

**Spatiotemporal multi-omics analyses of the barley (*Hordeum vulgare* L.)
inflorescence reveal a multilayered regulation of developmentally programmed
pre-anthesis tip degeneration**

Dissertation

zur Erlangung des
Doktorgrades der Agrarwissenschaften (Dr. agr.)

der

Naturwissenschaftlichen Fakultät III
Agrar- und Ernährungswissenschaften,
Geowissenschaften und Informatik

der Martin-Luther-Universität
Halle-Wittenberg

vorgelegt von

Herrn M.Sc. Nandhakumar Shanmugaraj

Geb. am: 28.04.1994 in Salem, Tamil Nadu, India

Gutachter

1. Prof. Dr. Thorsten Schnurbusch (IPK Gatersleben, Universität Halle-Wittenberg)
2. Prof. Dr. David Jackson (Cold Spring Harbor Laboratory, USA)

Gatersleben, den 03.07.2023

*To all the farmers for feeding my stomach,
To all the scientists for feeding my brain,
To my parents, my brother and my wife for their support*

Table of contents

Acknowledgments	vi
1. Introduction.....	1
1.1 Genetic strategies for improving grain yield potential in cereals	3
1.1.1 Grain yield enhancement by modification of inflorescence development targeting pre-anthesis phase of cereal crop life cycle.....	4
1.1.2 Inflorescence architecture in grasses	5
1.1.2.1 Inflorescence determinacy vs indeterminacy	7
1.2 Barley inflorescence development	8
1.3 Pre-anthesis decline of spikelets and florets among grasses	11
1.3.1 Floret fertility and sterility	11
1.3.2 Apical degeneration of inflorescence meristem	15
1.4 Molecular regulation of senescence and programmed cell death in plants	23
1.4.1 Definition of senescence and programmed cell death in plants.....	24
1.4.2 Morphological and ultrastructural changes associated with senescence and cell death	26
1.4.3 Phytohormonal control.....	27
1.4.4 Metabolic regulation	30
1.4.5 Transcriptional networks	32
1.5 Utilization of multi-omics for unwiring complex traits in crops	34
1.6 Spatial metabolomics by mass spectrometry imaging	36
1.6.1 Matrix-assisted laser desorption/ionization (MALDI) mass spectrometry imaging.....	37
1.7 Uncovering gene functions by targeted mutagenesis	39
1.8 Aims of this study	40
2.1 Plant materials and growth conditions	43
2.2 Methods	43
2.2.1 Phenotyping	43
2.2.2 Scanning electron microscopy (SEM) and Transmission electron microscopy (TEM).....	44
2.2.3 Live/cell death assay by FDA/PI staining	44
2.2.4 Phytohormone measurements in immature spike meristems	45
2.2.5 Primary metabolites profiling in immature spike meristems	47
2.2.6 ROS staining.....	49
2.2.7 Total RNA extraction.....	49
2.2.8 RT-qPCR	50

2.2.9 RNA-sequencing and gene expression analysis.....	50
2.2.10 Co-expression network analysis	51
2.2.11 Cis-motif enrichment analysis	51
2.2.12 Gene Ontology (GO) enrichment analysis	51
2.2.13 Subcellular localization	52
2.2.14 Generation of <i>gt1</i> knockout barley by targeted mutagenesis	52
2.2.15 De-tillering experiment	53
2.2.16 Association study and haplotype analysis	53
2.2.17 MALDI MSI	54
2.2.17.1 Spike sampling and tissue sectioning	54
2.2.17.2 Matrix application	55
2.2.17.3 MALDI-TOF MS measurements	55
2.2.17.4 MS imaging data analysis	56
2.2.18 Statistical analysis	57
2.2.19 Data availability	57
2.3 Data contribution by the author and the collaborators for the present thesis.....	57
3. Results.....	60
3.1 Morphological characterization of barley spike PTD	60
3.1.1 MYP, onset, and extent of PTD are reproducible in the main-culm spike.....	60
3.1.2 Live/death assay identifies the pattern of cell death during spike PTD	62
3.2 Physiological and biochemical characterization of barley spike PTD.....	63
3.2.1 Differential gradients of growth regulators separate the fate of apical spikelets.....	63
3.2.2 Dying apical parts display contrasting patterns of primary metabolites	66
3.2.3 ROS accumulates at higher levels in the degenerating apical parts..	71
3.3 Transcriptional reprogramming during barley spike PTD	72
3.3.1 Spatiotemporal transcriptome analysis uncovered molecular signatures that define the opposing developmental fates of degenerating and viable regions.....	72
3.3.2 ROKU analysis identifies putative candidates for barley spike PTD..	76
3.3.3 Transcription factors associated with barley spike PTD	81
3.3.4 WGCNA identifies putative hub genes for barley spike PTD	83
3.4 HvGT1 represses apical spikelet growth	85

3.5 Molecular changes leading to spike PTD are conserved in six-rowed barley.....	92
3.5.1 Natural variation in <i>HvGT1</i> regulatory region contributes to spikelet survival in six-rowed barley	100
3.6 Optimizing MALDI MS imaging pipeline for barley inflorescence meristems	102
3.7 MALDI MSI of immature barley inflorescences.....	105
3.7.1 Spatiotemporal distribution of specific amino acids and sugars	107
3.7.2 MSI identifies tissue-specific metabolites vital for proper spikelet development.....	111
4. Discussion	121
4.1 Spike PTD in barley is a preprogrammed meristematic senescence process	121
4.2 Spike PTD involves transcriptional regulators of senescence, plant defense, and light signaling	122
4.2 Barley GT1, a modulator of spike PTD	124
4.3 Later events of spike PTD are predominantly associated with higher ABA levels	126
4.4 Apical spikelets undergo metabolic reprogramming typical of organ senescence in plants	127
4.5 MALDI MSI has proven to be a valuable tool for studying the metabolism of barley spike meristems	130
5. Outlook.....	135
6. Summary	138
7. Zusammenfassung.....	140
8. References	143
9. Appendix	169
10. Abbreviations.....	182
11. Curriculum Vitae.....	184
12. Eidesstattliche Erklärung/Declaration under Oath	187

Acknowledgments

I am feeling grateful to reach one of the milestones in my research career. This part is devoted to all the people who supported me during the past five years and those who stood behind me to make this happen.

This work has been carried out in the research group Plant Architecture (PBP) at the Leibniz Institute of Plant Genetics and Crop Plant Research (IPK), Gatersleben, Germany, since November 2017.

Firstly, I sincerely thank my supervisor, Prof. Dr. Thorsten Schnurbusch, for allowing me to join his team. It was a life-changing moment when I received a green signal from you to pursue doctoral research in your lab on my long-time favorite research interest of inflorescence biology. You constantly motivated me to pursue this research independently from the beginning, sharing knowledge through our scientific discussions and constant guidance and support even at hard times. Further, your time-to-time career advice always helped me to plan for my career prospects. I am so grateful to pursue my doctoral research under you.

My sincere appreciation and gratefulness to my co-supervisor PD. Dr. Hans-Peter Mock for his guidance in performing research on metabolomics. Thanks for sharing your immense knowledge in this field. I started as a biologist, and after all these years, I feel overwhelmed performing some analytical techniques with fruitful outcomes and gaining some knowledge on this research direction.

I thank Prof. Dr. David Jackson from Cold Spring Harbor Laboratory, USA, for kindly accepting the invitation to review my doctoral thesis.

My deepest thanks to Dr. Thirulogachandar Venkatasubbu, Dr. Ravi Koppolu, and Dr. Yongyu Huang for constantly feeding me their knowledge and guidance on conducting quality research. I especially thank, Chandar for his constant advice on logical and critical thinking from the beginning of my doctoral research. I thank my fellow doctoral students, officemates, and friends, Guojing, Roop, and Ragav, for all these years of scientific and non-scientific discussions and support. I sincerely thank Dr. Guy Golan for his friendly attitude and fruitful scientific advice. My heartfelt thanks to all current and former members of the Plant Architecture group at IPK for their support and fruitful discussions during the group meetings. Sincere thanks to Corinna Trautewig for the excellent technical assistance. I also thank all the former research group members of

Applied Biochemistry at IPK for their support and cooperation. Especially thank Dr. Adriana Garibay for the excellent support, for sharing ideas, for solving all the research doubts related to metabolomics, and for being an office mate and friend.

This research would not be possible without the support of the people from the research groups of the physiology and cell biology department at IPK—my sincere thanks to all the collaborators. I especially thank Prof. Nico von Wiren, Dr. Yudelsy, Dr. Mohammed-Reza Hajirezaei, Dr. Twan Rutten, Dr. Michael Melzer, and Dr. Jochen Kumlehn for their excellent research support. I thank Dr. Sandip Kale for his contributions to RNAseq data analysis and Dr. Jeyaraman Rajaraman for developing Cas-9 plants and his guidance. Further, I want to acknowledge the tremendous support from Mr. Geyer and his team in the greenhouse. I thank IPK and European Research Council for funding.

I highly appreciate and thank Dr. Britt Leps, who helped me from the beginning to the end with all the administrative work and personal advice required during the past five years.

Besides research inputs, I thank Ravi, Chandar, Krishna, Sandip, Suresh, Sudharsan, and their families for their moral support and memorable times during my stay in Gatersleben and for helping with my mental wellness. I thank my dearest friend Ragav, my roommate and a doctoral student in the plant architecture group, who supported and motivated me during the good and most challenging moments. Thanks for your friendship!

Finally, as the most important people, I thank my parents, Shanthi and Shanmugaraj, for their prayings, hard work, sacrifice, and constant encouragement to follow my dreams and for their unconditional love. I thank my wife, Vedha, who supported me morally through challenging times and for her love.

Thank you all!

Nandhakumar Shanmugaraj

1. Introduction

Cereal crops are the primary component in ensuring global food security, providing food sources to humans and animals. The current global cereal production represents about 32 percent (2.9 billion tonnes) of the total crop production (9.3 billion tonnes) (FAO 2022). However, world crop production is challenged by climate change, industrialization, and soil erosion, thereby decreasing yield stability (Bailey-Serres et al., 2019, Ray et al., 2022). Increasing food production sustainably without expanding agricultural land is vital to feed the expected global population of 9.8 billion in 2050 (Clark et al., 2020, Ray et al., 2012). These projected demands on cereal grains worldwide urge researchers to find possible ways to increase the yield of cereal crops (Bailey-Serres et al., 2019, Burgess et al., 2022).

Barley (*Hordeum vulgare* L.) is one of the most ancient, economically important, and fourth most produced cereal food crops next to maize (*Zea mays* L.), rice (*Oryza sativa* L.), and wheat (*Triticum spp.*) (Badr et al., 2000) (Figure 1.1). Barley belongs to the Triticeae tribe (Poaceae) along with wheat, triticale (*x Triticosecale* Witt. ex A. Camus), and rye (*Secale cereale* L.). It is mainly used for animal feed and malting/brewing/distilling purposes, and only in recent years gained attention as direct food due to its high nutritional value (Baik and Ullrich, 2008). According to FAO, over 75% of barley produced worldwide was used as animal feed, where about 20% in malting industries and only about 5% for human consumption. However, malting barley represents a high-value use compared to feed barley because of its significant profitability (Langridge, 2018). Based on the arrangement of grains, cultivated barleys are commonly classified as two- and six-rowed (More detailed description in section 1.2). Globally, two-rowed barley varieties dominate the malting and brewing industries because of their grain uniformity, higher starch content, and a higher percentage of malt extracts (Schwarz and Li, 2010). In contrast, six-rowed are majorly preferred for feed because of their rich protein contents (Schwarz and Li, 2010, McKim et al., 2018). However, some parts of North America also use six-rowed barleys for malting and brewing purposes. In addition, several other factors are also considered for barley cultivation and end uses (Ullrich, 2014). Despite barley production being stagnant over the past two decades, a steady increase in global beer production reflects the rising proportion of barley used for malting (Langridge, 2018).

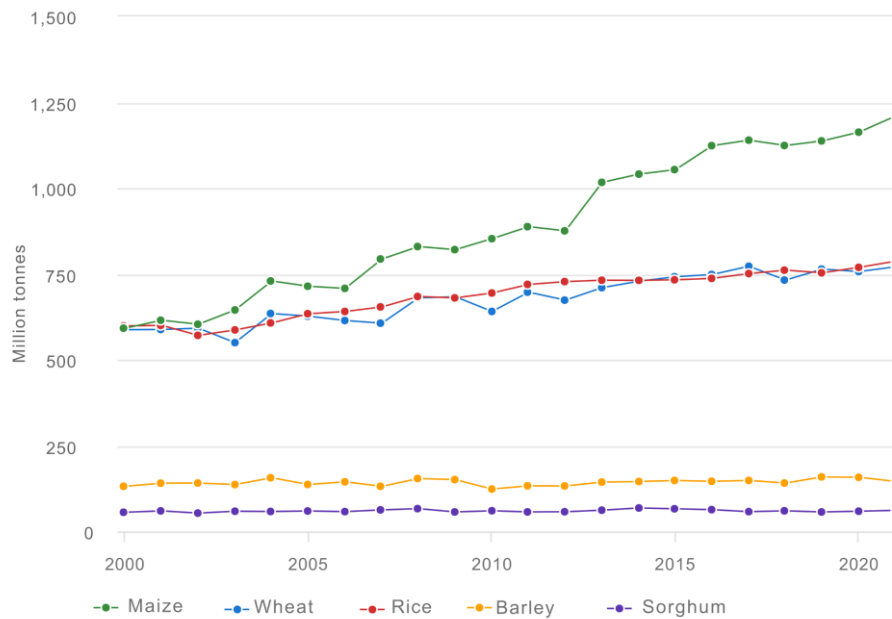


Figure 1.1. Global production of the major cereal crops in the past two decades. Data were obtained from <https://www.fao.org/faostat/en/#data/QCL> (FAOSTAT, 2023a).

Germany stands as the second most producer of barley in the world, with over ten million tonnes of production by 2021 (Figure 1.2A, B). Germany ranks fourth in barley beer production globally, followed by China, the U.S.A, and Brazil, and the third biggest exporter of malted beer, accounting for over one million tonnes (FAOSTAT, 2023b). Barley is a diploid ($2n=14$) annual crop with a comparatively low-complexity genome (= 5.1 Gb) among Triticeae and shows high collinearity to other related cereals, such as wheat and rye (Bauer et al., 2017). The extensive collection of genetic resources/mutants (Druka et al., 2010, Knudsen et al., 2022) and the availability of high-quality reference genome (Mascher et al., 2021) and pan-genome (Jayakodi et al., 2020) makes barley an excellent model crop for the tribe Triticeae, with the possibility of transferring the gained knowledge to other prime cereal crops such as wheat, maize, rice, and sorghum.

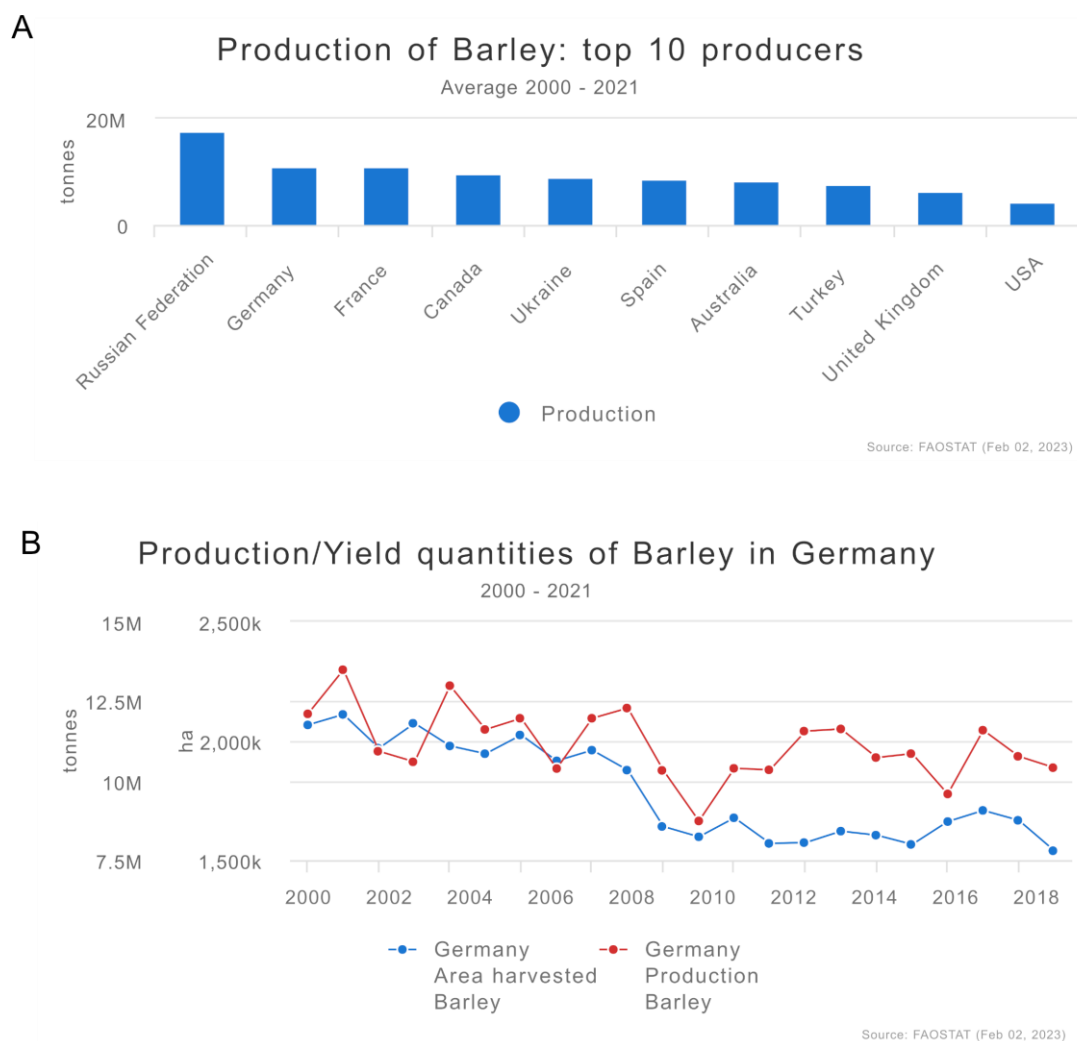


Figure 1.2. Barley production in the past two decades in Germany. (A) Top 10 major producers of barley and their production between 2000 and 2021. **(B)** Area under barley cultivation and production in Germany for the past two decades. M – Million. Data were obtained from <https://www.fao.org/faostat/en/#data/QCL> (FAOSTAT, 2023a).

1.1 Genetic strategies for improving grain yield potential in cereals

Crop grain yield potential is determined by complex traits that integrate multiple intrinsic and extrinsic factors. Due to this inherent complexity, the last decades of research have identified numerous ways and multiple potential targets to increase crop grain yield, ranging from crop management practices to diverse molecular and physiological processes at the whole plant, organ, and cellular levels. Understanding the subset of plant traits and biological processes crucial for determining crop grain yield will further pave ways to exploit crop productivity (Burgess et al., 2022). Here, “grain yield potential” is defined as grain yield without limitations by external inputs, biotic/abiotic stresses, or suboptimal growth conditions. The strategies for improving crop grain yield potential may differ depending on the species.

1.1.1 Grain yield enhancement by modification of inflorescence development targeting pre-anthesis phase of cereal crop life cycle

The architecture of cereal inflorescences and, in particular, the number of grains (GN) and grain size are the crucial traits directly related to grain yield in cereals. The final GN in cereals is primarily determined by the morphological transitions during the initial stages of inflorescence development (Sreenivasulu and Schnurbusch, 2012). Therefore, understanding how the inflorescence meristem maintains a proper size, shape, and numbers are vital in improving crop grain yields. However, GN and grain size of cereal crops are multifactorial traits controlled by numerous quantitative trait loci (QTL), which pose a significant challenge in identifying the underlying genes (Sakuma and Schnurbusch, 2020). Indeed, knowledge of early reproductive development and its manipulations using natural variations or generating novel alleles by new breeding techniques to improve final grain number are well described in rice and maize (Liu et al., 2021b). These findings suggest that knowledge of early inflorescence development and their manipulation can foster crop grain yield improvement. However, the understanding of early reproductive development and its genetic basis is still largely unknown in temperate cereals like wheat and barley. The yield potential of wheat and barley is closely related to the floret fertility at anthesis (Alqudah and Schnurbusch, 2014, Slafer et al., 2022). Therefore, identifying the possible ways by careful dissection of early reproductive development to maximize grain number per inflorescence in such crops will provide further opportunities to increase grain yield per unit area and crop productivity to meet the growing demands (Figure 1.3).

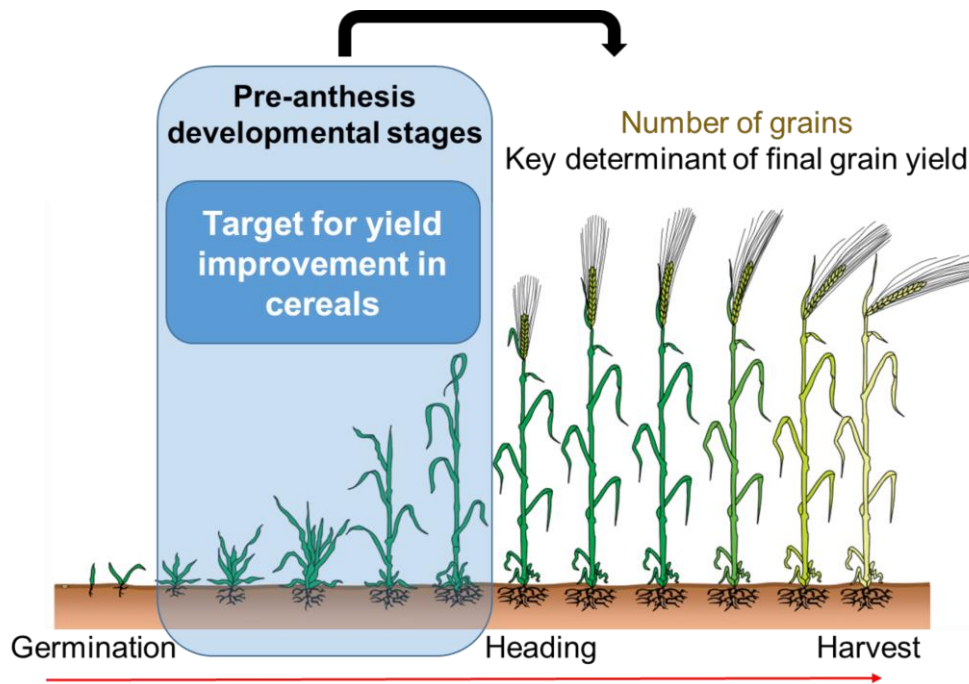


Figure 1.3. Pre-anthesis reproductive development as a target for yield enhancement in cereals. Representative image with major developmental transitions during cereal crop lifecycle. The final grain number in cereals is primarily determined by the morphological transitions during the initial stages (shaded in blue) of inflorescence development. Figure modified after (Sreenivasulu and Schnurbusch, 2012)

1.1.2 Inflorescence architecture in grasses

Plant development, in general, is governed by shoot apical meristem (SAM) and root apical meristem (RAM) activities (Wang and Li, 2008). In the vegetative phase, the shoot apical meristem produces leaves on its flanks and transforms into a reproductive inflorescence meristem (IM) after perceiving appropriate signaling cues for the transition. Inflorescences are flower-bearing structures that control plant reproductive success through a diverse and complex spatiotemporal arrangement of flowers (Kirchoff and Claßen-Bockhoff, 2013). Grass inflorescence architecture has been modified independently during domestication, contributing to improved yield, fitness, and harvestability (Pourkheirandish and Komatsuda, 2022, Olsen and Wendel, 2013). Inflorescences of the grass family (Poaceae) offer tremendous diversity primarily due to iterations of branching (Bommert and Whipple, 2018, Kellogg, 2022).

Moreover, the grass inflorescence possesses different types of branches, including a specialized short branch called a spikelet. The spikelet is the basic inflorescence unit in grasses that produces two glumes and encloses one to several florets (Kellogg, 2022). The spikelet resembles short inflorescence (little spike), either sessile, attached

directly to the inflorescence axis (called rachis), or produced on primary or higher order branches. Iterative transitions of different meristems, including IM, the branch meristem (BM), the spikelet pair meristem (SPM) in some grasses, the spikelet meristem (SM), and the floret meristem (FM) gives the architectural complexity to grass inflorescences (Figure 1.4A-D) (Koppolu and Schnurbusch, 2019). In all grasses, an IM or BM can function as a branch producing meristem, forming new BMs on its flanks, forming SM, or terminating by halting further cell division and growth. BM can also produce higher-order BMs and follows similar developmental transitions (Kellogg, 2022, Koppolu et al., 2022).

Based on the branching phenomenon, grass inflorescences are commonly classified as panicles, racemes, or spikes. The panicle inflorescences bear long or short branches, in which the spikelets are born on primary or higher order branches arising from the inflorescence axis (rice, sorghum (*Sorghum bicolor* L.), oats (*Avena sativa* L.)). Unlike other grasses, modern maize bears two distinct inflorescences: the male inflorescence (tassel) at the shoot apex and the female inflorescence (ear) in the leaf axils. IM in rice, sorghum, and maize produces branch meristems (BMs) (Tanaka et al., 2013). In rice, the BM produces a spikelet meristem (SM), and in maize and sorghum, BMs produce spikelet pair meristems (SPMs) (Figure 1.4A, B). Spikelets are arranged in a spiral phyllotaxis in most of the branched inflorescences. In the case of highly modified spike-type inflorescences, mostly the spikelets are sessile and attached directly to the inflorescence axis in a distichous manner [wheat, barley, rye (*Secale cereale* L.)] (Kellogg et al., 2013).

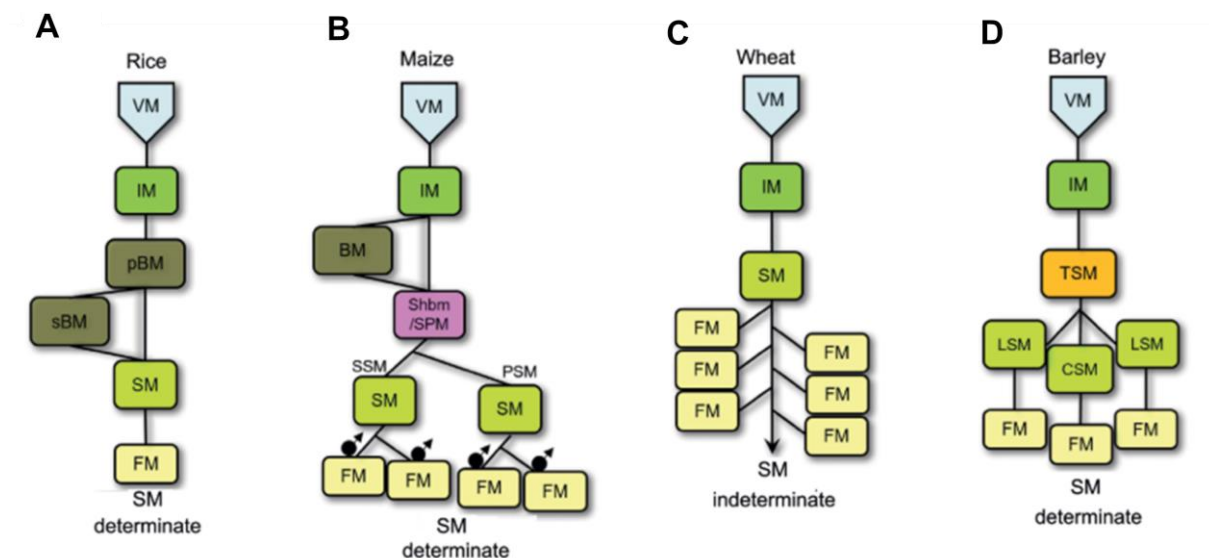


Figure 1.4. Meristem transitions and organization in major grass inflorescences. Meristem transitions and organization in the panicle inflorescence of rice (**A**), maize tassel (**B**), determinate wheat spike (**C**), and indeterminate barley spike (**D**). VM: vegetative meristem; IM: inflorescence meristem; PBM: primary branch meristem; SBM: secondary branch meristem; SM: spikelet meristem; FM: floret meristem; BM: branch meristem; ShBM/SPM: short branch meristem/spikelet pair meristem. TSM: triple spikelet meristem; LSM; lateral spikelet meristem; CSM: central spikelet meristem. The black circle with the arrow highlights male fertile florets of maize tassel inflorescence. Figure (Koppolu and Schnurbusch, 2019).

1.1.2.1 Inflorescence determinacy vs indeterminacy

Based on the determinacy of shoot meristems, inflorescences are either determinate or indeterminate. IMs are considered indeterminate if they remain undifferentiated by continuously forming lateral structures on their flanks. IMs are determinate when they produce a fixed number of lateral organs and are wholly consumed to develop into a FM to form a terminal flower (Prusinkiewicz et al., 2007). In grass IMs, lateral BMs or SMs are produced reiteratively and become determinate if the IM transforms to a terminal spikelet meristem in the case of wheat, sorghum, rye, ryegrass (*Lolium spp.*), and oat (*Avena sativa*) (Kellogg, 2022, Moncur et al., 1981). Alternatively, the IM ends as an undifferentiated dome or axis without any terminal spikelet for maize, barley, and rice (Bonnett, 1966, Kellogg et al., 2013, Yoshida et al., 2013). The fate of an IM to end in spikelet formation is independent of the primary BMs terminating in spikelets or ceasing growth (Moncur et al., 1981, Kellogg et al., 2013, Kellogg, 2022). For example, in the case of rice, primary and higher-order branches end with spikelet formation. In contrast, the IM ceases the growth with no terminal spikelet after forming the determined primary BMs. The presences or absences of terminal spikelets in IM are very labile between tribes and genera of grasses during evolutionary times (Kellogg et al., 2013).

In addition, SMs, in turn, become determinate or indeterminate, producing defined or variable florets, respectively. For example, in rice, the BM produces SMs, and each spikelet generates one floret. In maize and sorghum, BMs produce spikelet pair meristems (SPMs); each SM produces two florets. Whereas in Triticeae, the SM of barley and rye are determinate with only one and two florets, respectively. In contrast to the determinate IM, wheat possesses an indeterminate SM producing a variable number of florets along the rachilla (spikelet axis). Similarly, such indeterminate SMs with multiple florets are also present in the panicle-type inflorescence of oat (Poeae)

(Bonnett, 1966, Moncur et al., 1981, Koppolu and Schnurbusch, 2019, Sakuma and Schnurbusch, 2020).

1.2 Barley inflorescence development

Barley possesses an indeterminate 'spike'-type inflorescence in which the sessile spikelets are attached directly to the rachis in a distichous phyllotaxis (Koppolu and Schnurbusch, 2019). Reproductive development in temperate cereals such as barley and wheat are divided into different phases based on morphological transitions of the shoot apex: leaf initiation (vegetative phase), spikelet initiation (early reproductive phase), spike growth and differentiation (late reproductive phase), and grain filling phase. Many studies have developed scaling systems to identify and track the morphological transitions during apical meristem development in barley and other major cereals (Bonnett, 1966, Kirby and Appleyard, 1981, Waddington et al., 1983). The most popular scaling method for studying barley inflorescence development was proposed by (Kirby and Appleyard, 1981), which involves the most extensive and accurate scale covering the external and internal developmental changes. Nevertheless, after carpel initiation, this method limits to general growth characters (e.g., anther length, spike length) that vary significantly among genotypes. In addition, after the awn primordium (AP) stage, this scale is restricted to differentiate only four major developmental transitions until anthesis, based on anther development and meiosis *viz.*, white anther, green anther, meiosis and yellow anther stages. However, the quantitative scale for developing barley and wheat spikes commencing from vegetative apex to anthesis was proposed by (Waddington et al., 1983) based on spike initials and pistil morphogenesis of the most advanced floret primordium and carpel of the inflorescence. This scale gives decimal scores from 0 to 10 (W0 – W10; W - Waddington) and covers about 20 developmental transitions of spike axillary meristems for the precise identification of growth and differentiation of inflorescence development in wheat and barley (Figure 1.5A).

After the transition of SAM to IM, the barley IM differentiates into the double ridge (DR) stage, which marks the first reproductive stage with a lower leaf meristem ridge and upper spikelet meristem ridge. The leaf meristem ridge remains suppressed, while the SM ridge enlarges to differentiate into the triple spikelet meristem (TSM) or triple mound at each rachis node (Kirby and Appleyard, 1981). The TSM consists of a larger central spikelet meristem (CSM) bordered by two smaller lateral spikelet meristems

(LSMs), all of them are a unique feature of the entire genus *Hordeum*. Each SM in barley is determinate and uniflorous and thus produces a single grain. The development of the CSM is much more developmentally advanced than the LSMs, and the fate of the two LSMs to form fertile or sterile spikelets determines barley spike 'row types.' In wild barley and most cultivated varieties, each rachis node develops only central spikelets to produce fertile floret and grain. In contrast, floral organ development in the lateral spikelets (LSs) is inhibited and remains sterile. Since spikelet nodes are oppositely positioned in a distichous manner along the rachis, spikes have two rows of fertile central spikelets yielding barley's "two-rowed" spike types (Zohary et al., 2012, Koppolu and Schnurbusch, 2019, Sakuma and Schnurbusch, 2020). In six-rowed barleys, all three spikelets at each rachis node produce fertile florets to give 'six-rowed' spike architecture (Figure 1.5B). In both row types, the end of spikelet primordia initiation (spikelet initiation phase) along the rachis marks the maximum yield potential (MYP) stage after advancing to glume, lemma, stamen, and awn primordium stages. The total spikelet primordia number formed at the MYP stage represents the potential spikelet number (PSN) of the inflorescence. The number of spikelets or spikelet primordia per spike varies among barley genotypes and ultimately influences the final grain number (Alqudah and Schnurbusch, 2014, Kamal et al., 2021, Thirulogachandar et al., 2021b). Previous studies suggested that in most genotypes, the number of spikelets per spike is determined around the awn primordium (AP) stage (Alqudah and Schnurbusch, 2014). However, a recent study proposed a method called 'spikelet stop' for the precise identification of the MYP and found it can vary among barley genotypes and growth conditions (Thirulogachandar and Schnurbusch, 2021). After the MYP stage, during the spike growth phase, the IM dome ceases its activity and starts to collapse, followed by the gradual degeneration of spikelet primordia, spikelets, and rachis beneath the dome until a specific position along the spike is reached. In addition, the poor differentiation of a few spikelet nodes (usually 2-3) at the base of the spike generates rudimentary spikelets, which generally do not set grains either; however, some genotypes lack such basal rudimentary spikelets. Only the surviving spikelets during the late reproductive phase will later enter the anthesis, followed by the grain-filling phase (Alqudah and Schnurbusch, 2014, Kamal et al., 2021). The spikelets that survive after the completion of apical spikelet degeneration at anthesis and reach the grain-filling phase represent the final spikelet number (FSN). However, not all spikelets entering the grain-filling phase will produce grain; grain abortion might also result due

to poor pollination or source-sink dynamics at late senescence phase. Therefore, the grains retained at harvest represents the final grain number (GN) per spike (Figure 1.5C) (Kennedy et al., 2018, Thirulogachandar et al., 2021b, Slafer et al., 2022).

As mentioned above, degeneration of initiated spikelets/florets occurs during the course of inflorescence development in cereals. The following section will describe a detailed background on the different forms of pre-anthesis floral degeneration in cereals species and their significance.

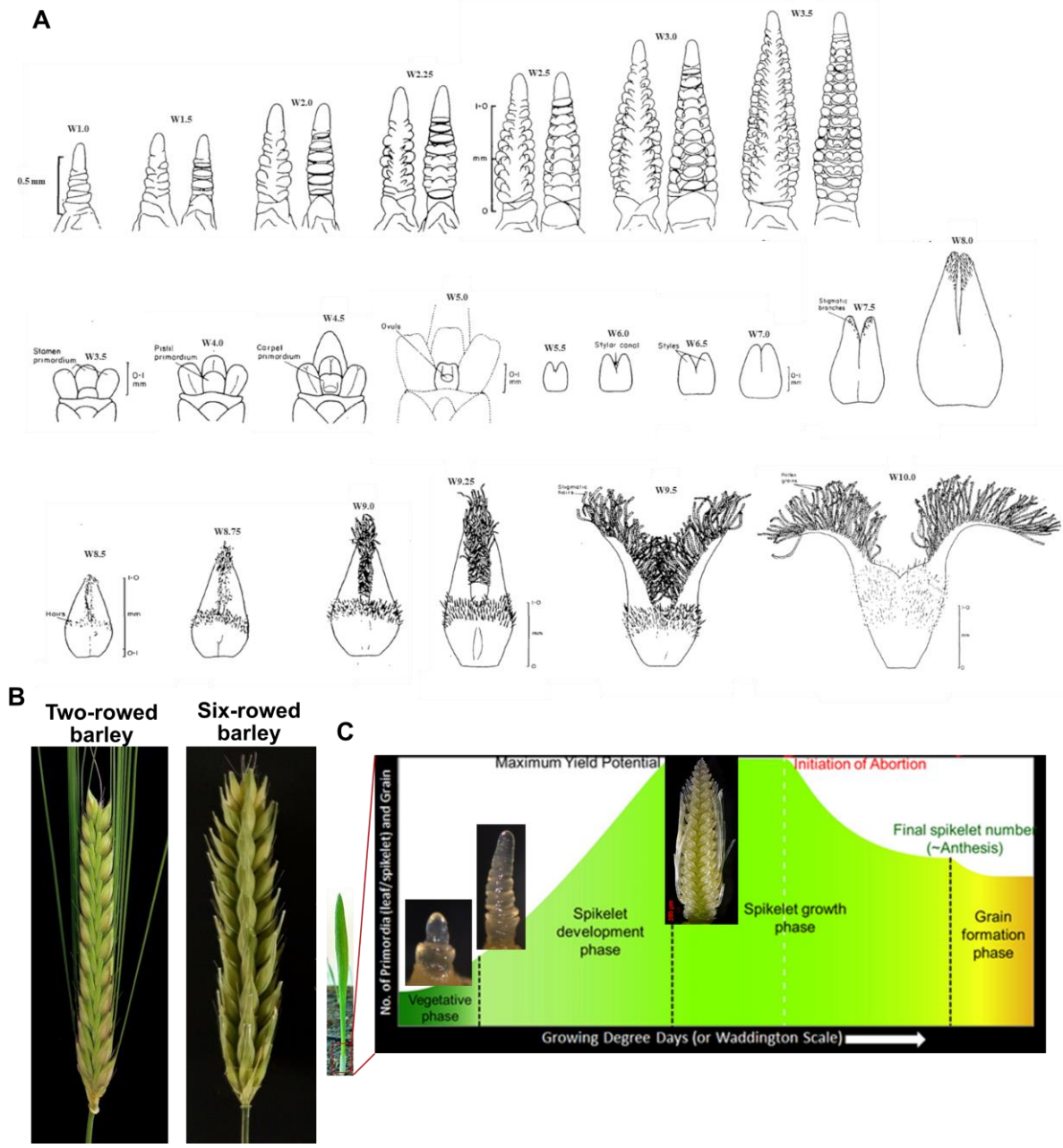


Figure 1.5. Inflorescence development in barley. (A) Quantitative scale with images of developing barley spike meristems commencing from vegetative apex to anthesis based on spike initials and pistil morphogenesis proposed by Waddington et al., 1983. **(B)** Representative two-rowed and six-rowed

spikes after heading. Awns clipped off from six-rowed barley. **(C)** Overview of the major reproductive developmental phases in barley. The image at vegetative phase represents the vegetative shoot apex followed by the double ridge stage containing the axillary spikelet meristem, the first reproductive structure in barley during the spikelet developmental phase. The immature spike in the center of the graph represents the end of spikelet primordia initiation. The x-axis shows the number of leaf/spikelet primordia and grain, the y-axis represents growing degree days or the Waddington scale. W, Waddington scale. Figure C (Source: <https://www.ipk-gatersleben.de/unabhaengige-arbeitsgruppen/pflanzliche-bauplaene/>)

1.3 Pre-anthesis decline of spikelets and florets among grasses

1.3.1 Floret fertility and sterility

In many cereal crops, not all the initiated floret primordia develop to become fertile florets that form grains. Aborted or sterile florets are widespread among cereal inflorescences (Moncur et al., 1981). Importantly, in some species, the fate of sterile or fertile florets is predetermined during the initial phase of reproductive development and fixed among individuals (Thiel et al., 2021, Yang et al., 2021). Alternatively, in some instances, floral sterility may also result due to unfavorable conditions (Kato et al., 2008). Altering the developmental fate of sterile to fertile florets will significantly improve final grain number and productivity in cereals (Sakuma and Schnurbusch, 2020). Studies in maize, sorghum, and barley have identified a few molecular determinants involved in floret abortion and the function of those sterile florets, which will be reviewed in this section.

Maize and sorghum

Many relatives in the grass tribe Andropogoneae bear their florets in pairs of spikelets in which one spikelet of the pair produces grain, and the other remains sterile or staminate (AuBuchon-Elder et al., 2020). In maize, floral meristems in the physically separated male (tassel) and female (ear) inflorescences become unisexual through sex determination that has long been studied (Acosta et al., 2009). SM in maize generates one upper and one lower floret in the tassel and ear. Each floret initiates a series of floral organs, including three stamen primordia and a central carpel primordium. The tassel florets become staminate through the selective elimination of a preformed carpel initial by programmed cell death (PCD) and sexual maturation of the stamen. The ear spikelets become pistillate through the development of the carpel only in the upper (primary) floret, while stamen suppression is in both (upper and lower)

florets (Yang et al., 2021). The carpel suppression trait has been well studied in maize using the classic *tassel/seed* (*ts*) mutants. The *ts1* and *ts2* mutant plants lose their carpel suppression ability to generate pistillate tassels and pistils in all ear florets (DeLong et al., 1993, Acosta et al., 2009). The PCD of carpel primordia involves TS1-dependent production of the phytohormone jasmonic acid (JA) by encoding plastid-localized lipoxygenase and TS2, a short-chain alcohol dehydrogenase whose specific function in the cell-death pathway remains elusive. Whereas brassinosteroids (BR) and gibberellic acids (GA) have also been reported to regulate sex determination in maize (Dellaporta and Calderon-Urrea, 1994, Hartwig et al., 2011). In addition to hormonal regulations, sex determination is also associated with the transcriptional regulation of the AP2-like transcription factor (*Ts6*), whose expression is controlled by a *microRNA172* (*ts4*) (Chuck et al., 2007). The tissue-specific transcriptome of upper and lower florets using laser-capture microdissection revealed the involvement of sugar signaling and cell wall modifications in the growth suppression of lower florets (Yang et al., 2021). Carpel PCD mediated by the axillary meristem suppression gene, *GRASSY TILLETSS1* (*GT1*), and inflorescence meristem determinacy gene, *RAMOSA3* (*RA3*), have been reported in maize (Klein et al., 2022). *RA3* and *GT1* genetically interact to regulate meristem determinacy in inflorescences and carpel suppression in both tassel and ear florets.

Unlike maize, sorghum possesses a determinate, terminally produced panicle-type inflorescence (Jiao et al., 2018). The main inflorescence bears primary branches, and subsequent secondary or tertiary branches develop from the primary branches. Each branch terminates in a trio of spikelets: one fertile sessile spikelet (SS) and two sterile pedicellate spikelets (PS), which fail in developing mature carpels and occasionally anthers. Below the terminal spikelets, several pairs of spikelets can be found with one SS and one PS and later being sterile due to carpel abortion (AuBuchon-Elder et al., 2020). Interestingly, like in maize, JA has been shown to play a significant role in the sterility of the PS in sorghum. The sorghum *multi seeded1* (*MSD1*) gene encoding a class II TCP (TEOSINTE BRANCHED1/ CYCLOIDEA/PROLIFERATING CELL NUCLEAR ANTIGEN FACTOR 1) transcription factor, *MSD2* encoding lipoxygenase that catalyzes the first step in JA biosynthesis and *MSD3*, a plastidial ω -3 fatty acid desaturase that catalyzes the conversion of linoleic acid (18:2) to linolenic acid (18:3), negatively regulates PS development (Jiao et al., 2018, Dampanaboina et al., 2019, Gladman et al., 2019). Whereas, *msd1*, *msd2*, and *msd3* mutants can produce

~200% more grains as both SS and PS are fertile to produce regular grains, increasing final GN per panicle. Transcriptome analysis revealed that MSD1 activates *MSD2* expression, thereby promoting JA biosynthesis and other gene networks, leading to the *multiseeded* phenotype. The *msd3* mutants have reduced levels of 18:3 fatty acid; a substrate for JA biosynthesis that may lead to reduced levels of endogenous JA. These results demonstrate the importance the JA pathway on floral organ abortion. However, the function of these sterile spikelets was not known until a recent study in sorghum using carbon isotope labeling, demonstrating that sterile spikelets (PS) perform photosynthesis and contribute to grain yield by increasing the grain size of fertile spikelets (SS) (AuBuchon-Elder et al., 2020).

Barley

As described previously in section 1.2, the cultivated barley inflorescence can be divided into two major spike forms, 'two-rowed' and 'six-rowed' spikes, based on their lateral spikelet (LSs) fertility. In most wild barleys (*Hordeum vulgare* ssp. *spontaneum*), the progenitors of cultivated barley, are two-rowed while the six-rowed phenotype has been selected during domestication (McKim et al., 2018). Natural and induced mutants displaying various degrees of fertility in lateral florets have been investigated, and the underlying genes have been characterized. So far, genetic studies have identified up to 11 independent loci associated with complete or partial changes in the fertility of LS (Koppolu and Schnurbusch, 2019). The LS fertility (six-rowed spike) phenotype is controlled by at least five known independent loci that include *Six-rowed spike1* (*Vrs1*, formerly for *vulgare row-type spike 1*), *Vrs2*, *Vrs3*, *Vrs4*, and *Vrs5* [*INTERMEDIUM SPIKE-C (Int-c)*] (Zwirek et al., 2019) (Figure 1.6A-F). However, two-rowed barley can be transformed into complete six-rowed barley by a single mutational event in the *Vrs1* gene (Komatsuda et al., 2007). Loss-of-function mutations of *Vrs1* contribute to higher GN per spike through a complete metamorphosis of sterile to fertile lateral florets. The *Vrs1* gene encodes a Homeodomain leucine zipper (HD-ZIP) class I transcription factor (*HvHox1*), which expresses in the lateral floret primordia (in the carpel, lemma, palea, and rachilla) of the developing spike and was found among natural row-type variants of the cultivated barley gene pool (Sakuma and Schnurbusch, 2020, Sakuma et al., 2013). Further allelic variation at the barley *Vrs1* locus was uncovered with the study of the barley mutant '*deficiens*'. In *deficiens* barleys, the LSs are highly suppressed compared to conventional two-rowed barleys due to a single amino acid

substitution (S184G) at the C-terminal region in a putative phosphorylation site of the VRS1 protein that results in extreme suppression of lateral florets (Sakuma et al., 2017). Similar to maize and sorghum, sterility in barley LSs results from the inhibition of carpel development (some two-rowed cultivars produce functional anthers), while the mechanism remains elusive (Sakuma and Schnurbusch, 2020). Similar to *Vrs1*, natural row-type variation for *Vrs5* was found among the cultivated barley gene pool. *Vrs5* encodes a class II TCP transcription factor, an ortholog of the maize domestication gene *TEOSINTE BRANCHED1* (*TB1*), and loss-of-function alleles of *Vrs5* promote LS fertility and an increased tiller number. The less functional allele of *Vrs5*, *Int-c.a* (*HvTB1*) promotes the growth of LS and grain size in commercial six-rowed cultivars together with *vrs1.a* six-rowed alleles (Ramsay et al., 2011, McKim et al., 2018).

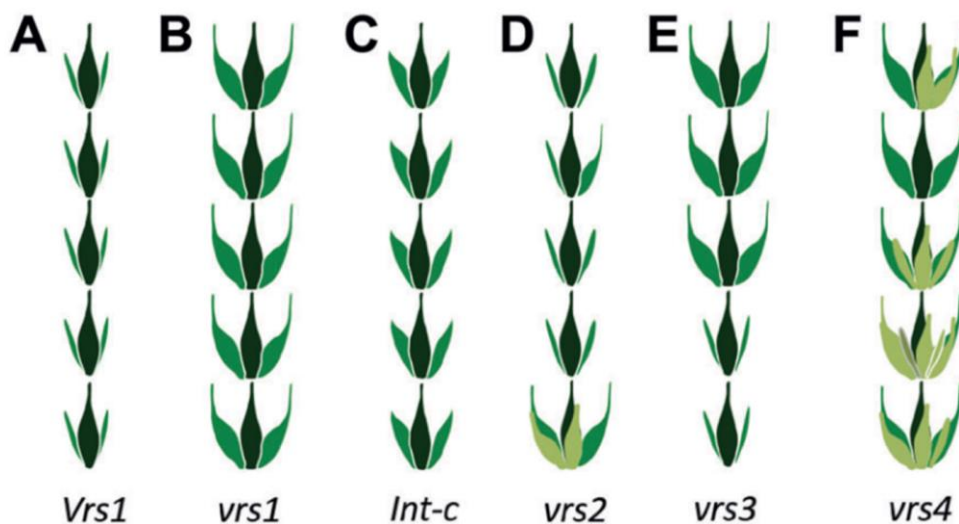


Figure 1.6. Regulation of spike row-type in barley. (A) Two-rowed spike (*Vrs1*) with fertile central spikelets (CS) and sterile lateral spikelets (LS). (B) *Six-rowed spike 1* (*vrs1*) with fully fertile CSs and LSs. (C) *INTERMEDIUM SPIKE-C* (*Int-c*)/*Vrs5*: shows enlarged LSs. (D) *Six-rowed spike 2* (*vrs2*): Fertile LSs in the middle and basal regions of the spike with occasional additional spikelets at the spike base. Additional spikelets (AS) - light green color. (E) *Six-rowed spike 3* (*vrs3*): Partial two-rowed and six-rowed phenotypes. (F) *Six-rowed spike 4* (*vrs4*): spike similar to *vrs1* with respect to LS fertility, bearing frequent AS (light green colored). LSs - Lateral spikelets; CSs – Central spikelets. Figure from Koppolu *et al.*, 2013.

Further, induced recessive mutant alleles in other loci (*vrs2*, *vrs3*, *vrs4*) exhibit varying degrees of six-rowed phenotypes. *Vrs4* confers a LATERAL ORGAN BOUNDARY (LOB) domain transcriptional factor, an ortholog of maize transcription factor

RAMOSA2 (RA2), which is essential for inflorescence branch formation in maize (Koppolu et al., 2013). *vrs4* mutants show complete LS fertility similar to *vrs1* but exhibit indeterminate triple spikelet meristems as it produces additional spikelets/florets. *Vrs2* mediates a plant-specific *SHORT INTERNODES (SHI)* transcriptional regulator, which modulates plant architecture and phase duration involving auxin biosynthesis and gibberellin (GA) responses. At the same time, the mutant (*vrs2*) shows a partial six-rowed condition with fertile LSs toward the center of the spike (Youssef et al., 2017). *Vrs3* underlies a putative Jumonji C-type (JMJC) H3K9me2/me3 demethylase, whose recessive allele *vrs3* restores lateral spikelet fertility and improves grain uniformity in six-rowed germplasm (with *vrs1* and *vrs5* alleles) (Bull et al., 2017). Based on mutant and transcript network analysis, *VRS3*, *VRS4*, and *VRS5* may regulate the expression of *VRS1* and other row-type genes to maintain the two-rowed spike form modulating hormonal pathways (auxin, cytokinin, GA, and JA) and sugar signaling (van Esse et al., 2017, Bull et al., 2017). Recently, the tissue-specific transcriptome of CSM and LSM between TM to AP stages revealed upregulation of processes related to stress responses and growth repression, including abscisic acid (ABA) response/signaling, GA catabolism, JA responses, and secondary metabolism (Thiel et al., 2021). In particular, this study postulates the involvement of ABA signaling in the initial growth arrest of LSs. However, unlike maize and sorghum, the hormonal regulation of floral sterility is still elusive in barley. Nevertheless, identifying and characterizing spike row-types (*VRS*) genes advanced our understanding of floret fertility/sterility and provided novel routes to enhance grain number in barley.

1.3.2 Apical degeneration of inflorescence meristem

In addition to the floret sterility or abortion in different cereal species described above, arrest and cessation of the IM or SM followed by the basipetal degeneration of apical spikelet/florets and axes is also found among cereals (Bonnett, 1966). In general, this phenomenon happens during the pre-anthesis phase of reproductive development in the cereal inflorescences possessing indeterminate meristems and negatively impacts yield potential and the final grain number. The occurrence of tip degeneration varies among cereal species depending on the position of indeterminate meristems. For example, in barley and maize, degeneration is confined to the tip of the immature IM, as it possesses an indeterminate IM (Alqudah and Schnurbusch, 2014, Meng et al., 2007). In wheat, rye, and oat, apical degeneration happens in each spikelet as these

species possess indeterminate SMs (Bonnett, 1966) (Figure 1.7). Previous studies in wheat and barley have described this process as floret abortion or spikelet abortion, respectively. To more clearly distinguish this phenomenon from developmental events described previously (see 1.3.1), it will be collectively referred to as pre-anthesis tip degeneration (PTD) in the present study. Reducing spikelet/floret loss during the pre-anthesis phase of reproductive development, thereby, represents an opportunity to increase grain yield in cereals. In rice, the IM is determinate in producing primary branch meristems, whereas the apex aborts and remains as a vestige structure at the base of the topmost primary branch (Yoshida et al., 2013). In addition, panicle apical degeneration/abortion also occurs in rice only under adverse conditions, where few spikelet-bearing primary branches in the upper part abort. Several genes responsible for this trait have been cloned using panicle abortion mutants (Ali et al., 2019). Under optimal growth conditions, such a phenomenon is absent in rice, unlike the developmentally orchestrated tip degenerations observed in the indeterminate meristems of barley, wheat, rye, oat, and maize. The current section will describe the phenomenon of PTD in major cereal crops harboring indeterminate IM/SM and review the available knowledge about the genetic basis and significance of unwiring this trait.

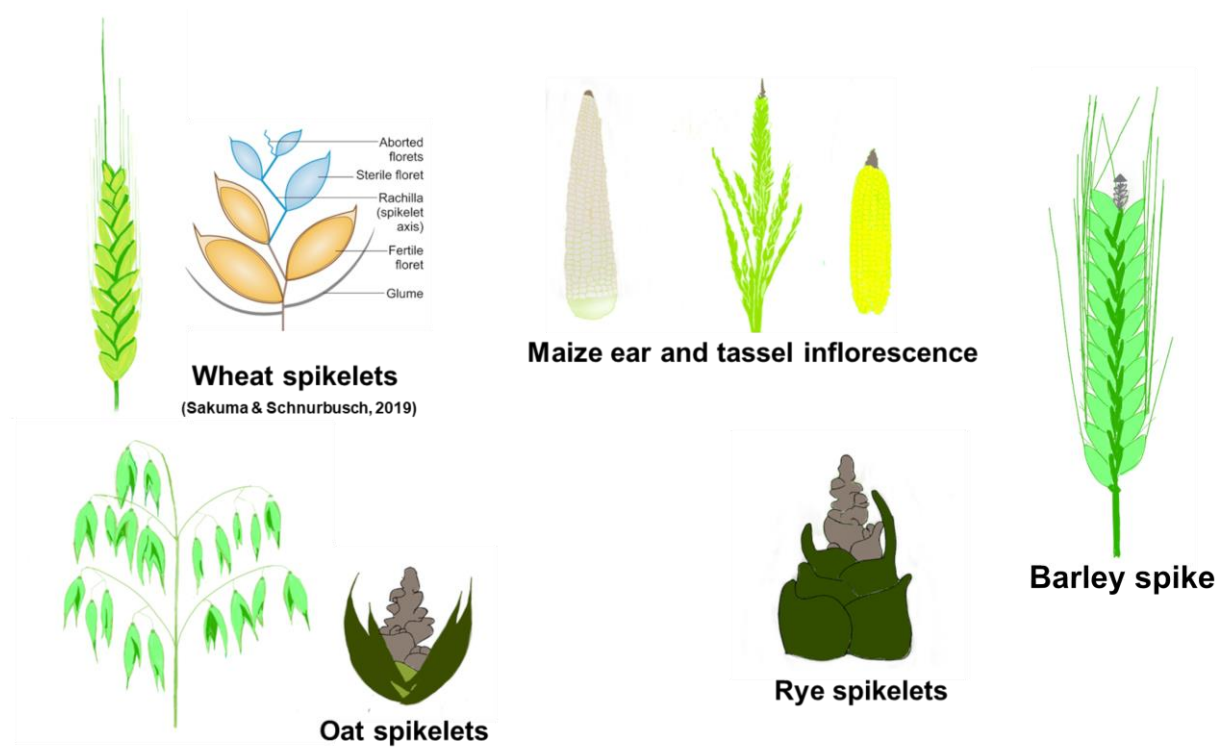


Figure 1.7. Pre-anthesis floral degeneration is widespread among major cereals. Floret degeneration in the apical part of each spikelet among wheat, rye, and oat. Tip degeneration in maize ear and tassel inflorescence and in barley spikes.

Ear apical degeneration in maize

Maize bears indeterminate tassels and ear IMs with dome-shaped apex (Bonnett, 1966). Apical degeneration is a common phenomenon in both IMs, perhaps more evident in the ear. In ear IMs, the death of apical organs leaves a rudimentary barren tip under normal development. However, this ear tip barrenness (ETB) is enhanced under unfavorable conditions leading to more aborted kernels in the tip and significantly reducing kernel number per ear, a key determinant of yield potential in maize (Meng et al., 2007). Few genetic and physiological studies previously described QTLs, hormone, and metabolic changes associated with ETB or apical kernel abortion that investigated after pollination or at harvest (Feng et al., 2011, Li et al., 2020). However, studies on early events of ETB in maize are still obscure.

The identification of genes involved in regulating ear IM size and activity has been a great value in improving kernel number in maize. The IM size is primarily determined by the activity of the SAM (Kitagawa and Jackson, 2019). The SAM consists of a specialized domain of cells, the organizing center (OC), stem cell niches of the central zone (CZ), peripheral zone (PZ), differentiation zone, and rib zone (RZ) (Heidstra and Sabatini, 2014, Wang and Li, 2008). A CLAVATA (CLV)-WUSCHEL (WUS) signaling pathway discovered first in eudicot *Arabidopsis* regulates stem cell maintenance and IM activity (Schoof et al., 2000, Williams and Fletcher, 2005). *WUS* encodes a homeodomain transcription factor and activates the expression of *CLV3* gene, a secreted peptide that is perceived by receptor complexes, including leucine-rich repeats (LRRs) kinases CLV1 and CLV2 that stabilize the meristem activity by signaling back to repress the *WUS* expression (Sharma et al., 2003). This pathway is also conserved in other species, including maize (Dodsworth, 2009, Zhang and Yuan, 2014). In maize, null mutants of the *CLV* orthologues, THICK TASSEL DWARF1 (ZmTD1, CLV1 ortholog), FASCIATED EAR2 (ZmFEA2, CLV2 ortholog), and CLAVATA3/EMBRYO SURROUNDING REGION-RELATED7 (ZmCLE7, CLV3 ortholog), show enlarged IM by restricting IM proliferation and produce fasciated ears losing dome-shaped apex that drastically affected kernel rows with reduced grain yield (Bommert et al., 2005, Bommert et al., 2013, Rodriguez-Leal et al., 2019). Besides, FASCIATED EAR3 (ZmFEA3), an LRR receptor-like protein, represses *WUS* expression by perceiving a distinct CLE peptide, FON2-LIKE CLE PROTEIN1 (ZmFCP1, CLV3 paralog) that acts in a distinct *CLV* pathway to repress

WUS expression (Je et al., 2016, Je et al., 2018). Weak coding sequence alleles and promoter-edited alleles of CLV-*WUS* pathway genes result in a quantitative increase of kernel rows, maintaining meristem organization without fasciation, highlighting the potential for yield enhancement (Bommert et al., 2013, Je et al., 2016, Liu et al., 2021a).

In contrast to genes regulating ear size through modifying IM width, *KERNEL NUMBER PER ROW6* (*KNR6*), *ZmACO2*, *YIGE1*, and *EAD1* were recently shown to regulate ear size by improving ear length (EL) (Jia et al., 2020, Ning et al., 2021, Luo et al., 2022, Pei et al., 2022). *KNR6* encodes a serine/threonine protein kinase that may function in auxin-dependent inflorescence development by mediating Arf GTPase-activating protein phosphorylation and enhances grain yield by raising EL and KNR (Jia et al., 2020). *ZmACO2* encodes 1-aminocyclopropane-1-carboxylate oxidase 2 regulating ethylene biosynthesis, and a loss-of-function allele leads to lower ethylene production in developing ears, resulting in higher grain yield per ear by improving floret fertility and number (Ning et al., 2021). *YIGE1* encodes an unknown protein and positively regulates EL by increasing pistillate floret number, altering genes related to sugar and auxin pathway (Luo et al., 2022). *EAD1* encodes an aluminum-activated malate transporter preferentially expressed in the xylem of immature ears. Loss of *EAD1* leads to reduced availability of malate in the apical part of developing inflorescences and undergoes premature ROS-mediated PCD resulting in shorter ears with reduced EL and KRN. However, overexpression of *EAD1* outperforms the wild type by positively regulating EL and KNR, shedding light on the importance of malate metabolism in early inflorescence development in maize (Pei et al., 2022).

Apical degeneration in Wheat, Rye, and Oat spikelets

Wheat, Rye, and Oat produce determinate IM, whereas the SMs in these species are indeterminate and produce a varying number of florets attached to the spikelet axis, the rachilla (Bonnett, 1966). A wheat spikelet typically produces up to 12 floret primordia; however, during development, about 70% of the florets abort due to SM tip degeneration (Guo and Schnurbusch, 2015, Guo et al., 2016). Floret fertility also varies depending on the position of the spikelet within the spike. At each spikelet, florets differentiate acropetally, leaving only developmentally advanced 3-5 basal fertile florets to produce typical grains. This pre-anthesis SM degeneration, followed by the death of

apical florets, significantly influences the final grain yield potential in wheat (Sreenivasulu and Schnurbusch, 2012, Slafer et al., 2022). The spike architecture of cultivated rye, in general, is more similar to wheat. Earlier studies on rye spike development showed the indeterminate nature of the SM, producing up to 6 florets while leaving only two basal florets fertile that produce two grains, whereas the remaining 3 to 4 apical florets degenerate (Bonnett, 1966). Spikelets of common oat (husked) produce a variable number of floret primordia ranging from 4-6 but eventually form only 2-3 fertile florets and grains (Bonnett, 1966, Ougham et al., 1996). In certain naked oat types, spikelets produce up to 10-12 florets with long rachilla and varying fertility of about 4-7 florets depending on genotype and environmental conditions (Burrows, 1986, Welch, 2012, Zimmer et al., 2019). In all these species, the phenotypic description of spikelet apex degeneration and terminal florets' death hints at the possibilities of similar molecular regulation and function.

In past decades, substantial research has been conducted to understand wheat floret fertility/survival (Slafer et al., 2022). Many studies on wheat floret death have proposed a prominent role for assimilate allocation (Miralles et al., 1998, Dreccer et al., 2014), the developmental age of florets (Bancal, 2009, Bancal, 2008), floret differentiation rate (Ferrante et al., 2013), hormonal regulations (Zheng et al., 2016) and poor vascular connections (Hanif and Langer, 1972, Wolde and Schnurbusch, 2019). It has been suggested that grain number determination in wheat is strongly influenced by the photoassimilate allocation to the growing spikes during the phase between terminal spikelet (TS) and anthesis (Gonzalez et al., 2011). The TS stage roughly coincides with the stem elongation phase, followed by booting and anthesis. Spike development between the TS-anthesis phase comprises floret development, death of floret primordia, and determination of surviving/fertile florets, which later enter into anthesis and grain-filling phases. It is assumed that rapid stem elongation, which coincides with active spike growth, might limit assimilate partitioning to the developing florets, thereby decreasing floret fertility (Miralles et al., 1998). Based on whole-spike measurements (Ghiglione et al., 2008), sugar starvation has been postulated to play a role in the death of more distal florets in wheat. A recent study reported that a faster rate of floret development was responsible for improved survival of labile florets in response to nitrogen fertilization supporting the hypothesis on resource allocation to the growing spike before anthesis (Ferrante et al., 2020). In addition, differences in survival might

be attributed to intra-spike partitioning of resources as the floret survival is dynamic between spikelets along different spike positions (Ferrante et al., 2013). Due to the significance of the pre-anthesis phase on grain number determination in wheat, previous studies have been conducted to extend the duration of the stem elongation phase, allowing more time for spike biomass accumulation, thereby improving floret growth (Miralles et al., 2000, González-Navarro et al., 2015). QTLs specific for the duration of this phase have been identified; however, the underlying genes are not yet studied (Borras-Gelonch et al., 2012). Studies on photoperiod (*Ppd-1*) genes showed adverse effects of photoperiod-insensitive alleles on floret survival (Prieto et al., 2018, Pérez-Gianmarco et al., 2018). In addition, other possible relationships to floret survival in wheat were attributed to anther and ovary size (Guo et al., 2015, Guo et al., 2018). However, the genetic basis of wheat floret death is not entirely unwired. Recently, a mutation in the *HD-ZIP I* gene *GRAIN NUMBER INCREASE 1-A* (*GNI-A1*) was reported to increase grain number by increasing floret fertility in a wheat spikelet (Sakuma et al., 2019). *GNI1* is an ortholog of the barley *VRS1* gene, which functions in lateral floret sterility. *GNI1* is expressed in rachillae and apical florets of wheat spikelets and inhibits their growth, while reduced *GNI1* expression increases floret fertility and, thus, grain number by ensuring lower rate of apical floret degeneration. A less functional *GNI-A1* allele with a single amino acid substitution (N105>Y: asparagine to tyrosine) in the highly conserved homeodomain has been selected in wheat after domestication for enhanced GN per spikelet (Sakuma et al., 2019). Interestingly, the field trials demonstrated the yield advantage of about 10 to 30% in the lines carrying the less functional allele without affecting thousand grain weight (TGW), which usually has a negative association with GN per spike (Würschum et al., 2018, Sakuma and Schnurbusch, 2020, Sakuma et al., 2019). This study demonstrates the significance on improving floret survival/fertility by altering apical degeneration as a strategy to increase grain number in cereals. In addition, a paralog of *GNI1*, *TaHox2* also suggested having a negative function on wheat spike development (Wang et al., 2017). However, the molecular basis of *GNI1* in enhancing floret survival is not known yet, which requires further studies in this direction. Moreover, the reduced function of *GNI1* seems to improve floret survival by reducing the extent of apical degeneration, thereby promoting the growth of labile floret (s); however, the upstream regulators controlling the onset of cell death remain elusive.

Barley spike pre-anthesis tip degeneration

As briefly described in section 1.2, the initiation of spikelet primordia along the rachis of the barley IM halt at the maximum yield potential (MYP) stage. After this, the IM enters into the spike growth and differentiation phase, where the IM dome is kept alive for a few developmental stages. Later, the developmental collapse of the IM dome occurs, followed by the death of all tissues beneath the dome, including spikelet primordia/spikelets and rachis. This tip degeneration (PTD) continues to a certain extent along the spike, and only the surviving spikelets enter towards anthesis and grain-filling phase (Figure 1.8). Barley PTD is common to both row types of barley. The proportion of degenerated apical spikelets is higher in six-rowed barley as they form three spikelets at each rachis node. Similar to the variation for potential spikelet number among genotypes, the proportion of the fertile spikelets reaching anthesis also varies among barley accessions. Previous studies on spikelet survival/fertility in barley suggest that this trait is firmly under genetic control with high repeatability and broad-sense heritability (Alqudah and Schnurbusch, 2014, Kamal et al., 2021). However, the plasticity of spikelet survival for the given genotype is not entirely understood, though few studies report some variation for this trait as it changes between tillers, temperature, environment, and abiotic stress (Kirby and Ellis, 1980, Ellis and Kirby, 1980, COTTRELL et al., 1985, Boussora et al., 2019, Gol et al., 2021). Phenotypic variation for PTD among diverse six-rowed spring barley accessions varied between ~13 to 51%, influencing the final spikelet number, highlighting the importance of understanding the genetic basis of this trait (Kamal et al., 2021).

Barley spike PTD resembles apical floret death in wheat spikelets (Sakuma et al., 2019). Similar to wheat, few morphometric or genetic studies have been conducted to dissect apical spikelet degeneration/survival in barley (Kirby and Ellis, 1980, Ellis and Kirby, 1980, COTTRELL et al., 1985, Miralles et al., 2000, Arisnabarreta and Miralles, 2006, Alqudah and Schnurbusch, 2014, Alqudah et al., 2021, Kamal et al., 2021, Thirulogachandar et al., 2021b, Kamal et al., 2022). Barley PTD also occurs during active stem elongation and when spikes are at their maximum growth rate between MYP and anthesis, like in wheat, ensuing a high competition for photoassimilates/nutrients between both organs (inter-organ competition). However, specifically in barley, the AP stage to tipping (first awns visible from the flag leaf sheath) is suggested to be a more critical subphase for spikelet survival (Alqudah and

Schnurbusch, 2014). In addition, intra-spike (intra-organ) competition for resources might also occur due to the asynchronous development of spikelets at apical, central, and basal positions.

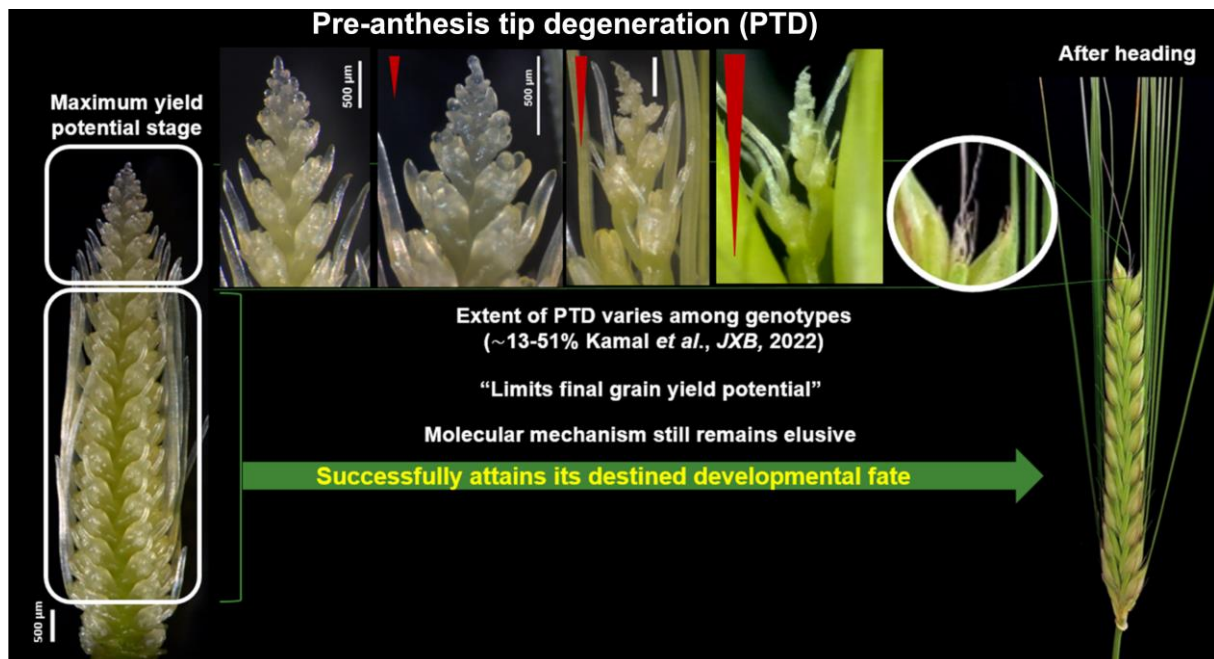


Figure 1.8. Pre-anthesis tip degeneration in the barley inflorescence. IM ceases the spikelet primordia initiation at the maximum yield potential stage. Later, during the spike growth phase, IM remains intact for a certain period, after which death initiates from the tip down to a particular spike position. Only the spikelets in the proximal to the central part of the spike normally develop to form a fertile spikelet and grain. After heading, the apical region is found as dried remnants. The extent of PTD varies among barley genotypes and impacts the final grain yield potential. The red arrow shows the direction of PTD progression.

Usually, the spike growth is more robust towards central and basal positions, where lately formed apical spikelets might be left with limited resources (Arisnabarreta and Miralles, 2006). It was also postulated, based on the wheat vascular development in spikelets (Wolde and Schnurbusch, 2019), that death might result from the inability to establish proper vascular connections between rachis and the apical spikelets to supply the required resources for its development. The rate of floret development during the spike growth phase also influences the survival of spikelets reaching anthesis. Arisnabarreta and Miralles (2006) showed that the floret reaching the stage of W7 by the beginning of PTD in barley had a higher chance of becoming fertile at anthesis. Thus, it was proposed that synchronization of floret development at different positions along the spike during the spike growth phase might help increase the spikelet survival at anthesis, which can be achieved by extending the stem elongation

phase without altering heading time (Miralles and Richards, 2000, Arisnabarreta and Miralles, 2006).

In recent years, several flowering time genes, such as *FLOWERING LOCUS T1/2/4* (*FT1/2/4*), *PHOTOPERIOD1* (*PPD-H1*), and *CENTRORADIALIS* (*CEN*), have been reported to regulate spikelet initiation, fertility, and grain yield in barley (Bi et al., 2019, Digel et al., 2015, Pieper et al., 2020, Shaw et al., 2019). However, these genes affect the vegetative-reproductive phase transition and spikelet initiation, altering floret fertility and grain yield. The involvement of phytohormones was also proposed for barley spike PTD (Youssef and Hansson, 2019). Despite this available knowledge on spikelet survival, the molecular mechanism and factors controlling spike PTD in barley remain unknown. It has consistently been insisted for a long time that there are active death-inducing internal cues that underlie PTD in barley, which requires a molecular and physiological understanding of the positional dynamics during the spike growth phase (COTTRELL et al., 1985, Arisnabarreta and Miralles, 2006).

Furthermore, spike PTD occurs in the early stages of plant development, which requires microscopic analyses to track the exact MYP stage and the onset of spike PTD, making a systemic description and analysis more challenging. Thus, a comprehensive chronological study that describes the morphological and molecular changes during the spike growth phase is necessary to better understand barley PTD. Improving spikelet survival by identifying and manipulating the molecular players behind PTD might help increase grain number per inflorescence in barley and can be translated to other temperate cereals, including wheat, oat, and rye.

In this doctoral thesis, the primary focus is understanding the molecular basis of barley spike PTD. Phenotypically, spike PTD in barley seems to be a genetically controlled cell-death process with unknown death-inducing mechanism(s). Thus, to gain some background on cell death, the following section describes the molecular regulation of well-characterized cell death processes in plants.

1.4 Molecular regulation of senescence and programmed cell death in plants

Cell death is a fundamental process of life that can affect the entire plant, whole organs, tissues, or individual cells, including meristems (Bleecker and Patterson, 1997, Gan, 2003, Van Hautegeem et al., 2015). Historically, molecular regulations of plant cell death were studied at multiple levels, and of all, leaf senescence is the most characterized

that involves an array of intrinsic and extrinsic factors, including hormones, metabolites, RNA, biotic stress, light, photoperiod, *etc.* (Woo et al., 2019) (Figure 1.9). The current section will introduce senescence and programmed cell death in plants, followed by the significant physiological and molecular factors regulating these processes.

1.4.1 Definition of senescence and programmed cell death in plants

The term “senescence” derives from the Latin word “*senescere*” meaning ‘to grow old’ (van Doorn and Woltering, 2004). Senescence is defined as the final phase of development of a cell, tissue, or organism that may or may not be followed by death, primarily dependent on cell viability and molecular status (Thomas et al., 2003, Thomas, 2013). Under optimal growth conditions, leaf senescence is initiated in an age-dependent manner. It involves a highly coordinated sequence of disassembly and degenerative events, whereby nutrients are recycled from older to younger tissues of the plant before the onset of cell death (Lim et al., 2007). Senescence in plants can be classified as mitotic or replicative senescence (occurrence in meristematic tissues involving cell-cycle/proliferative arrest) and post-mitotic senescence at organs (typically in organs like leaf, stem, floral petal, roots) or organismal level (annual crops undergo whole plant senescence for nutrient reallocation and grain filling) (Gan, 2003, Woo et al., 2019). In comparison, the term “programmed cell death” (PCD) refers to a tightly controlled fundamental cellular suicidal process activated during development and stress (Van Hautegeem et al., 2015). In plants, PCD can occur as a part of developmental processes such as self-incompatibility, sex determination, embryogenesis, senescence, or in cell-type-specific elimination during differentiation of tapetum cells, xylem tracheary elements, root cap cells and be categorized under developmental PCD (dPCD). PCD can also result due to biotic stress, such as pathogen invasive that includes hypersensitive responses (HR) or abiotic stresses, which comes under environmental PCD (ePCD) (Daneva et al., 2016).

In general, cell death is the end point of senescence. During senescence, for optimized nutrient recycling, senescing cells are kept viable; cell death is tightly controlled and executed once most nutrients are completely remobilized. However, during the early stages, senescence symptoms can be reversed, and the final death of the individual or an organ can be postponed. For example, Gan and Amasino (1995) showed expression of cytokinin biosynthesis gene under the control of senescence-specific

promoter delayed whole plant senescence and enhanced plant productivity. In addition, nitrogen (N) supplementation also reversed the primary leaf senescence in barley and Arabidopsis when N was resupplied even after the onset of senescence (Schildhauer et al., 2008, Balazadeh et al., 2014). Despite the viability and reversibility of the senescing tissue, there is a rapid and irreversible transitional phase between senescence and PCD during the last stages of senescence (Thomas, 2013). Degreening is one of the earliest senescence symptoms due to chlorophyll catabolism and seems reversible based on the above examples. Whereas DNA laddering, a hallmark of PCD, occurs at very late stages of senescence when most chlorophyll is degraded, pointing towards the presence of boundary between senescence and PCD (Delorme et al., 2000, Schippers et al., 2015, Tamary et al., 2019). Presence of tight sensing mechanism that progressively make cells or tissues competent for senescence followed by PCD (Daneva et al., 2016, Graham et al., 2018). Nevertheless, recent studies on organ senescence and PCD reports on the involvement of overlapping regulatory factors between (PCD vs. senescence) and within (e.g. age vs. stress-induced or leaf vs. root vs. floral organs or dPCD vs. ePCD) these two processes, though some unique regulators have also been identified (Lim et al., 2007, Olvera-Carrillo et al., 2015, Daneva et al., 2016, Wojciechowska et al., 2018) SAM/IM arrest and senescence come under mitotic/proliferative senescence, which has long been studied in Arabidopsis and some eudicots (Hensel et al., 1994, Davies and Gan, 2012). However, only in recent times, understanding the molecular control of SAM arrest and senescence has been gaining attention in the context of stem cell senescence (Merelo et al., 2022, Wang et al., 2022). At the same time, such a phenomenon of proliferative senescence is not yet described in stem cell systems of cereals. Therefore, in the present thesis, barley spike PTD is investigated in the frame work of SAM/IM senescence and/or PCD.

Among all organ senescence and cell death in plants, leaf senescence is the most widely characterized process under multilayered regulations, including phytohormones, metabolites, gene expression, chromatin remodeling, post-transcriptional, and post-translational modifications. At the same time, the emerging regulatory mechanisms include light signaling, circadian rhythm, and aging clock (Woo et al., 2019). Of these, phytohormonal, metabolic, and transcriptional regulations are the most well-characterized factors for their role in senescence (Balazadeh et al., 2008,

Breeze et al., 2011, Watanabe et al., 2013, Schippers et al., 2015). Because of these reasons, in the following sections, most of the examples will be provided based on the findings on leaf senescence in addition to the other growth inhibitory mechanisms in model and crop species.

1.4.2 Morphological and ultrastructural changes associated with senescence and cell death

At the senescence stage, cells show distinct structural changes with the sequential disintegration of intracellular organelles (Woo et al., 2019). In green tissues like the leaf, apparent changes occur in the chloroplast, including size, number, and internal structures, with a decline in photosynthetic activity. The earliest changes in the chloroplast are associated with thylakoid disintegration and an increase in the number and size of lipid droplets called plastoglobuli (Lim et al., 2007, Rottet et al., 2015). However, a recent study reported that chlorophyll degradation precedes the changes in chloroplast structure (Tamary et al., 2019). At the same time, nuclei and mitochondria remain intact until later stages for the expression of genes regulating senescence and continued energy production, respectively, for the effective recycling of cellular contents while chloroplasts are already being degraded (Chrobok et al., 2016). Apart from plastidial degradation, participation of extra plastidial degradative pathways is also found during plant senescence and cell death, mainly involving vacuoles (Gomez et al., 2019). It includes distinct specialized vacuoles such as senescence-associated vacuoles (SAV), chloroplast vesiculation (CV)-containing vesicles, and autophagy-derived vesicles (Otegui, 2017). Autophagy is a lytic process in eukaryotic cells that regulates the recycling of proteins and organelles via lysosomal/vacuolar degradation (ONO et al., 2013). Autophagy plays an essential role during senescence for N remobilization (Guiboileau et al., 2012). Senescent cells harbor large vacuoles implying terminal differentiation or loss of proliferative ability (Thomas et al., 2003, Hara-Nishimura and Hatsugai, 2011). The presence of autophagosome bodies and large vacuoles has been reported for distal floret degeneration in wheat spikelets (Ghiglione et al., 2008). A recent study on plant stem cell senescence reported the presence of large vacuoles in SAM cells that lost their proliferative activity (Wang et al., 2020). During the last stages of a senescing organ, typical symptoms of PCD, such as controlled vacuolar collapse, chromatin condensation, and DNA laddering/fragmentation, are detected in various plant species.

Later, visible disintegration of the plasma and vacuolar membranes leads to disruption of cellular homeostasis and ends the life of senescing cells (Lim et al., 2007).

1.4.3 Phytohormonal control

Distinct effects of all classical phytohormones and their crosstalk on senescence and PCD have been extensively studied in multiple plant species. The phytohormonal pathways show potential effects at all the stages of leaf senescence, including initiation, progression, and termination. In general, ethylene, abscisic acid, salicylic acid, and jasmonic acid promote senescence, whereas cytokinins, auxin, and gibberellic acids retard it. In addition, certain phytohormones exhibit opposing effects on senescence and developmental PCD. Nevertheless, hormonal signaling pathways play a significant role in plants mediating developmental and environmental responses.

Cytokinin

Cytokinins (CK) play vital functions in plant growth and development, including cell division, differentiation, and shoot branching (Wybouw and De Rybel, 2019). In general, cytokinins have long been known as a negative regulator of senescence, based on the findings on its effects on delaying leaf senescence when exogenously applied (Richmond and Lang, 1957) or enhanced endogenously using the senescence-specific promoter (Gan and Amasino, 1995). In addition, CK levels drop during leaf senescence with the downregulation of genes involved in its biosynthesis and the upregulation of its catabolism genes (Buchanan-Wollaston et al., 2005). External application of zeatin and synthetic CK, i.e. 6-benzylaminopurine, during the pre-anthesis phase decreased floret degeneration rates in wheat spikelets, thereby enhancing fertility and grain yield (Wang et al., 2001, Zheng et al., 2016). A recent study in *Arabidopsis* reported a temporal decrease in CK levels, and its signaling leads to proliferative arrest in reproductive SAM (Merelo et al., 2022). On the contrary, CK induces PCD at high levels in the suspension cultures (Vescovi et al., 2012) and dPCD of tracheary element (Milhinhos and Miguel, 2013), both mediated by CK signaling receptors, histidine kinases.

Abscisic acid

ABA is an isoprenoid-derived stress-associated plant hormone that promotes both age-dependent and induced leaf senescence (Zhao et al., 2020). Genes involved in ABA metabolism, such as key enzymes in ABA biosynthesis, 9-cis epoxycarotenoid

dioxygenase (NCED), and core signaling components PYRABACTIN RESISTANCE 1 (PYR1)/PYR1-LIKE (PYL)/REGULATORY COMPONENTS OF ABA RECEPTOR (RCAR), clade A type 2C PROTEIN PHOSPHATASES (PP2Cs), and subclass III SnRK2s, (ABA)-responsive element (ABRE)-binding transcription factors (ABFs) plays a significant role in promoting chlorophyll degradation and senescence (Gao et al., 2016, Mao et al., 2017, Woo et al., 2019). ABA antagonizes the CK-mediated delay of leaf senescence by upregulating the expression of *CKX* (Zhang et al., 2021). Exogenous application of ABA inhibited floret development and decreased floret fertility in wheat (Wang et al., 2001). Recently, an increase in ABA levels in the apical parts of the barley spike at the green anther stage was shown to be associated with spikelet abortion under control and salinity stress (Boussora et al., 2019). ABA metabolism and signaling may play a role in inhibiting lateral spikelet development in barley (Thiel et al., 2021). The role of ABA on barley age-dependent root senescence is also reported (Liu et al., 2019). Positive regulation of ABA signaling on axillary bud dormancy has been reported in *Arabidopsis* and Maize (González-Grandío et al., 2017). On the contrary, ABA works antagonistically in certain cell-type dPCD during seed maturation in cereals (Daneva et al., 2016).

Jasmonates

JA, a lipid-derived phytohormone, regulates diverse plant defense responses and development processes (Huang et al., 2017). The function of methyl jasmonate (Me-JA) and its precursor JA as a positive regulator of leaf senescence and cell death have long been known in various plant species, including barley (Reinbothe et al., 2009). In the senescing leaves, endogenous JA level increases with the increased expression of its biosynthesis genes, including *LIPOXYGENASE (LOX)*, *ALLENE OXIDE SYNTHASE (AOS)*, and *ALLENE OXIDE CYCLASE (AOC)* and while JA/Me-JA supplied externally induces leaf senescence (He et al., 2002). Exogenous application of both JA and Me-JA induces premature leaf senescence with rapid loss of chlorophyll and increased expression of *SENESCENCE-ASSOCIATED GENES (SAGs)* (Park et al., 1998, Kinoshita et al., 1999). JA-mediated leaf senescence requires a functional JA signaling receptor component CORONATINE INSENSITIVE 1 (COI1), as *coi1* mutant fail to induce JA-dependent senescence, indicating that key components of JA signaling pathway also have roles in leaf senescence (He et al., 2002). JA also

promotes carpel PCD and floret sterility in maize (Acosta et al., 2009) and sorghum (Jiao et al., 2018) inflorescences, respectively, as described previously in section 1.3.1

Ethylene

Ethylene, a gaseous phytohormone, is a major positive regulator of leaf senescence and PCD (Daneva et al., 2016). Exogenously supplied or endogenously produced ethylene accelerates senescence, while mutants defective in its biosynthesis, perception, or signaling display delayed leaf senescence and promote leaf longevity (Koyama, 2014). Studies on ethylene constitutive response and overproduction mutants suggest that ethylene does not directly regulate the onset of leaf senescence but instead modulates the timing of leaf senescence (Jing et al., 2002). The effect of ethylene on leaf senescence relies on leaf age, which led to the development of the 'senescence window' concept about the competence of the organ to respond to senescence signals (Schippers et al., 2015, Jing et al., 2002). Ethylene also crosstalk with other phytohormone signaling pathways, including JA (Li et al., 2013), and salicylic acid (SA) (Wang et al., 2021) to coordinate the leaf senescence process. Ethylene negatively regulates floret fertility and ear length in maize (Ning et al., 2021).

Salicylic acid

SA increases with leaf age and function in age-dependent senescence and cell death associated with plant defense responses. SA induces the expression of several SAGs, thereby regulating the onset and leaf senescence rate (Lim et al., 2007). Expression of SAGs altered with delayed senescence in the SA-signaling mutants, such as *phytoalexin deficient4 (pad4)* and *nonexpressor of pathogenesis-related genes1 (npr1)* (Morris et al., 2000). In Arabidopsis, SA and ethylene can synergistically promote leaf senescence (Wang et al., 2021).

Auxin and Gibberellins

Auxin is a major phytohormone regulating plant development, including cell division and expansion, shoot growth, vascular patterning, root expansion, apical dominance, and cell differentiation. Auxin function as a negative regulator of leaf senescence, as elevated levels of IAA (Indole acetic acid) by overexpression of *YUCCA6*, which encodes flavin-containing monooxygenases, delayed leaf senescence and enhanced longevity by decreasing the expression of SAG genes and activating genes involved in redox signaling and auxin redistribution (Kim et al., 2011, Cha et al., 2016). Auxin

application represses the expression of *SAG12* in senescing leaves (Noh and Amasino, 1999), implying its antagonistic activity. AUXIN RESPONSE FACTOR (ARF2), a repressor of auxin responses, increases during senescence, while the loss-of-function mutants result in higher chlorophyll content with delayed flowering and later onset of leaf senescence (Ellis et al., 2005). Whereas auxin positively regulates certain dPCD (Van Hautegeem et al., 2015). Recently, auxin has been identified as an arrest signal exported from proximal fruits to regulate proliferative arrest of the inflorescence apex in *Arabidopsis* (Ware et al., 2020).

Gibberellins (GAs), tetracyclic diterpenoid phytohormones, regulate many aspects of plant growth and development, including stem elongation, leaf expansion, seed dormancy and germination, and flowering (Binenbaum et al., 2018). Bioactive GAs, such as GA₃, GA₄ and GA₇ are generally considered as a repressor of senescence as endogenous GAs decline as leaves age, while the exogenous application of GA₃ retards the degradation of chlorophyll (Aharoni and Richmond, 1978, Li et al., 2010). Whereas the GA catabolism gene *GA2-OXIDASE2* upregulates in senescing leaves, suggesting that the decrease in active GA may cause leaf senescence (van der Graaff et al., 2006). GA₃ application increased the number of fertile florets in wheat spikelets (Wang et al., 2001). GA and ABA seem to function antagonistically in leaf senescence. On the other hand, GA can promote specific dPCD acting antagonistic to ABA (Daneva et al., 2016).

1.4.4 Metabolic regulation

Primary and secondary metabolites in plant tissues are crucial in maintaining plant growth, development, reproduction, stress responses, and cell death. During senescence, a dramatic metabolic transition from anabolism to catabolism occurs, accompanied by increased hydrolysis of macromolecules (Woo et al., 2019). The first visible sign of senescence in photosynthetic organisms is leaf yellowing due to chlorophyll degradation and chloroplast disassembly with a concomitant reduction in photosynthetic activity. It also involves progressive loss of proteins and lipids mediated by senescence-associated proteases and lipid-degrading enzymes. In contrast, nuclei and mitochondria are kept intact until later stages for the expression genes regulating senescence and alternate energy production, respectively, to effectively recycle cellular contents (Chrobok et al., 2016). A comprehensive overview of metabolic

rearrangements in senescing Arabidopsis (Watanabe et al., 2013) and barley (Avila-Ospina et al., 2017) leaves revealed significant alterations in amino acid levels, Tricarboxylic acid (TCA) intermediates and sugars.

Sugars are the primary cellular energy metabolites and signaling molecules in numerous physiological and developmental responses. In general, energy limitation or stress inhibits growth and development as an adaptive strategy (Lastdrager et al., 2014). The plant growth and development are mediated by Snf1-related kinase 1 (SnRK1) and the plant target of rapamycin (TOR) kinase, which functions as central regulators linking carbon and energy status. TOR promotes plant growth by sensing high sugar levels (Dobrenel et al., 2016). SnRKs promote catabolism under nutrient and carbon starvation conditions by coordinating transcriptional activation of bZIP (BASIC LEUCINE ZIPPER PROTEIN) transcription factors (Jamsheer et al., 2019). Though the role of sugars in the onset and progression of senescence has been under debate for decades, several studies reported starvation-induced senescence in multiple plant species (Kim, 2019). The death of distal florets in wheat spikelets has been reported to be associated with reduced water-soluble carbohydrate levels, including glucose and fructose, based on whole-spike measurements (Ghiglione et al., 2008, Dreccer et al., 2014). However, this study fails to measure sucrose and lacks information about the localized sugar status in the apically aborting florets. On the other hand, feeding a sucrose solution to the wheat flag leaves during the floret degeneration stage increased the number of fertile florets at anthesis (Ghiglione et al., 2008). Even though the mechanism is unclear, it suggests a possible role for sucrose in floret survival.

Reactive oxygen species (ROS) are metabolic products that serve as a signal to regulate growth, development, death, and survival in plants. A number of studies have revealed that developmentally regulated senescence and PCD are also associated with increased availability of ROS (Mhamdi and Van Breusegem, 2018). ROS crosstalk with phytohormones on regulating senescence and PCD have been reported previously. ROS homeostasis affects both SAM and RAM activities (Schippers et al., 2016). The molecular mechanism underlying the antagonistic actions of superoxide anion free radical and hydrogen peroxide (H_2O_2) shows dynamic changes in the SAM during the life cycle of Arabidopsis (Zeng et al., 2017). This study showed that superoxide is associated with transcriptional upregulation of *WUS*, whereas H_2O_2

inhibits *WUS* and promotes stem cell differentiation by accumulating at high levels in the peripheral zone. Recent studies in *Arabidopsis* also found that during the growth of SAM, the levels of superoxide anion free radical gradually declines, whereas H_2O_2 accumulates at the senescent stage suggesting its role as a signaling molecule in SAM arrest and death (Wang et al., 2020, Wang et al., 2022).

1.4.5 Transcriptional networks

Transcription factors (TFs) are proteins that bind to specific DNA sequences and regulate the transcription of genes by either activating or repressing them (Liu et al., 1999). TFs play a crucial role in the extensive reprogramming of gene expression of a few to thousands of genes involved in various metabolic and physiological processes that lead to senescence and PCD. Considering the significance of transcriptional control on events leading to senescence and cell death, with the advent of next-generation sequencing (NGS) techniques, extensive transcriptomic studies have been conducted to obtain a global picture of the complex regulatory networks behind senescence in model and crop species (Lee and Masclaux-Daubresse, 2021, Kim et al., 2018b, Breeze et al., 2011, Borrill et al., 2019). Gene regulatory networks (GRNs) involving NAC (NAM [no apical meristem], ATAF1/2, CUC [cup-shaped cotyledon]) and WRKY TF families have been studied extensively and implicated for their regulation of senescence and cell death in various plants (Woo et al., 2019). NAC TFs have been shown to regulate several aspects, including leaf yellowing, chlorophyll catabolism, and PCD. Members of NAC TFs function as both positive and negative regulators of senescence (Kim et al., 2018b). For example, ORESARA1 (ORE1) and NAP (NAC-LIKE, ACTIVATED BY AP3/PI) functions as positive regulator of leaf senescence both in *Arabidopsis* and rice (Bengoa Luoni et al., 2019). Crosstalk between phytohormones and TFs has been established to mediate senescence and cell death. The trifurcate pathway, downstream of ethylene involving *ETHYLENE INSENSITIVE2*, *miR164*, and *ORE1*, links leaf senescence, and age-induced cell death (Kim et al., 2009). EIN3, a key TF downstream of EIN2, induces ORE1 by directly repressing *miR164* transcription. NAP promotes ABA biosynthesis during the onset of senescence by positively regulating the ABA biosynthesis gene. The function of NAP in ABA-mediated senescence is conserved in *Arabidopsis* and rice (Liang et al., 2014, Yang et al., 2014). NAC TF also terminates floral receptivity, promoting senescence and cell death in *Arabidopsis* (Gao et al., 2018) and maize (Šimášková et al., 2022).

In addition, other TF families, including bZIP, MYB, AP2/ERF (APETALA2/ETHYLENE RESPONSIVE ELEMENT BINDING FACTOR), TCP (TEOSINTE BRANCHED/CYCLOIDEA/PCF), HD-ZIP, and ARF were also implicated to function in senescence and PCD (Koyama, 2014, Schippers, 2015, Woo et al., 2019). A diverse class of TF families in barley mediates lateral spikelet sterility (Koppolu and Schnurbusch, 2019). In wheat, the HD-ZIP TF gene, *GNI1*, suppresses the development of distal florets (Sakuma et al., 2019). JA biosynthesis mediated by TCP TF leads to pedicellate spikelet sterility in sorghum (Jiao et al., 2018).

Over the past, the significance of TF-mediated regulation as a critical regulatory mechanism underlying complex traits has clearly been illuminated. Overall, in many cases, the unraveling transcriptional networks helped to identify possible regulators committing tissues to undergo senescence/cell death while targeting the master regulators to reverse or delay the process (Figure 1.9). The following sections briefly overview the approach and techniques utilized in the present study to understand the complex process of spike PTD in barley.

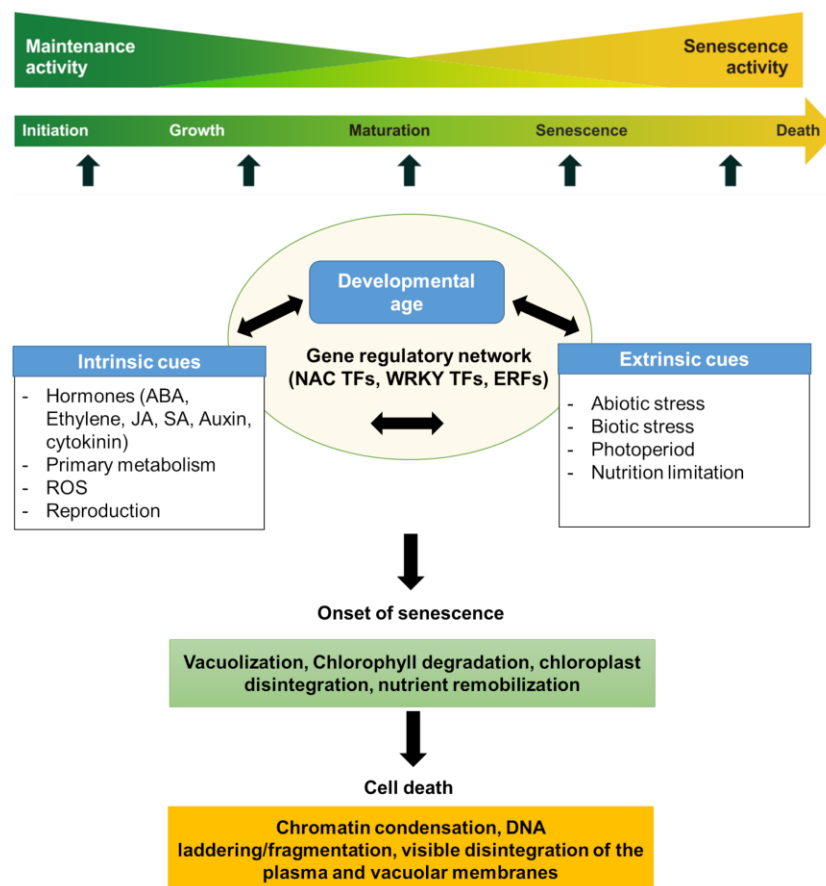


Figure 1.9. Overview of the molecular basis of organ growth and senescence. Modified after Woo et al., 2013.

1.5 Utilization of multi-omics for unwiring complex traits in crops

Extensive studies on complex plant traits impose the significance of utilizing multi-omics (genomics, epigenomics, transcriptomics, proteomics, metabolomics, phenomics) to obtain the complete picture of the trait. Multi-omics data enable a higher precision understanding of complex traits (Pazhamala et al., 2021). Transcriptomics is the study that refers to the collection of genome-wide RNA transcripts (both mRNAs and non-coding RNAs) produced in a cell or tissue. Initial gene expression studies used low-throughput methods. For example, initial attempts to identify differentially expressed genes using a DNA microarray technique for genome-wide profiling behind daylength-dependent changes in wheat floret fertility have led to identifying a distinct chronology of metabolic processes and signaling pathways regulating floret abortion (Ghiglione et al., 2008). The advancement in NGS technologies helped address the fundamental mechanisms behind complex traits such as leaf senescence in multiple plant species employing RNA sequencing (Borrill et al., 2019, Woo et al., 2019). Further, developing a gene expression atlas serve as a versatile resource for associating transcriptome to the specific developmental process and understanding the regulatory mechanism by tracking the expression profiles of the individual or set of genes (Ramirez-Gonzalez et al., 2018, Thiel et al., 2021, Xu et al., 2021).

On the other hand, in systems biology, network-based approaches have been helpful in mining gene function from high-throughput transcriptome data. Gene co-expression analysis has become a powerful tool for building transcriptional networks of genes involved in common biological events in plants. The use of co-expression networks has revealed candidate genes on regulating biological processes in many cereal crops, including barley (Thiel et al., 2021), wheat (Alabdullah et al., 2019), rice (Tan et al., 2017) and maize (Leiboff et al., 2021).

The large-scale or high throughput phenotyping of desired traits in the diverse natural population combined with population-wide genotyping data can be used to perform genome-wide association studies (GWAS) to dissect complex traits and identify QTLs/candidate genes by marker-trait associations using millions of single nucleotide polymorphisms (SNPs) markers (Singh et al., 2021). Further, gene-based associated studies may help identify the superior haplotypes/allelic variation for the candidate genes of interest derived from other methods, such as transcriptomic studies (Abbai et al., 2019). The present study also aimed at tracking transcriptome level changes in the

developing IM in barley during the spike growth phase by tissue-specific RNA sequencing in the degenerating and viable regions to unveil the GRNs behind spike PTD and spikelet development.

In metabolomics, mass spectrometry (MS) has been an invaluable tool as these methods are employed to characterize metabolites extracted from homogenized tissue and cell lysates (Taylor et al., 2021). MS is an analytical technique for measuring the mass of molecules in an ionized state on a mass spectrometer, which consists of three principal parts: an ion source, a mass analyzer, and a detector. In the source, the sample is evaporated to the gas phase, ionized, and introduced to the mass analyzer. In the analyzer, the ions are separated depending on their mass-to-charge ratios (m/z - dividing the mass of an ion by its charge number), typically under a high vacuum. The separated ions were then detected, and the data were collected using specific software tools connected to the MS system. The output, a mass spectrum, plots the intensities of the detected ions on the y-axis against their m/z values on the x-axis (Svatoš and Mock, 2013). Gas chromatography (GC) and liquid chromatography (LC) -MS has been the most extensively used analytical technology for metabolomics because of their high resolution, high sensitivity, broad application range, and excellent specificity (Zeki et al., 2020). Several studies have reported the combinations of transcriptomic and metabolomics to derive fruitful insights into the underlying mechanism and help identify candidates relating gene expression changes and metabolite modifications during leaf senescence (Woo et al., 2019). Thus, in addition to the invasive transcriptome analysis, the present study also aimed at profiling targeted metabolites, including sugars, amino acids, glycolysis, and TCA intermediates, to uncover the metabolic status of the developing IM during the spike growth phase and its relation to the spikelet development and PTD process.

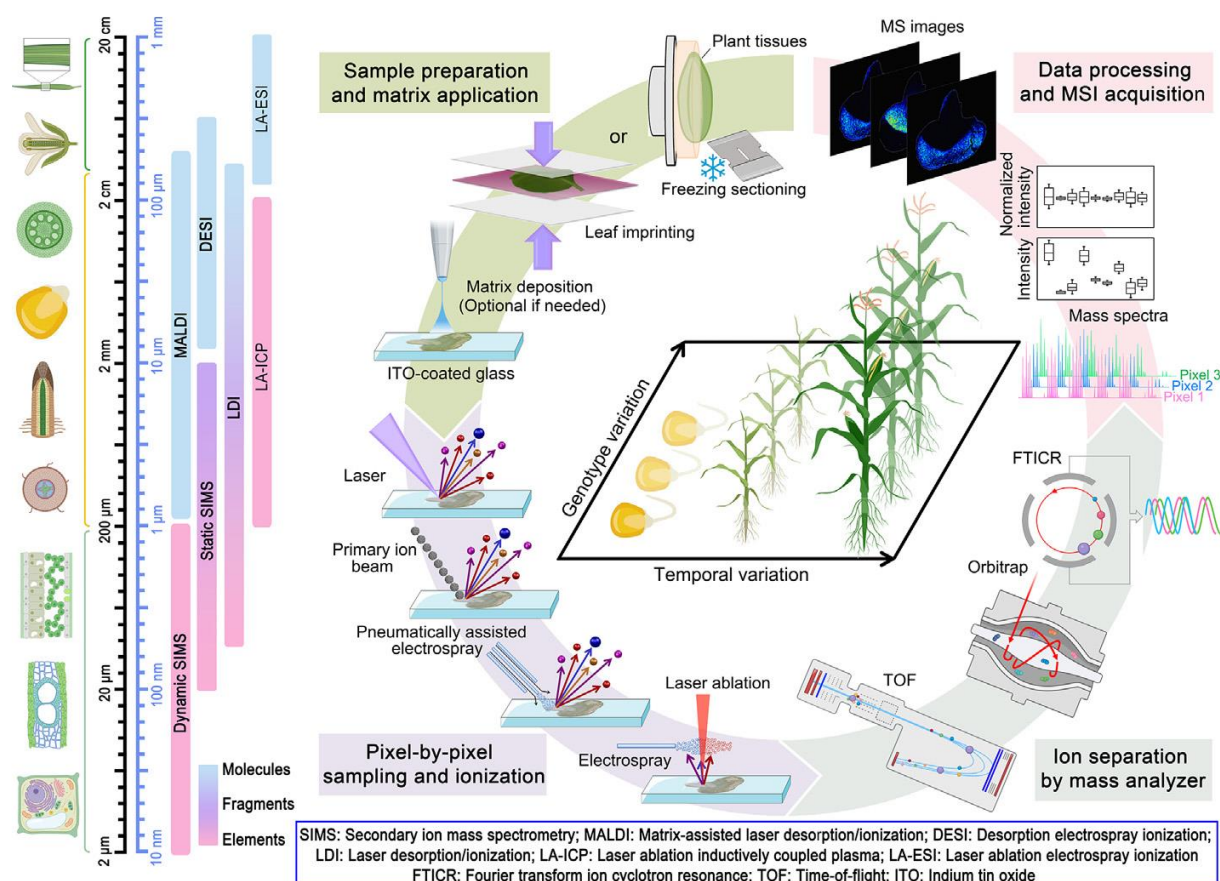
On the other hand, innovations in MS and spectroscopy have resulted in tremendous discoveries and technological advancements within this omic field over the last two decades (Taylor et al., 2021). However, in MS-based holistic studies, the spatial information is not retained as the analysis was performed on a tissue homogenate. Spatially resolved metabolite analysis enables us to understand the metabolic status of the tissue or individual cells. Earlier, tools used for transcriptomic studies, such as FACS (fluorescence-activated cell sorting), LCM (laser-capture microdissection), and organelle fractionation, were coupled with MS to retain the spatial information.

However, the sample preparation with these methods is time-consuming and poses the risk of molecules undergoing modification or degradation (Dong et al., 2016a). Genetically encoded FRET (fluorescence resonance energy transfer)-based sensor systems were also developed in plants for live cell imaging to monitor the real-time dynamics of target metabolites or hormones (Shaw and Honeychurch, 2022). However, this method requires stable transgenic plants encoded with a specific biosensor system that poses a major bottleneck. Whereas technical advancement in the MS and spectroscopy field led to the development of spatially resolved metabolomics methods, one can visualize metabolite distribution in the biological tissue sections or cells without losing spatial information. Metabolite imaging techniques offer excellent potential for understanding complex biological processes and have been advancing rapidly in recent years and gained much attention in plant research (Borisjuk et al., 2023). Even though there are several spectroscopy-based techniques, including NMR (Nuclear Magnetic Resonance) (Radchuk et al., 2021), FTIR (Fourier-Transform Infrared) spectroscopy (Guendel et al., 2018) are used for metabolite imaging, MS-based imaging methods are quite popular offering excellent sensitivity and broad molecular coverage (Emwas, 2015, Feenstra et al., 2017, Qin et al., 2018, Guendel et al., 2021).

1.6 Spatial metabolomics by mass spectrometry imaging

Spatial metabolomics is a rapidly developing field that combines metabolomics with spatially resolved analysis to visualize and identify metabolites *in situ* (Alexandrov, 2020). As several metabolites serve as signaling molecules, complete knowledge of spatial distribution is required to understand their role(s) in regulating specific biological processes in individual plant tissues or cells. Mass spectrometry imaging (MSI) is an MS-based molecular imaging technology for determining the spatial distribution of targeted or untargeted metabolites in specific tissues. The resolution, sensitivity, and accuracy make it a potent tool for determining where target metabolites accumulate. Based on the ion sources used, there are three primary MSI techniques, including secondary ion MS (SIMS), desorption electrospray ionization MSI (DESI-MSI), and matrix-assisted laser desorption/ionization MSI (MALDI-MSI). While other MSI techniques, including Laser desorption/ionization MSI (LDI-MSI), Laser ablation inductively coupled plasma (LA-ICP), laser ablation electrospray ionization (LA-ESI), NanoDESI and Atmospheric pressure MALDI (AP-MALDI) are the derivatives or

variations of the above-mentioned primary ionization techniques (Dong et al., 2016a, Yu et al., 2022). There are also different choices of mass analyzers for ion separation, such as TOF (Time-of-flight), FTICR (Fourier transform ion cyclotron resonance), and Orbitrap (Yin et al., 2023). Each method has its advantage and limitations, which were chosen mainly based on the nature of the sample, analytes of interest, spatial resolution, and the scope of application (Dong et al., 2016a) (Figure 1.10). MALDI-MSI is the most widely used method in spatial metabolomics.



studies were routinely conducted between 5 to 20 μm spatial resolution (Yu et al., 2022). In MALDI-MSI, the sample requires the deposition of an organic matrix to promote desorption and ionization. The basic workflow of MALDI-MSI of tissues involves preparing thin cryosections, tissue-embedding, matrix deposition over tissue-sections, vacuum drying, ionization, and vaporizing in the ion source. Ions are sorted according to their m/z ratio in the mass analyzer, followed by data preprocessing, image construction, and statistical analysis (Dong et al., 2016a). Data generates a mass spectrum specific to the region of the sample irradiated by the laser beam and can be displayed as an average spectrum. Images of selected individual ion m/z values can also be extracted, displaying their spatial distribution based on m/z signal intensities (single ion intensity maps). Multi-ion intensity maps can also be derived from distribution patterns of targets with different m/z values (Kaspar et al., 2011). In the past decade, several studies in plant research have utilized MALDI MSI to understand the distribution of metabolites as well as their biological relevance (Yu et al., 2022). Such studies covered diverse classes of compounds, including amino acids, sugars, TCA intermediates, hormones, flavonoids, lipids, peptides, and other specialized metabolites. Importantly, MALDI-MSI was also used in a variety of plant tissues, including seeds, roots, stems, leaves, *etc.* (Bjarnholt et al., 2014, Bhandari et al., 2015). The spatiotemporal distribution of sugars was studied during barley grain development (Peukert et al., 2014). The distribution of primary and specialized metabolized in the developing seedling was also studied in sorghum (Montini et al., 2020). Chemical derivatization procedures were used to increase the ionization efficiency and sensitivity of detection for profiling a variety of metabolites including amino acids and hormones (Enomoto et al., 2018, O'Neill and Lee, 2020) .

Sample preparation is the most crucial step for successful MSI analysis. It should be optimized according to the type of the sample and analytes of interest to maintain the actual localization without any modifications or degradations (Dong et al., 2016b). Moreover, sampling plant tissues is more challenging due to cuticle and cell walls, and plant tissues become more fragile upon freezing. Further, water-rich plant samples significantly challenge getting thin and intact sections. Thus, a proper sample preparation pipeline, including a uniform and reproducible matrix deposition, is a significant prerequisite for a successful MALDI-MSI experiment. Matrices can be deposited by 'wet' (e.g., spraying) or 'dry' (e.g., sublimation) coating methods for obtaining a homogeneous layer of matrix crystals over the sample surface. Sublimation

is one of the preferred methods for matrix deposition for high-resolution MALDI-MSI as it produces small (<1 μm) and homogeneous crystals over the tissues (Dong et al., 2016a).

As mentioned previously, in the present study, the processes leading to spike PTD are of the highest interest while tracking the developing IM of barley. A comprehensive MALDI MSI study on barley spike development may lead to new insights on spatiotemporal metabolite allocations or discovery of novel metabolic pathways concerning spikelet initiation, meristem maintenance, and PTD. Tissue-specific proceedings in the IM where the cell death is confined to the apical part initiating from the few cells in the IM dome suggest possibilities of defined spatial patterns for the metabolites underlying this process. Moreover, it may facilitate spatial metabolic reprogramming during spike development and assign specific metabolic markers/pathways confined to the specific cell-types of the complex spike tissues, including vascular cells, meristem dome, spikelet meristem, and rachis. However, considering the challenges of the sample preparation, in the present study, special attention have been paid to adapting the MALDI-MSI method for developing inflorescence meristems in barley (Shanmugaraj et al., 2023a and 2023b).

1.7 Uncovering gene functions by targeted mutagenesis

Previously, gene functional characterization studies exploited the available natural variations in the germplasm collections or mutants induced by chemical or ionization radiations. The most established reverse genetics tools include T-DNA or transposon tagging that randomly disrupts the gene function, and TILLING (Targeted Induced Local Lesions in Genomes), developed using chemical mutagens, which introduces random point mutations across the genome (Barkley and Wang, 2008). Though TILLING is a non-transgenic and high-throughput approach, it possesses a risk of a large number of background mutations. VIGS (Virus-induced gene silencing) and RNAi (RNA interference) have been used for the transient knockdown of target genes to elucidate the underlying function(s). VIGS is relatively rapid and inexpensive, but the resultant phenotype is not heritable and is limited by the narrow host range of the virus used for silencing, whereas concerns prevail over stability and off-target effects in the case of RNAi (Senthil-Kumar and Mysore, 2011, Singh et al., 2021).

The advancement in biotechnology and plant science led to the development of new breeding tools based upon customizable endonucleases to modify DNA sequences at a defined site of interest in the host genome (Koeppel et al., 2019). Targeted genome editing is a powerful tool to accelerate gene function analysis and facilitates crop improvement by creating favorable alleles. In particular, RNA-guided, clustered, regularly interspaced short palindromic repeats (CRISPR)-associated (Cas) endonucleases allow the generation of mutations in almost any gene of interest (Liu et al., 2021b). CRISPR/Cas9 uses the Cas9 enzyme to generate double-stranded breaks in a specific DNA sequence guided by sgRNA (single guide RNA) molecules that recognize a genomic region of interest. Double-strand breaks (DSBs) are introduced at the specific target sites in the plant genome, allowing targeted modifications to be induced when the breaks are repaired by non-homologous end joining (NHEJ) or homology-dependent repair (HDR) (Zhu et al., 2017). NHEJ is error-prone and generates small insertions and deletions in regions of interest or larger deletions/insertions that occur at low frequency (Liu et al., 2021b). Site-directed mutagenesis using CRISPR/Cas endonuclease technology is now well established and routinely used to knock-out genes in temperate crops, including barley and wheat, that was successful employed to alter various plant traits, including inflorescence architecture (Fan et al., 2023, Koeppel et al., 2019, Li et al., 2021).

1.8 Aims of this study

Improving spikelet/floret survival is one of the strategies to increase grain number in the major cereal crops, including wheat and barley. Spike (PTD) in barley reduces spikelet survival/fertility and ultimately influences final grain number, a key determinant of grain yield. Even though few morphometric or genetic studies have been conducted to dissect barley spikelet fertility/survival and grain number determination, the exact molecular mechanism and factors controlling spike PTD in barley remain elusive. Age-induced tissue degeneration can affect the entire plant, organs, and tissues, including meristems. Phytohormonal, nutritional, and transcriptional regulations are the most well-characterized factors in cell death/senescence-related processes. Metabolic and energy homeostasis strongly influence plant cell growth, viability, and death. The present study postulates that primary metabolism in the dying apical part is altered based on previous findings on apical floret fertility in wheat.

On the other hand, previous findings showed differential accumulation patterns of auxin, cytokinins, and gibberellins along barley spikes. Moreover, phytohormonal function on floral sterility is known in several cereal species and reviewed in sections 1.3.1 and 1.4.3. Thus, it was hypothesized that phytohormone patterning along the barley inflorescence might act as an endogenous signal that regulates spikelet/rachis development and death. In addition, identifying the GRNs behind spike PTD is of great significance to manipulating this trait and requires a high-resolution spatiotemporal transcriptome atlas during the spike growth phase.

Spatially resolved metabolomics will provide deeper insights into the distributions and regulatory mechanisms underlying growth, development, and response to stress(es) from complex biological samples. Mass spectrometry imaging (MSI) offers a significant advantage in visualizing various metabolites' spatial distribution in plant tissues and cells. Thus, applying such a technique to study early spike development provides novel insights into the metabolic signals governing events, including spikelet initiation, meristem maintenance, spikelet/rachis development, and spike PTD. More importantly, this eliminates extensive sampling for invasive measurements as it leads to the loss of spatial information.

Hence, the present study aimed to get a comprehensive chronological view of morphological, biochemical, and transcriptional changes in the developing barley spikes during the spike growth phase for a better understanding of spike PTD at high spatiotemporal resolution with the following objectives,

1. Morphological, physiological, and molecular characterization of PTD in barley inflorescence.
 - Detailed phenotyping of early developing barley inflorescence to track maximum yield potential (MYP) stage, onset, and progression of PTD in two- and six-rowed barley cultivars.
 - Spatiotemporal profiling of the transcriptome, plant hormones, and primary metabolites before and during the onset of PTD over a two-weeks period.
 - Functional validation of one of the candidate genes for spike PTD, barley *GRASSY TILLERS1*, using knockout mutant plants generated by RNA-guided Cas9 endonucleases.
2. Spatial metabolomics in the barley inflorescence meristems by MALDI-TOF MSI technique.

- Optimization of sample preparation for high spatial resolution MALDI-TOF MSI in barley IM.
- Exploring the metabolites distribution using the tissue-sections of developing IM

2. Materials and Methods

2.1 Plant materials and growth conditions

Two-rowed barley cultivar (cv.) Bowman (hereafter Bowman), *tip sterile 2.b (tst2.b)* mutant (BW833) in Bowman background (Backcrossed - BC₆F₅ - hereafter BW.*tst2.b*) and six-rowed barley cv. Morex (hereafter Morex) were grown in 9-cm (diameter) square pots (one plant per pot) in a climate chamber (IPK, Gatersleben) at 12°C/8°C and 12-h/12-h light-dark photoperiod with a light intensity of 300 μE at 80% humidity as described previously (Thiel et al., 2021). Two-rowed cultivar Golden Promise (GP) was used as the recipient for genetic transformation. GP.*Hvgt1* (CRISPR)-Cas9 knockout lines in T₂ generation were grown for spike and plant phenotyping in a glasshouse containing natural loamy soil under sunlight and porous metal netting on the sides to enable air circulation (the growth period was between April 2022 and August 2022). Lines were sown in jiffy pots in a controlled environment and ten days later transplanted in soil with approx—10 cm distance between plants within a one-meter row. For the greenhouse experiment, plants were grown in 9cm square pots under long-day conditions of the 16-h/8-h light-dark regime at 17°C/14°C.

2.2 Methods

2.2.1 Phenotyping

For all the spike phenotyping and molecular/biochemical analyses, the immature spike meristems were sampled only from the main culm of the plants between 6 and 10 h after initiating the light phase. Three independent experiments were conducted in a climate chamber to track the early spike development in two-rowed Bowman and six-rowed Morex. In all three experiments, at least five main-culm spike meristems were collected at each stage to identify the MYP stage (Thirulogachandar and Schnurbusch, 2021), the maximum number of rachis nodes (potential spikelet number), the onset of PTD, the progression of PTD, and the final spikelet number at anthesis. The spikelet survival rate was calculated using the formula below,

$$\text{Spikelet survival rate} = \frac{\text{Final spikelet number at anthesis}}{\text{Potential spikelet number at MYP stage}} \times 100$$

Optical images of the spike meristems were captured using a Zeiss stereomicroscope fitted with a digital camera (Carl Zeiss, Germany).

Early spike development patterns, including the MYP stage, the maximum number of rachis nodes, the onset of PTD, the progression of PTD, and the final spikelet number at anthesis were investigated in T₂ *Hvgt1* knockout and WT (azygous) lines. Data for the number of grains from the harvested spikes were collected using a MARVIN seed analyzer.

2.2.2 Scanning electron microscopy (SEM) and Transmission electron microscopy (TEM)

Scanning electron microscopy (SEM) and transmission electron microscopy (TEM) observations were done as described previously (Daghma et al., 2011, Poursarebani et al., 2020). For SEM, Bowman spikes were fixed in 50 mM cacodylate buffer (pH 7.2) containing 2% glutaraldehyde and 2% formaldehyde at 4°C. Samples were washed and dehydrated in an ascending ethanol series and critical-point-dried in a Bal-Tec critical point dryer (<https://www.leica-microsystems.com>). Dried spike specimens were gold-coated in an Edwards S150B sputter coater (<http://www.edwardsvacuum.com>) and examined in a Zeiss Gemini30 scanning electron microscope (<https://www.zeiss.de>) at 10 kV acceleration voltage. For TEM, Bowman spike samples were embedded in Spurr's resin. After ultrathin (70 nm) sectioning and staining, samples were analyzed in a Tecnai Sphere G2 transmission electron microscopy (FEI, Netherlands) at 120 kV.

2.2.3 Live/cell death assay by FDA/PI staining

For the live-death assay, spike meristems were incubated in 2 ml Eppendorf tubes containing water supplemented with 10 µg/ml FDA (stock 2.5 mg/mL in acetone) and 2 µg/ml PI (stock 1 mg/ml in distilled water) and incubated in the dark for 5 min on a lab shaker at 100 rpm. Stained meristems were mounted onto the chambered coverglass (Thermo Scientific, USA). FDA and PI were imaged simultaneously on a LSM780 laser scanning microscope (Carl Zeiss, Germany) as previously described using a 488-nm laser line to excite FDA and a 561-nm laser line to excite PI (Feng et al., 2022). Emission was detected with a 500-540 nm bandpass for FDA and a 580 640 nm bandpass for PI.

2.2.4 Phytohormone measurements in immature spike meristems

For phytohormone measurements of Bowman grown in a climate chamber, apical, central, and basal spike parts were collected in stages W5.0, W6.5, W7.5, and W8.0, with the apical part covering all the dying rachis nodes/ridges, central and basal, with 11 rachis nodes each leaving three under-developed spikelets at the base (Figure 2.1A). Additionally, greenhouse-grown Bowman plants were subjected to phytohormones measurements by collecting spikes parts at stages W5.0, W6.5, and W7.0. In the case of Morex, spikes parts at stages W5.5, W6.5, W8.25, and W8.5 were collected, with the apical part covering all dying spikelet nodes/ridges and central and basal parts with 11 rachis nodes, each leaving two under-developed spikelets at the base from the plants grown in climate-chamber (Figure 2.1B). Four biological replicates per sample were used. For each biological replication, 15 (W5.0, W5.5), 10 (W6.5), and 5 (W7.5, W8.0, W8.25, W8.5) spike meristems were dissected and collected as apical, central and basal parts in separate vials, frozen in liquid nitrogen and stored at -80°C . Two stainless steel beads were added to each sample tube, placed in pre-cooled (-80°C) Tissuelyser II (QIAGEN, USA) racks, and homogenized at 30 Hz for 1.5 min. Fresh weights were measured using a precision balance. Samples of 3.5 – 30 mg (fresh weight) were weighed into 2 mL safe lock tubes (Eppendorf AG, Germany) and kept at -80°C until use. Before extraction, two 3 mm ceria-stabilized zirconium oxide beads were placed into each tube. The samples were extracted and purified as described previously with minor modifications (Simura et al., 2018). For UHPLC-ESI-MS-MS analysis, samples were dissolved in 50 μL of 30% ACN (v/v) and transferred to insert-equipped vials. The absolute quantification of targeted phytohormones was performed as described (Eggert and von Wiren, 2017). Ten microlitres of purified extracts were injected into an Acquity Ultra-performance LC system coupled with a Xevo TQ mass spectrometer (Waters, USA). All targeted phytohormones but gibberellins were separated on an Acquity UPLC® BEH C18 1.7 μm , 2.1 \times 100 mm column coupled to a VanGuard pre-column BEH C18 1.7 μm , 2.1 \times 5 mm. A ten points external calibration curve was used for quantification. MassLynx software (version 4.1; Waters) was used to control the instrument and data acquisition. MS data were processed with TargetLynx V4.1 SCN 904. Gibberellins baseline separation was achieved on a reversed-phase Acquity The UHPLC system was coupled to Q Exactive Plus Mass Spectrometer (San Jose, CA, USA) equipped with a HESI source operating

in negative ion mode. MS data were acquired and processed by Trace Finder Software (v. 4.1, Thermo Scientific, San Jose, CA, USA). The peak area on the extracted ion chromatogram (XIC) of the deprotonated molecule ion $[M-H]$ was measured to generate the calibration curve. A least-square linear regression was used to fit the linearity curve best. The identification of compounds found in extracts was based on comparing their retention time, high-resolution m/z spectrum, and isotope pattern with standards. Additionally, generated MS2 spectra were searched in a custom spectral library to confirm compound identification. For the greenhouse experiment, Bowman spikes were collected at stages W5.0, W7.0, and W8.0 and performed the hormone profiling similarly as described above.

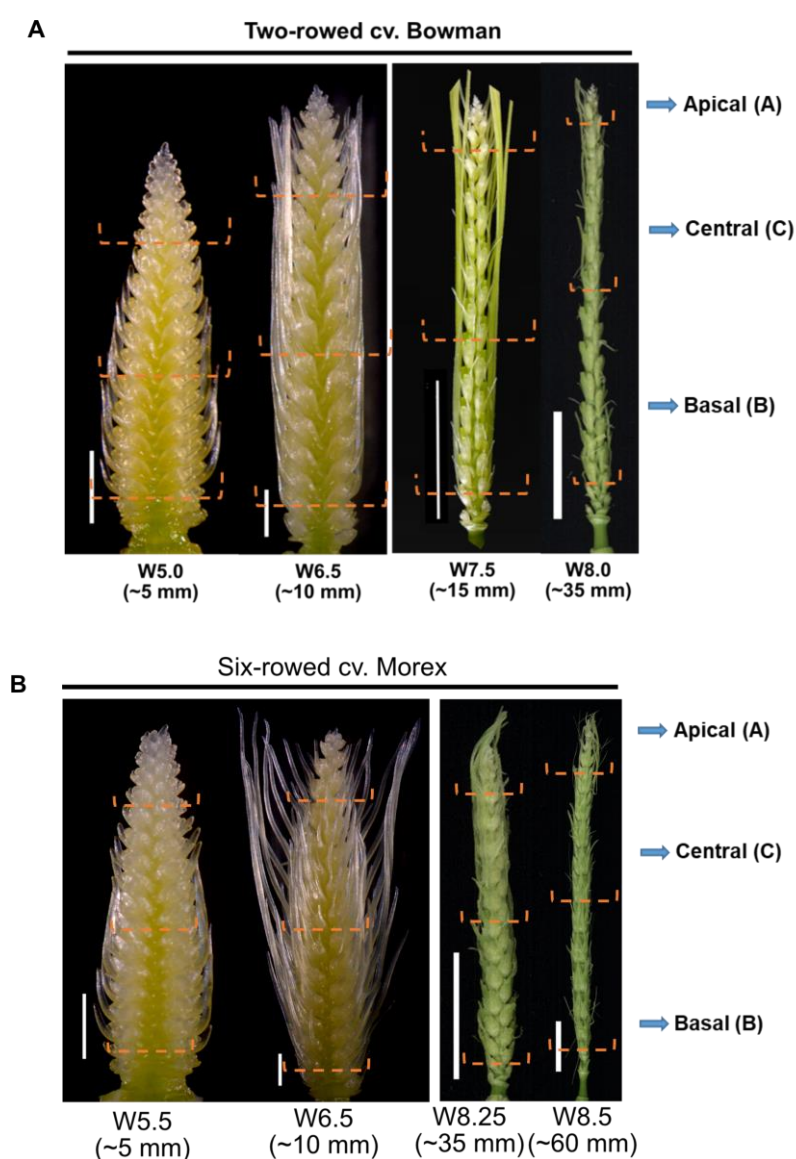


Figure 2.1. Spike sampling for hormones and primary metabolite profiling. (A-B) Four spike developmental stages in the two-rowed cv. Bowman **(A)** and six-rowed cv. Morex **(B)**. Orange dashed lines show the point of partitions that divide spikes into apical, central, and basal parts. Apical parts

include all nodes that undergo PTD. Scale bar 1 mm (W5.0, W6.5); 1 cm (W7.5, W8.0, W8.25, W8.5). W, Waddington scale.

2.2.5 Primary metabolites profiling in immature spike meristems

Spike samples were collected from the plants grown in a climate chamber similar to hormone measurement to extract polar metabolites, frozen immediately in liquid nitrogen, and stored at -80°C (Figure 2.1A-B). Five biological replicates per sample were used for this analysis. Two stainless steel beads were added to each sample tube and placed in pre-cooled (-80°C) TissueLyser II (QIAGEN, United States) racks and homogenized at a frequency of 30 Hz for 1.5 min. Samples of 3.5 – 40 mg (fresh weight) were weighed into 2 mL safe lock tubes (Eppendorf AG, Germany) and kept at -80°C until use. One mL of the extraction buffer containing chloroform: methanol in a 1:1 (v/v) ratio was added. Samples were mixed thoroughly and placed on a vortex at 4°C while shaking carefully for 20 min. Afterward, 300 μL LC-MS grade water was added to each sample and mixed. After centrifugation at 14000 rpm at 4°C for 10 min, the polar upper phase was transferred to a new reaction tube (Eppendorf AG, Germany) and used directly for the measurement or stored at -80°C for further analysis. Soluble sugars (sucrose, glucose, and fructose) were measured enzymatically as described previously (Ahkami et al., 2009). For the targeted analysis of amino acids, 100 μL of vacuum-dried polar phase from each sample extract were re-dissolved in 10 μL of water. The amino acids were derivatized with AQC (6-aminoquinolyl-N-succinimidyl carbamate) using the Bioanalytics Gatersleben Amino-Acid kit (Germany). Briefly, 10 μL samples were added with 70 μL of the derivatization buffer and 20 μL of the AQC reagent, followed by a 10-min incubation at 55°C , and cooled down for analysis. One μL of the derivatized amino acids was analyzed through RP-UPLC-PDA-FLR (RP-UPLC-PhotoDiode Array-Fluorescence detection) using an Acquity UPLC system (Waters, Germany). Amino acids were separated in an AccQTag Ultra (1.7 μm , 2.1 x 100 mm; Waters, Germany) column coupled to an Acquity In-Line filter (Waters, Germany) at 60°C and $0.7\text{ ml}\cdot\text{min}^{-1}$. The separation gradient was: starting isocratic hold with 0.1% eluent B for 0.5 min, from 0.1 to 2% B from 0.5 to 5.7 min, from 2 to 9% B from 5.7 to 7.5 min, from 9 to 9.7% B from 7.5 to 8.7 min, from 9.7 to 13% B from 8.7 to 9.2 min, from 13 to 14% B from 9.2 to 12 min, from 14 to 60% B from 12 to 12.2 min, and an isocratic hold from 12.2 to 12.7 min to clean the column; after each run, the column was equilibrated to the starting conditions (0.1% B). Eluent A was the AccQTag Ultra Eluent A concentrate diluted 1:10 (v/v) in water, and eluent B was the

AccQTag Eluent B concentrate (Waters, Germany). The derivatized amino acids were analyzed by fluorescence (excitation/emission 266/473 nm, PMT gain 1.0, data rate 10 points.s⁻¹) and PDA (260 nm, 4.8 nm resolution, sampling rate 10 points.s⁻¹) detection. For the targeted quantitation of each amino acid, we used calibration curves of commercial standards in the column range of 0.1 to 75 pmol. Data processing and analysis were done with the Empower 3 software (Waters, Germany).

Sugar phosphates and organic acids were measured as described previously (Ghaffari et al., 2016). Briefly, the separation and detection of metabolites were carried out using an ion chromatography system with a conductivity detector (Dionex, Thermofisher Germany) connected to a triple quadrupole mass spectrometer QQQ6490 (Agilent Technologies, Waldbronn Germany). ESI-MS/MS analysis was conducted in the negative ionization mode. The following parameters were employed: desolvation temperature of 250°C, nitrogen gas of 720 l per hour with a heater temperature of 250°C, a capillary voltage of 3.5 kV, and different dwell times between 40 and 200 sec. Collision energy (CE) differed among the compounds and was in the range between 6 and 50 for different masses. Deprotonated ions [M-H]⁻ were monitored with a span of 1 amu. Multiple Reactions Monitoring (MRM) was performed to identify individual compounds accurately. This allows for minimizing parallel monitoring and enhancing sensitivity. Quantification was performed with authentic standards (Sigma-Aldrich, Germany) at different concentrations.

The relative abundance of additional polar metabolites was analyzed through untargeted LC-MS-based profiling. Polar extracts were added 4:1 (v/v) with 0.5% v/v formic acid. Samples were analyzed by RP-UPLC-ESI-UHR-QTOF-MS (Reversed Phase Ultra Performance LC-Electrospray Ionization-Ultra-High-Resolution-Quadrupole Time Of Flight MS) using an Acquity UPLC system (Waters, Germany) coupled to a maXis Impact ESI-QTOF MS (Bruker Daltonik GmbH, Germany) with an injection volume of 5 µl. The separation was done in an Acquity UPLC HSS T3 (1.8 µm, 2.1 x 100 mm; Waters, Germany) column coupled to an Acquity UPLC HSS T3 VanGuard (1.8 µm, 2.1 x 5 mm; Waters, Germany) pre-column, at 30°C and 0.4 ml.min⁻¹, using the following gradient (eluent A, 0.1% v/v formic acid in water; B, 0.1% v/v formic acid in acetonitrile): starting isocratic hold with 0.1% B for 1 min, from 0.1 to 5% B from 1 to 3 min, from 5 to 12.6% B from 3 to 6 min, isocratic hold from 6 to 7 min, from 12.6 to 50% B from 7 to 10 min, from 50 to 99%B from 10 to 10.5 min, and an

isocratic hold from 10.5 to 12.5 min to clean the column; after each run, the column was equilibrated to the starting conditions (0.1% B, 99.9% A). MS profiling for small molecules (50-1000 m/z) was done in MS1 using a positive ionization mode as described (Garibay-Hernández et al., 2021). MS/MS was performed in selected samples using auto MS/MS mode for annotation purposes (Garibay-Hernández et al., 2021). Data processing and quantitative analyses were performed with MetaboScape 5.0 (Bruker Daltonik GmbH, Germany) using an intensity threshold of 1500 counts and a minimum peak length of 7 spectra. The Compass DataAnalysis 4.4 SR1 package (Bruker Daltonik GmbH, Germany) was used for manual data inspection. Amino acids and trehalose were confirmed with a commercial standard by retention time (0.75 min), exact mass (error < 3 ppm), isotopic pattern, and MS/MS fragmentation. The relative quantitation of trehalose was based on the most intense ion, $[M+H-H_2O]^+$ m/z 325.1138. The MS/MS fragmentation of this precursor mass resulted in the characteristic ions $[M+H-C_6H_{10}O_5]^+$ m/z 163.0643 and $[M+H-C_6H_{12}O_6]^+$ m/z 145.0495. The absolute or relative measurements of all the polar metabolites described above were calculated by normalizing them to the fresh weight of starting extracted material.

2.2.6 ROS staining

Reactive oxygen species (ROS) distribution was observed using fluorescent dye 2',7'-dichlorodihydrofluorescein diacetate (H_2DCFDA). Bowman spike samples at stages W5.0, W6.5, and W7.5 with were incubated for 30 min with 20 μM H_2DCFDA in 20 μM HEPES-NaOH buffer (pH 7.4) as well described previously (Feng et al., 2020). Fluorescence was examined using a laser scanning confocal microscope (LSM780, Zeiss) using a 488 nm excitation line in combination with a 490-540 nm emission bandpass.

2.2.7 Total RNA extraction

Total RNA was extracted from the apical, central, and basal spike parts of the stages W5.0, W6.5, W7.5 (Bowman) and from W5.5, W6.5, W8.25 (Morex) using TRIzol (Invitrogen) (Figure 2.2). Three biological replicates per tissue type were used for this analysis. To remove genomic DNA contamination, RNA was treated using RNase-free DNase (TURBO, Invitrogen). RNA integrity and amounts were checked via Agilent 2100 Bioanalyzer (Agilent Technologies) and Qubit (Invitrogen).

using ClustVis online tool (Metsalu and Vilo, 2015). Barley reference transcriptome is publicly available at (https://ics.hutton.ac.uk/barleyrtd/bart_v2_18.html). Gene IDs of barley MorexV3 genome reference (Mascher et al., 2021) were also obtained by the reciprocal blast against BARTv2.18 transcriptome reference.

2.2.10 Co-expression network analysis

TPM data of all expressed transcripts from 27 samples each from Bowman and Morex were used for constructing the co-expression network, module detection, and identification of hub genes from the chosen PTD modules. The data processing and co-expression analysis was carried out as described previously (Thiel et al., 2021). The expression profile of each module was summarized by module eigen-gene defined as its first principal component, and modules with highly correlated (>0.75) eigen-genes were merged. This way, ten modules in Bowman and thirteen in Morex were identified. Furthermore, modules with expression patterns similar to genes of interest were selected to identify hub genes. For hub gene identification, the "degree" and "betweenness centrality" statistics were calculated separately for all the transcripts from each module. These values were used to rank the genes, and the top 10 genes from each module were considered hub genes. The networks were visualized using Cytoscape 3.7.1 (Shannon et al., 2003).

2.2.11 Cis-motif enrichment analysis

For cis-motif identification and enrichment analysis, the first 1.5 Kb upstream promoter sequences for all the genes were extracted from MorexV3 (Mascher et al., 2021). The "findMotif.pl" HOMER suite (Heinz et al., 2010) program was used for the promoter sequences of apical, central, and basal enriched genes identified in ROKU analysis. Identified motifs were searched against the 1.5 kb promoter sequences of remaining genes for enrichment, and binomial distribution was used to calculate P values.

2.2.12 Gene Ontology (GO) enrichment analysis

Arabidopsis homologs were used for GO term enrichment analysis. The protein sequences of barley annotated genes (BARTv2.18) were used to query the Arabidopsis protein dataset in TAIR10. Genes with the highest hit of BLASTP (e-value < 1e-5) were considered the closest homologs in Arabidopsis. GO term enrichment was performed for the DETs from pairwise comparisons and tissue-specific DETs from ROKU analysis using their corresponding TAIR IDs with Metascape

(<http://metascape.org>) following default parameters with a p-value cutoff of 0.05 (Zhou et al., 2019).

2.2.13 Subcellular localization

For subcellular localization, the full-length sequence of *HvGT1* (NIASHv2033D08, Genebank accession no. AK365295) (Matsumoto et al., 2011) was amplified from a full-length cDNA clone obtained from NIAS, Japan (<http://barleyflc.dna.affrc.go.jp>) and directionally cloned into the pENTR/D-TOPO entry vector (ThermoFisher, Inc). After sequence verification, entry vectors were N- and C-terminally fused in-frame to yellow fluorescent protein (YFP) gene in pIPKTA48 and pIPKTA49 vectors (https://figshare.com/articles/dataset/Sequence_information_of_pIPKTA48_and_pIPKTA49/6652415/1), respectively, using Gateway® cloning technology (ThermoFischer Scientific, New York, NY, USA). The resulting YFP-fusion constructs were transiently expressed in 7-day-old leaf segments of barley cv. Golden Promise by particle bombardment and examined after 24 h of incubation using an LSM 780 confocal microscope (Zeiss). For primer information, refer to Appendix Table 1.

2.2.14 Generation of *gt1* knockout barley by targeted mutagenesis

A suitable Cas9 target motif was selected in the first exon of *GT1* (Figure 8a) using the genomic sequence of barley cv. 'Golden Promise' (Schreiber et al., 2020) and the DESKGEN (Doench et al., 2014) and WU-CRISPR (Wong et al., 2015) platforms followed by modeling and validating the gRNA's secondary structure using the RNAfold tool (Gruber et al., 2008) according to criteria outlined previously (Koeppel et al., 2019). The *GT1*-specific 5'-end of the gRNA-coding transgene was synthesized as single DNA strands with overhangs (forward: 5'-TGGCGAAGCTGTCCGGGAAGACGA -3' and reverse: 5'-AAACTCGTCTTCCCGGACAGCTTC-3') that then were annealed and cloned into the intermediate vector pSH121 (GeneBank-ID: MW145140.1) (Hoffie et al., 2021) using *BsaI* restriction sites. Subsequently, the plasmid fragment containing the expression cassettes of *GT1*-specific gRNA and cas9 was sub-cloned into the binary vector p6i-d35S-TE9 (DNA CLONING SERVICE, Hamburg, Germany) using *SfiI* restriction sites. The sequence-verified binary vector was introduced into the hypervirulent *Agrobacterium tumefaciens* strain AGL1 via electroporation. A resulting AGL1 clone was then used to inoculate immature embryos of barley cv. 'Golden Promise' as previously described (Hensel et al., 2009). To verify the T-DNA transfer,

T0 plants were analyzed for the presence of *cas9* and *hpt* transgenes using a PCR-based approach, which was followed by Sanger-sequencing of target region-specific PCR amplicon to detect mutations (Supplemental table 16). In total, 29 T0 events (41 sister lines) were generated and based on the analysis, and eight independent events were selected for further investigation in subsequent generations. In the T1, 24 sister lines per event were germinated and analyzed for mutation by PCR amplification of the target region as described above. Based on the zygosity of the mutation and phenotypic characterization, two independent homozygous mutant events (*gt1^{CR1}* and *gt1^{CR2}*) and an azygous (WT) event were selected for detailed analysis in T2. For primer information, refer to Appendix Table 1.

2.2.15 De-tillering experiment

For the detillering experiment, the WT (azygous) and *Hvgt1* knock-out lines were grown in a greenhouse in 9cm square pots under long-day conditions of 16-h/8-h light-dark regime at 17°C/14°C. Tillers were removed once every three days, starting from the first visible outgrowth of tillers until harvest. Free-tillered plants were used as a control. Three to five plants from azygous WT (control, de-tillered) and mutants (control, de-tillered) were used to score the spike traits.

2.2.16 Association study and haplotype analysis

We have the whole genome sequenced from 358 six-rowed spring barley accessions (unpublished). Here gene-based association study was performed with 752 SNPs (MAF ≥ 0.03) from the two flanking genes of *HvGT1* that covered ~200-kb genomic region. To control for both false positives and false negatives, the FarmCPU model was used to detect SNPs traits association under GAPIT (version3) (Liu et al., 2016, Wang and Zhang, 2021). SNPs for the same interval from 300 diverse barley accessions reported elsewhere (Jayakodi et al., 2020) was also included, for which 121 SNPs were identified. SNPs were merged and phased with BEAGLE5.0 with default settings (Browning et al., 2018). Merged accessions were grouped with phylip using DNADIST method. The tree was visualized with ggtree (Yu, 2020). Our association study identified a peak SNP situated closed to an open chromatin region from ~8-kb upstream of *HvGT1* (Lu et al., 2019). The haplotype analysis was performed by considering SNPs surrounding the peak SNP and the ATAC-seq peak

encompassing a 5-kb interval from the 358 six-rowed barley accessions (112 SNPs). TF binding motif was predicted using PlantPAN3.0 (Chow et al., 2018).

2.2.17 MALDI MSI

This methodology is partly based on the following publication and reproduced with the kind permission of the publisher.

Shanmugaraj, N., Rutten, T., Svatos, A., Schnurbusch, T., Mock, H. P. (2023). "Fast and Reproducible Matrix Deposition for MALDI Mass Spectrometry Imaging with Improved Glass Sublimation Setup." Journal of the American Society for Mass Spectrometry **34**(3): 513-517.

2.2.17.1 Spike sampling and tissue sectioning

Bowman and *BW.tst2.b* spike samples at W2.5, W3.0, W3.5, W4.5, W5.0, W6.5, and W7.5 were collected and frozen immediately in liquid nitrogen and stored at -80°C . Measurements were done in the whole spike sections at stages W3.0, W3.5, and W4.5, whereas the measurements were done in the divided spikes at stages W5.0, W6.5, W7.5 due to the technical difficulties in sectioning large spikes and complexity caused by awns. Spike was divided based on the extent of PTD in the mutants, in which all the spikelets above node 17 usually degenerates. Thus, for comparisons, both WT and mutant spikes were divided into two halves at node 17 and studied further. The data presented in this study are from one biological sample from each stage. Samples were then embedded in a freshly prepared 10% w/v gelatin (Sigma-Aldrich, Germany) medium. Briefly, 1g of gelatin was weighed and mixed in 10 mL of Millipore water in a glass beaker. This was allowed to swell at room temperature for 45 – 60 min. Then the mixture was heated at 55°C using a laboratory heater. The medium was carefully mixed using a glass rod at regular intervals until the solution turned clear. The embedded blocks were placed over a cold metal block in the liquid nitrogen. The disposable intermediate square (15x15x5mm) cyromolds (Tissue-Tek Sakura Finetek Europe) were filled with freshly prepared gelatin medium. Then the frozen barley inflorescence meristems were positioned quickly in the gelatin medium in the desired orientation under the microscope, and placed them immediately in a cold metal block to freeze. With 10 mL of medium, about 4-5 embeddings was done. The samples were then transferred to the cryostat (Thermo scientific Cryostar NX70, Germany) at -20°C and equilibrated for 1 hour. Embedded material was fixed onto the sample holder using a few drops of optimum cutting temperature compound (O.C.T. Tissue-Tek Sakura

Finetek Europe). The lateral sections of 10 μm thickness were prepared with the sample holder and blade at -10°C and -9°C , respectively, and thaw mounted onto indium tin oxide (ITO, Bruker Daltonics, Germany) coated glass slides (75mm x 25mm). The slides were then placed into a vacuum desiccator for ~ 30 min before making optical images (Keyence digital microscope) and matrix application.

2.2.17.2 Matrix application

2,5-dihydroxybenzoic acid (DHB) matrix was deposited over the tissue surface by sublimation process with an improved lab-made glass sublimation setup modified from the previously published methods (Shanmugaraj et al., 2023a, Caughlin et al., 2017, Hankin et al., 2007). The preparation of the DHB matrix was slightly modified from the previously published method (Hankin et al., 2007). About 100 mg of DHB was weighed and dissolved using 1 mL of acetone. The matrix solution was spread over the bottom of the Chemglass sublimation chamber and allowed to crystallize at room temperature (RT). The ITO glass slide containing the tissue section was weighed using a precision balance (Mettler Toledo XPE205 DeltaRange[®] Balance) and attached to one side of the thermally-conductive double-sided tape (3M, USA) and fixed to the bottom of the cold finger using the other side of the tape. The chambers were sealed using two metal clamps. The temperature was set at 120°C using a digital temperature controller connected to the heating mantle. The vacuum pressure was set at 0.066 mbar to evacuate the chamber using a mechanical pump (Vacuubrand RZ 6, Germany) connected to the VACUU-SELECT[®] digital controller (Vacuubrand GmbH, Germany). After reaching the desired pressure (~ 2 min), the cold finger was filled with ice for about 3 cm and 100 mL of cold water to create a slurry. After cooling the sample for 3 min, the sublimation chamber was placed into the heating mantle, allowing the sublimation process for 10 min. After this time, the chamber was moved out from the mantle and cooled down at RT for 5 min with pressure set at 15 mbar. After 5 min, the pump was turned off and slowly released the pressure by loosening the micro-vent valve in the top condenser to reach the atmospheric pressure (~ 2 min). The final amount of sublimated matrix was measured using the same precision balance.

2.2.17.3 MALDI-TOF MS measurements

MALDI-TOF MS measurements were performed using an Ultraflex extreme MALDI-TOF/TOF MS instrument (Bruker Daltonics, Germany) equipped with a smartbeam II

laser in a positive ionization mode at a repetition rate of 1000 Hz as described previously with few modifications (Peukert et al., 2014). The software tools flexControl v3.3 and flexImaging v.2.1 (Bruker Daltonics) were used to set the measurement parameters. The data was acquired in the small mass range between the mass window of m/z 80-1000 Da and the sample rate at 1 Gs s^{-1} . The laser width was set to $15 \mu\text{m}$, and 600 shots per raster spot were acquired in reflectron mode. The laser power was adjusted to exhaust the analyte signals, and the images were acquired in random sampling mode. The instrument was calibrated with $0.25 \mu\text{L}$ polyethylene glycol mixture (1:1 PEG 200 and 600, diluted 1:300 in 30% (v/v) acetonitrile and 0.1% (w/v) trifluoroacetic acid) and from the DHB background before each experiment. The monoisotopic masses of the respective calibrants were determined as described previously (Peukert, 2013).

2.2.17.4 MS imaging data analysis

The unprocessed data were loaded into flexImaging v4.1 and SCiLS lab 2021c pro software (Bruker Daltonics, Germany). Data processing in the SCiLS lab was done according to the instruction manual. Reduced spectra (.mis file) were loaded into the SCiLS lab and proceeded with the default automatic mass axis setting (constant: equidistant). A convolution algorithm was used for baseline removal with a peak width value of 20. MALDI ion images were processed using total ion count (TIC) normalization and visualized.

2.2.17.5 Validation of compounds by MALDI-TOF MS

Distribution patterns of specific polar metabolites obtained by MALDI MSI were further validated using manually extracted spike samples by LC-MS/MS analysis. Specific polar metabolites were confirmed as described in section 2.2.5.

One μL of commercial standards of amino acids, sucrose, trehalose, spermidine, and spermine were prepared at the concentration of 1mM and were spotted directly onto an AnchorChip 800 target plate (Bruker Daltonics, Germany). One μl of DHB matrix (30 mg/ml in 50% v/v methanol, 0.2% w/v TFA) was added to the standard spots. Additionally, 1 mg of grounded spike samples were subjected to metabolite extraction using $100 \mu\text{l}$ of 50 % (v/v) methanol and mixed thoroughly for 1 min. One μl of spike extract and DHB matrix each were also spotted on the target plate. The spots were measured manually in positive ionization mode at the mass range of 80-1000Da using

MALDI TOF MS instrumentation calibrated using the PEG200 + PEG600 mixture. The laser intensity was adjusted according to the measurement requirements. Later, the data were analyzed in flexAnalysis software v3.3 (Bruker Daltonics).

In addition, a publicly available online database (<https://metaspace2020.eu/>) and previously published datasets were used to annotate the detected ions.

2.2.18 Statistical analysis

Bar plots and statistical analysis were generated using the GraphPad Prism software, version 9.3.1 (LLC). One/two-way ANOVA with post hoc Tukey's or Dunnett's test ($p \leq 0.05$) was performed for multiple comparison analyses. An unpaired t-test with Welch's correction was applied for the heteroscedastic data.

2.2.19 Data availability

RNA-seq raw data have been deposited at the European Nucleotide Archive (ENA) under accession number PRJEB51523. GeneBank accession numbers; *HvGT1* - AK365295, *HvNCED1* - AB239297.1. Other related data are openly available in the Dryad Digital Repository at doi:10.5061/dryad.j0zpc86k9.

2.3 Data contribution by the author and the collaborators for the present thesis

Most of the data presented in this thesis has been generated in the research group Plant Architecture (AG PBP), IPK-Gatersleben, by the author of the thesis (*Nandhakumar Shanmugaraaj*). However, this work required technical expertise and infrastructure from diverse research groups to conduct experiments such as MALDI-TOF MS imaging, phytohormones/metabolites profiling, barley transformation, and microscopic analysis. For this purpose, collaborations have been established between the research group Plant Architecture (AG PBP, Prof. Dr. Thorsten Schnurbusch) and other research groups at IPK, including Applied Biochemistry (AG ABC, Dr. Hans-Peter Mock), Molecular Plant Nutrition (AG MPE, Prof. Dr. Nicolaus von Wirén), Plant Reproductive Biology (AG PRB, Dr. Jochen Kumlehn), Structural Cell Biology (AG SZB, Dr. Michael Melzer). In order to make this thesis a complete and understandable story, our collaborators have considerably contributed to the results. The following provides a detailed description of the various efforts completed by the author (*Nandhakumar Shanmugaraaj*) and the other collaborators to accomplish the goals of the current thesis.

Spike and plant phenotyping

- Microscopic dissection of immature spike meristems, imaging, plant and mature spike phenotyping of all WT and mutant lines used in this thesis was carried out by *Nandhakumar Shanmugaraj*.

Histological studies

- Spike sampling for all histological studies – *Nandhakumar Shanmugaraj*; ROS staining & FDA/PI staining – sample preparation and confocal microscopy – *Nandhakumar Shanmugaraj* and *Dr. Twan Rutten*; SEM preparation and image recordings - *Dr. Twan Rutten*; SEM preparation and image recordings – *Dr. Michael Melzer*.

Phytohormone measurements

- Experimental design – *Dr. Thorsten Schnurbusch* and *Nandhakumar Shanmugaraj*; spike sample collection and grinding - *Nandhakumar Shanmugaraj*; phytohormone extraction and absolute quantification - *Dr. Yudelsy Antonia Tandron Moya* and *Prof. Dr. Nicolaus von Wirén*; phytohormone data interpretation – *Nandhakumar Shanmugaraj*.

Metabolite profiling

- Experimental design – *Prof. Dr. Thorsten Schnurbusch*, *Dr. Hans-Peter Mock*, and *Nandhakumar Shanmugaraj*; spike sample collection, grinding, and extraction- *Nandhakumar Shanmugaraj*; Amino acid measurements and data analysis - *Nandhakumar Shanmugaraj* and *Dr. Adriana Garibay-Hernández* led by *Dr. Hans-Peter Mock*; Sugars, TCA metabolites profiling and data analyses - *Dr. Mohammad-Reza Hajirezaei* and *Nandhakumar Shanmugaraj*.

MALDI-MSI

- Experimental design – *Nandhakumar Shanmugaraj*, *Prof. Dr. Thorsten Schnurbusch*, and *Dr. Hans-Peter Mock*; spike sample collection, embedding, cryosectioning, matrix application, MALDI-MSI, and data analysis - *Nandhakumar Shanmugaraj*; LC-MS validation - *Nandhakumar Shanmugaraj*, *Dr. Adriana Garibay-Hernández*.

Gene expression analyses

- RNA sequencing experimental design – *Prof. Dr. Thorsten Schnurbusch, Nandhakumar Shanmugaraj, and Dr. Thirulogachandar Venkatasubbu*; spike sampling, RNA preparation - *Nandhakumar Shanmugaraj*; RNA sequencing data analysis *Dr. Sandip Kale and Nandhakumar Shanmugaraj* with inputs from *Dr. Venkatasubbu Thirulogachandar and Dr. Ravi Koppolu*; RT-qPCR - *Nandhakumar Shanmugaraj*.

Barley transformation and subcellular localization

- cas9/gRNA vector for barley *GT1* was designed by *Dr. Jeyaraman Rajaraman* along with *Dr. Nagaveni Budhagatapalli*; Barley transformation work and generation of *gt1* knockout lines were led by *Dr. Goetz Hensel and Dr. Jochen Kumlehn*; Subcellular localization of HvGT1, identifying and sequencing of the *gt1* mutant lines were conducted by *Dr. Jeyaraman Rajaraman*. Phenotyping of *gt1* knock-out lines - *Nandhakumar Shanmugaraj*.

Association study and haplotype analysis

- Association panel selection and experimental design– *Prof. Dr. Thorsten Schnurbusch, Dr. Ravi Koppolu, and Dr. Venkatasubbu Thirulogachandar*; Association study - field and greenhouse experimental design and phenotyping – *Roop Kamal, Dr. Yongyu Huang, Dr. Venkatasubbu Thirulogachandar, Nandhakumar Shanmugaraj*; Haplotype analysis and data interpretation - *Dr. Yongyu Huang* along with *Nandhakumar Shanmugaraj*.

3. Results

3.1 Morphological characterization of barley spike PTD

3.1.1 MYP, onset, and extent of PTD are reproducible in the main-culm spike

To better understand the sequential events leading to barley spike PTD and dissect its molecular basis, the plants were under controlled conditions to limit possible environmental influences (Methods section 2.1). The early spike development was tracked in the main culm of the two-rowed barley cv. 'Bowman' using the Waddington scale (Waddington et al., 1983) and determined the MYP stage using the 'spikelet stop' method (Thirulogachandar and Schnurbusch, 2021). Importantly, the developing inflorescence showed robust and reproducible developmental patterns in terms of spikelet initiation and degeneration (Figure 3.1A-B). Under these standardized growth conditions, each Bowman spike produced 38–39 rachis nodes/ridges at stage W5.0 (38 days after sowing [DAS]), of which 13–14 aborted, reaching a spikelet survival rate ($[\text{Final spikelet number}/\text{Potential spikelet number}] \times 100$) of about 64%. In Bowman, at stages W5.0, W6.5, W7.5, and W8.0, the spikes were about ~5 mm, ~10 mm, ~15 mm, and ~35 mm in length, respectively, with awns elongating drastically from stage W6.5. At the MYP stage (W5.0), spikes displayed a lanceolate phenotype with an acropetal developmental gradient of spikelets (advanced spikelets toward the basal part). Developmental differences became more evident between spikelets from the degenerating apical region and those from the viable central and basal regions as growth progressed after the MYP stage. With the onset of spike elongation at W6.5 (44 DAS) (pre-death stage), the spike shape became more oblong with a higher degree of developmental synchronicity between the spikelets with central and basal positions. Spike elongation also occurs mainly in the viable central and basal zones with active internode elongation and differentiation of the spike (Figure 3.1B). However, spikelets and spikelet primordia at the spike tip still showed a developmental gradient until the visible collapse of the inflorescence dome (visible death initiation stage), which takes place around W7.5 (48 DAS) and death progresses basipetally at stage W8.0 (52 DAS) (Figure 3.2). These observations indicate that the fate of the apical and destined-to-die spikelets and spikelet primordia is determined prior to visible signs of this decision. In addition, early spike development and PTD in barley main-culm spikes respond to strict developmental control for a given genotype when using defined growth conditions.

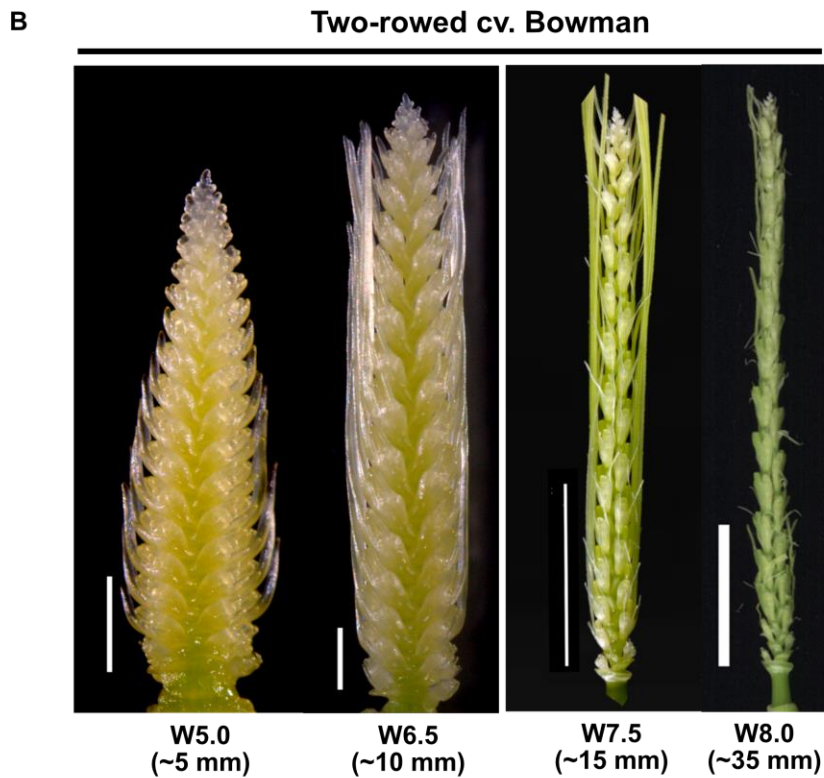
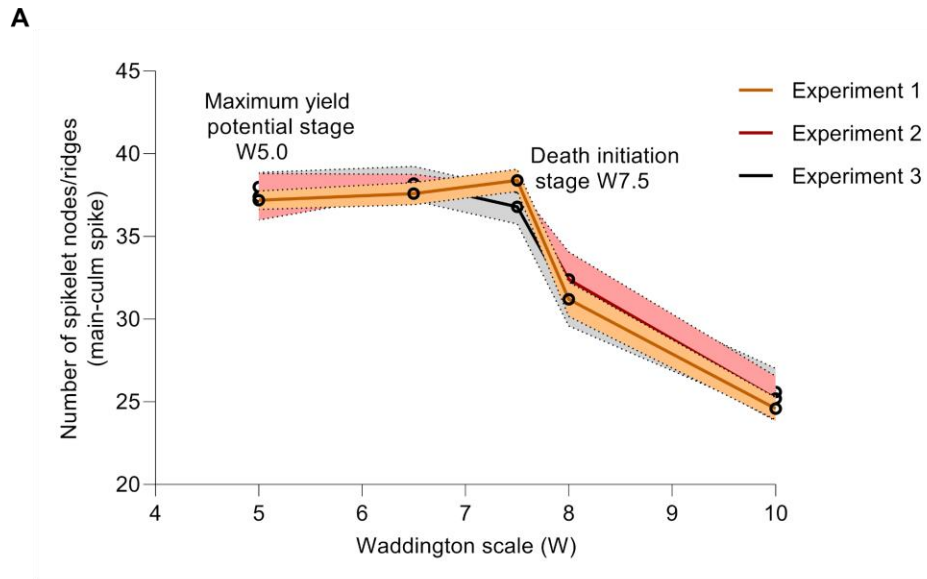


Figure 3.1. MYP, onset, and extent of PTD are reproducible in the main-culm spike. (A) Spike developmental pattern in the two-rowed cv. Bowman. Plots represent mean and error with a 95% confidence interval from three independent experiments in standardized phytochamber conditions. The x-axis indicates stages, and the y-axis shows the number of spikelet nodes/ridges produced in the main-culm spike. **(B)** Four developmental stages and their respective lengths within the spike growth phase of cv. Bowman considered in this study. Scale bar 1 mm (W5.0, W6.5); 1 cm (W7.5, W8.0). W, Waddington scale.

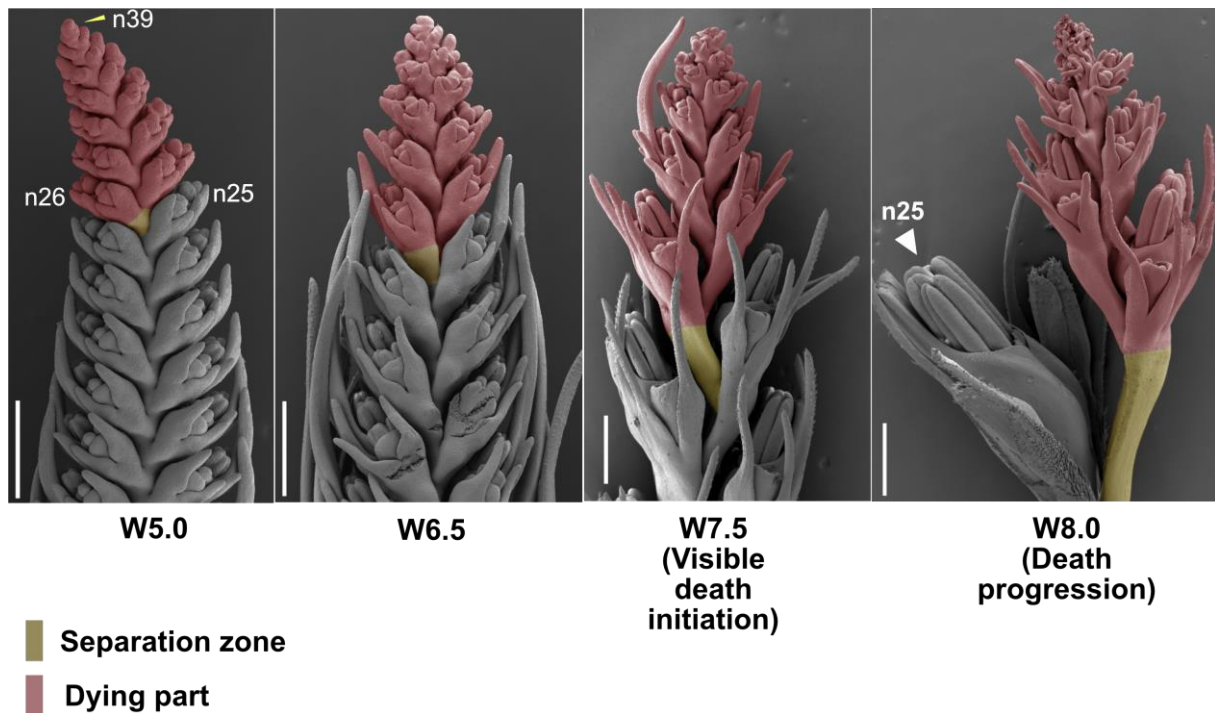


Figure 3.2. Changes in spike morphology leading to PTD in cv. Bowman. Representative Scanning Electron Microscope (SEM) images show the suppressed growth of dying apical spikelets from the central region at four developmental stages between MYP and death progression in Bowman. Dying spikelets are colored red, whereas the yellow-colored internode represents the separation zone of dying and viable parts. The yellow arrow points to the final spikelet ridge (node 39) at W5.0, and the white arrow points to the well-differentiated last surviving spikelet (node 25). Scale bar 500 μ m, n- rachis node.

3.1.2 Live/death assay identifies the pattern of cell death during spike PTD

Visualization of cells with a fluorescent dye is a helpful tool for characterizing cellular dynamics, including viability and death. Fluorescein diacetate (FDA) and propidium iodide (PI) are commonly used fluorescent dyes for visualizing viable and dead cells, respectively. FDA passes through the plasma membrane, hydrolyzed by intracellular esterases to produce fluorescein in the cytoplasm of metabolically active viable cells. In contrast, PI stains the nuclei of dead cells. PI enters only the disrupted cell membranes and binds with DNA to exhibit fluorescence and stains plant cell walls regardless of cell viability (Jones et al., 2016). Staining the tissues using the both FDA and PI will help us differentiate viable and dead cells simultaneously in a single live-cell imaging analysis and studied in various plants (Feng et al., 2022, Jones et al., 2016). This study employed PI-FDA staining to distinguish between viable and dead cells in barley spike meristems of cv. Bowman. Fluorescence imaging using confocal microscopy clearly showed that no PI signals found detected until W6.5, with FDA signals in all the cells, including the IM dome. In contrast, the initiation of cell death

starts from the inflorescence dome at around W7.5 (48 DAS) and progresses basipetally at stage W8.0 (52 DAS). Typically, anthers died before other tissues were affected in the spikelets, while the central rachis kept viable during the initial stages and was found dead during later events (Figure 3.3). Similar patterns were observed for most of the spikes investigated, suggesting that the PTD undergoes a spatiotemporally coordinated cell death process.

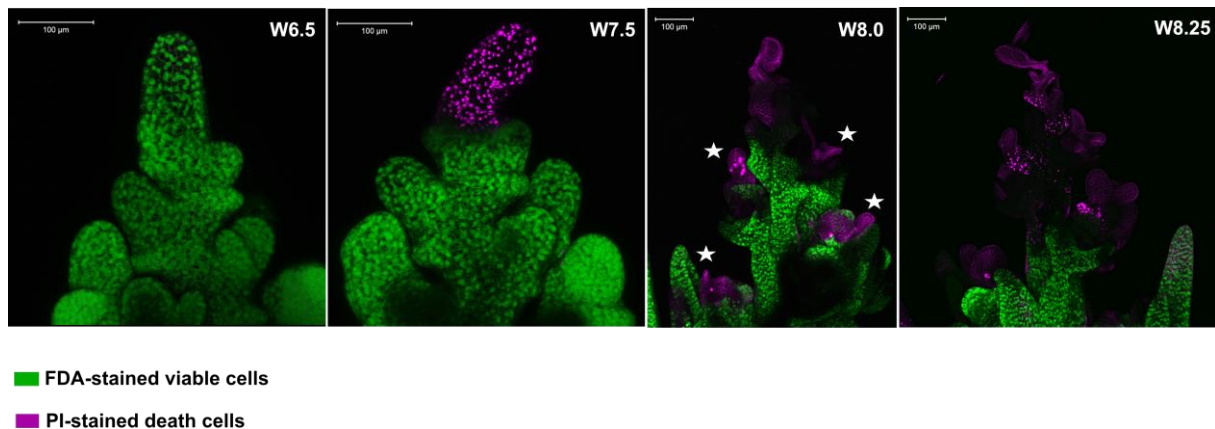


Figure 3.3. Live-death staining assay. Fluorescent dyes, Fluorescence diacetate (FDA), and Propidium Iodide (PI) were used to label Bowman spikes and imaged the fluorescence under a confocal microscope. FDA (green) stains viable cells, and cells undergoing death were stained with PI (Magenta). Star in panel 3 (W8.0) points to the death of anthers in the spikelets. Scale bar 100 μm. W, Waddington scale.

3.2 Physiological and biochemical characterization of barley spike PTD

3.2.1 Differential gradients of growth regulators separate the fate of apical spikelets

Previous findings showed differential accumulation patterns of auxin, cytokinin, and gibberellins along barley spikes (Youssef et al., 2017). We thus hypothesized that phytohormonal patterning along an inflorescence might act as a signal that regulates apical spikelet/rachis development and death. Indeed, endogenous phytohormone measurements at four early developmental stages (W5.0 to W8.0) in three different spike parts of cv. Bowman revealed that ABA steadily increased in the apical parts under controlled conditions (phytochamber) (Methods section 2.2.4; Figure 3.4A). Notably, higher apical ABA levels (~three-fold) coincided with the arrest of the inflorescence dome (W7.5), and these levels continued to increase (to ~four-fold) at the death progression stage (W8.0). Similar patterns were observed for the ABA catabolite phaseic acid (PA) (Figure 3.4A), which has ABA-like functions in Arabidopsis

(*Arabidopsis thaliana*) (Weng et al., 2016). Reverse transcription-quantitative PCR (RT-qPCR) analysis detected higher expression levels for the key ABA biosynthesis gene *HvNCED1* (*NINE-cis-EPOXYCAROTENOID DIOXYGENASE1*) in apical parts (Figure 3.4B). These results indicate that a higher accumulation of ABA and its catabolite PA in the apical part of the spike accompany growth repression and death of apical organs.

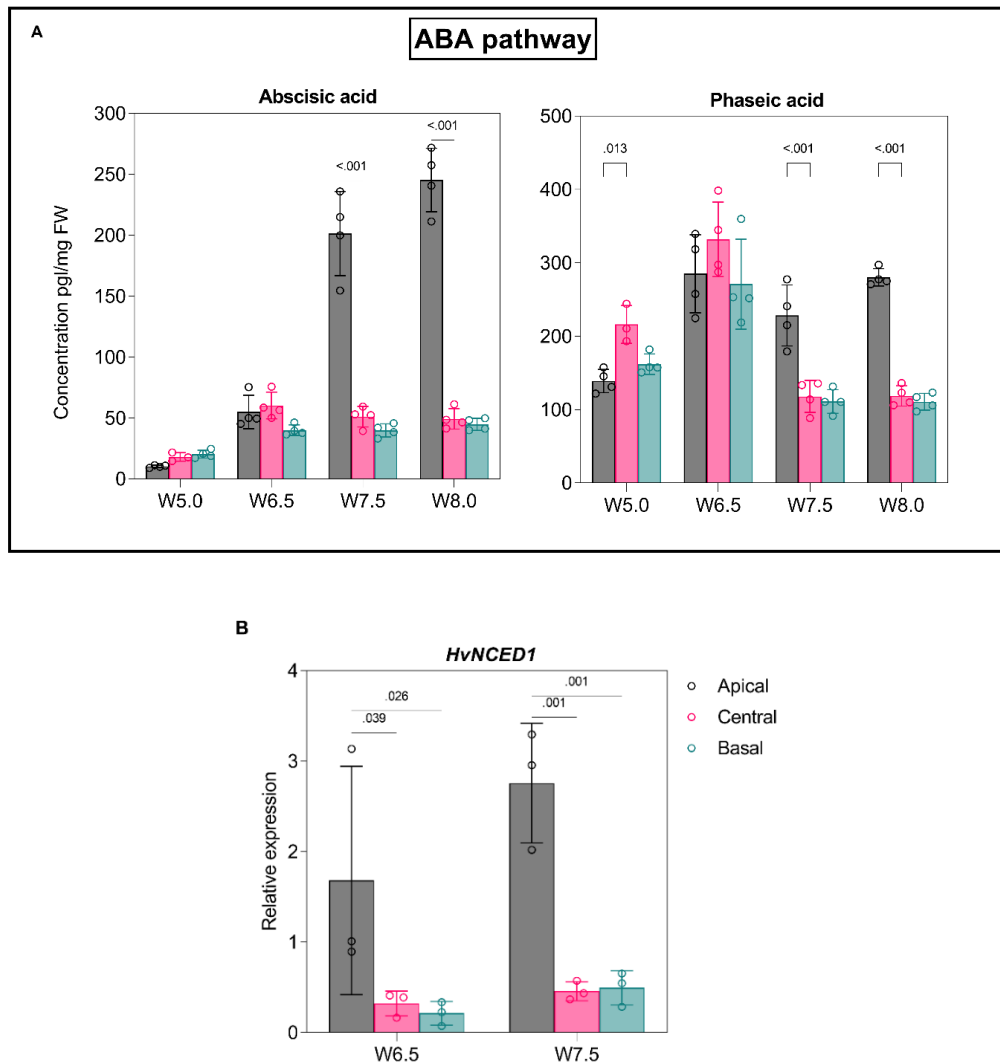


Figure 3.4. Involvement of ABA pathway on spike pre-anthesis tip degeneration. (A) Absciscic acid and its catabolite phaseic acid distribution along with the three spike positions of two-rowed Bowman in four developmental stages. Plots show means \pm SD with significant p values calculated from three to four biological replicates. **(B)** The bar plot shows the relative expression (qRT-PCR) of the ABA biosynthesis gene *HvNCED1* in the two-rowed Bowman. Plots show means \pm SD with significant p values calculated from three biological replicates. Significance was tested by Two-way ANOVA with Tukey's multiple comparison tests to evaluate the difference between apical, central, and basal positions at each stage. W, Waddington scale.

In contrast to ABA, the growth-promoting phytohormones auxin (IAA, indole-acetic acid) and cytokinin (CK) ribosides (iPR, N^6 -(Δ^2 -isopentenyl) adenine 9-riboside; and cZR, *cis*-zeatin 9-riboside) accumulated in the central and basal parts of spikes (Figure 3.5). This pattern was maintained for IAA in all four stages tested, which is consistent with its role in meristem growth and differentiation (Yamaguchi et al., 2013, Wang and Jiao, 2018). By contrast, IAA levels remained low in the apical parts after W5.0, consistent with poor differentiation of apical organs. Interestingly, we measured a sharp increase for iPR and cZR levels in the central and basal parts of stage-2 spikes (W6.5), followed by a drop in later stages. The gibberellic acid (GA) precursors GA15, GA44, and GA19 accumulated at high levels in the apical part at W5.0 and declined over time (Figure 3.5), consistent with a role for GA in barley floral induction (Boden et al., 2014). Both GA44 and GA19 levels were high at W6.5 in the central and basal positions, coinciding with spike elongation and spikelet differentiation; their levels later decreased. These patterns in phytohormones were relatively conserved in samples collected from plants grown under long-day conditions in the greenhouse rather than in the phytochamber (Appendix figure 1). Overall, the observed auxin and CK patterns clearly indicate that the levels of these phytohormones are higher in the central and basal parts of spikes to support their continuing growth and differentiation, whereas PTD is highly associated with ABA and PA levels.

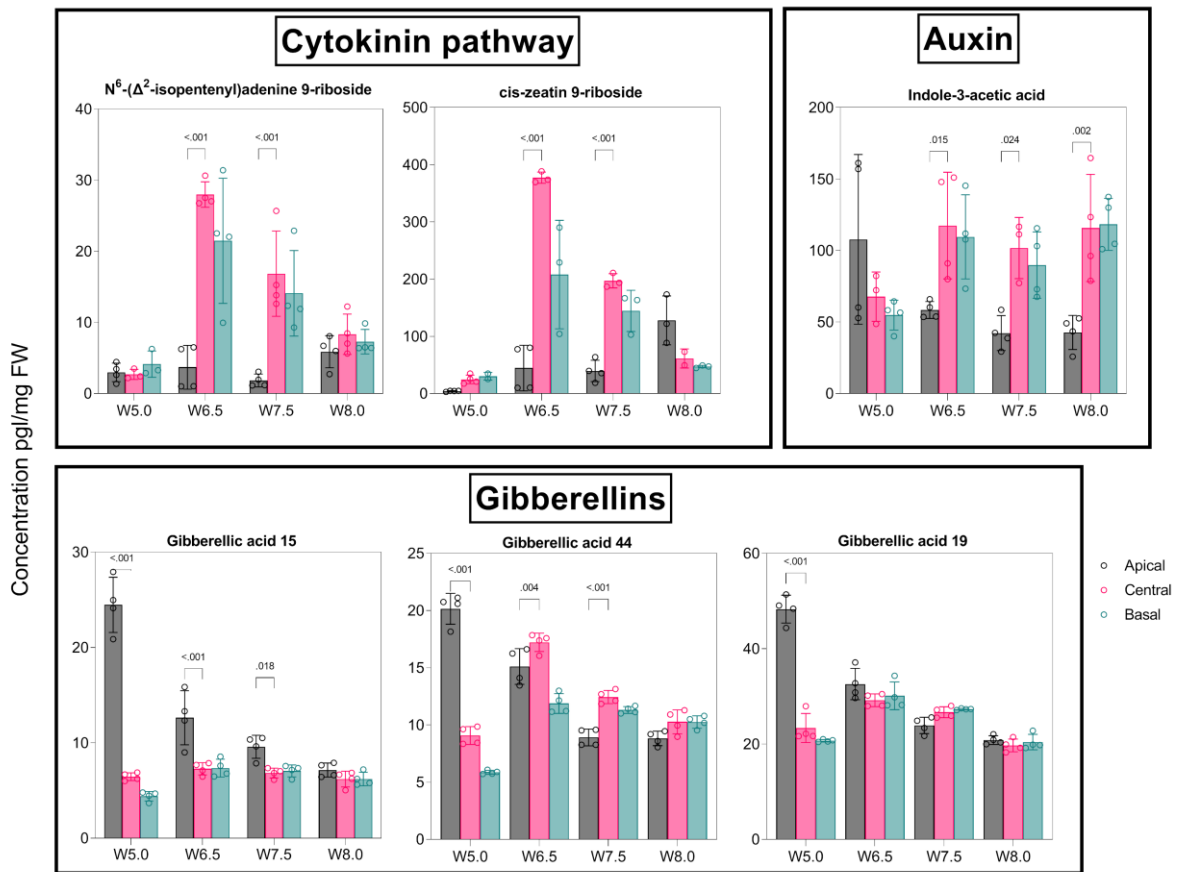


Figure 3.5. Influence of spike hormonal patterning on barley pre-anthesis tip degeneration. Bar plots depicts the distribution of cytokinins, auxin and gibberellins along with the three spike positions of Bowman in four developmental stages. Plots show means \pm SD with significant p values calculated from three to four biological replicates. Significance was tested by Two-way ANOVA with Tukey's multiple comparison test to evaluate the difference between apical, central, and basal positions at each stage. W, Waddington scale.

3.2.2 Dying apical parts display contrasting patterns of primary metabolites

Metabolic and energy homeostasis strongly influence plant cell growth, viability, and death (Kabbage et al., 2017, Skylar et al., 2011). We postulated that primary metabolism is altered in the dying apical part based on previous findings on apical floret fertility in wheat (Ghiglione et al., 2008). Amino acids can also function as signaling molecules in plants and for metabolic adaptation in response to stress (Heinemann and Hildebrandt, 2021). Soluble sugars, amino acids, glycolysis, and tricarboxylic acid (TCA) cycle intermediates were quantified in the dissected spike parts at similar stages used for phytohormone profiling by analytical approaches (Methods - section 2.2.5). Sucrose (Suc), a vital energy metabolite and signaling molecule for plant metabolism and growth (Wind et al., 2010), might be critical to support spike growth, as we observed that its levels increase over time in non-dying

parts (central and basal), but stopped rising in dying apical parts after W6.5 (Figure 3.6A). Trehalose-6-phosphate (T6P), which acts as a signaling metabolite in multiple aspects of plant development linking sucrose metabolism (Eveland and Jackson, 2012, Figueroa and Lunn, 2016), was present in significantly lower amounts in apical tissues relative to central and basal spike regions (Figure 3.6B). By contrast, fructose (Fru) and trehalose (Tre) contents increased in dying tissues (W8.0) (Figure 3.6A; Appendix Figure 2).

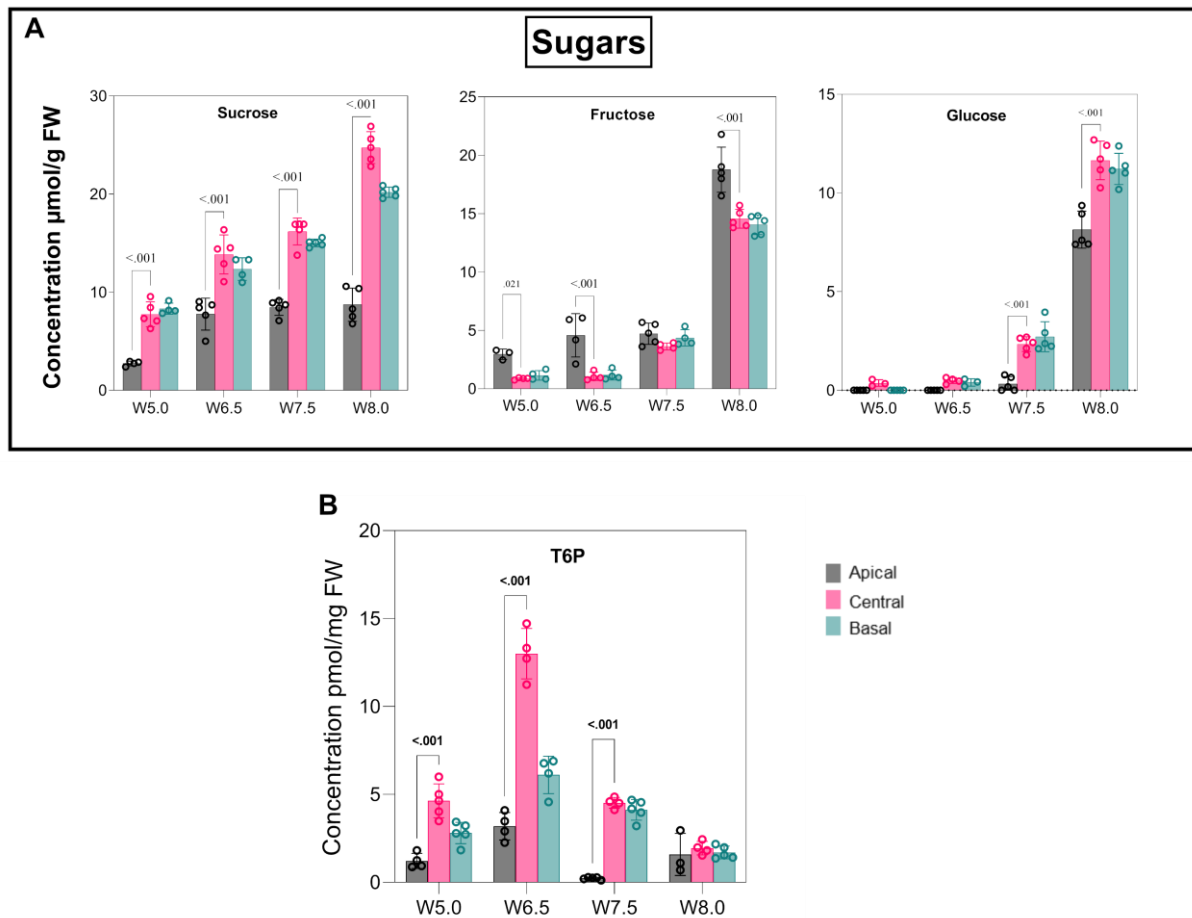


Figure 3.6. Influence of sugars on barley pre-anthesis tip degeneration. Bar plots depicts the distribution of sugars and trehalose-6-phosphate along with the three spike positions of Bowman in four developmental stages. Plots show means \pm SD with significant p values calculated from three to five biological replicates. Significance was tested by Two-way ANOVA with Tukey's multiple comparison test to evaluate the difference between apical, central, and basal positions at each stage. W, Waddington scale.

Among vital amino acids (AA) with a high N:C ratio, Asn (Gaufichon et al., 2010) steadily increased ~five-fold in the apical part at the death progression stage (W8.0) and was the most abundant among the free AA pool (Figure 3.7). By contrast, the content of Gln, a central metabolite of plant nitrogen metabolism (Chellamuthu et al.,

2014), was lower in the apical parts (Figure 3.7), which might limit the proper growth of apical spikelets as its levels were higher in the other spike parts, which undergo normal differentiation. In contrast, we detected the highest concentration for all three aromatic AAs (AAAs), phenylalanine (Phe), tyrosine (Tyr), and tryptophan (Trp), which serve as precursors for a diverse class of primary and specialized metabolites (Lynch and Dudareva, 2020), in the visible death initiation (W7.5) and progression (W8.0) stages in apically dying parts (Figure 3.8). Similar patterns were observed for the two branched-chain amino acids (BCAAs), leucine (Leu) and isoleucine (Ile), which act as alternate respiratory substrates under energy-limited conditions (Peng et al., 2015) (Figure 3.8). By contrast, another BCAA, valine (Val), and stress-responsive proline (Pro) (Alvarez et al., 2022) accumulated in the apical part only at the death progression stage (Figure 3.8; 3.9). High levels of lysine (Lys) and histidine (His) were also detected from W7.5 onward in the dying parts (Figure 3.9). Additionally, differential accumulation patterns of other TCA and glycolysis intermediates were noticed (Figure 3.9). Thus, the apical part of the spike accumulates low levels of certain key carbon and nitrogen metabolites and undergoes specific metabolic reprogramming that distinguishes it from the non-dying central and basal parts to regulate spike PTD.

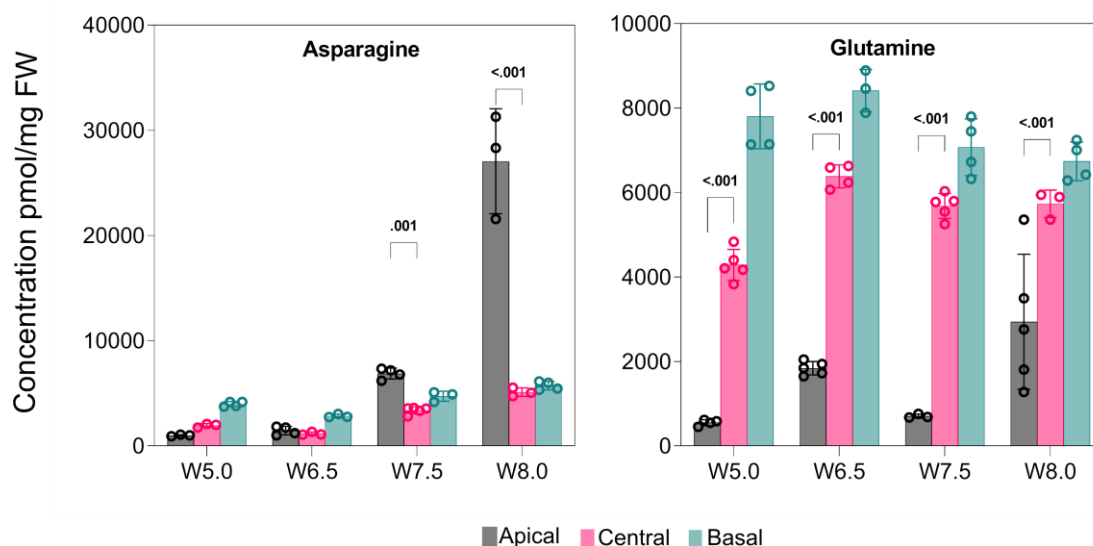


Figure 3.7. Distribution of primary amino acids involved in nitrogen metabolism during spike PTD. Bar plots depict the distribution of asparagine and glutamine along with the three spike positions of Bowman in four developmental stages. Plots show means \pm SD with significant *p* values calculated from three to five biological replicates. Significance was tested by Two-way ANOVA with Tukey's multiple comparison test to evaluate the difference between apical, central, and basal positions at each stage. W, Waddington scale.

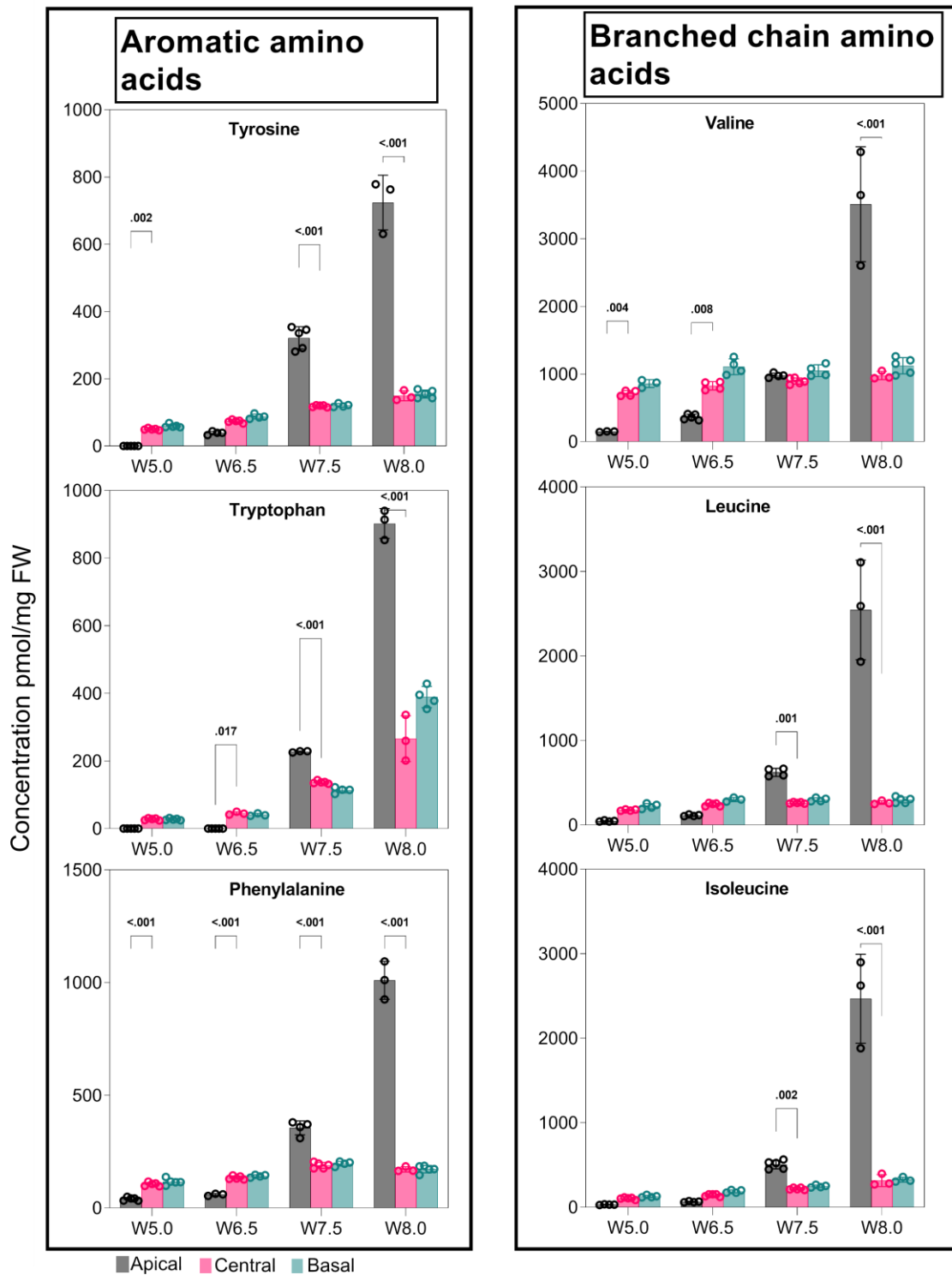


Figure 3.8. Distribution of branched-chain and aromatic amino acids during spike PTD. Bar plots depict the distribution of branched-chain and aromatic amino acids along with the three spike positions of Bowman in four developmental stages. All these amino acids accumulate significantly at high levels in the apical parts at W6.5 and W7.5, except valine, with increases at W8.0. Plots show means \pm SD with significant p values calculated from three to five biological replicates. Significance was tested by Two-way ANOVA with Tukey's multiple comparison tests to evaluate the difference between apical, central, and basal positions at each stage. W, Waddington scale.

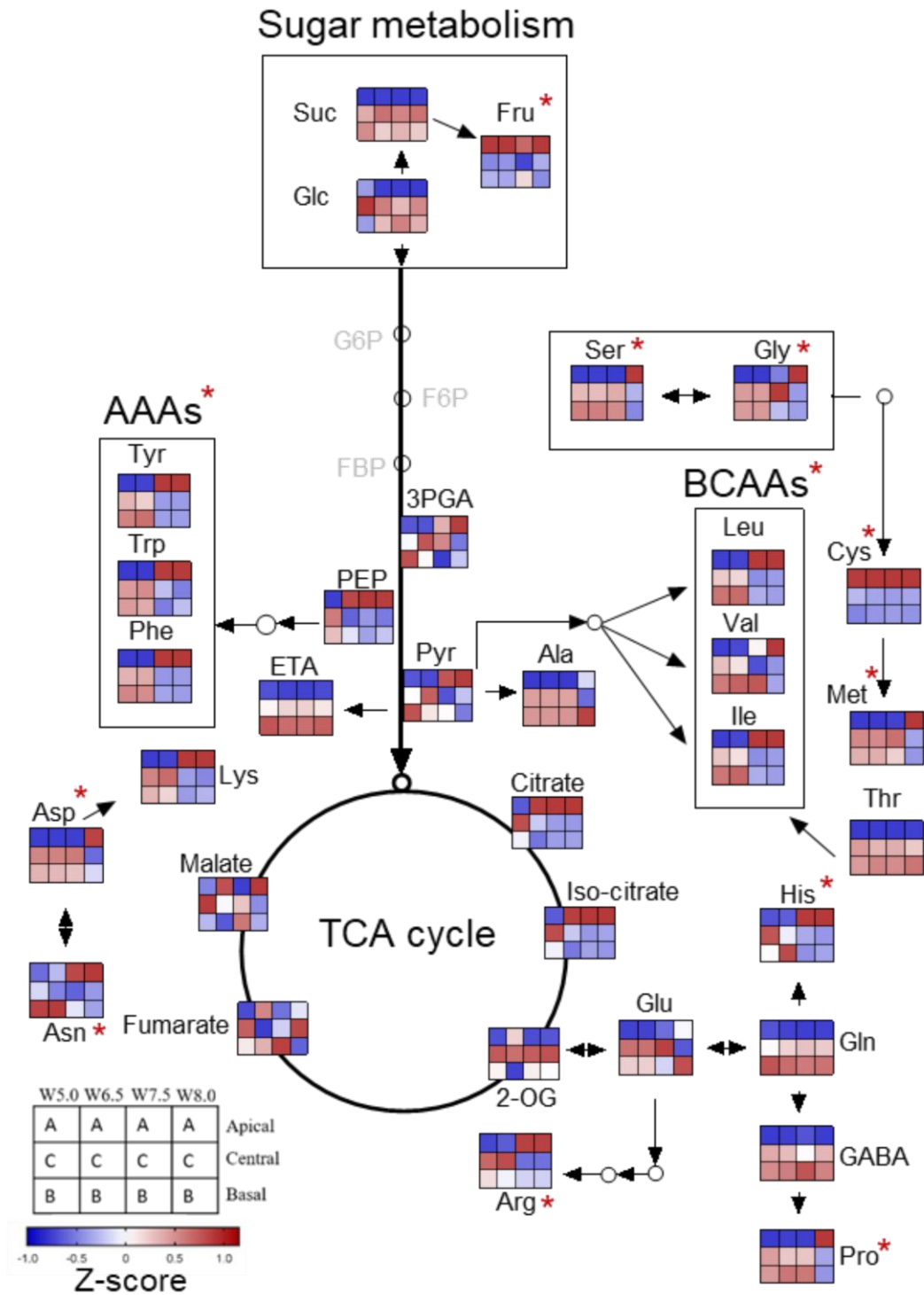


Figure 3.9. Dying apical parts display contrasting patterns of primary metabolites in two-rowed barley. Heatmap of primary metabolite changes during the spike growth phase in Bowman. Colors represent the Z-transformed ratios of apical, central, and basal parts at each stage. Suc, sucrose; Glc, glucose; Fru, fructose; T6P, trehalose-6-phosphate; Asn, asparagine; Asp, aspartate; Arg, arginine; Ala, Alanine; Glu, glutamate; Gln, glutamine, Cys, cysteine, Met, methionine; Gly, glycine; Ser, serine; His, histidine; Val, valine; Leu, Leucine; Ile, isoleucine; Phe, phenylalanine; Tyr, tyrosine; Trp, tryptophan, Thr, threonine; Lys, lysine; GABA, gamma-aminobutyric acid; Pro, proline; 3-PGA, 3-Phosphoglyceric

acid; PEP, phosphoenolpyruvate; Pry, pyruvate; 2-OG, 2-Oxoglutarate; AAAs, aromatic amino acids; BCAAs, branched-chain amino acids; TCA, tri-carboxylic acid; W, Waddington scale. The red asterisk points to the amino acids and sugar enriched at high levels in the apical part during PTD.

3.2.3 ROS accumulates at higher levels in the degenerating apical parts

ROS is a signaling molecule during senescence and cell death (Mhamdi and Van Breusegem, 2018). In order to verify the involvement of ROS in barley spike PTD, whole-mount staining and imaging were performed using ROS-specific dyes. The experiment was initially conducted using non-fluorescent dyes such as DAB (3,3'-diaminobenzidine) and NBT (Nitroblue tetrazolium). However, DAB was not sensitive enough to detect ROS in the barley spikes at early developmental stages, while NBT is non-specific (data not shown). Later, the staining was performed using ROS-specific fluorescent dye, H₂DCFDA, in Bowman spikes at W5.0, W6.5, and W7.5. Indeed, ROS fluorescence was detected high in the apical part of the spike in all three stages investigated (Figure 3.10). However, the fluorescence was found weak or absent in the IM dome in all the stages, and the specific reason for this pattern in the IM dome is unclear. Nevertheless, a similar pattern of high ROS fluorescence in the apical parts was observed for all three biological replicates at each stage, suggesting the involvement of ROS during spike PTD prior to the visible onset.

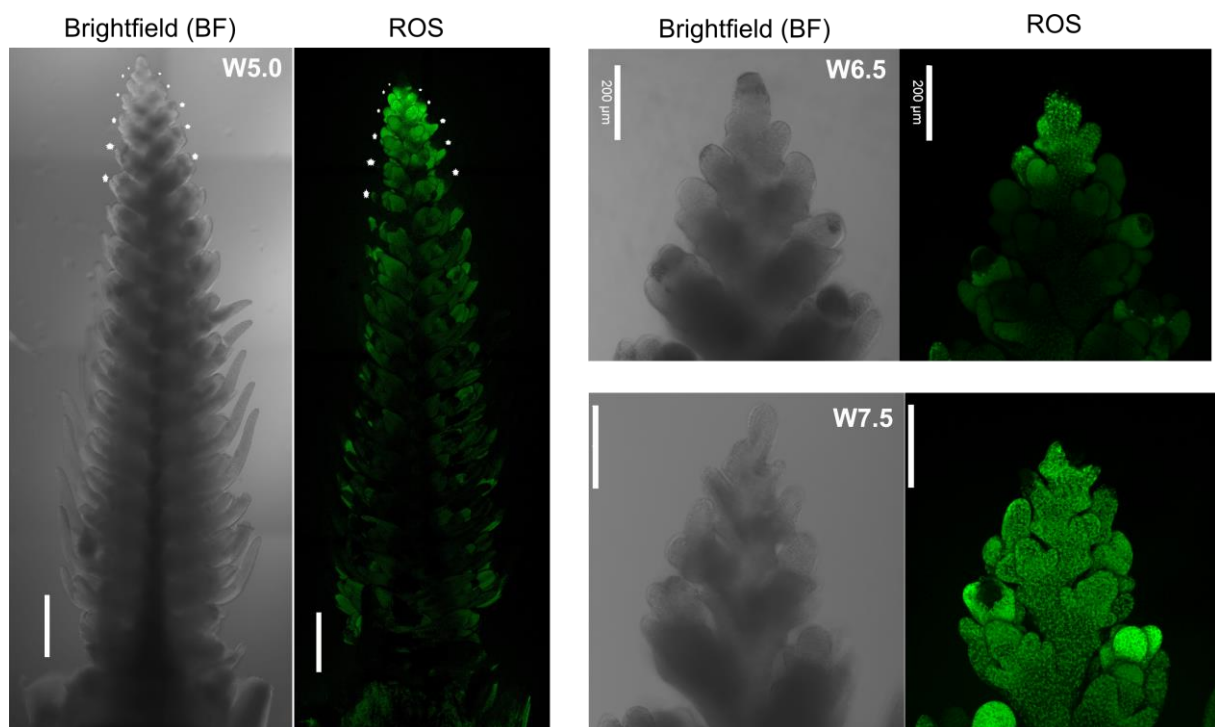


Figure 3.10. ROS staining in Bowman spike meristems. Reactive oxygen species (ROS) were stained using H₂DCFDA fluorescent dye and examined under a confocal microscope. The left panel

shows the brightfield images, while ROS fluorescence is shown in the right panel at W5.0 as a whole spike, W6.5, and W7.5 with magnified apical parts. The white asterisk points depict the PTD nodes. Scale bar 500 μm . W, Waddington scale.

3.3 Transcriptional reprogramming during barley spike PTD

3.3.1 Spatiotemporal transcriptome analysis uncovered molecular signatures that define the opposing developmental fates of degenerating and viable regions

Transcriptome deep sequencing (RNA-seq) in spike parts between W5.0 and W7.5 in Bowman was performed to assess the transcriptional reprogramming that leads to the death of the apical part (Methods section 2.2.7, 2.2.9). A principle component analysis showed trajectories associated with spike growth stages and a developmental gradient along the spike (Figure 3.11). In total, 83,177 transcripts were expressed (at least in one sample), of which 47,220 transcripts (~57%) were differentially regulated (DETs; $\log_2[\text{Fold-change, FC}] > 1$) among the 15 pairwise comparisons made within and across developmental stages (Methods section 2.2.9; Figure 3.11). The number of DETs was higher (~16%) between apical (dying) and central (viable) parts, pointing to their opposite developmental fates, compared to those between the central and basal parts (~2%), reflecting their normal developmental progression and synchrony.

Gene Ontology (GO) enrichment analysis of these DETs identified distinct biological processes differentially regulated between viable (central and basal) and degenerating apical parts (Figure 3.12, 3.13). KEGG (Kyoto Encyclopedia of Genes and Genomes) pathway enrichment of DETs in central and basal parts across development (from W5.0 to W7.5) also showed a clear enrichment for pathways related to photosynthesis, sugar, and starch metabolism, the TCA cycle, and glycolysis (Appendix Figure 3). These observations suggest that the developed transcriptome dataset may provide some novel insights into the mechanisms governing spike PTD and spikelet growth/differentiation.

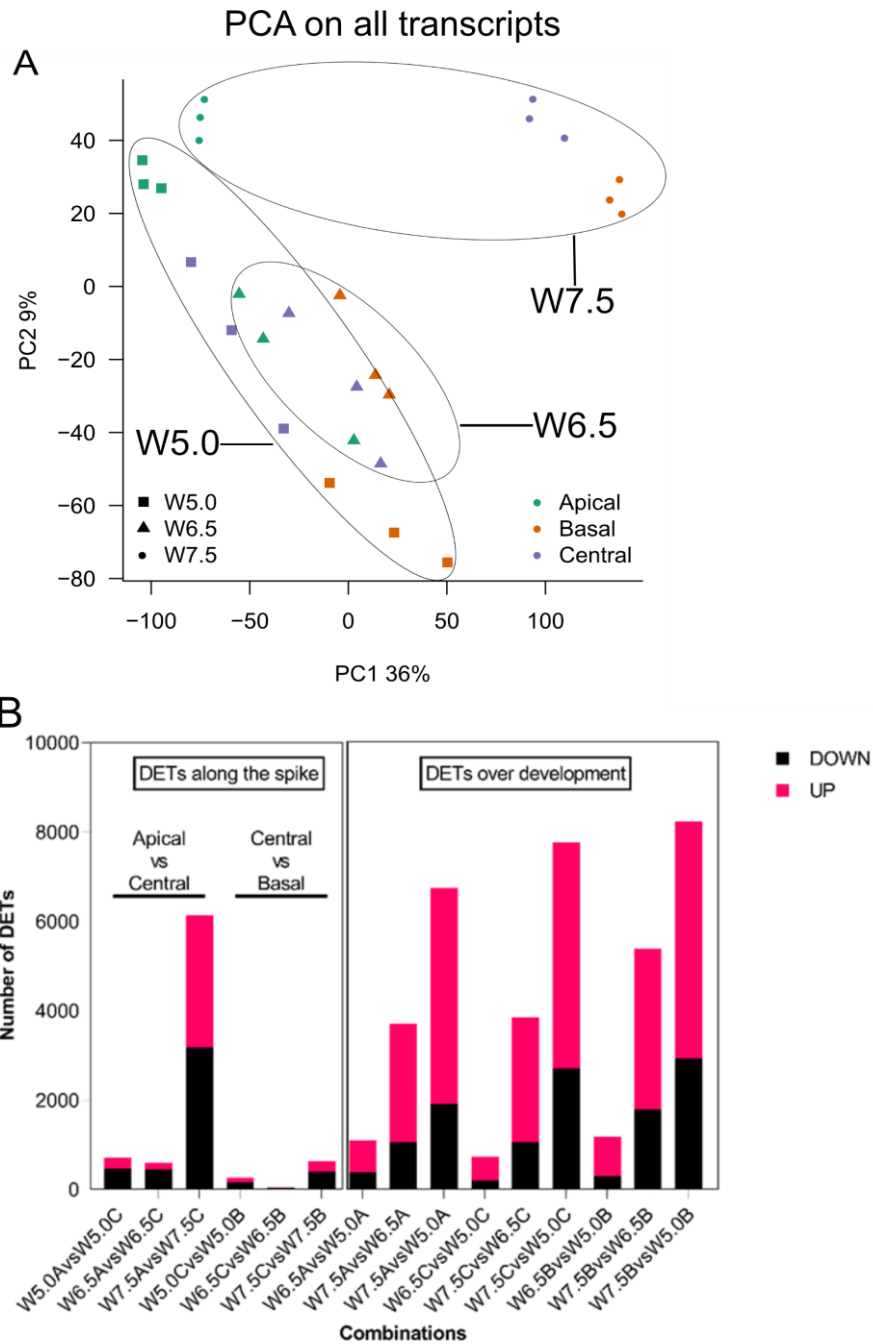


Figure 3.11. Position-specific transcriptomic analysis in viable and degenerating spike parts. (A) Principal component analysis (PCA) of normalized expression levels (counts per million, cpm) of all expressed transcripts in cv. Bowman. **(B)** The number of differentially expressed transcripts (\log_2 FC > 1) between 15 pairwise combinations. A- apical, C-central, B- basal. W, Waddington scale.

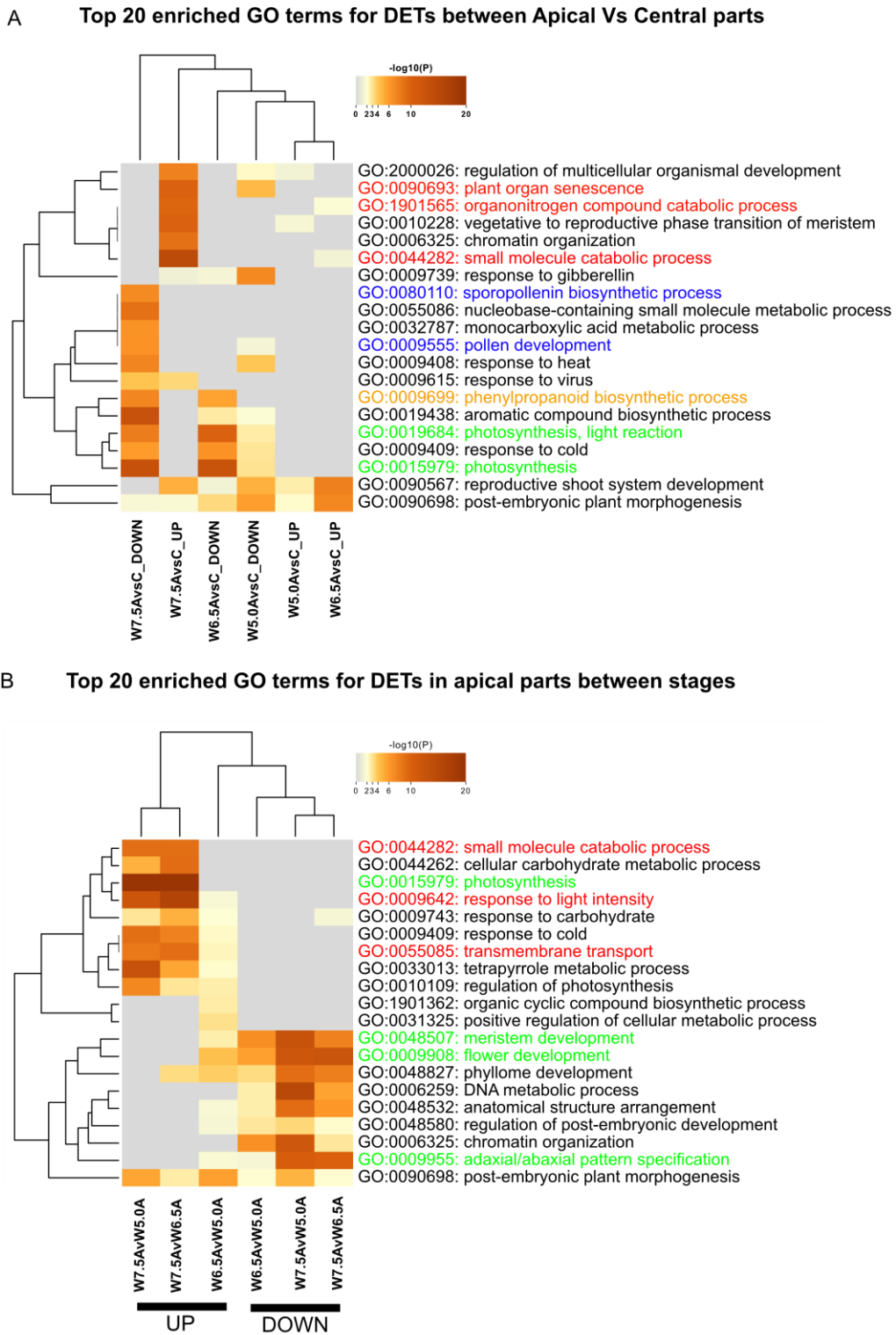
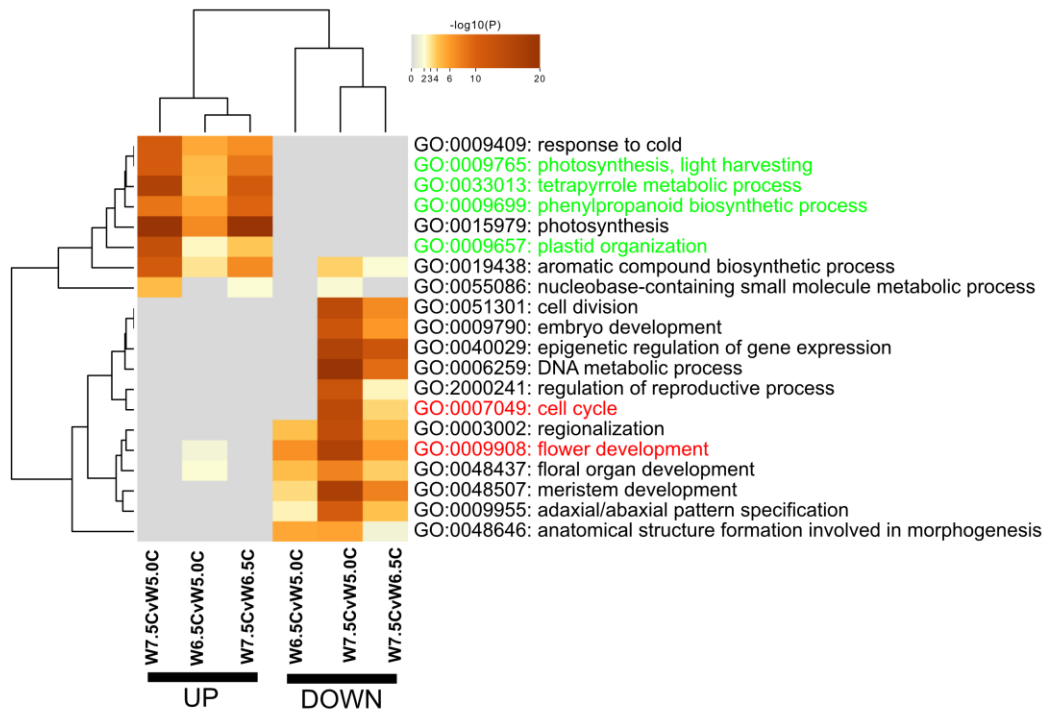


Figure 3.12. GO enrichment for DETs found within and between stages in Bowman. (A) Top 20 GO terms enriched for the differential expressed transcripts (DETs) between degenerating apical and viable central parts. **(B)** Top 20 GO terms enriched for the differential expressed transcripts (DETs) between degenerating apical parts in the three developmental stages. Color saturation corresponds to the degree of enrichment. A- apical, C-central, B- basal. W, Waddington scale.

A Top 20 enriched GO terms for DETs in Central parts between stages



B Top 20 enriched GO terms for DETs in basal parts between stages

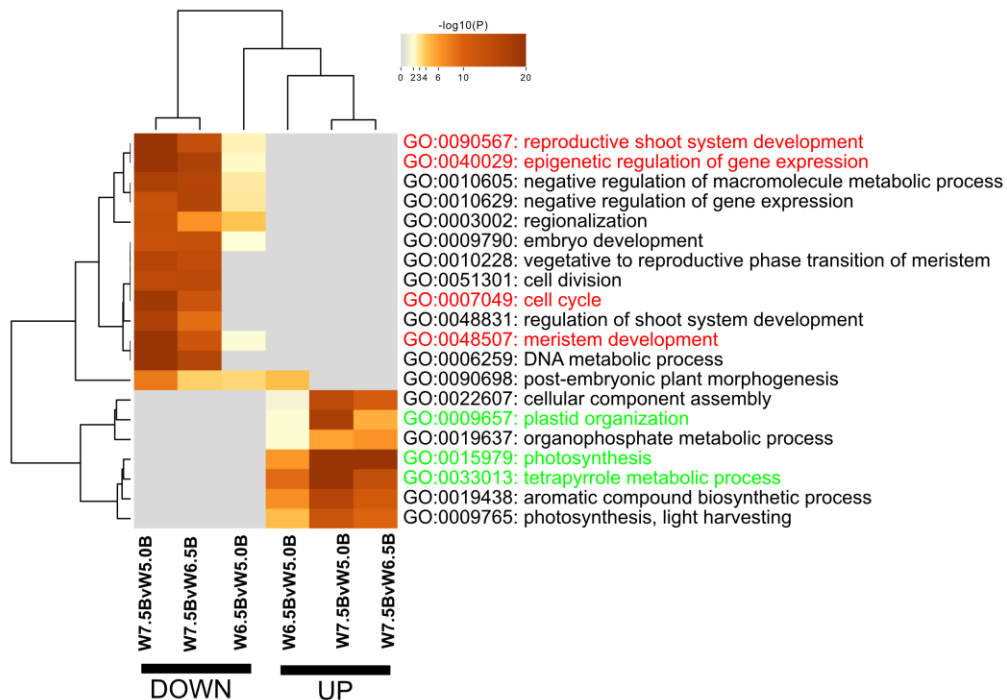


Figure 3.13. GO enrichment for DETs found in central and basal parts between stages in Bowman. (A&B) Top 20 GO terms enriched for the differential expressed transcripts (DETs) between viable central (A) and basal (B) parts in the three developmental stages. Color saturation corresponds to the degree of enrichment. A- apical, C-central, B- basal. W, Waddington scale.

3.3.2 ROKU analysis identifies putative candidates for barley spike PTD

One primary aim of this study is to identify the putative regulators involved in spike PTD. Thus, the developed position-specific transcriptome data were subjected to tissue-specific gene expression analysis using a method called ROKU. ROKU ranks genes based on their overall tissue specificity using Shannon entropy and detects tissue-specificity for each gene using an outlier detection method (Kadota, 2006). All expressed transcripts were subjected to ROKU analysis to identify apical, central, and basal position-specific transcripts and filtered those differentially expressed among the 15 pairwise comparisons ($\log_2FC > 1$; expression ≥ 1 TPM [transcripts per million] in at least one tissue), resulting in 3968 transcripts (apical – 2561, central – 387, basal – 1020) (Methods section 2.2.9; Figure 3.14) (Kadota et al., 2006). The transcripts were ranked based on their tissue specificity. Genes enriched in central spike parts at W5.0 and W6.5 were highly related to cell cycle, flower development, embryo development, or post-embryonic morphogenesis, followed by floral organ development, carbohydrate metabolism, and xylem/phloem patterning at W7.5 (Figure 3.14). In basal parts, genes identified were enriched with processes related to the cell cycle, carbon metabolism, organ development, and post-embryonic development at W5.0 and W6.5. At W7.5, genes were related to photosynthesis, plastid organization, energy metabolism, chlorophyll biosynthesis, and phenylpropanoid metabolism, in line with the substantial spikelet development and greening observed in the basal to the central part of the spike (Figure 3.14). These findings underscore the significance of photosynthesis, plastid organization, and energy metabolism for the constant supply/biosynthesis of assimilates to support proper growth and differentiation of spikelets in the viable (central and basal) regions.

By contrast, apically enriched genes at W5.0 were highly associated with biological processes related to cell division, flower development, meristem maintenance, chromatin organization, auxin transport, and phytohormone metabolism (Figure 3.14; Appendix Figure 4A). However, the expression of most of these genes declined in later stages. Furthermore, the promoters of W5.0 apical genes were significantly enriched in cis-motifs related to the REM (Reproductive Meristem) protein family (Mantegazza et al., 2014) and 'GAGA' (binding target of BARLEY B RECOMBINANT/BASIC PENTACYSTEINE [BBR/BPC] family proteins), regulating flower development (Theune et al., 2019). These data suggest that at W5.0, the apical region is still intact,

displaying normal meristem development and differentiation with no signs of death to come.

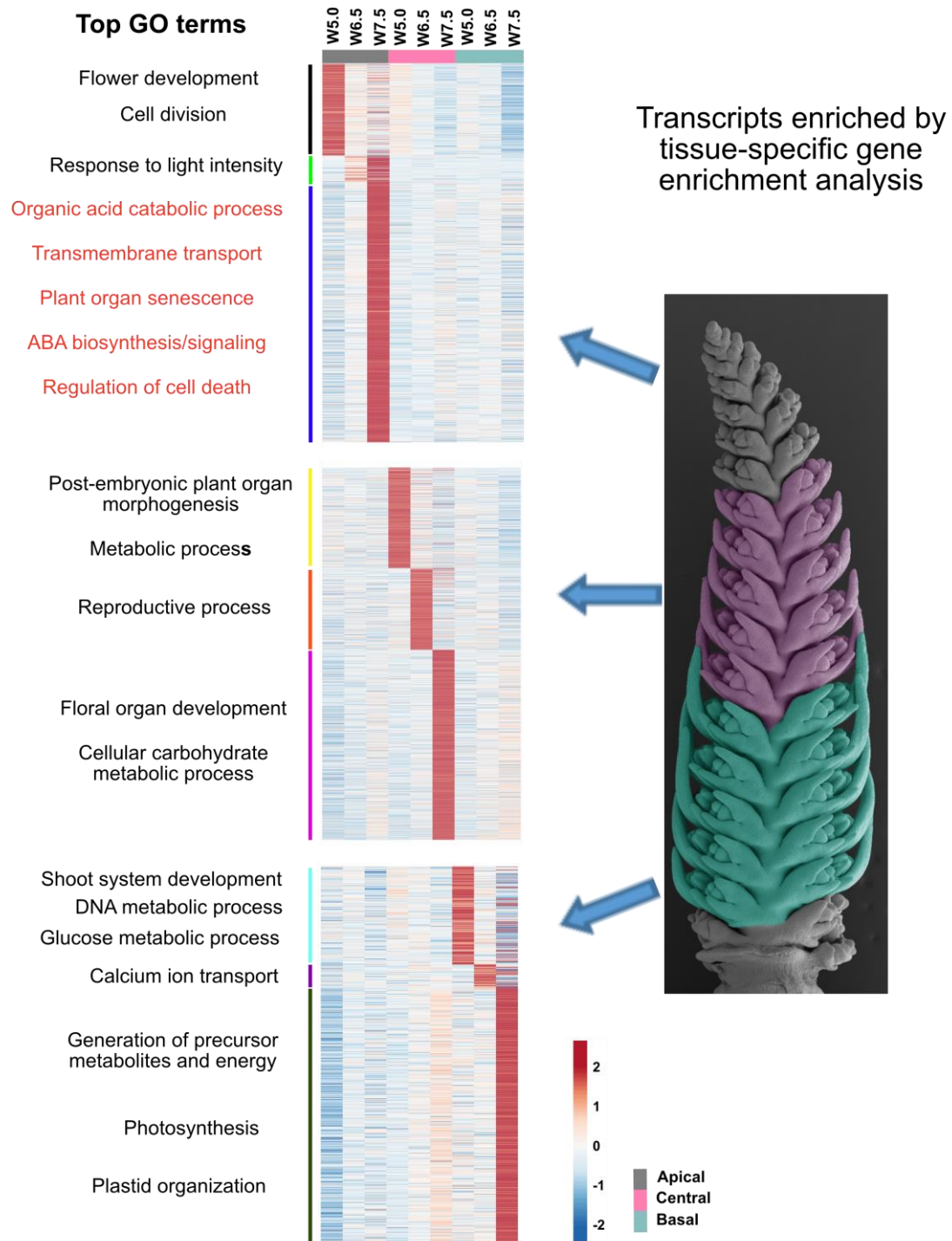


Figure 3.14. Position-specific transcriptomic analysis identifies genes and biological processes differentiating viable and degenerating spike parts. Heatmap shows the expression clusters of apical, central, and basal position-specific transcripts identified by entropy-based ROKU analysis and stage-wise representative significant biological process. Heatmaps represent $\ln(X+1)$ transformed mean TPM values depicted by color code: red, high; blue, low expression. W, Waddington scale.

At W6.5, DETs were enriched in GO categories related to response to light intensity, transcriptional regulation, plant organ senescence, organic acid catabolism, and chlorophyll catabolism (Figure 3.14; Appendix Figure 4B). The expression of most of these genes continued to increase in W7.5 (Figure 3.14; Appendix Figure 4C). Furthermore, genes at W7.5 were highly related to ABA biosynthesis/signaling, proteolysis, amino acid/chlorophyll catabolism, transmembrane transport, reactive oxygen species (ROS), and lipid oxidation (Figure 3.15). Consistently, we noticed *HvNCED1* (Leymarie et al., 2008), encoding a critical rate-limiting enzyme; *ABA INSENSITIVE4 (ABA4)* (Perreau et al., 2020), involved in ABA biosynthesis; and several ABA-responsive/signaling genes among apically enriched genes. Moreover, dying tissues showed high expression of several defense response genes, including *DORMANCY-ASSOCIATED GENE/AUXIN-REPRESSED FAMILY PROTEIN (HvDRM/ARP)* (Roy et al., 2020) and *HYPERSENSITIVE-INDUCED REACTION (HvHIR3)* (Rostoks et al., 2003). The list of DEGs in dying tissues also included several kinase genes, including *STRUBBELIG-RECEPTOR FAMILY3 (SRF3)* and *OPEN STOMATA1 (OST1)*, which participate in circadian-regulated immunity (Alcázar et al., 2010, Li et al., 2011) and ABA signaling (Acharya et al., 2013), respectively.

In green tissues like leaves/culm, the earliest changes during senescence involve degreening due to chlorophyll degradation, followed by chloroplast disintegration (Tamary et al., 2019). We observed the typical basal-to-apical gradient of chlorophyll pigmentation (less pigmentation toward the spike tip) in developing barley spikes. Interestingly, genes involved in chlorophyll catabolism, such as *STAYGREEN1 (SGR1)*, *NON-YELLOW COLOUR (NYC1)*, *PHEOPHYTINASE (PPH)*, and *ABA-RESPONSIVE ELEMENT BINDING PROTEIN2 (ABRE2)*, were also enriched in the apically dying tissues of barley spikes (Yang et al., 2014) (Figure 3.16). Strikingly, the histone deacetylase-like gene *CHLOROPLAST VESICULATION (HvCV)*, an ortholog of Arabidopsis *CV* that is involved in stress-induced chloroplast disassembly, was also highly expressed in the spike apical part (Figure 3.15 (Wang and Blumwald, 2014). Another exciting candidate previously associated with the leaf senescence detected here was the senescence-regulator gene *HvS40-like*, whose leaf senescence-associated functions have been studied in barley and other species (Fischer-Kilbiński et al., 2010, Jehanzeb et al., 2017, Krupinska et al., 2013) (Figure 3.15). Genes participating in proteolysis, amino acid catabolism, and nutrient remobilization were also highly expressed in the apical part, including *PAPAIN-LIKE CYSTEINE*

PEPTIDASEs (*HvPAP14* and *HvPAP20*), *RESPONSIVE TO DESICCATION19* (*RD19*), and *RD21*, as well as genes encoding senescence-associated vacuolar processing enzymes (Hollmann et al., 2014) and several transporters. Consistent with the Asn accumulation observed in the apical part, genes involved in ammonium assimilation and nitrogen remobilization, such as *ASPARAGINE SYNTHETASEs* (*HvASN1* and *HvASN5*) (Avila-Ospina et al., 2015), showed a significant increase in their expression in dying parts. Similarly, *AUTOPHAGY-RELATED (ATG)* genes were highly expressed in these tissues as well (Figure 3.15). Observation of cells from the longitudinal sections of spikes by transmission electron microscopy (TEM) analysis revealed the presence of large vacuoles, plastoglobules, vesicular bodies, lipid droplets, and loosened cell walls in the apical part of the spike (Appendix Figure 5). Furthermore, genes involved in ROS metabolism, for example, those encoding catalases, peroxidases, and glutathione S-transferases were also highly expressed (Figure 3.15). These results indicate that spike PTD involves chlorophyll and cellular degradation by the expression of chlorophyll catabolism and senescence-related genes.

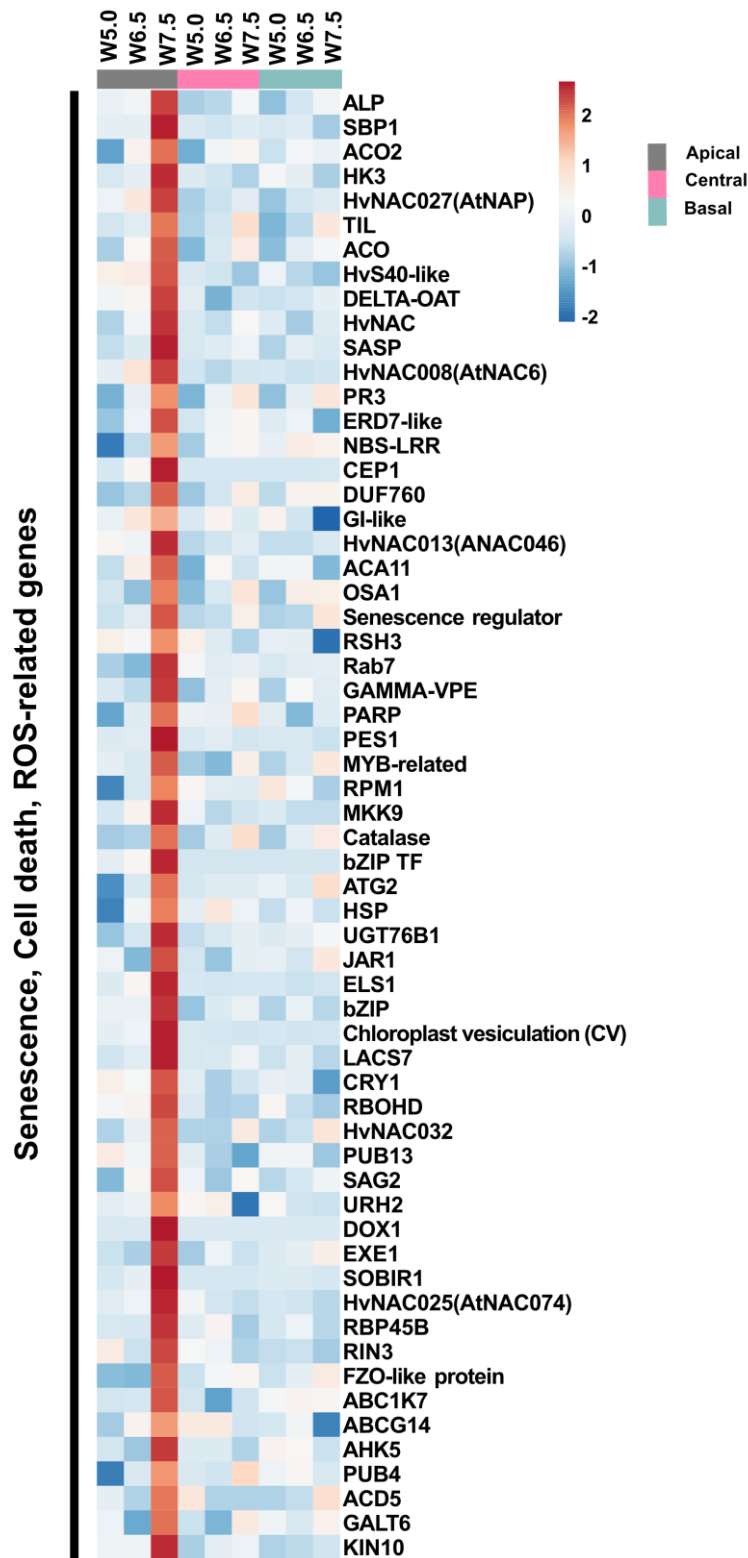


Figure 3.15. Expression heatmap of apically enriched senescence, cell-death, ROS-related genes. Heatmaps represent $\ln(X+1)$ transformed mean TPM values were depicted by color code: red, high; blue, low expression. Each rows were depicted with respective gene identifiers. W, Waddington scale.

Apically enriched Chlorophyll catabolism genes

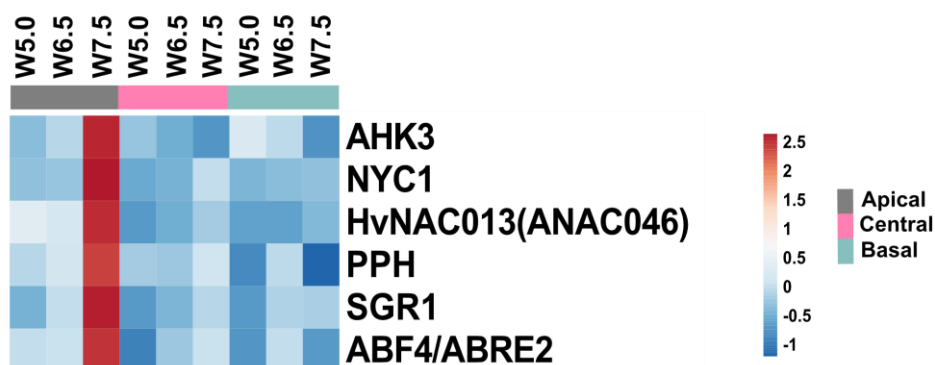


Figure 3.16. Association of chlorophyll catabolism genes and spike PTD. Heatmaps represent $\ln(X+1)$ transformed mean TPM values were depicted by color code: red, high; blue, low expression. Each rows were depicted with respective gene identifiers. W, Waddington scale.

3.3.3 Transcription factors associated with barley spike PTD

Transcription factors (TFs) tightly regulate and coordinate cell-death-related processes in plants by functioning as master regulators of transcription (Borrill et al., 2019, Schippers, 2015). To search for transcriptional regulators of barley spike PTD, we specifically analyzed TF genes among apically expressed PTD candidate genes, which represented about 9%. Among those TF genes, the MYB TF family accounted for the most, followed by genes encoding bZIPs (basic LEUCINE ZIPPERs), NACs (NAM [no apical meristem], ATAF1/2, CUC [cup-shaped cotyledon]), bHLH (basic HELIX LOOP HELIX), ERFs (ETHYLENE RESPONSE FACTORs), HD-ZIPs (HOMEODOMAIN-LEUCINE ZIPPERs), and WRKYs (Figure 3.17A). The promoters of apical-specific genes at the W6.5 were highly enriched in HOMEODOMAIN and NAC binding cis-motifs (Figure 3.17B). Consistently, many genes of the NAC TF family were expressed in the dying part, most of which have been reported to function in leaf senescence (Breeze et al., 2011, Christiansen and Gregersen, 2014, Christiansen et al., 2011) (Figure 3.18). Thus, the degeneration-associated expression of these NAC TF genes suggests the importance of the NAC regulatory network in the apical degeneration of barley spikes.

We also observed the significant enrichment of MYB-related 'GATAAG' and ABA-responsive element-binding (AREB/bZIP) 'CACGTG' cis-motifs in apical genes at W7.5, suggesting light (Kim et al., 2016) and ABA regulation (Gómez-Porrás et al., 2007), respectively, during spike PTD (Figure 3.17B). We ranked TF genes based on

their apical tissue specificity, which indicated that the top 50 genes include leaf senescence-associated NAC genes, ERF genes, and *HvGT1*, the ortholog of a key maize domestication gene (*GT1*) functioning in suppression of axillary tiller bud outgrowth (Whipple et al., 2011) (Figure 3.18), suggesting their possible involvement in spike PTD.

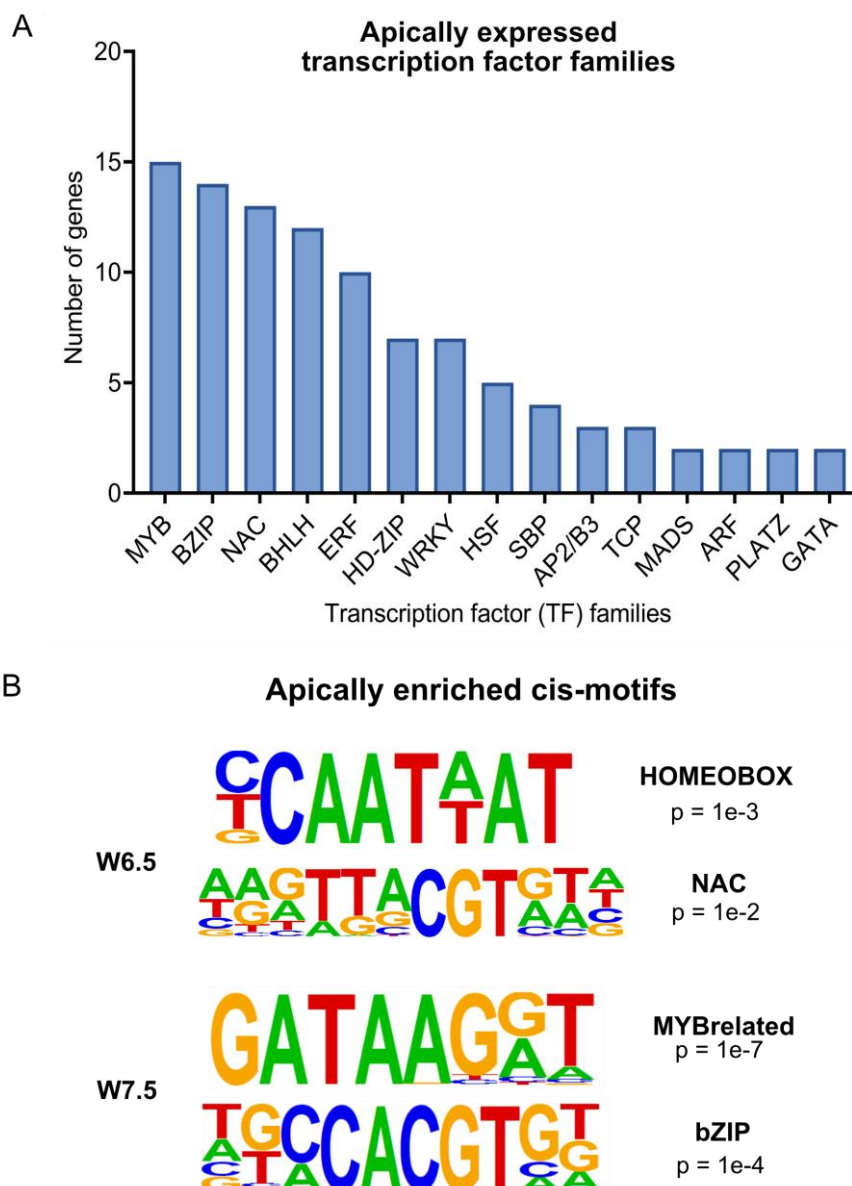


Figure 3.17. Apically expressed transcription factors families in Bowman. (A) The bar graph represents the number of transcription factor (TF) genes found among each TF family identified among apically expressed genes. **(B)** Top cis-motifs enriched with their respective p-values among the PTD-associated apical genes at W6.5 (pre-death) and W7.5 (death initiation). W, Waddington scale.

Top 50 apically enriched TFs (Ranked based on tissue-specificity)

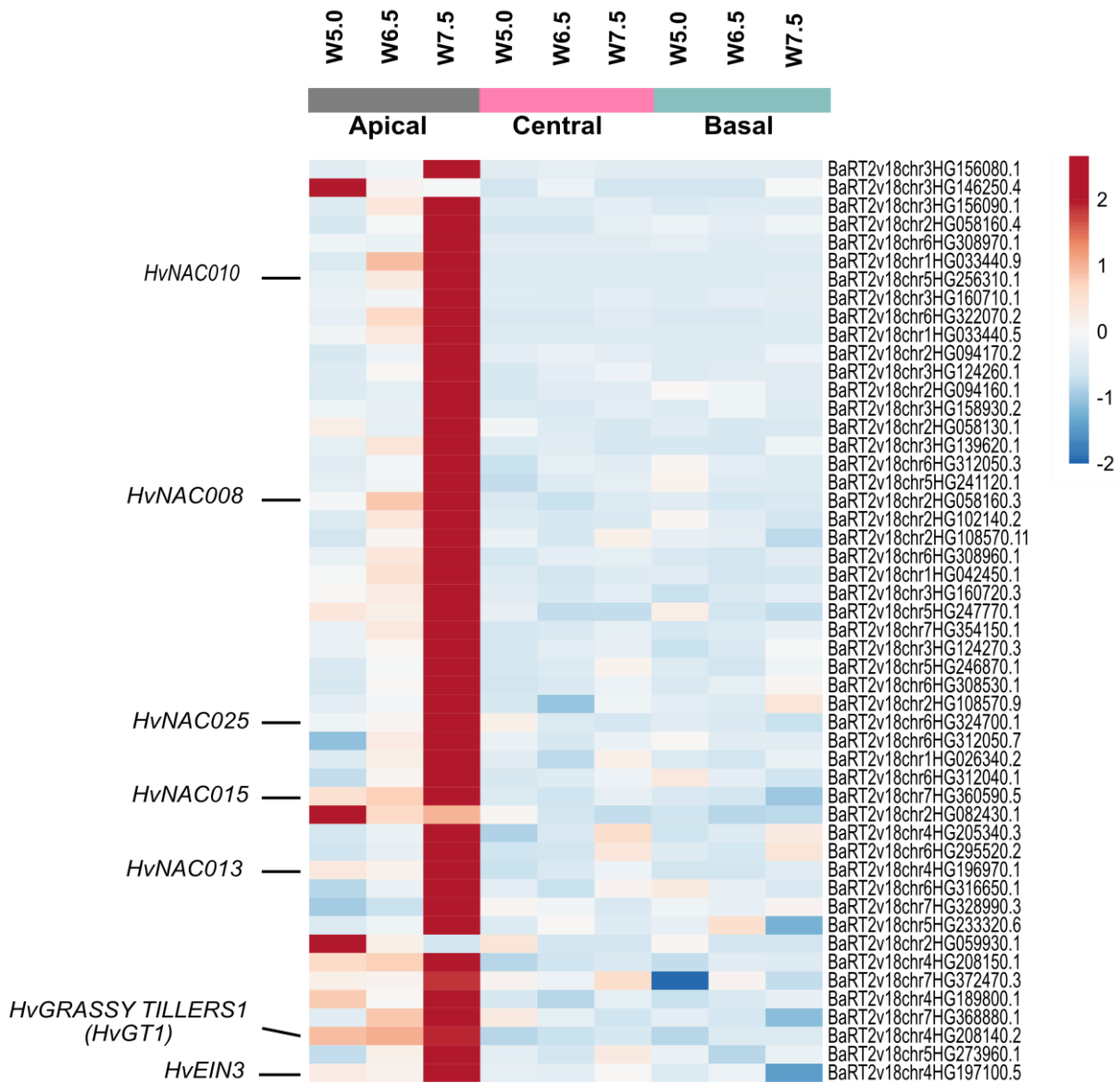


Figure 3.18. Highly ranked apical tissue-specific TF genes in Bowman. Expression heatmap of top 50 transcription factor genes ranked based on apical tissue-specific expression in Bowman and highlighted some senescence-associated genes and the barley *GRASSY TILLERS1* (*HvGT1*) gene. Heatmap represents $\ln(X+1)$ transformed mean TPM values are depicted by color code: red, high; blue, low expression. W, Waddington scale.

3.3.4 WGCNA identifies putative hub genes for barley spike PTD

Additionally, a weighted gene co-expression network analysis (WGCNA) was performed, and identified ten major modules showing different expression shapes (Methods section 2.2.10; Figure 3.19). Among those modules, the yellow module showed an increasing expression in the apical parts over the development with the genes enriched for cell-death-related processes and is chosen as a PTD-associated

gene network module (Figure 3.20A; Appendix Figure 6A). The top 10 genes were considered hub genes for the PTD module based on betweenness and centrality scores. The leaf senescence regulator *HvS40*-like gene is among the top 10 hub genes identified in the PTD-associated gene network module, which showed increased expression in the apical parts of the spike (Figure 3.20B). The putative undirected targets of *HvS40*-like were identified in this PTD-associated module, which included several *NAC* genes and *HvGT1*, while GO enrichment analysis of these targets suggested a role in cellular catabolism, autophagy, senescence, trehalose metabolism, and circadian rhythms (Figure 3.20C; Appendix Figure 6B).

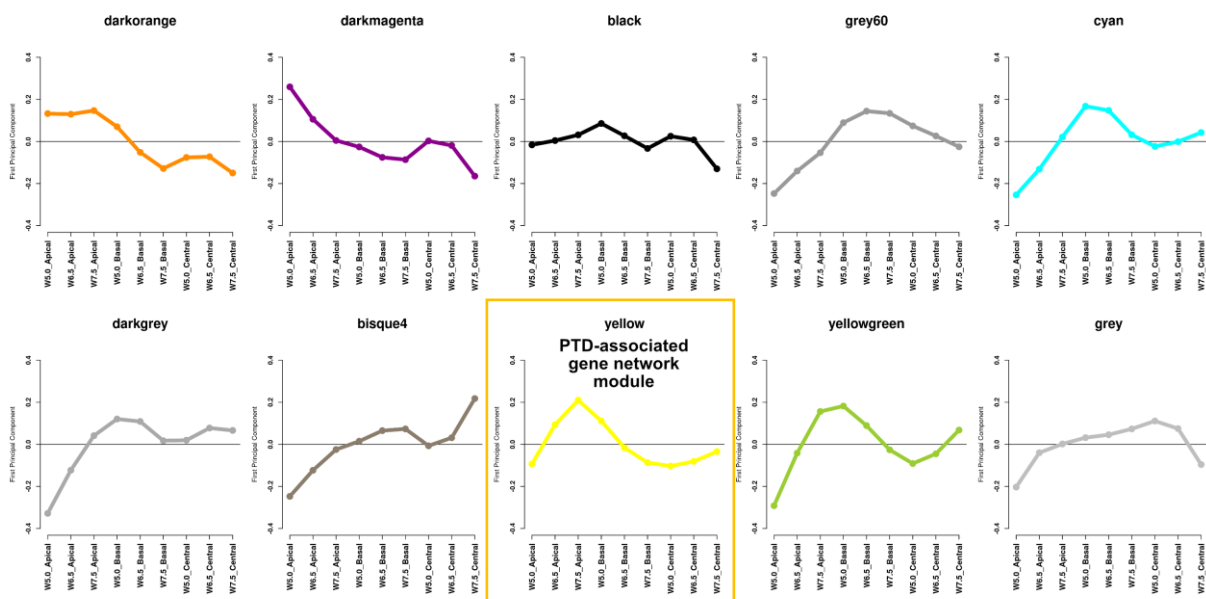


Figure 3.19. WGCNA co-expression modules in apical, central, and basal positions in cv. Bowman. Expression shapes of 10 merged modules, generated based on the correlation among the original modules in cv. Bowman. The highlighted yellow module was considered as a PTD-associated gene network module.

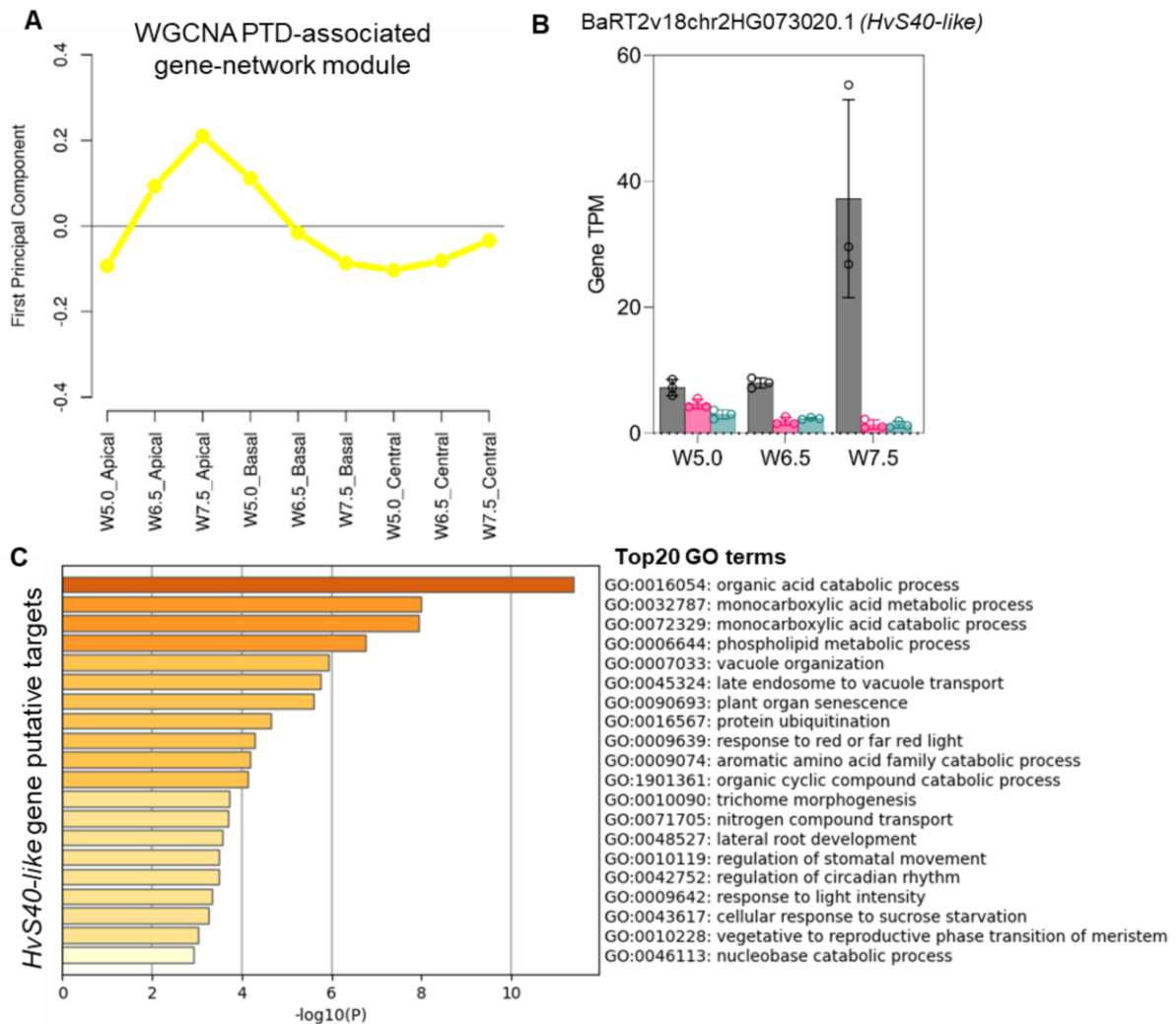


Figure 3.20. Gene co-expression network module for the barley spike PTD. (A) Expression shapes of death modules identified in cv. Bowman (yellow) by WGCNA. **(B)** Bar plots show the expression of the senescence-associated gene, *HvS40-like*, in Bowman, which has been identified as a key hub gene in Weighted Gene Co-expression Network analysis (WGCNA). Plots show means \pm SD of TPM values from three biological replicates. **(C)** GO term enrichment of putative targets of *HvS40-like* gene identified in Bowman. Color saturation corresponds to the degree of enrichment. W, Waddington scale.

3.4 HvGT1 represses apical spikelet growth

Among the top 50 transcription factor genes ranked based on their apical tissue-specific expression, we identified the class I HD-ZIP gene *HvGT1* (BaRT2v18chr4HG208140/ HORVU.MOREX.r3.4HG0399240.1) (Figure 3.21A). An independent transcriptome atlas of the barley inflorescence meristem with laser-capture microdissected tissues revealed the IM dome-specific expression of *HvGT1* at the MYP stage (Thiel et al., 2021) (Appendix Figure 7). Repressive growth functions are known for *GRAIN NUMBER INCREASE 1* (*GNI-A1*), HD-ZIP gene, and a wheat

ortholog of the barley row-type gene *VRS1* (*six-rowed spike 1*), that is expressed in rachillae and apical florets of wheat spikelets and inhibits their growth, whereas reduced *GNI-A1* function increases floret fertility and thus, grain number (Sakuma et al., 2019). *VRS1* represses lateral spikelet development in two-rowed barley (Komatsuda et al., 2007). In addition, maize *GT1* represses carpel development in tassel florets (Klein et al., 2022, Whipple et al., 2011). Moreover, *GT1* orthologs in maize (Klein et al., 2022, Whipple et al., 2011) and Arabidopsis (*HB21*, *HB40*, *HB53*) (González-Grandío et al., 2017) mediate growth repression of axillary tiller buds by ABA biosynthesis and sugar depletion. In agreement, the phytohormonal and metabolite analyses in the present study detected higher ABA levels with limited sucrose and T6P levels in degenerating apical parts, pointing to the conservation of this growth repression module during barley spike PTD. Further, HvGT1-YFP protein targets the nucleus by subcellular localization study, suggesting a transcriptional activation for HvGT1 (Appendix Figure 8A). Predicted targets of HvGT1 (undirected) identified by WGCNA co-expression network analysis included the senescence regulator *HvS40-like* and other growth repressors (Appendix Figure 6B). Hence, we focused on *HvGT1* as a candidate gene with a role in suppressing apical spikelet growth and regulating spike PTD.

To examine the HvGT1 function during barley spike PTD, we generated *Hvgt1* knockout mutants in the two-rowed cv. 'Golden Promise' (GP) using CRISPR-associated nuclease 9 (Cas9)-mediated gene editing (Figures 3.21B; Appendix Figure 8B).

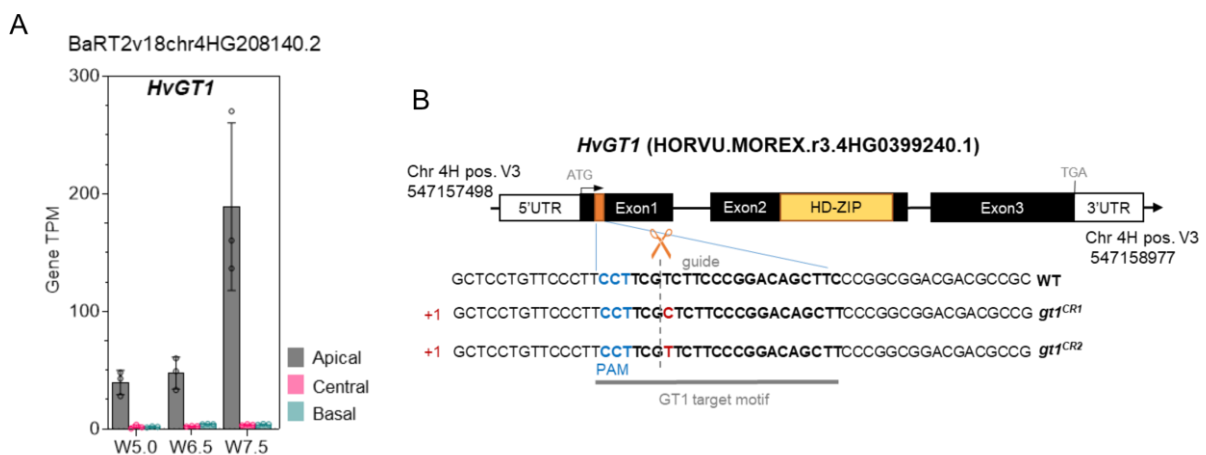


Figure 3.21. Site-directed mutagenesis of barley *GRASSY TILLERS 1* (*GT1*) by RNA-guided Cas9 endonucleases. (A) Bar plot shows the increasing apical-specific expression of the PTD candidate gene *HvGT1* in Bowman. Plots show means \pm SD of TPM values from three biological replicates. W,

Waddington scale. **(B)** Graphical representation of the guide RNA sequence with Protospacer Adjacent Motif (PAM) and a putative cutting site used to generate *HvGT1* Cas9 mutants. Chromosome position and gene ID is based on Morex reference genome version 3. Black boxes and solid black lines depict gene exons and introns, respectively. The yellow box in exon2 depicts the HD-ZIP domain. Single nucleotide insertions in the cut site are indicated in red.

No phenotypic difference was observed in the main-culm spikes at the MYP stage (W5.5) between the azygous wild type (WT) and the mutants in the T₂ generation when grown under long-day conditions in pots or natural loamy soil, as both showed a similar number (45–47) of spikelets/spikelet primordia (Methods section 2.1, 2.2.1; Figure 3.22A-B). Notably, significant differences appeared at W8.5 when visible apical death was initiated in the WT but not in mutant spikes (Figure 3.22B). During later stages, WT spikes displayed a basipetal degeneration of their apical spikelets. However, apical spikelets in the *Hvgt1* mutant plants remained alive longer, and the collapse of their inflorescence dome only commenced at around W9.5, whereas apical degeneration was nearly complete in WT spikes at the same stage (Figure 3.22C). In the *Hvgt1* mutant, many apical spikelets were still viable even at anthesis (W10), suggesting that the mutant undergoes a slower rate of degeneration progression. At the heading stage, the degenerated apical tip in WT spikes was clearly visible with dead spikelets (Figure 3.22D-E). The delayed death in the *Hvgt1* mutant was accompanied by pronounced floral organ differentiation in apical spikelets, including awns, lemma, palea, stamens, and carpel, resulting in higher spikelet survival at heading (Figure 3.23A-I). In both growth conditions tested, the *Hvgt1* mutant showed higher spikelet survival, thereby increasing the final spikelet number (Figure 3.24A-B). No differences in heading time between the WT and *Hvgt1* mutants. Although the final spikelet number was higher in the mutants at heading, the extra-surviving spikelets did not produce any regular grains in most spikes investigated. Instead, most extra-spikelets remained as a rudimentary structure with empty chaff, while no significant difference was found for the final grain number per main-culm spike between WT and *Hvgt1* mutant plants grown in both growth conditions, except for the significant decrease in *gt1^{CR2}* mutant grown in pots (Appendix Figure 9).

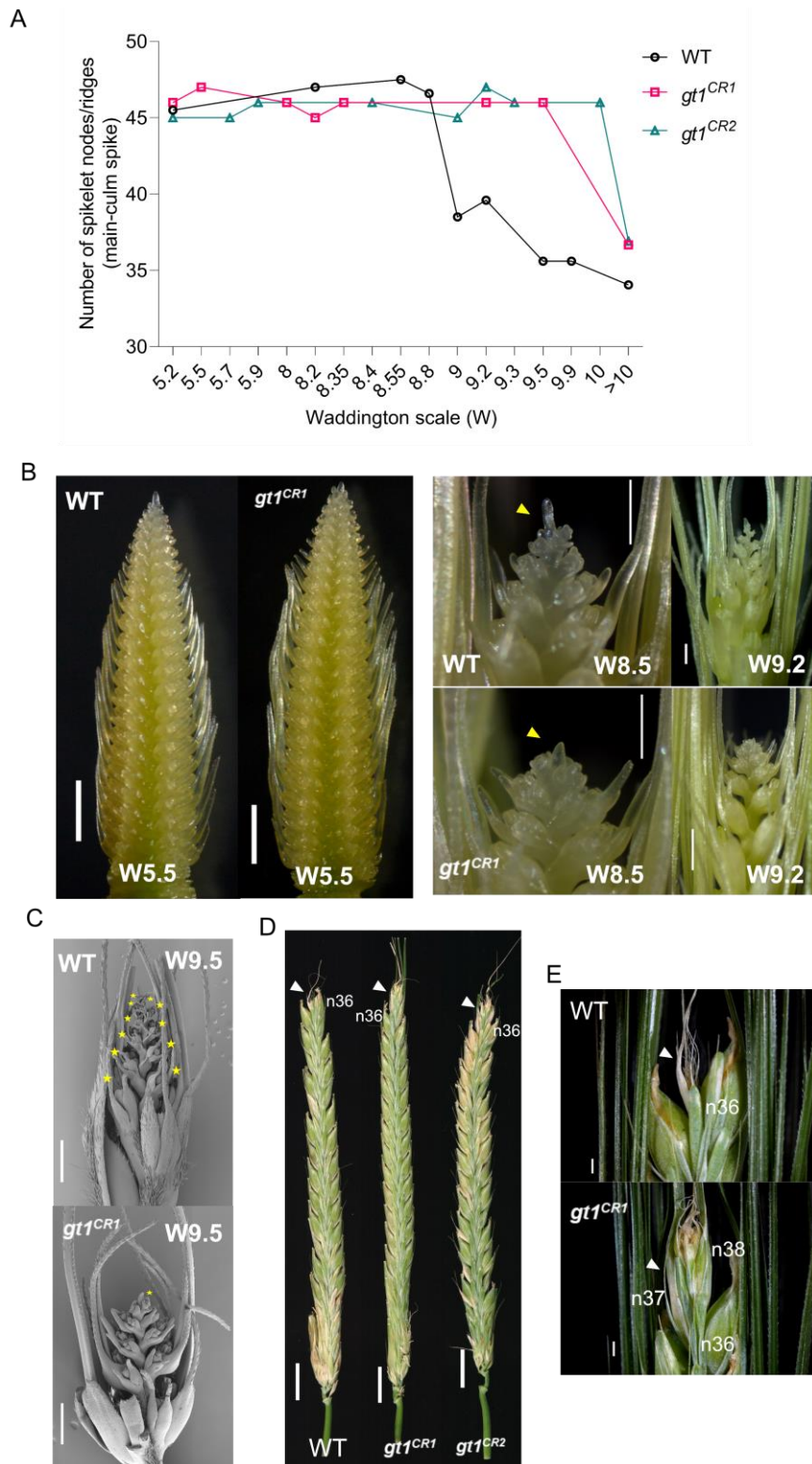


Figure 3.22. Mutation in barley *GT1* shows delayed PTD and derepressed apical growth. (A) A spike development pattern in the main-culm spike of azygous wild-type (WT) and *gt1* mutant lines (*gt1^{CR1}* & *gt1^{CR2}*) in the background of two-rowed barley cv. Golden Promise. [n=2 to 4 spikes for each data point until W10 and for >W10 n=22 (WT), 24 (*gt1^{CR1}*), 26 (*gt1^{CR2}*)] grown in pots. The x-axis shows Waddington stages and y-axis represents the number of spikelet nodes/ridges. **(B)** Representative stereomicroscope images of WT and *gt1^{CR1}* spikes. At the MYP stage (W5.5), no significant difference

was found between WT and mutant spike. Whereas at W8.5, the yellow arrows point IM that initiated PTD in WT spike, and the IM remains intact in *gt1^{CR1}* mutant spike. Mutant W9.2 in the right panel shows an intact apical part compared to degenerated WT spike. Scale bar 1 mm (left panel) and 500 μ m (right panel). **(C)** SEM images show the spike's apical part at stage W9.5 in the WT and *gt1^{CR1}*. A yellow asterisk marks the aborted nodes. Scale bar 500 μ m. **(D)** Whole spikes of WT and *gt1* mutants (*gt1^{CR1}* & *gt1^{CR2}*) at heading. The white arrow points to the region above node 36 that differs between WT and mutants. Scale bar 1 cm. **(E)** Magnified view of spike tips of WT and *gt1* mutants at heading. The white arrow points to the degenerated tip above node 36 in the WT spike and the surviving tip of the *gt1* mutant spike. Scale bar 1mm. n, node; W, Waddington scale.

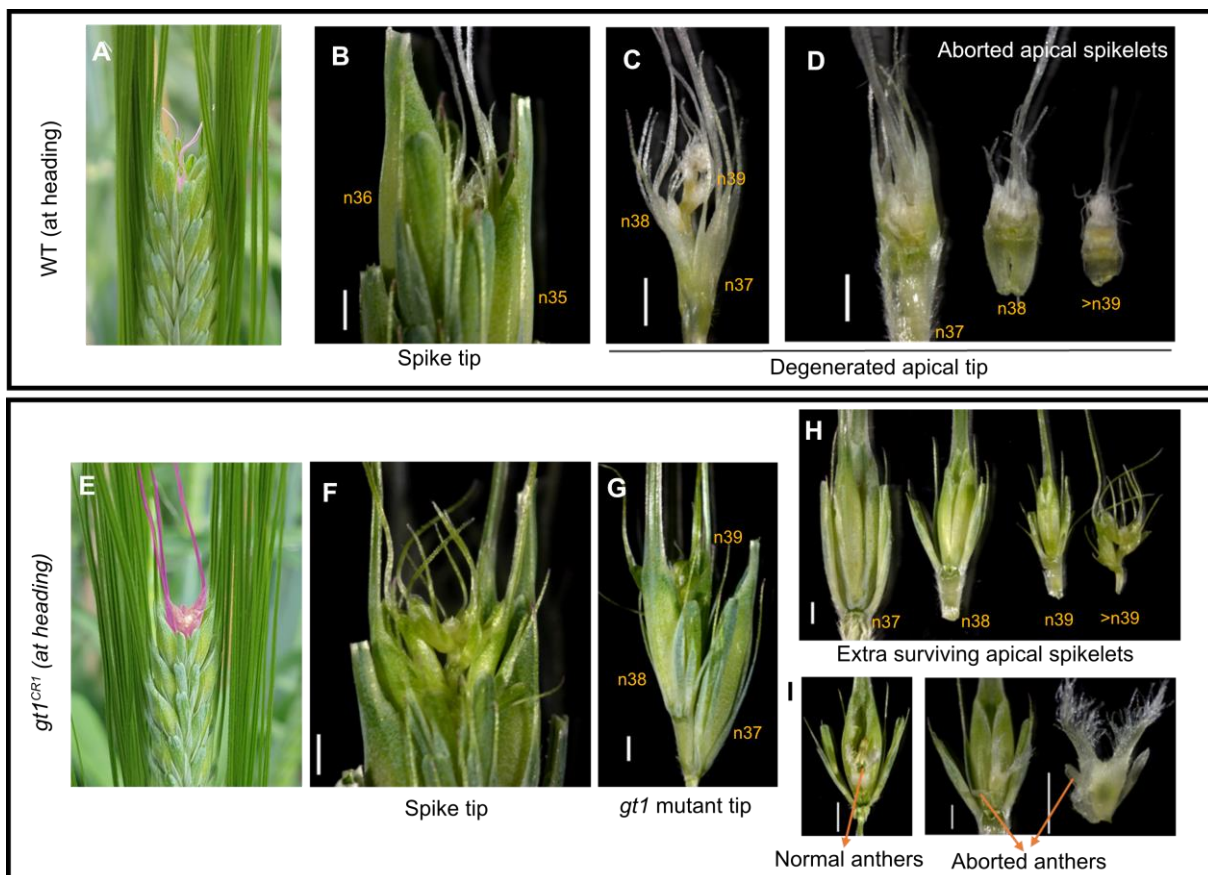


Figure 3.23. Enhanced differentiation of apical spikelets in *Hvgt1* knockout mutants. (A-D) Wild-type (WT) spike at the heading, and the images show dissected aborted tip and spikelet remnants **(D)**. **(E-I)** *Hvgt1* mutant spike at heading, and the images show dissected tip and extra-surviving spikelets **(H)**. However, the fertility of the few extra-surviving spikelets might be affected due to aborted anthers, as highlighted with the yellow arrow **(I)**. Scale bar 1mm. n, node.

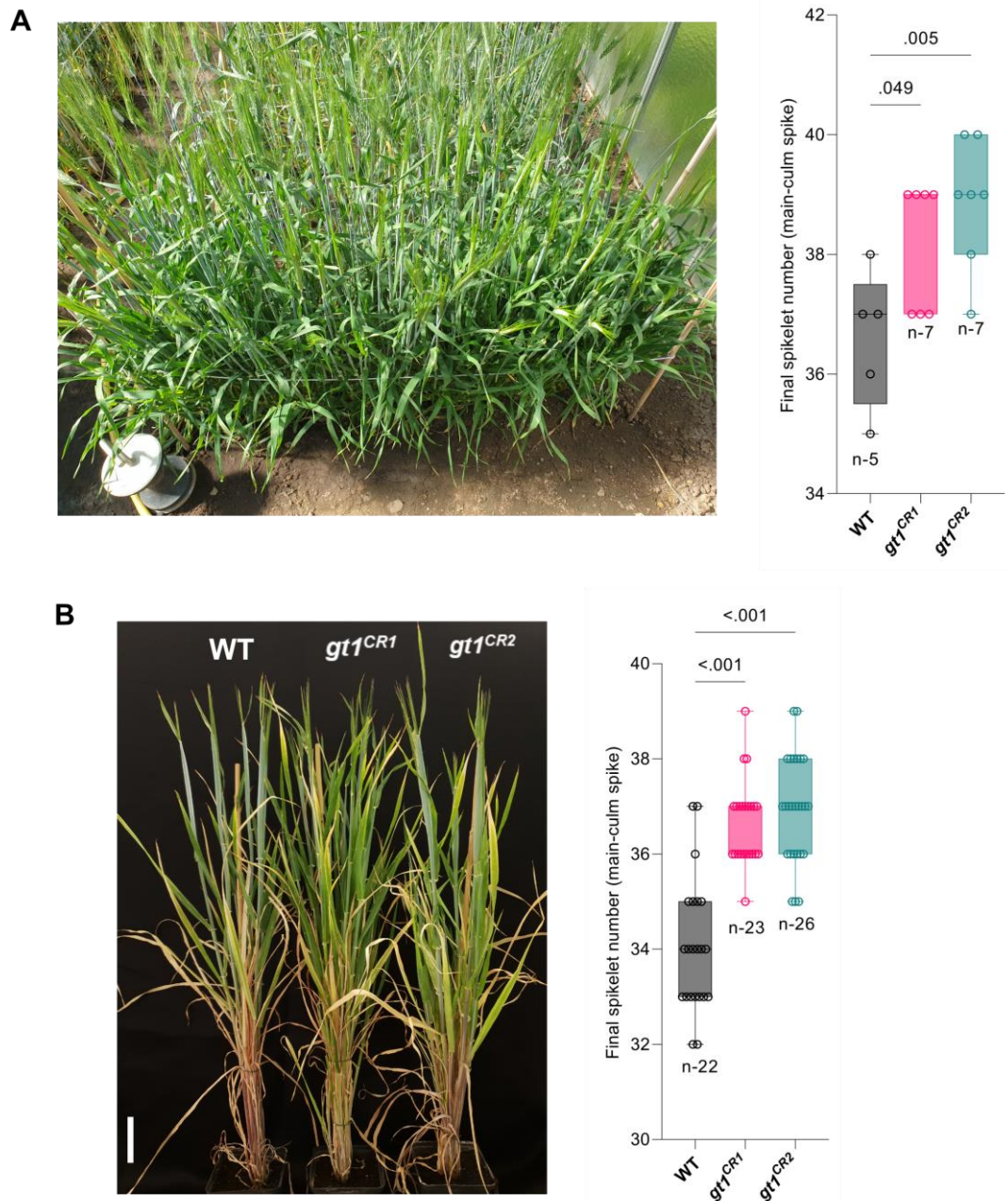


Figure 3.24. Mutation in barley *GT1* improves spikelet survival and increases the final spikelet number at anthesis. (A&B) The box plot shows the final spikelet number at the heading in the main-culm spikes of azygous WT and *gt1* mutant lines grown under a greenhouse directly in soil **(A)** and pots **(B)** (Methods section 2.1). Plots show means \pm SD with all replicate values. Significant levels are determined from the Unpaired Student's *t*-test with Welch's correction. W, Waddington scale. W, Waddington scale.

Additionally, *Hvgt1* mutant plants were found to produce significantly more tillers than their WT counterparts, as previously observed with *gt1* mutants in maize (Klein et al., 2022, Whipple et al., 2011) (Figure 3.25A-B). Later, we asked whether high tillering in the mutants might limit the sink fertility in the main-culm spike, so we performed a de-

tillering assay and found that the spikelet survival was more distinct in the de-tillered mutants compared to the de-tillered WT (Figure 3.25C-E). These observations indicate that HvGT1 plays a crucial role during spike PTD in barley and that its loss of function can delay the onset of tip death and improve spikelet survival at heading.

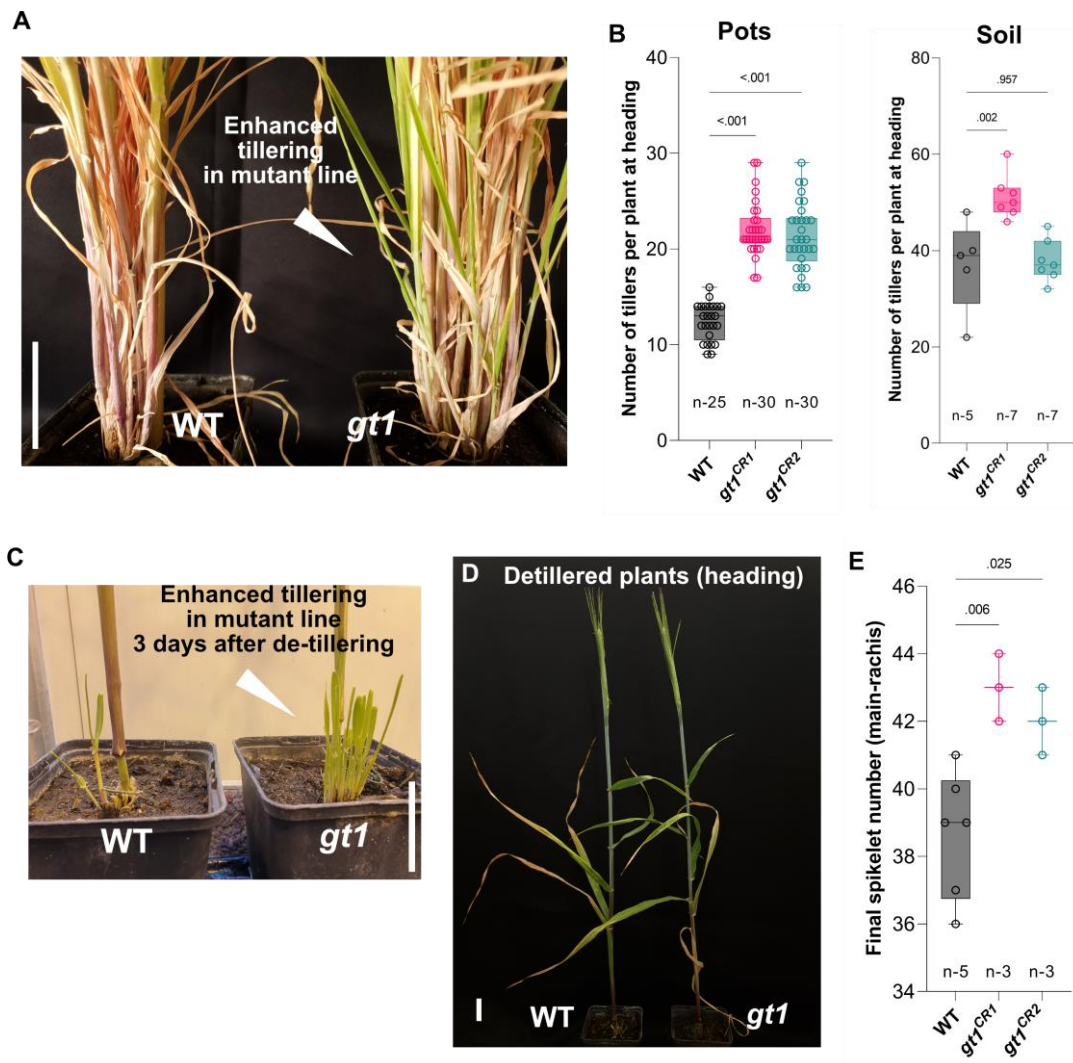


Figure 3.25. Tillering effect of barley *GRASSY TILLERS1*. (A) Pronounced tillering in *gt1* mutant lines compared to the azygous WT. The white arrow points to the enhanced tillering in the *gt1* mutant. (B) The phenotypic difference for the number of tillers in WT and *gt1* mutant lines (*gt1^{CR1}* & *gt1^{CR2}*) in soil-grown and pot-grown plants at heading. (C) Enhanced tiller outgrowth in the de-tillered *gt1* mutant plant compared to the de-tillered WT plant. The white arrow points to the enhanced tillering in the *gt1* mutant three days after detillering. (D) Representative de-tillered WT and mutant plants at heading. (E) The phenotypic difference in the final number of spikelets at heading in the de-tillered WT and *gt1* mutant lines. Bar plots show means \pm SD with all replicate values. Significant levels are determined from unpaired Student's *t*-test with Welch's correction. W, Waddington scale. Scale bar 5 cm.

3.5 Molecular changes leading to spike PTD are conserved in six-rowed barley

In barley, the fertility of the two lateral spikelets specifies spike row types: two- and six-rowed barley. In six-rowed barley, all three spikelets per rachis node are fertile and set grains, whereas both lateral spikelets are sterile in two-rowed barley. At least five genes control the lateral spikelet sterility mainly via carpel and anther abortion with growth inhibition already initiating from the triple mound stage (W2.25): *VRS1* (*six-rowed spike 1*), *VRS2*, *VRS*, *VRS4*, and *VRS5* (also named *INT-C* [*INTERMEDIUM SPIKE-C*] and *HvTB1* [*TEOSINTE BRANCHED1*]) (Koppolu and Schnurbusch, 2019, Thiel et al., 2021). However, apart from this difference between two- and six-rowed barley, we found that barley spike PTD is common in both row types. Hence, the developmental and molecular events led to a spike PTD in six-rowed cv. Morex was also investigated.

Six-rowed cv. Morex also showed robust and reproducible spike developmental patterns when grown in precisely controlled growth conditions (Figure 3.26A). Under similar growth conditions, Morex produced 35–36 rachis nodes/ridges at W5.5 (46 DAS), after which 10–11 nodes degenerated with the visible collapse of the inflorescence dome (visible death initiation stage) around W8.25 (62 DAS), with a spikelet survival rate of ~72% (Figure 3.26). PI-FDA staining also showed that cell death begins from the inflorescence dome and progresses basipetally at W8.5 (66 DAS), affecting the anthers first, similar to cv. Bowman (Figure 3.27).

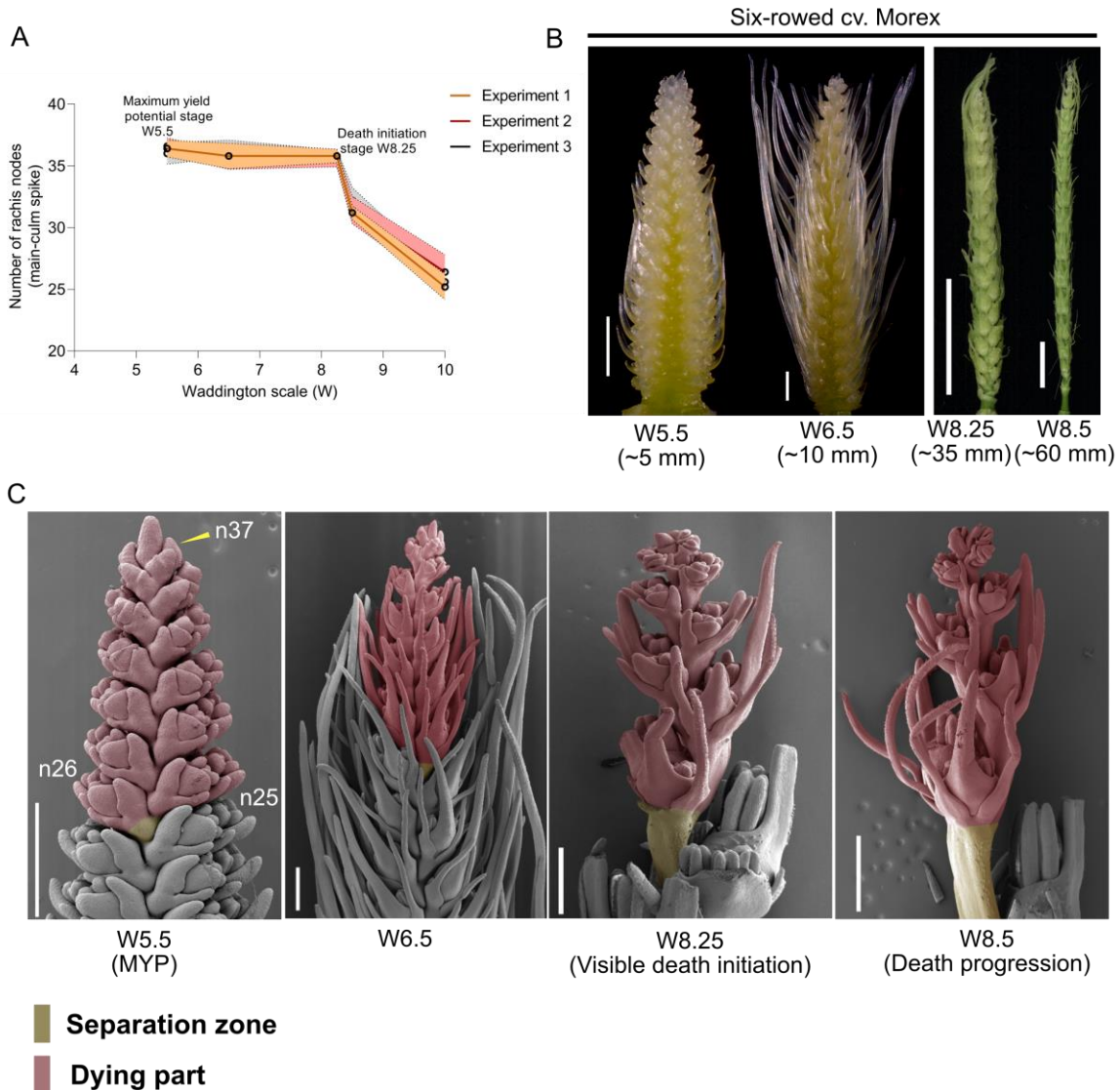


Figure 3.26. MYP, onset, and extent of PTD are reproducible in the main-culm spike of six-rowed. (A) Spike developmental pattern in the six-rowed cv. Morex. Plots represent mean and error with a 95% confidence interval from three independent experiments in standardized phytochamber conditions. The x-axis indicates stages, and the y-axis shows the number of rachis nodes produced in the main-culm spike. (B) Four developmental stages and their respective lengths within the spike growth phase of cv. Morex was considered in this study. Scale bar 1 mm (W5.5, W6.5); 1 cm (W8.25, W8.5). (C) Representative Scanning Electron Microscope (SEM) images show the suppressed growth of dying apical spikelets from the central region at four developmental stages between MYP and death progression in Morex. Dying spikelets are colored red, whereas the yellow-colored internode represents the separation zone of dying and viable parts. The yellow arrow points to the final spikelet ridge (node 37) at W5.5. Scale bar 500 μ m. n, rachis node; MYP, Maximum yield potential; W, Waddington scale.

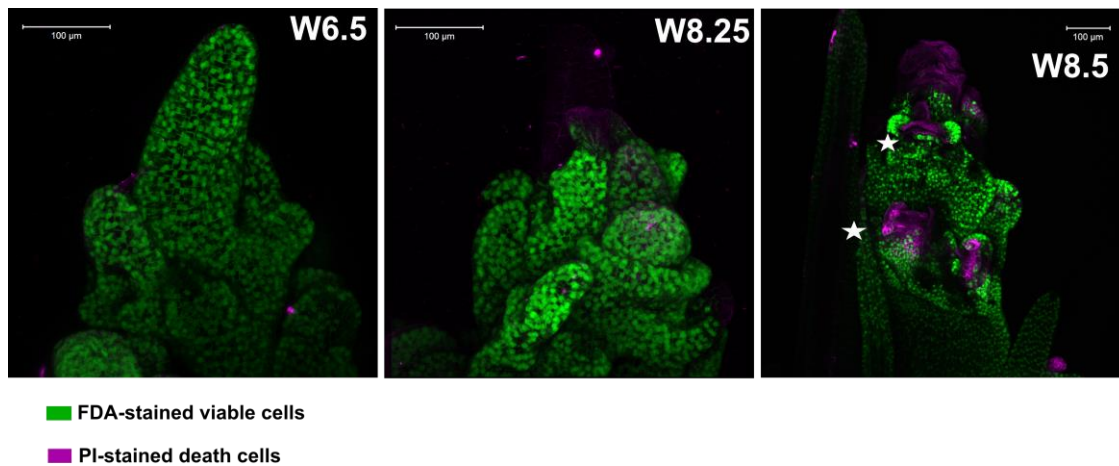


Figure 3.27. Live-death staining assay. Fluorescent dyes, Fluorescence diacetate (FDA), and Propidium Iodide (PI) were used to label Morex spikes and imaged the fluorescence under a confocal microscope. FDA (green) stains viable cells, and cells undergoing death were stained with PI (Magenta). Star in panel 3 (W8.5) points to the death of anthers in the spikelets. Scale bar 100 µm. W, Waddington scale.

Most phytohormones and metabolites showed consistent patterns similar to those seen in cv. Bowman with few differences. ABA levels peaked at W8.25 (visible death initiation) and increased ~five-fold in apical parts at the death progression stage (W8.5), pointing to a strong association between ABA and spike PTD (Figure 3.28). Auxin, CK, sucrose, T6P, and Gln levels were limited in the apical parts of Morex spikes, in contrast to the well-differentiating central and basal parts, which was consistent with their proposed importance for spikelet growth and differentiation (Figure 3.28, 3.29, 3.30). High levels of Asn, branched-chain, and aromatic AAs accumulated in apical parts, similar to cv. Bowman (Figure 3.30). However, most of these amino acids started to increase by the pre-death stage in Morex (W6.5), although visible death initiation was reasonably delayed (W8.25) compared to Bowman (W7.5) (Figure 3.30). Nevertheless, degenerating apical parts of Morex underwent a similar metabolic reprogramming as Bowman, suggesting conserved regulation of spike PTD in both barley row types.

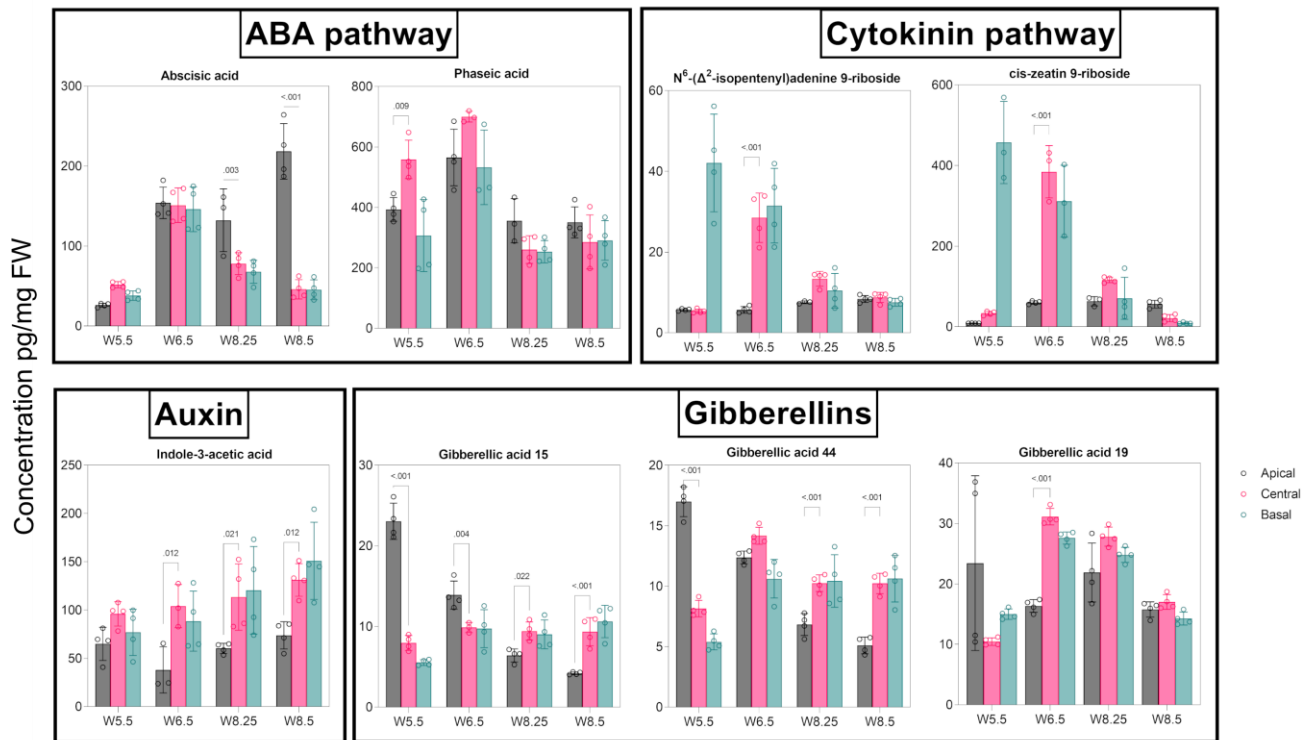


Figure 3.28. Influence of spike hormonal patterning on barley spikes PTD in Morex. Bar plots depict the distribution of ABA, cytokinins, auxin, and gibberellins, along with the three spike positions of Morex in four developmental stages. Plots show means \pm SD with significant p values calculated from three to four biological replicates. Significance was tested by Two-way ANOVA with Tukey's multiple comparison tests to evaluate the difference between apical, central, and basal positions at each stage. W, Waddington scale.

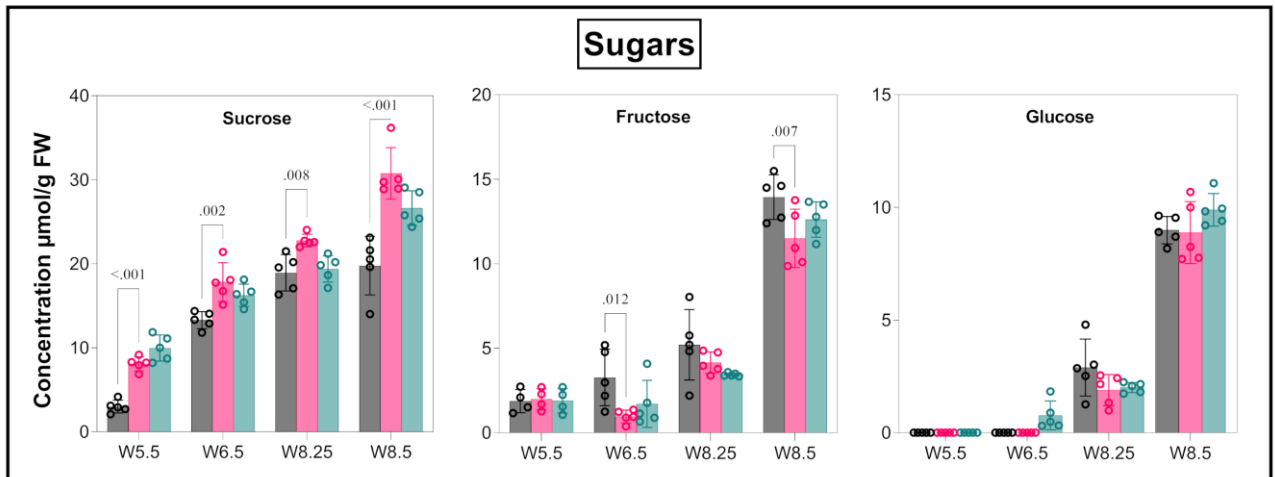
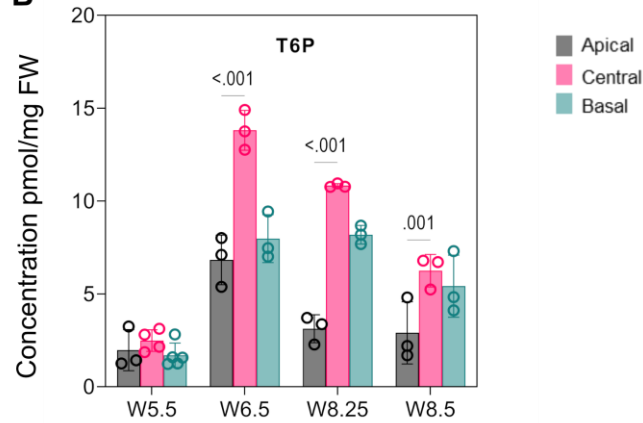
A**B**

Figure 3.29. Influence of sugars on barley spikes PTD in Morex. Bar plots depict the distribution of sugars and trehalose-6-phosphate along with the three spike positions of Morex in four developmental stages. Plots show means \pm SD with significant p values calculated from three to five biological replicates. Significance was tested by Two-way ANOVA with Tukey's multiple comparison tests to evaluate the difference between apical, central, and basal positions at each stage. W, Waddington scale.

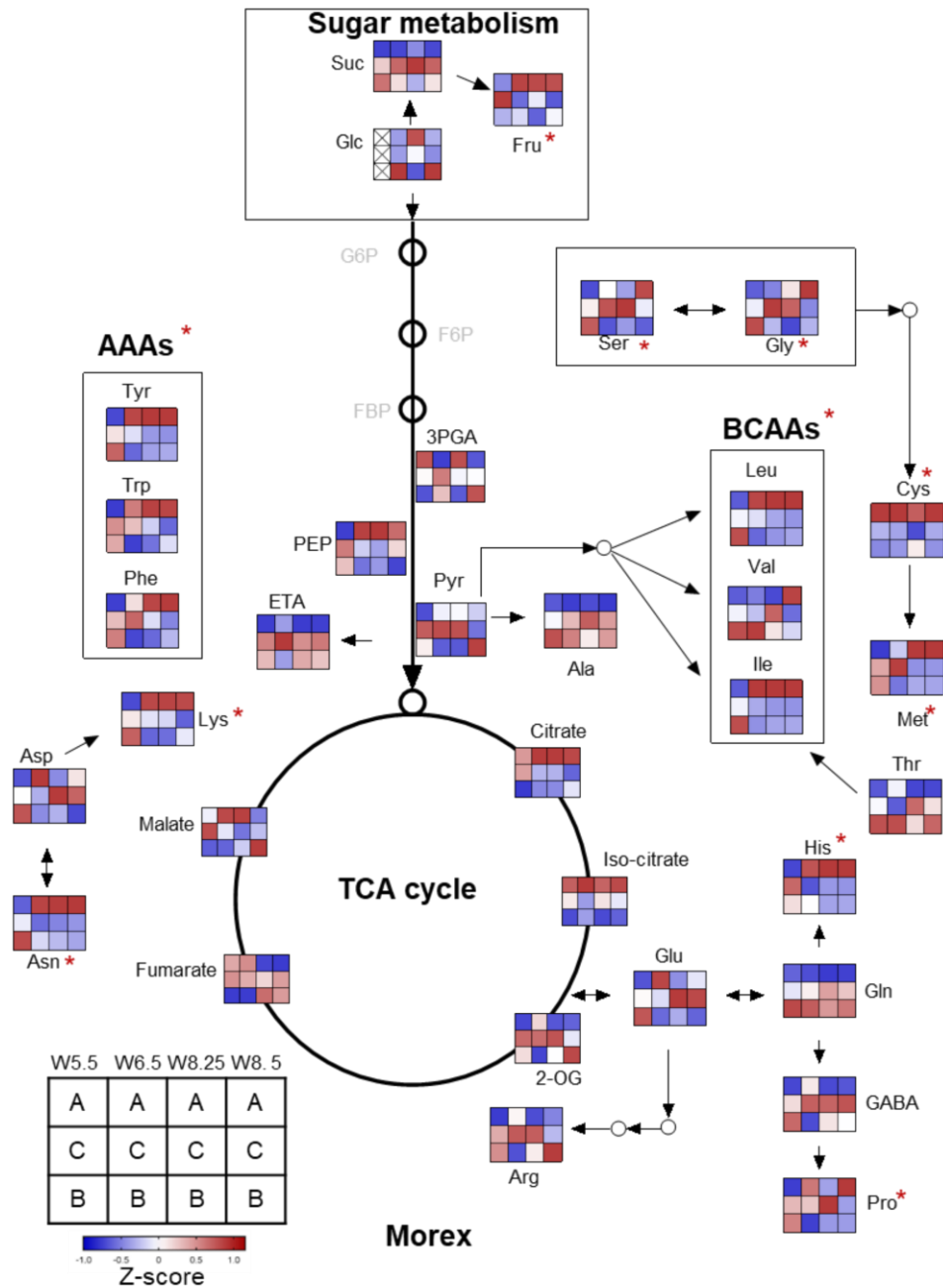


Figure 3.30. Dying apical parts display contrasting patterns of primary metabolites in Morex.

Heatmap of primary metabolite changes during the spike growth phase in Morex. Colors represent the Z-transformed ratios of apical, central, and basal parts at each stage. Suc, sucrose; Glc, glucose; Fru, fructose; T6P, trehalose-6-phosphate; Asn, asparagine; Asp, aspartate; Arg, arginine; Ala, Alanine; Glu, glutamate; Gln, glutamine, Cys, cysteine, Met, methionine; Gly, glycine; Ser, serine; His, histidine; Val, valine; Leu, Leucine; Ile, isoleucine; Phe, phenylalanine; Tyr, tyrosine; Trp, tryptophan, Thr, threonine; Lys, lysine; GABA, gamma-aminobutyric acid; Pro, proline; 3-PGA, 3-Phosphoglyceric acid; PEP, phosphoenolpyruvate; Pry, pyruvate; 2-OG, 2-Oxoglutarate; AAAs, aromatic amino acids; BCAAs, branched-chain amino acids; TCA, tri-carboxylic acid; W, Waddington scale. The red asterisk points to the amino acids and sugar enriched at high levels in the apical part during PTD.

RNA-seq analysis also highlighted the overlap in transcriptional reprogramming behind spike PTD in six-rowed Morex and two-rowed Bowman (Appendix figure 11). Enriched GO terms among DETs identified distinct biological processes differentially regulated between viable (central and basal) and degenerating apical parts similar to two-rowed Bowman (Figure 3.31A). Strikingly, most genes enriched in the apical parts of Morex significantly overlapped (623 genes; $P\text{-value} < 2.2e^{-16}$) with apically enriched genes in Bowman (Figure 3.31B). The overlapping genes included transcriptional regulator genes of light signaling, senescence, cell death, defense responses, or growth repression. Additionally, a weighted gene co-expression network analysis (WGCNA) identified the senescence regulator *HvS40*-like among the top 10 hub genes in the PTD-associated gene network module in which *HvGT1* is also co-expressed, similar to Bowman. Importantly, we also identified *HvGT1* among the top 50 (based on TPM) overlapping genes highly expressed in apical parts at all three stages (Figure 3.31C). Predicted undirected targets of *HvGT1* identified by our WGCNA co-expression network analysis included the senescence regulator *HvS40-like* similar to Bowman and other growth repressors. These observations suggest a conserved transcriptional regulation of spike PTD in both barley row types.

A Top 20 enriched GO terms for apically enriched genes in six-rowed cv. Morex

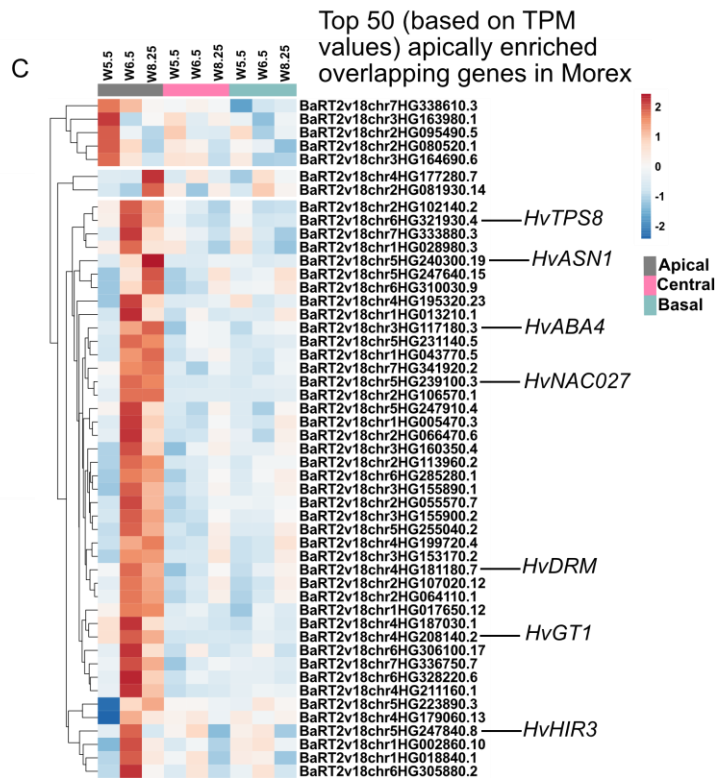
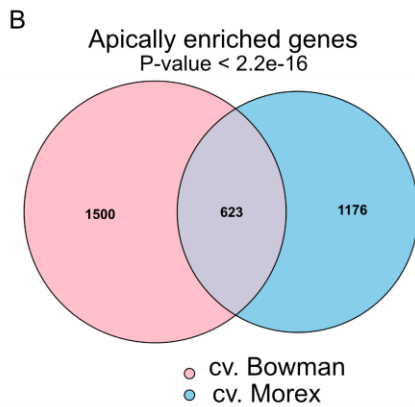
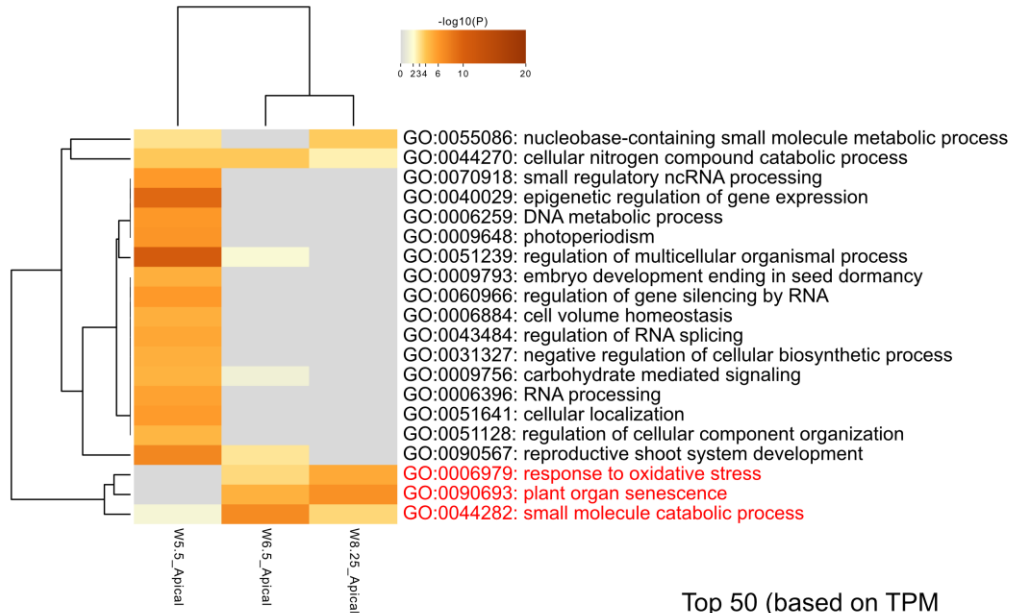


Figure 3.31. Molecular changes associated with barley spike PTD are conserved in Morex. (A)

Top 20 GO terms enriched for the apically expressed genes in the three developmental stages of six-rowed cv. Morex. Color saturation corresponds to the degree of enrichment. **(B)** Venn diagram depicting the number of genes identified as apical-specific in cv. Bowman and cv. Morex, as well as shared genes among both genotypes and p-value, showing the significance of overlap. **(C)** Expression heatmap with Euclidian distance of top 50 (based on TPM values) apically enriched overlapping genes in cv. Morex highlighted a few genes related to growth repression, senescence, abscisic acid biosynthesis, and cell death, including *HvGT1*. Heatmap represents $\ln(X+1)$ transformed mean TPM values are depicted by color code: red, high; blue, low expression. A- apical, C-central, B- basal. W, Waddington scale.

3.5.1 Natural variation in *HvGT1* regulatory region contributes to spikelet survival in six-rowed barley

In six-rowed Morex, *HvGT1* was also found to be highly expressed in the apical parts of the spike at all three stages (Figure 3.32A). Induced knockout of *HvGT1* improved spikelet survival and final spikelet number at heading in two-rowed barley. Therefore, we asked whether natural variation in and around *HvGT1* associates with spikelet survival by conducting a candidate gene association study using a panel of 358 six-rowed spring barley association (Kamal et al., 2021) and 300 diverse barley accessions (Jayakodi et al., 2020) (Methods section 2.2.16). We identified significantly associated SNPs (single nucleotide polymorphisms) ~8 kb upstream of *HvGT1* (Figure 3.32B), which is close to an open chromatin region identified by a previous study (Lu et al., 2019). We predicted that this region is recognized by bZIP TFs that play roles during stress responses and plant development, suggesting that sequence variation in this region is likely to have functional consequences (Figure 3.32C). We thus conducted a haplotype analysis based on the SNPs located close to this region. We determined that the haplotype group 6, which contained the alternative allele at the peak SNP, is associated with significantly higher spikelet survival compared to the other groups, based on phenotypic data collected from both glasshouse and field conditions (Figure 3.32D). These findings suggest that natural *HvGT1* genomic variation may contribute to phenotypic differences for barley spikelet survival.

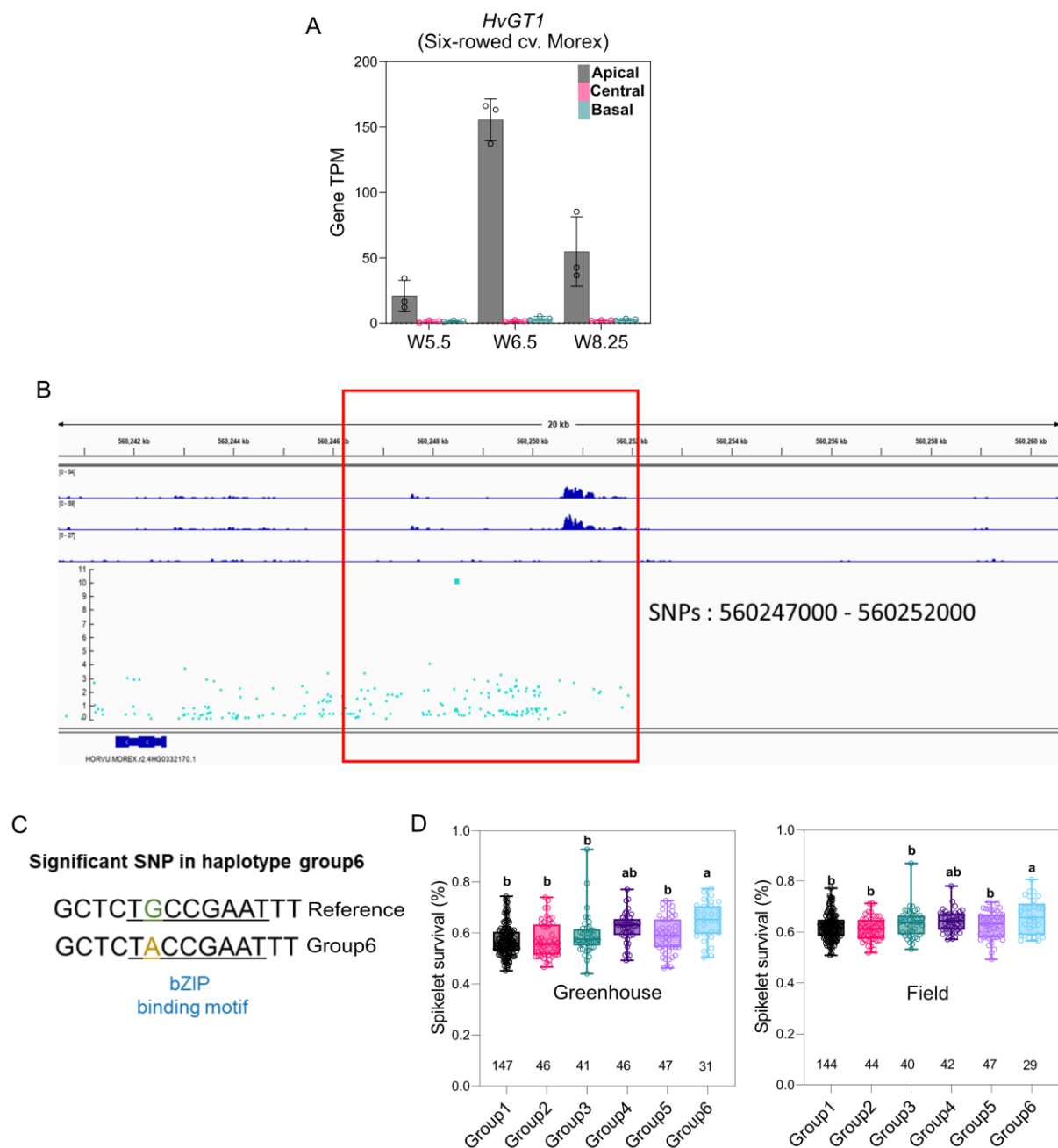


Figure 3.32. Natural variation in *HvGT1* enhances spikelet survival in six-rowed barley. (A) The bar plot shows the increasing apical-specific expression of the PTD candidate gene *HvGT1* in Morex. Plots show means \pm SD of gene TPM values from three biological replicates. (B) Significant SNPs were identified within \sim 8-kb upstream regulatory region of *GT1* from 358 six-rowed spring barley accessions (Kamal *et al.*, 2021) and 300 diverse barley accessions reported in Jayakodi *et al.*, 2020. The first and second tracks are the two replicates of the ATAC-seq data; the third is background control. (C) Significant SNP identified among the haplotype group 6 with high spikelet survival affects bZIP transcription factor binding cis-motif. (D) Spikelet survival phenotype in the six major haplotype groups (minor allele frequency \geq 0.05) among 358 six-row accessions grown in the greenhouse and field. The letters above box plots depict significant levels determined from ordinary one-way ANOVA with Tukey's multiple comparison test. W, Waddington scale.

3.6 Optimizing MALDI MS imaging pipeline for barley inflorescence meristems

As described in sections 1.4.4 and 3.2.2, the significance of metabolic regulation on plant growth and development is inevitable. However, its functions governing the developmental fate of specific organ, tissues, or cells requires our understanding of the metabolism at higher spatial resolutions. For spatial metabolomics, MALDI MSI serves as an excellent tool. Since MALDI MSI studies have not been conducted previously in immature inflorescence meristems, it was essential to adapt the method specifically for the barley meristems. A proper sample preparation pipeline, including sample embedding, cryosectioning, and uniform matrix deposition, are the major prerequisites for a successful and reproducible MALDI MSI experiment. The freshly prepared 10 % gelatin solution was suitable for embedding the barley meristems and preparing optimum cryosections with a thickness of about 10 μm . The size of the barley meristems subjected to the current MALDI MSI study ranged from ~2mm (W3.0) to ~10 mm (W7.5). Therefore, a high spatial resolution MALDI MSI was required to get better insights into the tissue- or cell-type specific distribution of metabolites. For the high-resolution MALDI MSI, the width of the laser used to irradiate the sample and the matrix crystal's size plays a significant role. However, the minimum laser size of the instrument used for MALDI MSI in the present study was limited to ~15 μm . Sublimation is one of the preferred methods for matrix deposition for high-resolution MALDI-MSI, as it produces small and homogeneous crystals over the tissues. Moreover, several studies have reported imaging of small molecules and lipids in diverse plant samples using the sublimated matrix. A glass sublimation setup is the most commonly used as it is easy to build at a low cost; however, optimizing the matrix deposition to get reproducible results between the tissues and experiments is necessary. For this purpose, a rapid and reproducible matrix deposition method was developed using an in-house sublimation setup with improved monitoring components (Shanmugaraj et al., 2023a).

Using 2,5-Dihydroxybenzoic acid (DHB), a commonly used matrix for MALDI MSI of small molecules and lipids, reproducible matrix deposition with uniform and smaller DHB crystals of less than 1 μm in width that required for high spatial ion imaging was obtained with the improved in-house built sublimation setup (Figure 3.33). Based on preliminary imaging experiments in positive ionization mode, the ion images were obtained in 15 μm /pixel resolution using a laser spot as the “minimum.” With this raster

width, endogenous metabolites of diverse classes, including amino acids, sugars, chlorophyll, and lipids, were detected in the range of 80-1000Da, distributed in specific cell types or the whole meristem section. Further, the analytes' distribution patterns and signal intensities were reproducible in the serial tissue sections and among biological replicates, confirming the method's robustness (Shanmugaraj et al., 2023a). The overall steps involved in MALDI MSI of the barley inflorescence meristems are presented in figure 3.34.

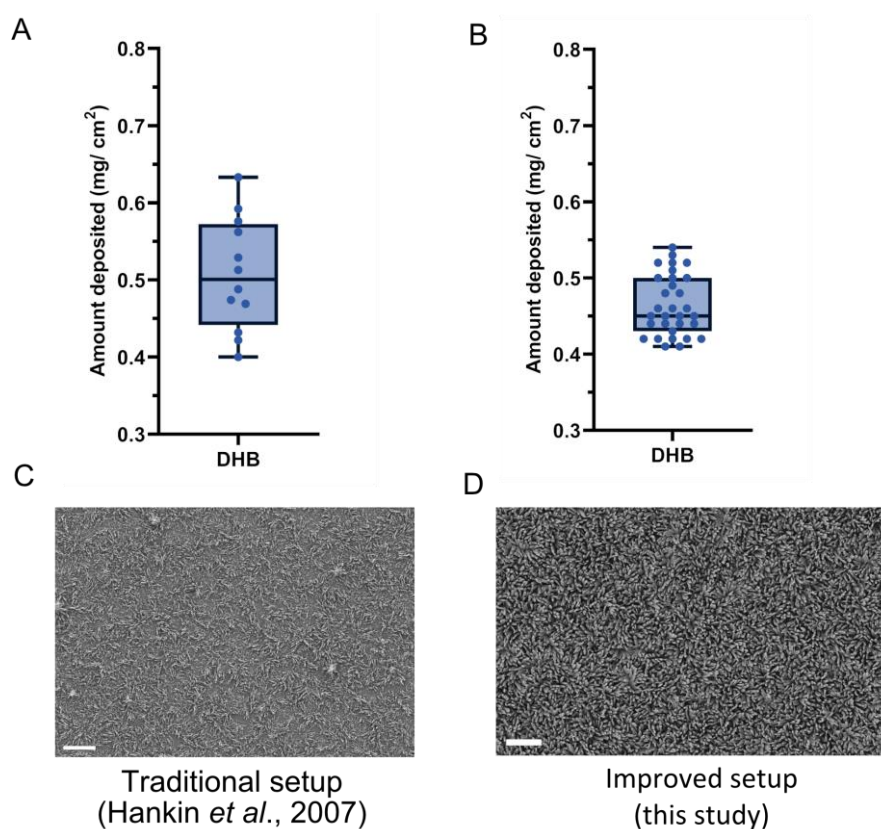


Figure 3.33. Density and size of sublimated matrix crystals. (A and C) Amount of matrix deposited per cm² in the ITO glass slides (A) and SEM images of DHB crystals (C) sublimated with a traditional setup. (B and D) Amount of matrix deposited (B) and SEM images of DHB crystals (D) sublimated with our improved setup used in this study. Scale bar 10 μ m.

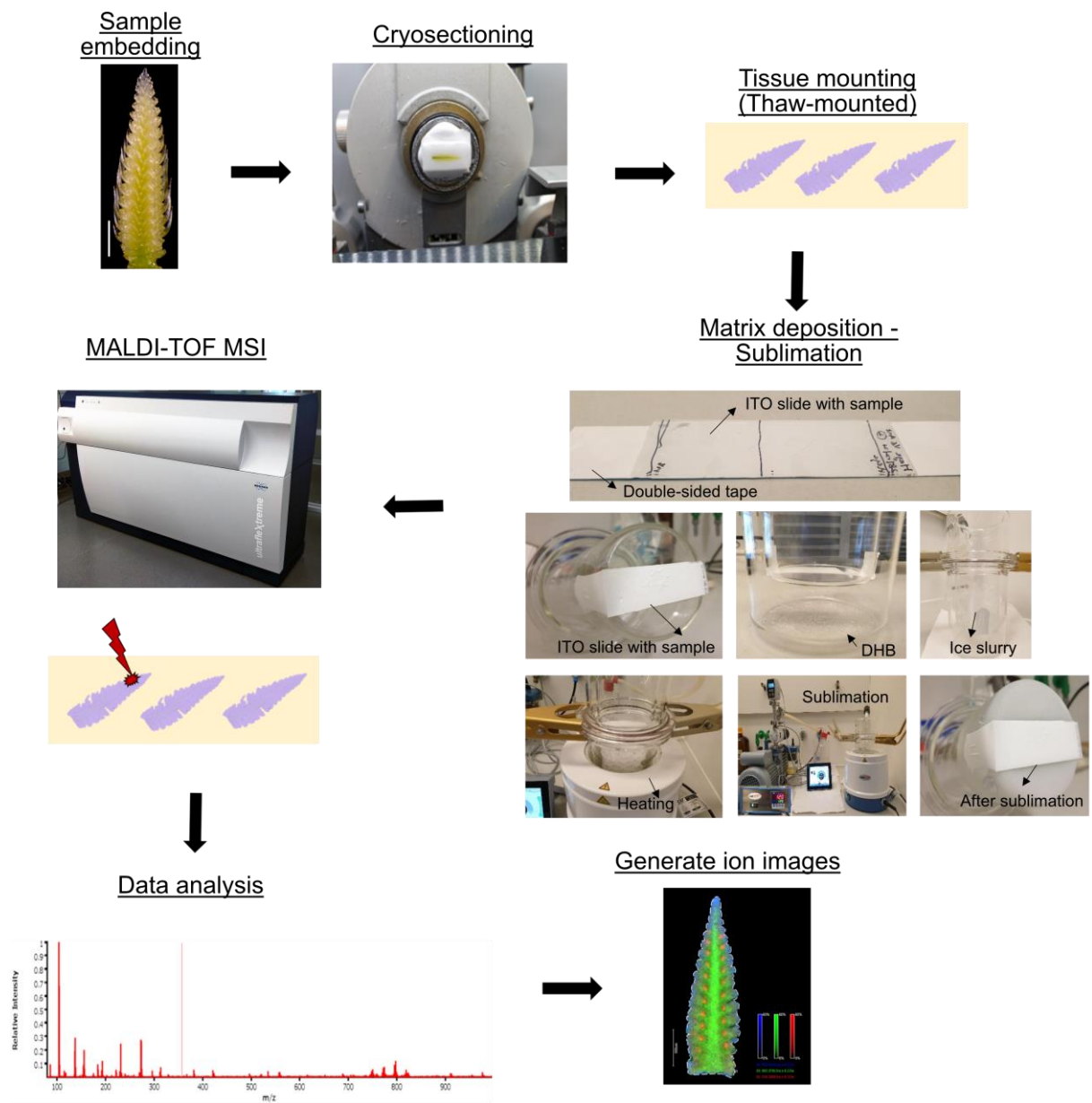


Figure 3.34. Overview of the MALDI MSI pipeline followed in this study for barley inflorescence meristems.

3.7 MALDI MSI of immature barley inflorescences

The primary aim of this study is to resolve the distribution patterns of small molecules using MALDI MSI during the early developmental stages of barley spike development in two-rowed barley (Bowman), covering spikelet initiation (W3.0, W3.5, W4.5, W5.0) and spike growth (W5.0, W6.5, W7.5) phases. Further, to identify and confirm the significance of the detected molecular ions on normal spike/spikelet development, an induced barley mutant (BW.*ts2.b*) defective in spike development was also subjected to a similar analysis. The key features of *ts2.b* mutant spikes compared to the wild type (WT - Bowman) include shorter spikes with poor spike greening, early onset and increased spike PTD, poor vascular development, altered energy and hormonal homeostasis. The percentage of dying apical nodes in the mutant is about 60% compared to the WT, which accounts for about 36% Figure 3.35A. However, no noticeable phenotypic differences between WT and mutant spikes were observed until stage W4.5. In contrast, apparent developmental differences in the mutant can be seen after W5.0. Moreover, in mutants, the visible death initiates around stage W6.0, while in WT, it starts only at around W7.5. The underlying gene responsible for the mutant phenotype was recently identified as *HvCMF4*, a CCT [CONSTANS(CO), CO-like, and TIMING OF CAB1 (TOC1)] motif family gene and functionally characterized to play a role during spikelet survival and growth by regulating spike greening, primary metabolism, light signaling, chloroplast, and vascular development (Huang et al., 2023). Considering these defective features, the mutant spikes were used as a proxy to identify metabolic signals governing normal spike/spikelet development.

Measurements were done in the whole spike sections at stages W3.0, W3.5, and W4.5, whereas the measurements were done in the divided spikes at stages W5.0, W6.5, W7.5 due to the technical difficulties in sectioning large spikes and complexity caused by awns (Section 2.2.17.1). An overview representing the samples and developmental stages investigated is shown in Figure 3.35B. All the measurements were performed using thin longitudinal sections (10 µm) of spikes from each developmental stage at a lateral resolution of about 15 µm in the mass range between 80 and 1000 Da. Although MSI was performed in a non-targeted manner, data analysis was focused on amino acids and sugars, as these classes of metabolites were also recorded by invasive metabolic analysis (Section 3.2.1). Further, the distribution of chlorophyll metabolites and the molecular ions showing interesting tissue-specific distributions and/or governing developmental stage-dependent changes were manually picked and

annotated. The results are interpreted to specify developmental stage-wise differences for specific metabolites within the spike sections and also assign their significance on spikelet development and spike PTD comparing WT and mutant.

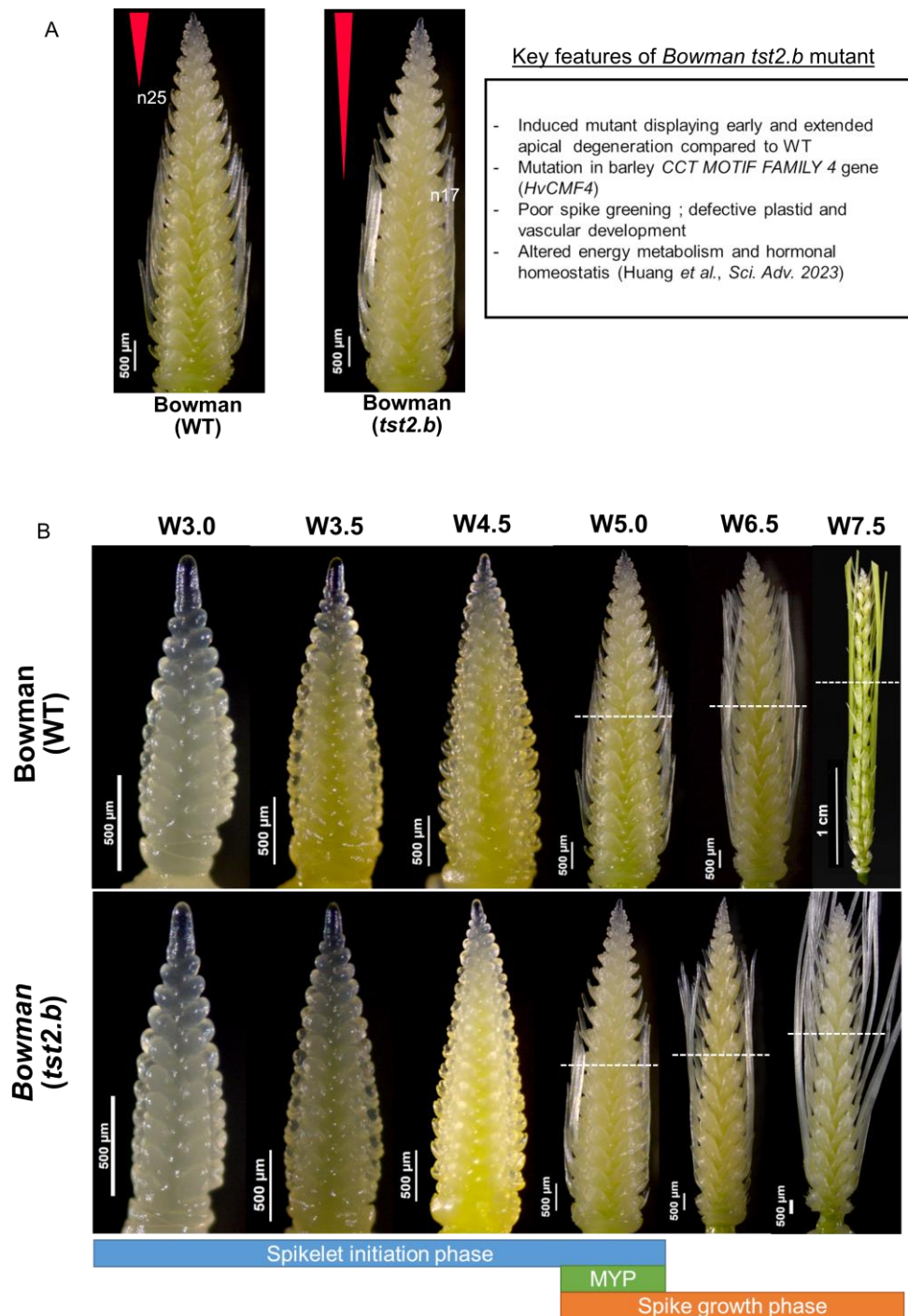


Figure 3.35. Overview of the spike samples subjected to MALDI MSI. (A) Representative stereomicroscope images of spikes from two-rowed barley Bowman (WT) and BW.*tst2.b* mutant at W5.0. The red arrow depicts the extent of spike PTD. Nodes marked represent the last surviving spikelet nodes. Text in the box brief the key phenotypes of *tst2.b* mutant. **(B)** Six spike developmental stages in WT and mutant covering spikelet initiation and spike growth phases subjected to MALDI MSI. Dashed

lines depict the position at which spikes were divided at the growth phase for MALDI MSI studies. n, rachis node; MYP, Maximum yield potential; W, Waddington scale.

3.7.1 Spatiotemporal distribution of specific amino acids and sugars

The average mass spectrum from the MALDI MSI done in positive ionization mode at each developmental stage showed the presence of molecular ions typically derived from the sample regions. The representative mass spectrum from the WT section at W5.0 is shown in figure 3.36A. The m/z values and the descriptions of the detected ions are presented in Table 1. Tentative identification of detected m/z values based on database and literature search indicated the presence of sugars and amino acids. Further, absolute quantification of sugars and amino acids done previously (section 3.2.2) using the spike parts was also used for validation and interpretation of MSI-detected signals. Ion signals corresponding to sugars (disaccharide, m/z 381.1 \pm 0.1 Da; trisaccharide, m/z 543.1 \pm 0.1 Da; tetrasaccharide m/z 705.2 \pm 0.1 Da; pentasaccharide m/z 867.2 \pm 0.1 Da) with potassium adducts [M+K]⁺ and amino acids (asparagine, Asn m/z 133.1 \pm 0.1 Da; glutamine, Gln m/z 147.1 \pm 0.1 Da; histidine, His m/z 156.1 \pm 0.1 Da, alanine, Ala m/z 90.1 \pm 0.1 Da, valine, Val m/z 118.1 \pm 0.1 Da) in protonated [M+H]⁺ forms were detected (Figure 3.36B, C).

Table 1. Tentative identifications of detected molecular ions in the present study.

Compound class	Compound	Monoisotopic mass (Da)	Sum formula	Obtained $m/z \pm 0.1$ Da	Corresponding ion(s)
Amino acids	Glutamine	146.069	C ₅ H ₁₀ N ₂ O ₃	147.1	[M+H] ⁺
	Asparagine	132.053	C ₄ H ₈ N ₂ O ₃	133.1	[M+H] ⁺
	Histidine	155.069	C ₆ H ₉ N ₃ O ₂	156.1	[M+H] ⁺
	Alanine	89.047	C ₃ H ₇ NO ₂	90.1	[M+H] ⁺
	Valine	117.078	C ₅ H ₁₁ NO ₂	118.1	[M+H] ⁺
Sugars	Disaccharide	342.116	C ₁₂ H ₂₂ O ₁₁	381.1	[M+K] ⁺
	Trisaccharide	504.169	C ₁₈ H ₃₂ O ₁₆	543.1	[M+K] ⁺
	Tetrasaccharide	-	C ₂₄ H ₄₂ O ₂₁	705.1	[M+K] ⁺
	Pentasaccharide	-	C ₃₀ H ₅₂ O ₂₆	867.1	[M+K] ⁺
Polyamines	Spermidine	145.157	C ₇ H ₁₉ N ₃	146.1; 129.1	[M+H] ⁺ ; [M+H-NH ₃] ⁺
	Spermine	202.215	C ₁₀ H ₂₆ N ₄	203.2	[M+H] ⁺
Lipid	LPC (16:0)	495.332	C ₂₄ H ₅₀ NO ₇ P	496.3; 534.3	[M+H] ⁺ ; [M+K] ⁺
Tetrapyrrole	Chlorophyll <i>a</i>	892.535	C ₅₅ H ₇₂ MgN ₄ O ₅	893.5	[M+H] ⁺
	Pheophytin <i>a</i>	870.565	C ₅₅ H ₇₂ N ₄ O ₅	871.5	[M+H] ⁺

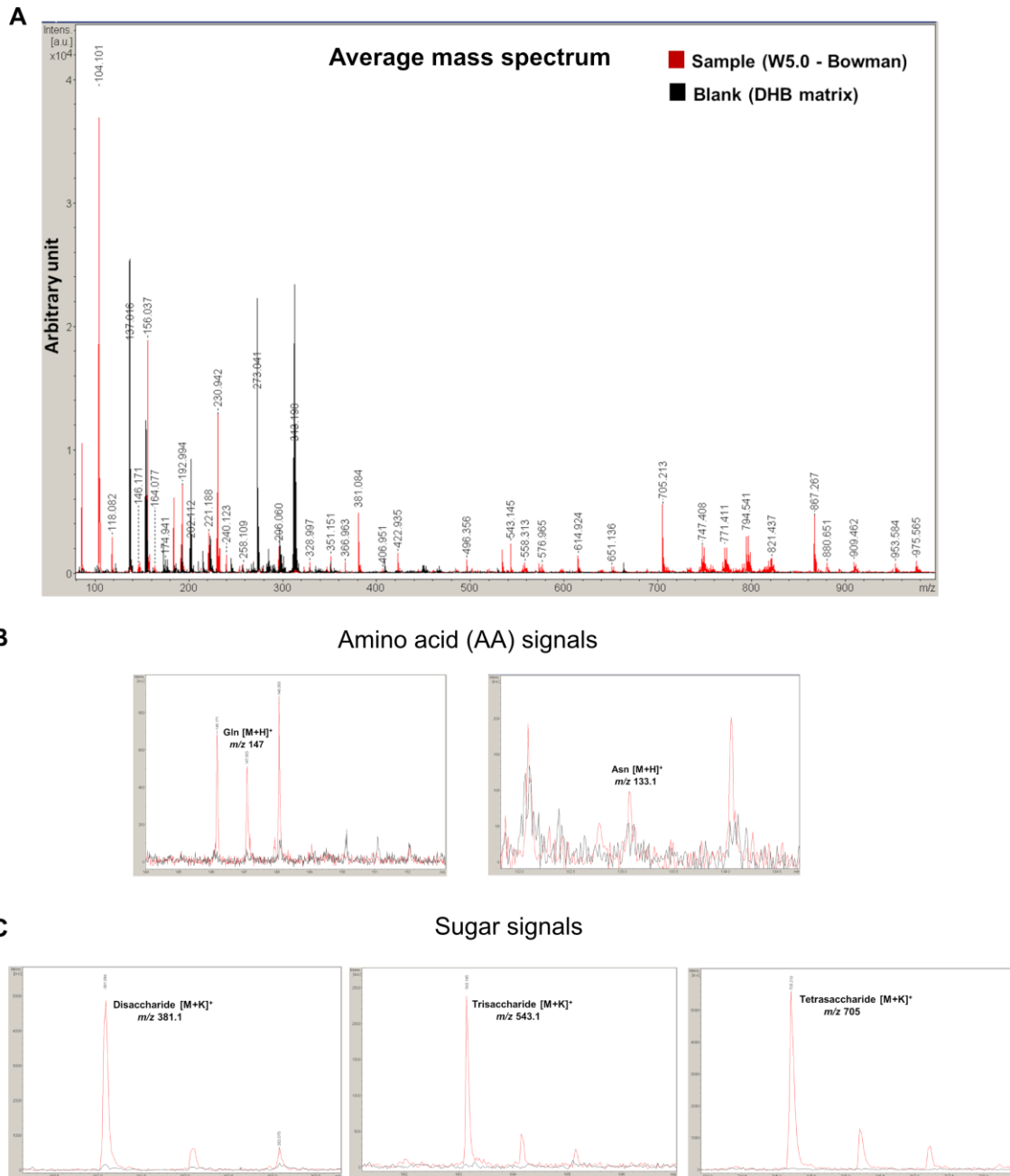


Figure 3.36. MALDI MSI in barley inflorescence meristem sections. **(A)** Representative normalized average mass spectrum from MALDI-MSI on meristem sections at W5.0 using DHB matrix in positive ionization mode. The horizontal axis shows m/z values, whereas the vertical axis shows the relative intensity of the signals. **(B)** MALDI spectra of amino acid Glutamine (Gln) and Asparagine (Asn) signals and their corresponding m/z values. **(C)** MALDI spectra of sugar signals and their corresponding m/z values.

The primary amino acid Gln, which plays a significant role in plant N metabolism, showed prominent patterns during the spikelet initiation phase in both WT and mutant (Figure 3.37A). Starting from W3.0, the distribution of Gln was more towards proximal to central parts of the section, while weak signals were in the few apical nodes. The

striking difference was found in the mutant at W4.5, where the signal is more restricted towards the basal half and almost absent in the apical half of the section. Whereas, during the spike growth phase from W5.0, the corresponding Gln peak is almost absent in the apical half of the mutant section. In contrast, WT apical section showed a gradient acropetally from node 17 towards the apex at W5.0, while at W6.5, the Gln signal was almost lost in the PTD region starting from node 24. Free Asn that plays a central role in N storage and transport in plants also accumulates at high levels in stressed and senescing tissues in several plant species. The m/z signal corresponding to Asn showed a typical pattern of enriching high in the apical part of the sections in both WT and mutant during the spike growth phase (Figure 3.37B). Specifically, it was high in the PTD zone at stages W6.5 and W7.5, which was lowest until W5.0 in WT and uniformly distributed in the mutant. Further, previous invasive measurements (section 3.2.2) in the WT also showed a higher accumulation of Asn in apical spike parts during later stages. The distribution of Asn is extended to a few more nodes down in the PTD zone at stages 6.5 and W7.5 of the mutant section compared to WT. However, at W7.5, Asn is absent in the topmost nodes in the mutant section as they are already degenerated, which points to the direction that the changes in Asn distribution might be associated with PTD.

Regarding the spatial distribution of sugars detected at stage W3.0, signals corresponding to disaccharides, m/z 381.1 ± 0.1 Da $[M+K]^+$, were found distributed in the whole spike with more abundance towards the base (Figure 3.37C). At W3.5 and W4.5, signals are almost absent in the IM and a few apical nodes underneath, while higher abundance is seen in the proximal region of the sections in both WT and mutant. Whereas, during the spike growth phase, at W5.0 and W6.5 in WT sections, the signals corresponding to disaccharide were found low towards the apex but showed higher signals in the apical nodes at W7.5. In contrast, disaccharide signals were present at higher intensities in mutants starting from W5.0 in the whole apical sections above node 18. Signals were absent in the few topmost nodes in the mutant at W7.5, as they have already degenerated.

Plants also produce several oligosaccharides that are composed of different hexose subunits. For example, raffinose family oligosaccharides such as raffinose and stachyose were found to play a role in plant development, stress responses as well as storage of carbohydrates in sink tissues (Yan et al., 2022). Signals m/z 543.1 ± 0.1 Da

$[M+K]^+$, m/z 705.2 \pm 0.1 Da $[M+K]^+$ and m/z 867.2 \pm 0.1 Da corresponding to tri-, tetra-, and pentasaccharides respectively, were detected at high levels during the spike growth phase in WT and mutant sections (Table 1; Appendix Figure 11). In contrast, all three signals were absent in the IM dome at W5.0. The striking difference is seen at W6.5 and W7.5, where the signals are weak or almost absent in PTD nodes in mutant and WT. Moreover, both oligosaccharide signals were distributed at high levels only in the viable nodes of the sections at W6.5 and W7.5, pointing their function towards the growth of surviving spikelets.

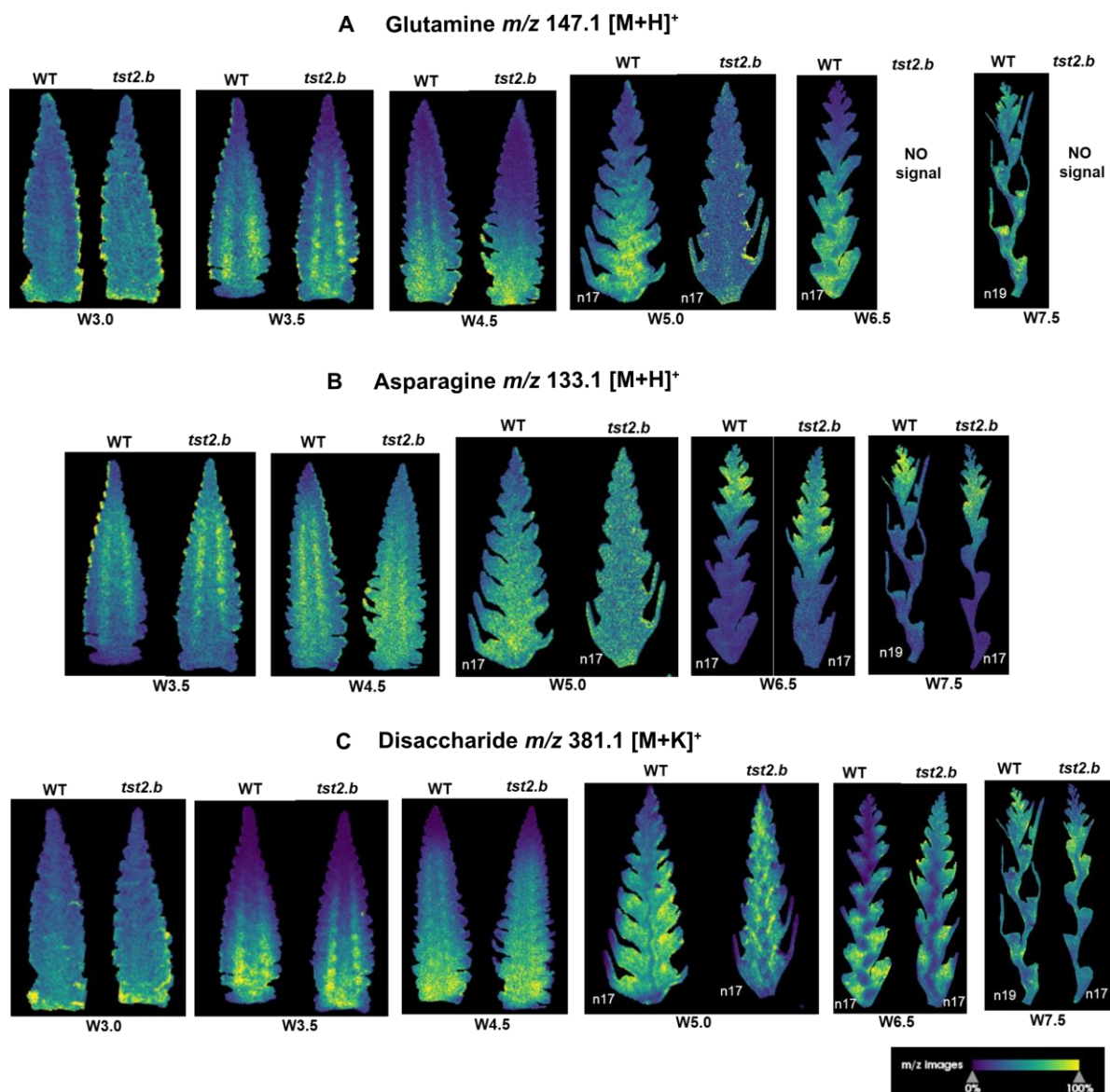


Figure 3.37. Spatial distribution of amino acids and sugar signals identified by MALDI MSI in barley inflorescence meristem sections. (A) Distribution of Glutamine in Bowman and *BW.tst2.b* mutant sections. Gln signals are absent in the mutant sections at W6.5 and W7.5 stages. **(B)** Distribution of asparagine in Bowman and *tst2.b* mutant sections which shows higher intensities in the apical part at

W6.5 and W7.5. **(C)** Distribution of disaccharide signal in Bowman and *tst2.b* mutant sections. Distributions are presented in the whole spikes at W3.0 to W4.5 while divided apical sections from W5.0 to W7.5. Images are shown as normalized single ion intensity maps with 15- μ m pixel size generated from Scils lab software. The color map corresponds to the intensity of ions. n, rachis node; W, Waddington scale.

3.7.2 MSI identifies tissue-specific metabolites vital for proper spikelet development

As mentioned earlier, MSI offers excellent potential for untargeted metabolomics. MALDI MSI in barley spike sections revealed the interesting tissue-specific distribution of several unknown metabolite signals, among which a few were selected manually and annotated. Developing barley inflorescence is a complex structure with multiple cell types with distinct identities and fates. A brief representation of the spike section at W4.5 with multiple cell types and identities is shown in figure 3.38. Revealing the distribution of metabolites in each specific cell type in spikes may help identify metabolic pathways governing differentiation, developmental transitions, meristem maintenance, spikelet growth or survival, and vascular development.

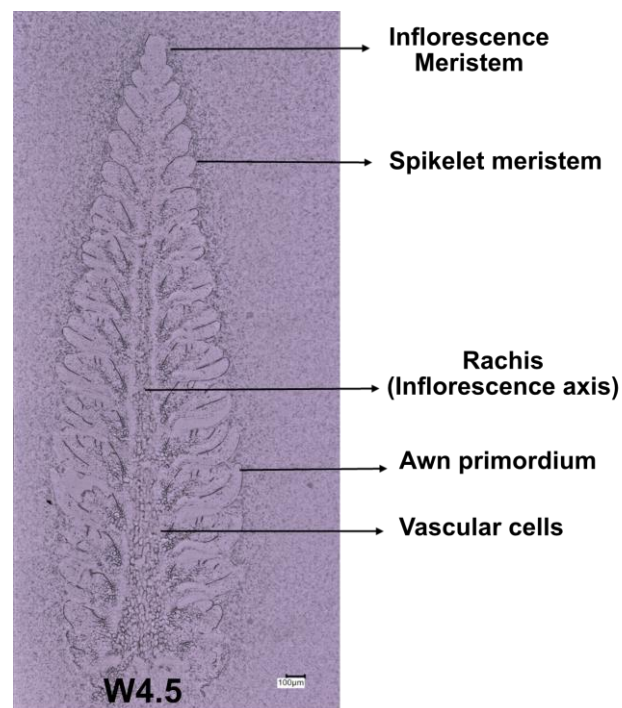


Figure 3.38. Representative longitudinal section of barley inflorescence meristem at W4.5 marked with different tissue types.

Chlorophyll metabolites

Early inflorescence greening is proposed to be unique to cool-season grasses, Pooideae (Huang et al., 2023) and might have contributed to adaptation to temperate regions (Zhang et al., 2022). The difference in the spike greening between WT Bowman and BW.*tst2.b* mutant and its significance on normal spike/spikelet growth was recently identified. This study also found an acropetal gradient of three chlorophyll metabolites, including chlorophyll *a* 893.1 ± 0.1 Da $[M+H]^+$ and pheophytin *a* 871.1 ± 0.1 Da $[M+H]^+$ in longitudinal tissue sections (Table 1). No significant difference between WT and mutant was seen until W4.5 in the distribution of chlorophyll metabolites (Figure 3.39). During spike growth at W5.0 and W6.5, chlorophyll *a* and pheophytin *a* are distributed similarly in the central axis of both WT and mutant sections. However, in the mutant, both molecules were absent in the spikelet axis that connects to the central rachis in most of the PTD nodes (from node 18). Whereas these compounds were distributed normally in the spikelet axes in most of the apical nodes, except for the spikelets in the PTD zone in WT sections, suggesting a link between spikelet greening and spikelet growth (Figure 3.39).

Pheophytin a m/z 871.5 [M+H]⁺

Chlorophyll a m/z 893.5 [M+H]⁺

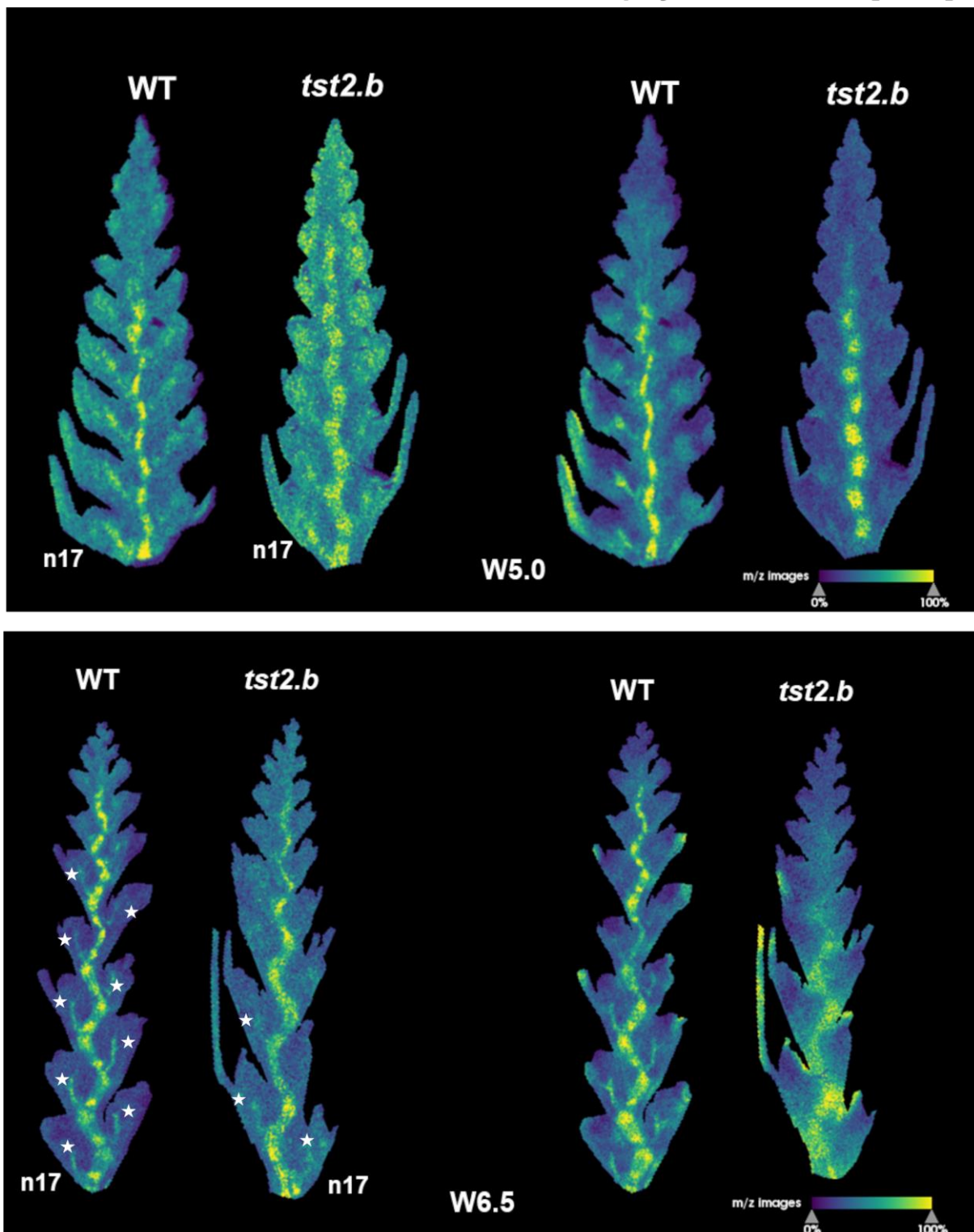


Figure 3.39. Distribution of chlorophyll metabolites in barley inflorescence meristem sections. The m/z images show Chlorophyll a and pheophytin a distribution in Bowman and *tst2.b* mutant sections at stages W5.0 and W6.5. The distribution of chlorophyll signals in the spikelet axes (depicted with a white star) is limited or almost absent in the *tst2.b* mutant sections compared to WT. Images are shown as normalized single ion intensity maps with 15- μ m pixel size. The color map corresponds to the intensity of ions. n, rachis node; W, Waddington scale.

MSI signals confined to IM and spikelet meristems

The tissue-specific distribution pattern was observed for the m/z value 146.1 ± 0.1 Da (Figure 3.40A, B). At W3.0, the signal intensity was very high in the IM dome for both WT and mutant (Figure 3.40C). Whereas, at W3.5 and W4.5, the signal intensity was still high in the IM dome but also distributed in the spikelet meristems, typically restricted towards the periphery of spikelet meristems, including awn primordia. However, a significant difference was found between WT and mutant from W5.0 for the distribution of this candidate ion. At W5.0, the signal intensity is still strong and distributed in the IM dome and spikelets of WT, while the signals are weakly distributed in the mutant section. At stages W6.5 and W7.5, signals of this candidate ion are weak in the topmost apical nodes of the mutant compared to the WT. Within the WT section, at W7.5, signals are weaker in the few topmost apical spikelet nodes compared to bottom spikelets (Figure 3.40C). Considering these interesting distributions of the candidate ion m/z value 146.1 ± 0.1 Da during spikelet initiation and growth phases, a database and literature survey were made to further determine the molecule's identity. Initial search for m/z 146 in the Metaspace MSI annotation platform (Palmer et al., 2017) using the filters positive polarity, MALDI source, and DHB matrix resulted in spermidine (Spd), a polyamine that plays a role in meristem activity, ROS homeostasis, TOR signaling, floral organ identity, longevity and delaying leaf senescence in plants (Chen et al., 2019, Salazar-Diaz et al., 2021). In plants, Spd is produced from its precursor putrescine, while another polyamine, spermine (Spm), is derived from Spd; however, the back conversions are also found (Figure 3.41A) (Chen et al., 2019). Considering these interesting functions, spermidine standards and polar extracts of the spikes were subjected to LC-ESI-MS and MALDI-TOF MS analyses. In both, spermidine is detected majorly as protonated form m/z 146.1 $[M+H]^+$ and a weak fragment ion at m/z 129.1 $[M+H-NH_3]^+$ with a loss of ammonia. However, in MALDI-TOF MS of Spd using DHB matrix produced m/z 146.1 ± 0.1 Da $[M+H]^+$ as the major strong peak, while m/z 129.1 ± 0.1 Da $[M+H-NH_3]^+$ fragment is very weak (Figure 3.41B). Nevertheless, ESI-MS/MS fragmentation resulted in an additional weak fragment at m/z 203.2. The m/z 203.2 corresponds to another polyamine Spm. Therefore, to test whether Spm is present in the spike section, co-localization analysis was performed for the MALDI MSI data to identify the masses co-localized with m/z 146.1 ± 0.1 Da. The co-localized m/z values 203.2 ± 0.1 Da and m/z 129.1 ± 0.1 Da are highly correlated with m/z 146.1 ± 0.1 Da and showed similar spatial distribution;

however, the intensities are very low (Figure 3.41C). Then, the Spm standard was also analyzed in MALDI-TOF MS, resulting in m/z 203.2 \pm 0.1 Da as the major peak with additional peaks at m/z 143.1 \pm 0.1 Da and m/z 129.1 \pm 0.1 Da (Figure 3.41B). However, ESI-MS of Spm standard resulted in three fragments m/z 203.2, 146.1, and 129.1 (Appendix Figure 12). Based on MALDI-TOF MS, Spm standard, fragment m/z 143.1 \pm 0.1 Da also showed similar spatial distribution at IM and spikelet meristems at W3.0, W4.5 as other peaks; however, the intensity of this mass is very weak in the spike sections and mostly on par with matrix background, so not detected strongly in all stages. Altogether, it conveys that both Spd and Spm are present in the spike sections; however, the abundance of Spd may be higher. Absolute quantification of these compounds from the spike extracts at different stages may confirm their ratios. Nevertheless, the differential distribution of these detected polyamines in the apical nodes of WT and mutant sections during spike growth phase suggests a possible role in the viability of IM and spikelet meristems.

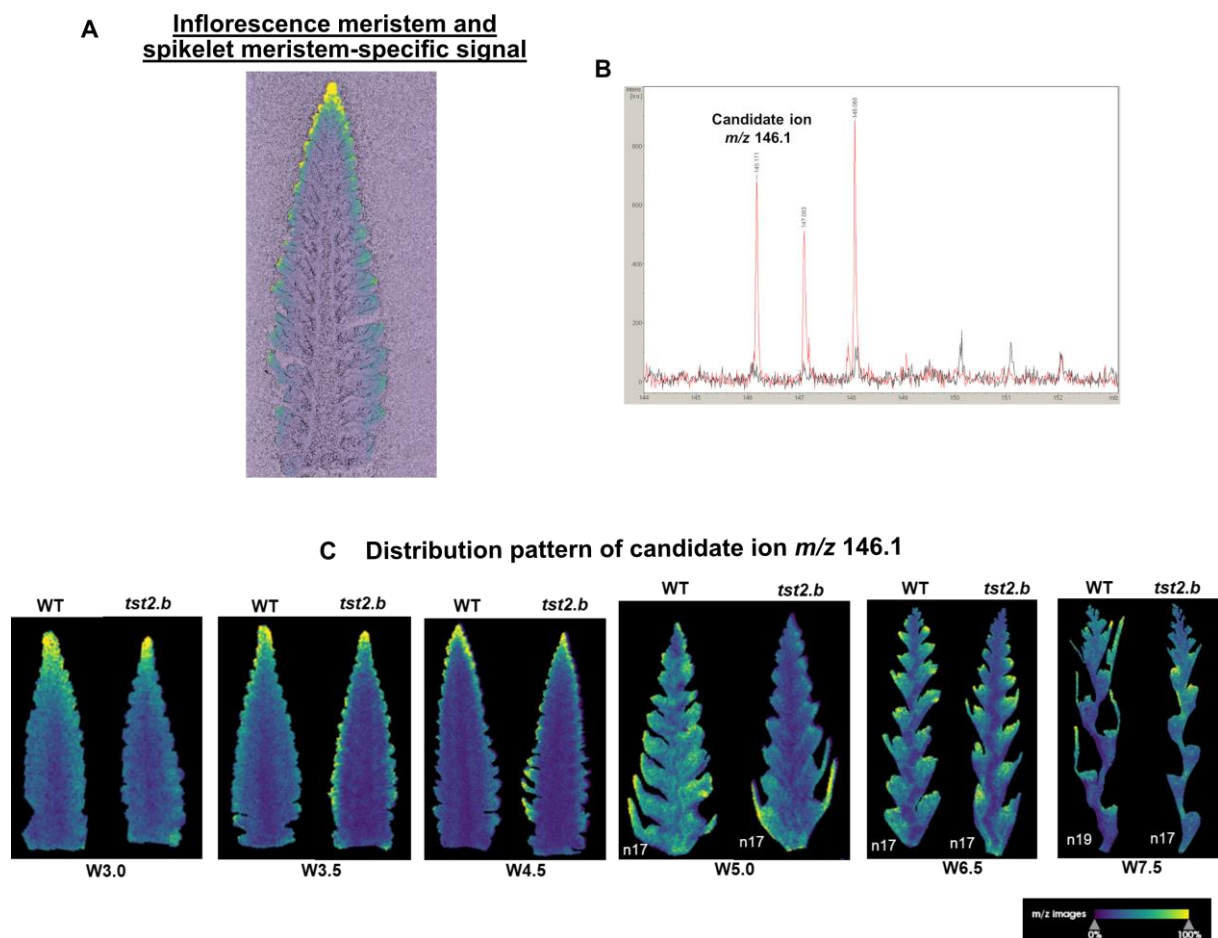
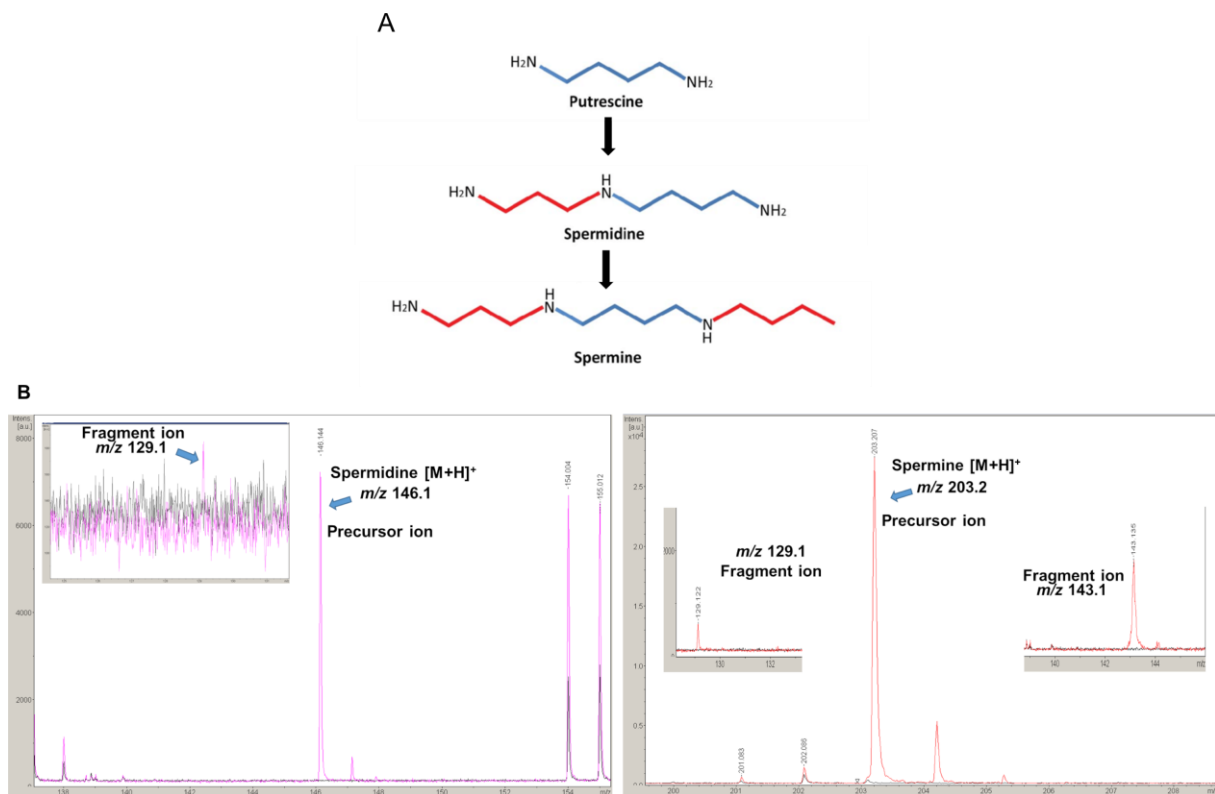


Figure 3.40. IM and spikelet meristem-specific distribution of candidate ion m/z 146.1. (A) Superimposed MALDI MSI signal m/z 146.1 on the optical image of the longitudinal section at W4.5

shows the distribution in IM and spikelet meristems. **(B)** Representative average mass spectrum highlighted with candidate ion m/z 146.1 peak. Black spectrum – from the blank area; Red spectrum – from sample tissue. **(C)** Distribution of m/z 146.1 signal in Bowman and *ts2.b* mutant sections over the development. The signal intensity gets weaker in the IM of the mutant section at W5.0 compared to WT. Images are shown as normalized single ion intensity maps with 15- μm pixel size. The color map corresponds to the intensity of ions. n, rachis node; W, Waddington scale.



C Similar distribution of precursor and fragment ions of spermidine/spermine

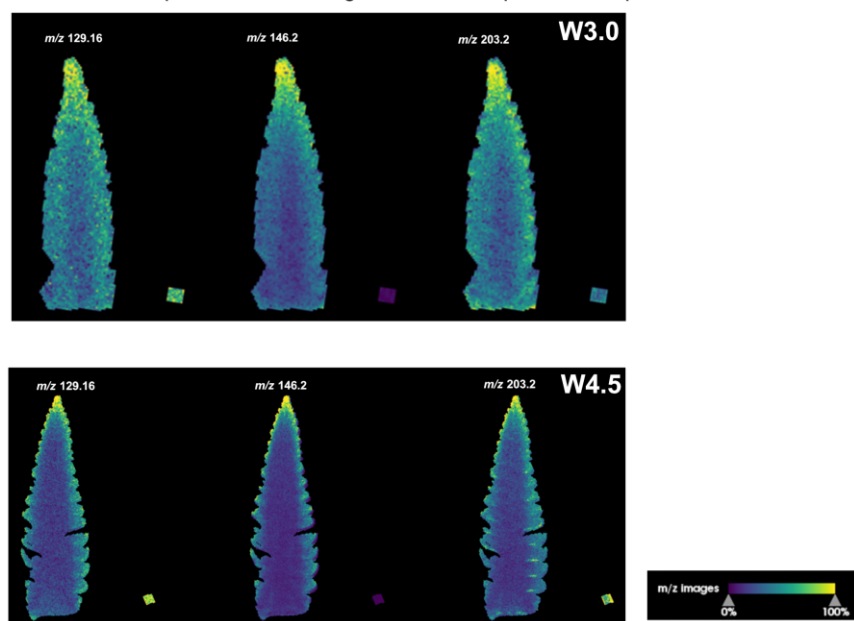


Figure 3.41. Identification of candidate ion m/z 146.1 as polyamine. (A) Chemical structures of three major forms of free polyamines in plants. **(B)** MALDI-TOF MS analysis with spermidine and spermine standards using DHB matrix. The mass spectrum in the left panel highlights the precursor ion of spermidine with m/z 146.1 with maximum intensity, and the enclosed box with magnified spectrum shows the weak fragment ion of spermidine m/z 129.1. Magenta spectrum – spermidine standard. The mass spectrum in the right panel highlights the precursor ion of spermine with m/z 203.2 with maximum intensity and two inner mass spectra showing weak fragment ions of spermine at m/z 129.1 and m/z 143.1. Red spectrum – spermine standard. **(C)** m/z images show the three fragment ions of spermidine/spermine with similar distribution patterns in the spike sections of WT at W3.0 and W4.5. Square boxes are the blank matrix area imaged simultaneously with each sample tissue. Superimposed MALDI MSI signal m/z 146.1 on the optical image of longitudinal section at W4.5 showing distribution in IM and spikelet meristems. Images are shown as normalized single ion intensity maps with 15- μ m pixel size. The color map corresponds to the intensity of ions. W, Waddington scale.

MSI signals confined to vascular cells

Another interesting m/z signal, 496.3 ± 0.1 Da, showed vascular cell-specific distribution within and between the developmental stages investigated (Figure 3.42A, B). During the spikelet initiation phase, at W3.0, the signal corresponding to the above-mentioned m/z value was distributed as a trail from the most advanced spikelet primordia and canalized strongly towards the base of each spikelet primordia (Figure 3.42C). At 3.5, the signal intensity gets stronger and localized at the junction or boundary between two spikelet primordia. Later at W4.5, in addition to the strong signal found at the junctions between two spikelet primordia, a few more spots arise in the spikelet primordia and at the boundary where the spikelets are found attached to the central axis. During the spike growth phase at W5.0 and W6.5, strong spots can be seen along the two lateral vascular axis underneath the spikelets, and weak spots within the spikelets resembling a zig-zag/distichous patterning (Figure 3.42C). The intensity is higher for the signal detected with potassium adduct at m/z signal 534.3 ± 0.1 Da $[M+K]^+$ which shows similar spatial distribution (Figure 3.43A). Importantly, a significant difference between WT and mutant for the distribution of this particular signal was found at W5.0 and W6.5 (Figure 3.42C, 3.43B). In particular, the pattern was distorted and almost absent in the apical nodes (above node 21) in the *tst2.b* mutant. In addition, this patterning is also missing above node 26 at W6.5 in the WT section, suggesting a possible association with the PTD (Figure 3.43B). Based on the MSI database, literature survey, and the fragments detected, the m/z 496.3 ± 0.1 Da $[M+H]^+$ signal was found to be lysophosphatidylcholine (LPC 16:0).

Lysophosphatidylcholine is a class of phospholipid, which can function as a signaling lipid in plants (Poulsen et al., 2015). Magnified superimposed images of LPC(16:0) 534.3 [M+K]⁺ signals over optical images highlighted the development of signals in putative vascular cells of the rachis as well as in spikelet over the development (Figure 3.43C). Multiple ion intensity map with chlorophyll a 893.5±0.1 Da and LPC (16:0) 534.3±0.1 Da showed a non-overlapping distribution of these two signals (Figure 3.43D). However, the specific identity of the vascular cells or veins where the LPC are distributed, including their functions, are yet to be revealed, which requires further study. Thus, the preliminary data analyses and validation of the compounds distributed in a tissue- or cell-type-specific manner confirmed the presence of Spd, Spm, LPC (16:0), and chlorophyll metabolites. The summary of their distribution is shown as a multi-ion intensity map in figure 3.43D.

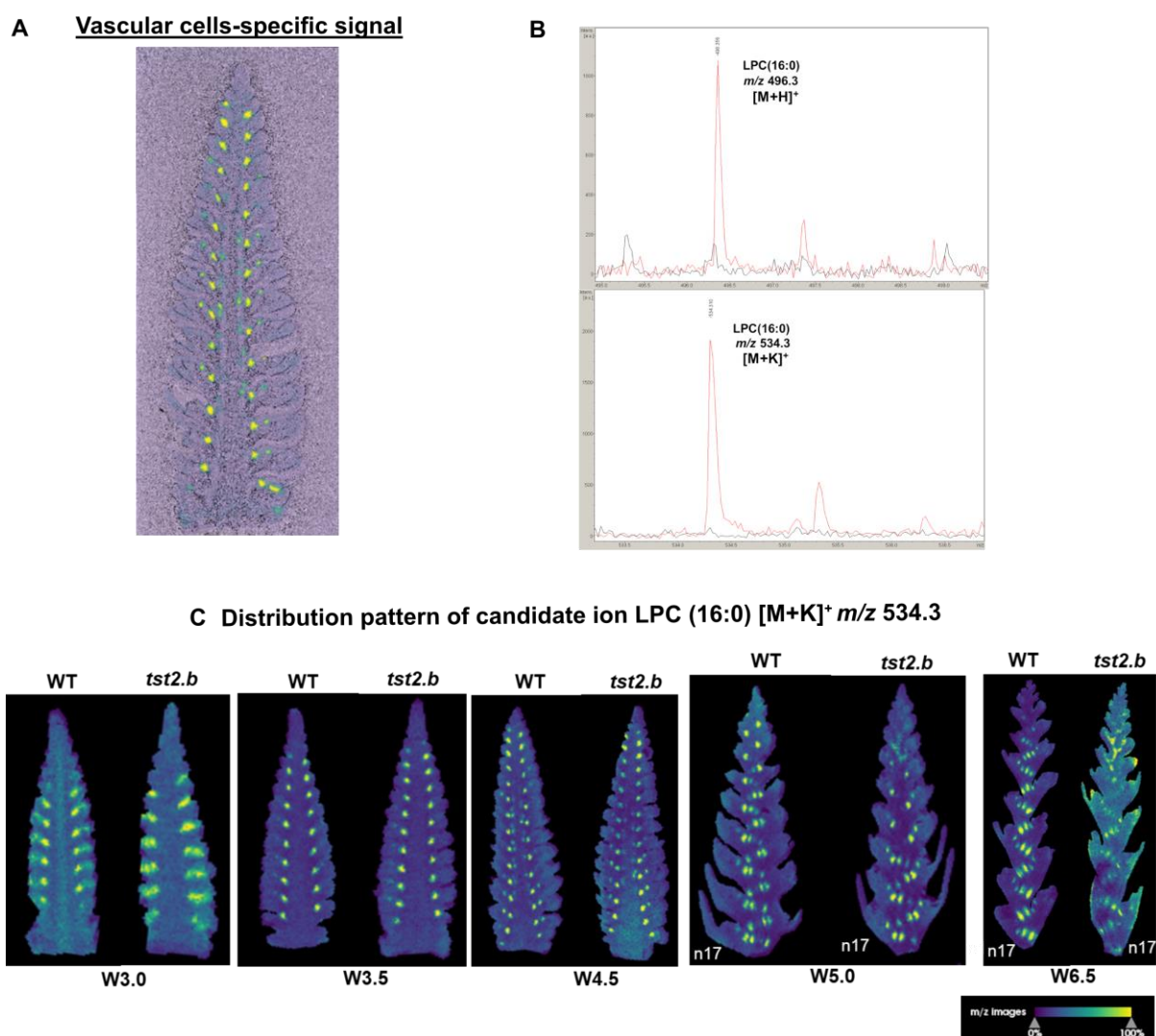


Figure 3.42. Vascular cell-specific distribution of a lipid signal lysophosphatidylcholine LPC(16:0). (A) Superimposed MALDI MSI signal m/z 496.3 on the optical image of the longitudinal

section at W4.5 shows the distribution in IM and spikelet meristems. **(B)** Representative average mass spectrum highlighted with candidate lipid LPC(16:0) as protonated form at m/z 496.3 [M+H]⁺ and more intense peak at m/z 534.3 [M+K]⁺ with potassium adduct. Black spectrum – from the blank area; Red spectrum – from sample tissue. **(C)** Distribution of LPC(16:0) signal m/z 534.3 [M+K]⁺ in Bowman and *tst2.b* mutant sections over the development. Images are shown as normalized single ion intensity maps with 15- μ m pixel size. The color map corresponds to the intensity of ions. n, rachis node; W, Waddington scale.

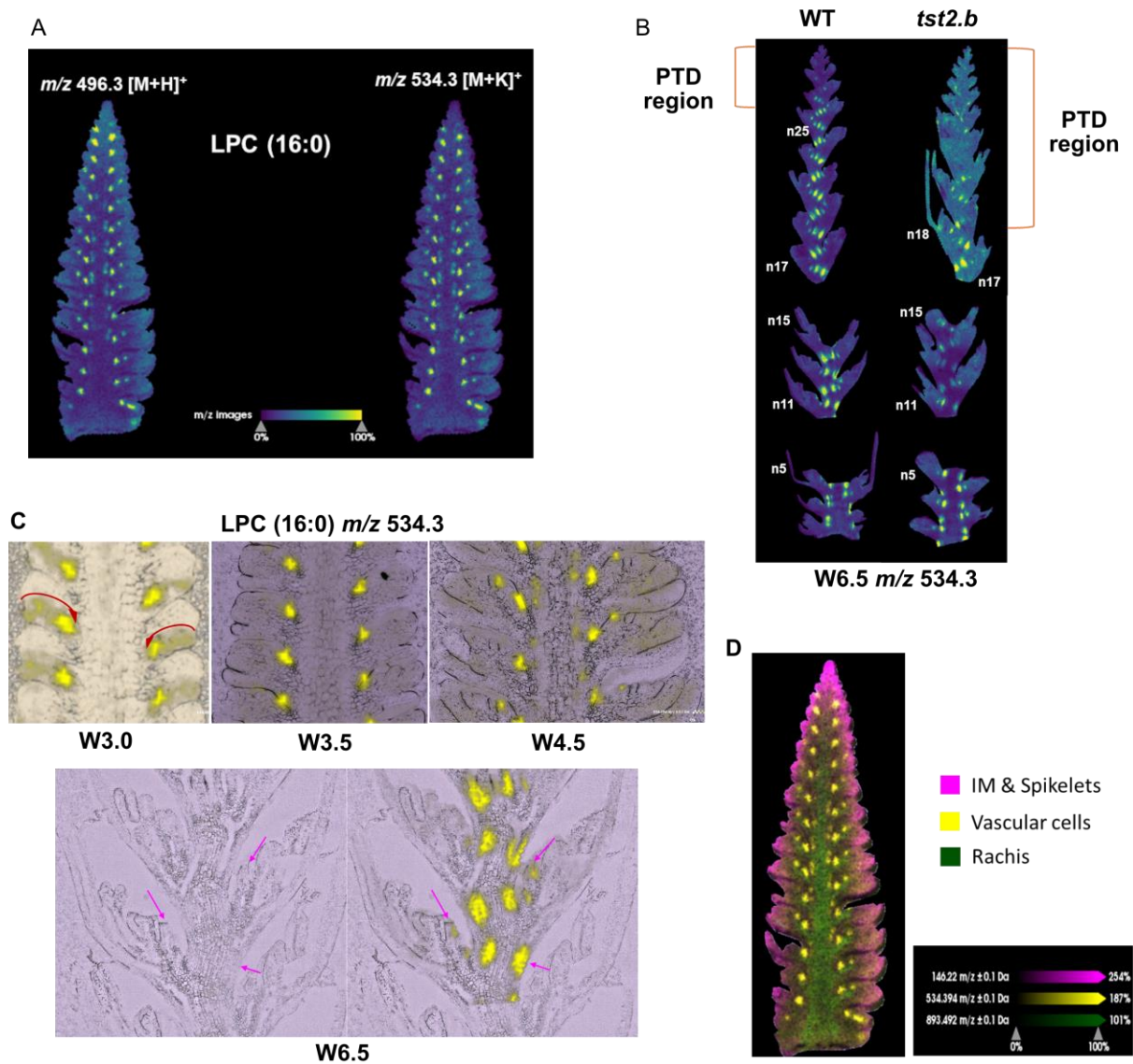


Figure 3.43. Putative association of vascular cell-specific distribution of LPC, spike vascular patterning, and PTD. (A) Representative images of LPC(16:0) signals m/z 496.3 3 [M+H]⁺ and m/z 534.3 [M+K]⁺ in WT spike section at W4.5 shows similar spatial distribution. (B) Difference in the distribution of LPC (16:0) between WT and *tst2.b* mutant sections at W6.5. Signals were found weak/absent and distorted in *tst2.b* in most of the PTD nodes above node 17 compared to the WT. In the WT section, signals were also found to be absent in a few topmost nodes under the PTD zone,

suggesting LPC (16:0) role in spikelet development and PTD. **(C)** Representative magnified superimposed optical images of WT sections at W3.0, W3.5, W4.5, and W6.5 with LPC(16:0) 534.3 [M+K]⁺ signals. The red arrow marks the path of LPC (16:0) at each spikelet meristem. For W6.5, the magenta arrow points to the cells where the LPC signals are distributed. **(D)** Summary of the tissue-specific metabolite signals identified in this study is shown in a multi-ion intensity map. Images are shown as normalized single ion intensity maps with 15- μ m pixel size. The color map corresponds to the intensity of ions. n, rachis node; W, Waddington scale.

4. Discussion

Unraveling the molecular regulations behind spike pre-anthesis tip degeneration (PTD) is vital for understanding the basis of spikelet survival and grain number determination in barley. The present study has assembled a comprehensive molecular framework of spike PTD, a phenomenon that decreases the grain yield potential of barley and related cereals. Identifying and manipulating the major players behind this process provides excellent potential for improving grain number in barley and other related cereals.

4.1 Spike PTD in barley is a preprogrammed meristematic senescence process

It was proposed for a long time that the presence of active death-inducing internal cues behind PTD in barley (COTTRELL et al., 1985, Arisnabarreta and Miralles, 2006). Based on the observations found in the spike development studies, the MYP stage, the maximum number of spikelet/spikelet primordia, the onset of death, and the number of dying spikelet nodes were highly reproducible in the standardized growth conditions for both barley row types suggest this as a preprogrammed process (Figure 1A, B). In *Arabidopsis* and some eudicots, shoot apical meristem and IM arrest/senescence have long been studied (Hensel et al., 1994, Davies and Gan, 2012). However, recent studies on the molecular control of SAM arrest and senescence revealed the involvement of local changes in the SAM cells, including dynamic ROS accumulation, vacuolization, auxin, and cytokinin signaling (Merelo et al., 2022, Wang et al., 2022). The present study on barley spike meristem also found ROS accumulation in the apical parts already at the MYP stage (W5.0) (Figure 3.10). However, FDA/PI- staining assay revealed that initiation of cell death occurs only at around W7.5 (Figure 3.3). While the SEM observation depicts the overall growth arrest of the apical spikelets commencing before W7.5. These findings suggest that the ROS accumulation found before visible cell death may function in the overall arrest of the spike apex by shutting down stem cell activity, similar to the SAM arrest in *Arabidopsis* (Wang et al., 2020a; Wang et al., 2022). However, during the present study only one type of ROS staining dye was successfully apply, implying that the found signals are absent or weak in the IM dome in all the three stages studied. Future studies may use other ROS-specific dyes or ROS-reporter lines to study the ROS dynamics in detail, even before the MYP stage, and to understand how it contributes to IM arrest and barley spike PTD. Further, FDA/PI staining showed that initiation of cell death in the IM occurs prior to the death of spikelets beneath the dome. Also, in spikelets, death

occurred initially in anthers, suggesting these male organs may be more sensitive to the death cues as observed in other stress-induced floret sterility in grasses (Begcy et al., 2019, Callens et al., 2022). Thus, the observations indicate that the locally induced cell-death within the IM dome may signal cell death in regions below the dome. Altogether, it suggests spike PTD appears as a preprogrammed cell death process that can be categorized in plants as proliferative/meristematic senescence.

4.2 Spike PTD involves transcriptional regulators of senescence, plant defense, and light signaling

Senescence in plants often classified as mitotic or replicative senescence (involves meristematic tissues and cell-cycle/proliferative arrest) and post-mitotic organ senescence (typically in organs like leaf, stem, floral petal, roots) or the organismal level (annual crops undergo whole plant senescence for nutrient reallocation during grain filling) (Gan, 2003, Woo et al., 2019). Leaf senescence, the most widely studied type of organ degeneration, involves several transcriptional regulators (Woo et al., 2019). During spike PTD, we detected the enrichment of several leaf senescence-related genes in the dying parts of the spike, including *HvS40-like* and NAC TF genes (Figure 3.17, 3.20). Identifying *HvS40-like* as a joint top hub gene in both barley row types within the WGCNA degeneration-associated gene network modules underscored its potential importance for spike PTD (Figure 3.20). Its homolog, *HvS40*, encodes a senescence regulator domain-containing nuclear-targeted protein and was expressed during age/dark-induced leaf senescence and pathogen response (Krupinska et al., 2002). Interestingly, many of the homologs of enriched NAC TF genes play a significant role during leaf senescence in barley and other species. For instance, *HvNAC027* (homologous to Arabidopsis *NAP*) is expressed during flag leaf senescence in barley and is highly responsive to ABA and methyl jasmonate (Christiansen et al., 2011). Nevertheless, its orthologs in wheat (*TaNAC69*) and rice (*ONAC122*) play a role in disease resistance and abiotic stress tolerance, respectively (Sun et al., 2013, Xue et al., 2011). Additionally, in Arabidopsis and rice, *NAP* is involved in ABA biosynthesis for the upregulation of transcripts involved in chlorophyll degradation during leaf senescence (Liang et al., 2014, Yang et al., 2014), which might function similarly in barley spike PTD (Figure 3.16). *HvNAC008/SF6*, highly expressed in apical tissues, was previously reported to have leaf senescence-associated expression in barley. Its closest homolog in Arabidopsis, *ORESARA1 (ORE1)*, is a

well-characterized regulator of leaf senescence and programmed cell death (Matallana-Ramirez et al., 2013). These pieces of evidence strongly suggest that the *HvNACs* identified here might function very similar during spike PTD. Future research on increasing yield potential should also explore the potential role of these NACs during PTD in barley and related cereals.

The effects of light/circadian regulators on environmental adaptation and flowering as well as their relevance to spike development, have been documented in barley (Boden et al., 2014, Bi et al., 2019). Molecular mechanisms connecting leaf senescence and light signaling have also emerged in recent years (Kim and Hong, 2019, Kim et al., 2018a, Lee et al., 2021). Very recent research also suggested the presence of a vascular-specific clock within the developing barley spike that might regulate spikelet growth and spike PTD (Huang et al., 2023). Similarly, this study found regulators involved in light senescence cross-talk, such as *ETHYLENE INSENSITIVE3 (HvEIN3)*, a homolog of Arabidopsis *EIN3*, which regulates age-dependent leaf senescence (Li et al., 2013), indicating the possibility of such a control mechanism for barley spike PTD (Figure 3.18). We also observed the enrichment of plant defense response genes, including *HvDRM/ARP* and *HvHIR3 (HYPERSENSITIVE INDUCED REACTION3)*. Their Arabidopsis homologs, *AtDRM1/2/ARP*, function in axillary bud dormancy, stress responses, and negative regulation of local and systemic acquired resistance (Rae et al., 2013, Rae et al., 2014, Roy et al., 2020), whereas *HvHIR3* functions as a positive regulator of hypersensitive response (HR)-like cell death (Rostoks et al., 2003). An independent study found a 35-fold increase in *HvHIR3* expression in the leaves of barley disease lesion mimic mutants, which show spontaneous HR-like cell death (Rostoks et al., 2003). Recently, a mutant in a proton pump *ATPase* gene exhibiting lesion mimic leaf and panicle abortion was characterized in rice (Hu et al., 2022). Although rice panicle abortion is morphologically distinct from barley spike PTD, characterizing barley lesion mimic mutant resources might help us better understand this cell death phenomenon. In fact, stem cell-derived immune signaling in the shoot apical meristem was previously hypothesized (Wu et al., 2020a), and loss of key immune signaling regulators may cause autoimmunity leading to death (Wu et al., 2020b). Thus, we postulate that PTD in barley might also occur due to the inability of the inflorescence tip to maintain proper immune signaling. This link suggests that spike PTD may be collectively regulated by senescence, autoimmunity/defense responses, and light signaling (Figure 4.44A).

4.2 Barley *GT1*, a modulator of spike PTD

Gene editing of one of the putative candidates, *HvGT1*, enhanced apical spikelet development and differentiation, substantially delayed degeneration, and increased final spikelet number in two-rowed barley (Figure 3.21-3.25). This result supports the evolutionarily conserved function of HD-ZIP class I family members in growth repression, as observed in grasses and eudicots (Komatsuda et al., 2007, Whipple et al., 2011, González-Grandío et al., 2017, Sakuma et al., 2019, Gallagher et al., 2023). The maize ortholog *GT1* is an essential domestication gene that suppresses carpel development in tassel florets and elongation of lateral ear branches and promotes axillary bud dormancy putatively regulated by the other domestication gene *TB1*, encoding a TCP transcription factor (Dong et al., 2019, Klein et al., 2022, Whipple et al., 2011). This domestication module in maize induces tiller bud dormancy by recruiting inhibitory phytohormones, such as ABA and jasmonate, thereby altering carbohydrate homeostasis (Dong et al., 2019). The findings from maize suggest that *HvGT1* might also function similarly in barley by modulating ABA and sugar signaling to suppress apical spikelet growth. However, barley *gt1* mutants did not show any carpel derepression phenotype in the spikelets of the non-dying region, in contrast to that seen in maize tassel florets (Klein et al., 2022). Notably, in barley, carpel suppression in lateral spikelets is controlled by the row-type *VRS* genes (Koppolu and Schnurbusch, 2019). The *TB1* ortholog in barley, *VRS5/INT-C/HvTB1*, functions in lateral spikelet fertility/sterility, and its loss of function causes increased tillering in the early phase of plant development and partial fertility in the lateral spikelets of two-rowed barley (Ramsay et al., 2011, Zwirek et al., 2019). Moreover, the expression domains of *HvTB1* and *HvGT1* were different in the barley inflorescence meristem, suggesting that they might function independently during barley spike growth, in contrast to maize, aside from their conserved tillering function. Thus, *HvGT1* may have gained a novel function in barley during the onset of spike PTD and suppression of apical spikelet growth, most likely involving ABA pathway genes, which will require further downstream analysis of *Hvgt1* mutants. Further, it was previously discussed in section 4.1 that initiation of cell death in the IM might serve as a vital signal for further progression of PTD. The phenotype observed in *Hvgt1* mutant plants also supports the notion that barley spike PTD is related to proliferative/meristematic senescence since extended IM longevity during the spike growth phase allowed more time for the growth

of spikelets in the PTD zone, thereby increasing their chances of survival. While once the IM collapse commences in *Hvgt1*, PTD progresses downwards and degenerates those rachis nodes susceptible to the death signal(s).

On the other hand, most of the excess tillers formed in *Hvgt1* mutants were unproductive and might impact assimilate partitioning and spikelet survival in the fertile tillers. The de-tillering experiment showed a more substantial effect on spikelet survival/fertility in *Hvgt1* mutants, which helped us uncouple the effect of *GT1* on spike PTD from tillering (Figure 3.25). Indeed, future studies targeting the regulatory elements of *HvGT1* may help us discover motifs responsible for its tissue specificity and exploit its full potential to improve apical spikelet survival in barley. Indeed, identifying the downstream targets of HvGT1 could help us understand the observed phenotype in the mutant. Predicted targets of HvGT1 (undirected) identified by our WGCNA co-expression network analysis included the senescence regulator *HvS40-like* and other growth repressors. These results identify GT1 as a new modulator of spike PTD in barley independent of the flowering time pathway and further demonstrate the significance of manipulating PTD to increase yield potential in cereals (Figure 4.44B).

However, the extra-surviving apical spikelets in *gt1* mutants fail to produce regular grains in most of the examined spikes. This could be attributed to various reasons such as growth conditions, genetic background, and border effect. On the other hand, the two-rowed cultivar 'Golden Promise' (used for transformation) often showed irregular ectopic spike branches in the basal nodes under a glasshouse light regime when grown in pots independent of *gt1* mutations as reported in previous studies (Brown and Bregitzer, 2011). However, such ectopic spike branches were utterly absent in the plants grown in soil under natural sunlight. Hence, it is still necessary to test the grain yield advantage of the *gt1* mutation by growing more plants and testing the mutant effects in other genetic backgrounds. Further, the loss of HvGT1 function achieved by targeted mutagenesis only delayed, but did not abolish, PTD, thereby facilitating more differentiation. Still, upstream regulators of spike PTD need to be identified, which requires further study.

4.3 Later events of spike PTD are predominantly associated with higher ABA levels

Phytohormones serve as local or long-distance signals in several developmental and stress-related processes (Lacombe and Achard, 2016, Mazzoni-Putman et al., 2021, Blazquez et al., 2020). Stress-responsive plant hormones, including ABA, jasmonic acid (JA), salicylic acid (SA), and ethylene, were previously characterized for their role in plant cell death and senescence (Woo et al., 2019). The phytohormonal profiling in the present study revealed high levels of ABA in the apical part, which coincided with the onset and basipetal progression of tip degeneration. ABA was recently suggested to be involved in spikelet primordia abortion in six-rowed barley under salinity stress (Boussora et al., 2019). The present study unequivocally demonstrates the involvement of ABA during spike PTD of both row types, even under standardized growth conditions (Figure 3.4; 3.28). ABA levels correlate with the increased transcript levels of the key ABA biosynthesis gene *HvNCED1* (Leymarie et al., 2008, Seiler et al., 2014). Additionally, the alternative ABA biosynthesis route was also active, as indicated by the upregulation of *ABA4* (Figure 3.31). The homologous encoded proteins in Arabidopsis and rice are plastid-localized and involved in stress-induced ABA accumulation (North et al., 2007), photoprotection (Dall'Osto et al., 2007), and root growth inhibition (Ma et al., 2014). ABA also represses the transcription of chloroplast genes (Yamburenko et al., 2015), supports reduced chlorophyll levels, and causes poor chloroplast differentiation toward the apex. Importantly, ABA also inhibits specific developmental PCD processes by regulating the proper onset and slow progression of cell death (Van Hautegeem et al., 2015, Young and Gallie, 2000). Similarly, barley spike PTD is not a rapid cell death event; instead, it undergoes a gradual progression that may last for weeks, depending on the genotype. Notably, ABA levels peak in the apical part during or after the collapse of the IM dome (Figure 3.4; 3.28). In such cases, ABA might regulate the timing/onset and progression of PTD antagonistically or mutually with other possible regulators; however, this question will await studies until the end of tissue death. Importantly, these observations identify ABA as one of the major players during the later events of spike PTD in barley.

Although we did not measure the absolute quantities of SA, JA, or ethylene, we observed an enrichment of genes involved in ethylene biosynthesis/signaling and JA and SA responses, suggesting a role for these phytohormones during barley spike

PTD. The ethylene biosynthesis gene *1-aminocyclopropane-1-carboxylate oxidase2* (ACO2) controls floret fertility and kernel number in maize ears (Ning et al., 2021). Interestingly, our study also identified its barley ortholog *HvACO* as a highly expressed gene in degenerating apical parts (Figure 3.15). Indeed, apical spike parts had reduced levels of growth-promoting phytohormones, such as IAA, GA precursors, and CK ribosides (cZR and iPR), which might limit further growth and differentiation (Figure 3.5; 3.28). A recent study in barley showed the significance of local auxin biosynthesis for the maturation of pollen grains by enhancing the expression of central metabolism genes, thereby promoting growth and differentiation (Amanda et al., 2022). Overall, differential gradients of growth-promoting and -repressing phytohormonal regulation in dying and viable spike parts may establish the final spikelet number in barley.

4.4 Apical spikelets undergo metabolic reprogramming typical of organ senescence in plants

Maintaining energy homeostasis is a key survival factor in all living organisms. During organ senescence/cell death, such as in leaves, drastic structural and biochemical changes take place sequentially, involving a metabolic transition from anabolism to catabolism and hydrolysis of macromolecules (Woo et al., 2019). Based on whole-spike measurements (Ghiglione et al., 2008), sugar starvation has been postulated to play a role in the death of more distal florets in wheat. We found that dying apical parts were low in carbohydrates, particularly Suc and T6P, whereas viable central and basal parts contained high levels of these metabolites (Figures 3.6; 3.29). Such metabolic gradients strongly identify carbohydrate homeostasis as one of the main factors during spike PTD, thereby confirming the significant role of sugars in plant growth and development (Eveland and Jackson, 2012). While Suc and T6P are essential factors during plant development and signaling, respectively, high Fru and Tre levels were previously observed during leaf senescence (Watanabe et al., 2013). Our transcriptome analysis also showed a strong enrichment of carbon metabolism and photosynthesis-related genes being highly expressed in the central and basal parts of the spike. Similarly, a very recent study showed the significance of photosynthates availability from the spike rachis; proper plastid differentiation and early inflorescence greening are essential to fuel the growth of developing spikelets in barley (Huang et al., 2023). A barley mutant (*Hvcmf4*), defective in these processes resulted in as poor spike development with early and extended apical degeneration.

Amino acids (AAs), which also serve as precursors for phytohormones, nucleotides, and several secondary metabolites, are involved in plant development, stress responses, and building proteins (Huang and Jander, 2017, Lynch and Dudareva, 2020, Yadav et al., 2019). The distribution of AAs in degenerating apical parts resembles that of stressed or senescent cells, which show increased levels of protein degradation due to proteolysis, which might explain the increase in AA contents (Hildebrandt et al., 2015). High levels of AAAs, BCAAs, Lys, and Pro in degenerating apical tissues may serve as precursors for stress-related secondary metabolites and alternate substrates under energy-limited conditions, as observed in *Arabidopsis* (Peng et al., 2015, Watanabe et al., 2013) and wheat (Heyneke et al., 2019, Zhu et al., 2022). Here, the apical part, limited in carbon supply, may use the degraded AAs as alternative substrates for energy production (Law et al., 2018). Notably, transcriptome analysis also revealed significant enrichment for genes related to AA catabolism in the apical parts.

The most abundant AA accumulating in the apical part of both genotypes was Asn, which fitted well with the high expression of *ASPARAGINE SYNTHATASE* genes (*HvASN1* and *HvASN5*) in degenerating tissues. An independent study in barley showed increased expression of these genes in developmental and dark-induced senescing leaves, probably serving a role in nitrogen (N) remobilization (Avila-Ospina et al., 2015). The Asn distribution and associated gene expression pattern favor a role for this AA as a major form of N transport and supply during spike PTD, whereby N might become available in the dying parts. During leaf senescence, mitochondria, and nuclei, required for energy production and gene expression, remained intact to mobilize cellular contents until senescence was completed effectively. Besides changes in AA levels, the expression of several transporter genes and those involved in autophagy and vesicle trafficking increased in the apical part, suggesting that newly available nutrients in the degenerating apical region become reallocated to the viable region. It is also evident from the FDA/PI cell-death staining assay, which shows PTD initiates first in the IM and then in spikelets, that the rachis is kept viable until later stages of PTD (Figure 3.3), supporting the notion that tissues around the vascular system are required for nutrient export/signaling and senesce at last (Gan and Amasino, 1997).

In summary, spike PTD in barley is a complex quantitative trait that likely involves multiple regulatory layers, including molecular processes typical for organ senescence/cell death (Woo et al., 2019). Despite the discovery of several molecular regulators in the present study, fundamental questions remain about the signal(s) determining the precise timing, initiation, and marking of the affected spikelet primordia (i.e., extent of death zone) (Figure 4.44A). Nevertheless, the candidates identified here may serve as an excellent resource for exploiting their natural allelic variants, while their functional validation and editing may lead to an increase in grain yield potential in barley and other related cereals.

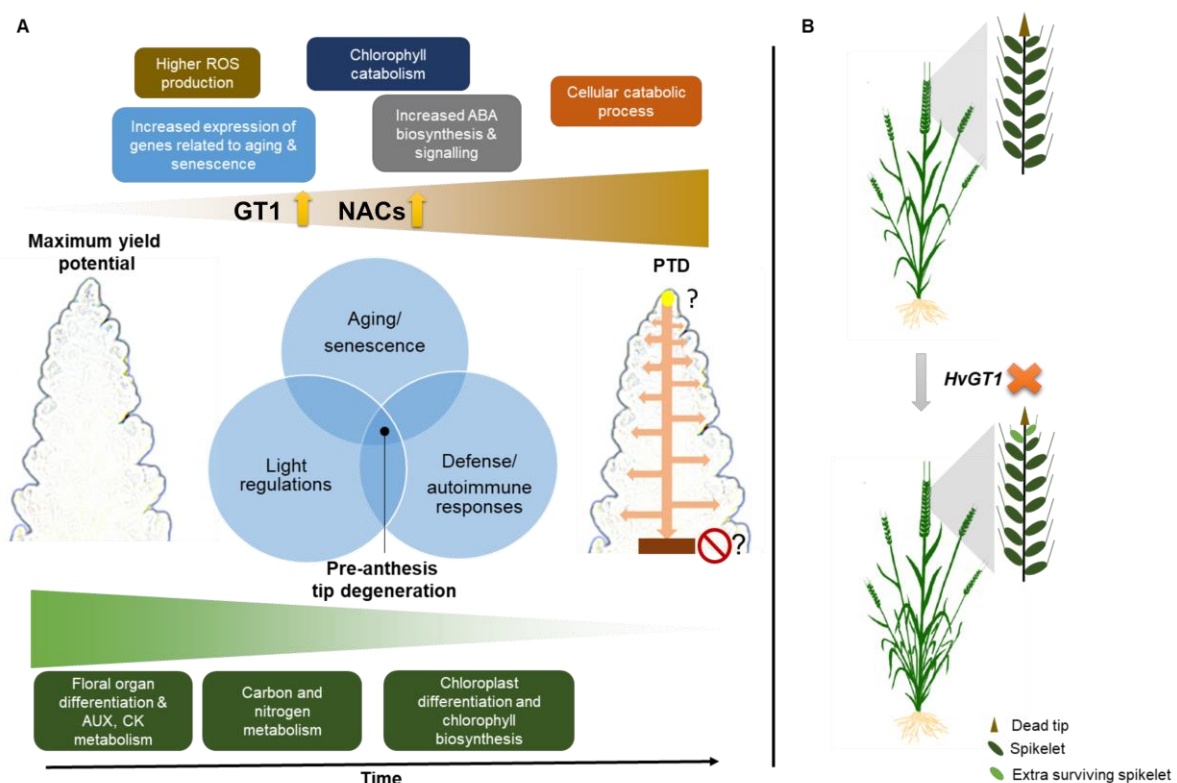


Figure 4.44. Proposed model of spike pre-anthesis tip degeneration (PTD) in barley. (A) Apical spikelets in the barley inflorescence undergo death, involving processes related to senescence, ABA biosynthesis, and increased ROS, chlorophyll, and protein catabolism. Increased expression of GT1 and NAC genes suggest their functions as a positive regulator of spike PTD. At the same time, dying apical parts were limited with primary metabolism, auxin, cytokinin biosynthesis, and chloroplast differentiation, which seems significant for spike growth and proper spikelet differentiation. Moreover, there seems to be an overlapping function of aging/senescence, light, and autoimmune response regulators on PTD. However, the actual signal(s) (solid yellow circle) that might originate from the IM tip and the signal(s) that defines the death zone (solid brown box) remains elusive. **(B)** *HvGT1*, identified as one of the putative modulators of spike PTD, acts as a growth repressor that negatively affects the development of apical spikelets. Its loss-of-function promotes apical growth with delayed degeneration and enhanced differentiation of apical spikelets, thereby increasing the final spikelet number.

4.5 MALDI MSI has proven to be a valuable tool for studying the metabolism of barley spike meristems

MALDI MSI has been utilized for the first time to study the spatial metabolic patterning in the early developing inflorescence meristems of barley. Initially, the MALDI MSI method was adapted for developing barley inflorescences based on published protocols for other tissues while optimizing specific key steps, like matrix deposition, by developing a reproducible sublimation method in the current study. Overall, this led to the detection of molecular ions between 80 and 1000Da of diverse classes, including amino acids, sugars, polyamines, chlorophyll, and lipids (Table 1). Preliminary data analysis revealed highly tissue-specific and developmental differences for the metabolites distributed in the developing spike sections. Furthermore, performing MALDI MSI in WT and mutant defective in normal spike development led us to relate the significance of a few metabolites on spikelet development and growth. This thesis presents the metabolic status of small molecules, including sugars and amino acids, over the development covering spikelet initiation and spike growth phases. In all the stages investigated here, Gln, a primary amino acid involved in N assimilation, was found limited towards the apex in both WT and mutant. In addition, glutamine is a major amino donor for the synthesis of other amino acids and other nitrogen-containing compounds in plants (Forde and Lea, 2007). Similarly, high abundance in basal to central parts was observed when measured using spike extracts during the spike growth phase in WT. The results seen here with MALDI MSI from W3.0 also suggest that the acropetal gradient for Gln was maintained already from the early spikelet initiation phase and may relate to high N assimilation or availability in basal and central parts. Further, the absence of any Gln signals in the PTD zones in both WT and *tst2.b* mutant implies its significance for proper spikelet development and spike greening by either functioning as a major N source or as a signaling metabolite (Nishimura et al., 1982, Kan et al., 2015).

On the other hand, a high accumulation of Asn found in the invasive measurement was also confirmed by the pattern observed here in MALDI MSI. Further, Asn found higher PTD zones in both WT and mutant sections, suggesting their role in dying cells as described previously in section 4.4.

Signals corresponding to disaccharides were detected in spike sections. Different disaccharide sugars are produced in plants, including sucrose, trehalose, maltose, and cellobiose, containing different combinations of hexose sugars. For example, sucrose, a major transport form in plants that plays a central role in primary metabolism and plant development, consists of one molecule of glucose and fructose bonded by an α , β -linkage, whereas trehalose is made up of two glucose units (Figuroa and Lunn, 2016, Nagy et al., 2019). This MSI study did not detect hexose sugars such as glucose and fructose. The disaccharide isomers mentioned above have similar molecular mass and are most likely detected with the same m/z value. Because of this reason, it is difficult to assign a specific identity to the detected sugar signals in a single MSI run. Other possibilities include performing MALDI MS/MS fragmentation and on-tissue digestion with specific enzymes. However, MS/MS is unsuitable in this case as hexose fragments will have similar molecular masses, while the digestion requires a specific experimental setup (Peukert et al., 2014). Therefore, the results obtained for the disaccharide sugars in this MSI study in barley spike sections are interpreted based on the tissue-specific distribution and invasive measurement of sucrose and trehalose performed in the WT spike parts (section 3.2.2). Invasive measurements showed low sucrose levels in the dying apical parts, in contrast to higher trehalose levels at W7.5 and W8.0 in the WT spike. Reduced intensity of m/z 381.1 found in the apical parts of WT sections until W6.5 may correspond to sucrose levels. As trehalose accumulation during stress and senescence have been reported in several species, the observed increase in disaccharide signal in the apical nodes of WT at W7.5 and from W5.0 in mutant sections may correspond to trehalose. However, this requires further investigation. Recent studies have reported a method for imaging all the disaccharide isomers mentioned above using LESA–SLIM SUPER Ion mobility-MSI workflow (Nagy et al., 2019). Such an approach may help us visualize specific disaccharide sugars in the developing barley spikes.

4.5.1 Identification of novel metabolic pathways governing barley inflorescence development

Apart from targeted screening of small molecules such as sugars and amino acids, this study also found a few unknown molecular ions with specific spatial distribution in the meristem sections. The ion signal m/z 146.1 that was found to be restricted to the IM and spikelet meristems during the spikelet initiation phase was identified as a

polyamine (PA), i.e. spermidine (Spd). In addition, another PA, spermine (Spm), was also detected with similar spatial distribution with weak signals at m/z 129.1 and m/z 203.2. The possible reasons for the weak intensity of the precursor ion of Spm m/z 203.2 could be due to the interference of matrix background found at the same m/z value or the compound itself available in limited amounts in the samples tested. However, this requires further absolute quantification of both Spd and Spm in the polar extracts of barley spikes. Notably, the specific distribution of these detected polyamines in the actively growing IM dome and spikelet meristems places them as novel putative modulators of inflorescence development in barley.

PAs are low molecular weight organic cations containing two or more amino groups, function in several physiological and developmental processes, as well as stress tolerance in plants and animals (Sobieszczuk-Nowicka et al., 2019). Putrescine (Put), Spd, and Spm are the major free forms of PAs in higher plants, while their biosynthesis majorly occurs by decarboxylation of amino acids ornithine and arginine. Spd and Spm are majorly derived from Put catalyzed by Spd synthase and Spm synthase, respectively. Furthermore, a back conversion reaction is possible from Spm to Put. Another route for Spd and Spm synthesis occurs via the S-adenosylmethionine pathway, which also serves as a precursor for the hormone ethylene. Amine oxidases such as polyamine oxidase and diamine oxidase are involved in the catabolism that generates H_2O_2 or back conversion of PAs (Mattoo and Sobieszczuk-Nowicka, 2019). Endogenous levels of PAs and activities of their biosynthesis genes were found to be highest in the meristem and actively growing cells while lowest in senescent tissues. The relationship between meristem development through WOX protein and polyamine biosynthesis has been characterized in *Arabidopsis* (Zhang et al., 2011). At the same time, its function on floral organ identity, floral bud initiation, and differentiations was also reported (Chen et al., 2019).

Similarly, the present study found Spd and Spm distributed in the IM dome and spikelet meristems during the spikelet initiation phase suggesting roles in meristem activity/initiation in barley. Further, many pieces of evidence suggest PAs function as anti-senescent molecules, particularly exogenous applications of Spd and Spm delayed leaf senescence in several plant species, including barley, by preventing chlorophyll loss and protein degradation (Sobieszczuk-Nowicka, 2017). In the present study, a reduction in the levels of Spd signals happened during the spike growth phase

in the IM and a few apical nodes of the WT section from W6.5 and earlier from W5.0 in the *tst2.b* mutant sections. This reduction seems to happen in both sections before their respective onset of PTD, suggesting a decrease in IM activity. Previous studies on PA metabolism during inflorescence development in cereals provide convincing evidence for their positive regulation of growth and development (Lv et al., 2021). Higher levels of Spd and Spm in the apical kernels in maize resulted in higher grain set depending on high sugar availability acting antagonistic to ethylene biosynthesis (Feng et al., 2011). A recent study found increased levels of Spd and Spm in wheat spikelets mediated by trehalose at low-temperature stress conditions (Liang et al., 2021). Exogenous trehalose increased endogenous levels of Spd and Spm in wheat spikelets, as well as activities of ROS scavenging enzymes at low-temperature stress, suggesting possible involvement of PA signaling on ROS homeostasis to regulate wheat floret fertility. The present study also found high ROS levels and increased ethylene biosynthesis and ROS-related gene expression in the apical parts during the spikelet growth phase (sections 3.2.3, 3.3.2, and 4.3). These pieces of evidence suggest that high Spd and Spm levels found in the IM dome and spikelet meristems during early developing stages might help for ROS homeostasis, while either their reduction caused by their catabolism or absence of biosynthesis might trigger the onset of PTD. Thus, identification and manipulation of polyamine pathway genes in barley inflorescence development may further help in elucidating their function on spikelet initiation, development, and spike PTD.

In addition to PAs, an exciting distribution was observed for m/z 496.3 \pm 0.1 Da [M+H]⁺ and 534.3 \pm 0.1 Da [M+K]⁺ corresponding to the lipid species lysophosphatidylcholine [LPC(16:0)]. Vascular cell-specific distribution of LPC(16:0) seems to play a role in spike vascular patterning. A recent study found reduced vascularization towards the spike apex in the WT Bowman, and the *tst2.b* mutant may account for apical degeneration (Huang et al., 2023). The mutants have a more substantial reduction in the vascular area towards the apex compared to the WT, reasoning for its enhanced apical degeneration. The present study also found vascular-specific patterning of LPC(16:0) showing an acropetal reduction in both WT and mutant during the spike growth phase, while the patterning found disturbed earlier at W5.0 in a mutant with weak and absence of LPC signal in most of the apical nodes. Though the functions of LPC on plant development are not much known, LPC species were found to have some

cell-to-cell signaling functions in root development (Poulsen et al., 2015), arbuscular mycorrhizal symbiosis (Drissner et al., 2007) and stomatal openings (Seo et al., 2008). Though the molecular mechanisms are unclear, it seems to modulate the plasma membrane H⁺-ATPase that functions in the nutrient transport process (Viehweger et al., 2002).

Similarly, we can speculate that LPC has a function in signal transduction during vascular patterning in barley spikes. On the other hand, the pattern for LPC(16:0) observed at W3.0 resembles the patterns observed for auxin efflux carriers PIN-FORMED (PIN) proteins during primordia initiation in *Brachypodium* spikelet meristem which also functions in vascular patterning (O'Connor et al., 2014). These LPC species are generated by specific phospholipase A₂ (Poulsen et al., 2015). The mechanism linking the requirement of phospholipase A₂ for PIN protein trafficking is also reported (Lee et al., 2010). Thus, these shreds of evidence also suggest the possibility of LPC to function during auxin-transport mediated patterning of vascular development in barley spike meristems. Overall, patterns observed in both WT and mutant suggest that proper vascular establishment, thereby connecting each spikelet to the central axis, is essential for normal spikelet development, possibly through regulated assimilate transport and signaling. Altogether, MALDI MSI in barley spike meristems has revealed novel metabolic pathways that may open new questions and research directions. These findings also pose the significance of using spatial metabolomics for studying spike metabolism because such vital spatial information will be missed in conventional invasive metabolomics studies.

5. Outlook

The present study has identified several gene modulators that might potentially involve in spike PTD. Functional knockout of a single gene, *HvGT1*, among the putative PTD candidates has already shown a significant effect on spikelet survival, suggesting the data generated here may serve as an excellent resource for future studies. Moreover, the loss of *HvGT1* function achieved by targeted mutagenesis only delayed but did not abolish PTD, suggesting upstream regulators of spike PTD need to be identified. Therefore, by carefully mining other apically expressed genes, particularly those designated here as putative PTD candidates, and exploiting the natural allelic variants, their functional validation and multiplex editing may increase grain yield potential in barley and other related cereals.

Growth suppression function of HD-ZIP class I gene family members on developmental traits have been identified in grasses such as maize (*GT1*) (Klein et al., 2022), wheat (*GNI-A1*) (Sakuma et al., 2019) and barley (*VRS1*) (Komatsuda et al., 2007). A recent study also reported that *GT1* and *VRS1* homologs in *Brachypodium* showed conserved growth repression function and discussed the evolutionary recruitment of duplicated HD-ZIP class I members as growth repressors for different developmental contexts (Gallagher et al., 2023). The present study confirms *GT1*'s function as a growth repressor in apical spikelet and axillary bud growth in barley. In addition to *GT1*, three other HD-ZIP TFs were highly expressed in the degenerating apical parts, including *HvHOX2*, a duplicated paralog of *VRS1*. While *VRS1* is well-known for its function on lateral spikelet suppression, the role of *HvHOX2* still remain elusive in barley, though it has been postulated to promote lateral spikelet development (Thirulogachandar et al., 2021a). Independent analysis of the barley spike transcriptome atlas also showed high expression in the IM for *HvHOX2* and two other HD-ZIP TFs. It would be interesting to study these paralogs or homologs within barley, which are co-expressed with *GT1*, to get more insights on their functional redundancy, as *gt1* mutants have only partially restored apical spikelet growth. Further downstream analyses in the *Hvgt* mutant generated during this study may help identify those pathways/genes that are associated with the possible mechanisms or regulators behind spike PTD.

On the other hand, an interesting observation in the present study is the increased expression of several members of senescence-associated NAC TFs and other senescence-associated genes in the degenerating apical parts. Considering that

several members of NAC have been shown to function in leaf senescence and other cell-death related processes in several plant species, including barley, dissecting functions of NAC regulatory networks on spike PTD seems to be essential. Moreover, studying the function of senescence-associated *HvS40-like* gene on spike PTD is necessary as this was found among the top 10 hub genes identified in the PTD-associated gene network module generated by WGCNA analysis. Altogether, I propose, multiplex-editing or stacking the loss-of-function/weak alleles of these negative regulators of apical growth may be a potential target for increasing grain number in barley.

Apart from focusing on genes functioning on spike PTD, the transcriptome resource generated in the present study is an excellent source for studies on spike shape. The lanceolate spike shape at W5.0, with the onset of spike elongation at W6.5, became oblong with a higher degree of developmental synchronicity between the spikelets at central and basal positions. WGCNA also identified several gene network modules with specific expression shapes that can be related to developmental synchrony and changes in spike shape. Identifying top hub genes in those modules and functionally characterizing key genes may help us reveal novel information on gene regulatory networks behind spikelet development and spike growth.

MALDI MSI in barley spike meristems revealed potentially novel metabolic pathways, which open new questions and research directions. Considering the anti-senescence or pro-survival functions of spermidine/spermine (Sobieszczuk-Nowicka et al., 2019), identifying specific polyamine catabolism genes, such as polyamine oxidases expressing high in apical parts of the spikes, is necessary. Developing barley mutants with reduced or loss-of-function of these genes to increase polyamine levels may help us to unveil the function of spermidine/spermine in barley spikelet development, IM longevity, and (or) spikelet survival. However, the study here was conducted only in the positive ionization mode using sublimated DHB as a matrix. Sublimation is a solvent-free method for matrix deposition; therefore, diffusion of most analyte molecules during matrix application is almost eliminated compared to wet deposition methods. Though sublimation is simple, fast, and reproducible while avoiding analyte delocalization, it is crucial to consider reduced analyte extraction efficiency due to the absence of a solvent. However, some rehydration of sections after sublimation has been reported to improve the detection sensitivity (Dong et al., 2016b). Detection of a

particular class of compounds also depends on the ionization mode, the type of matrices, deposition methods, and instrumentation used. Performing MALDI MSI in both ionization modes with the state-of-art MSI instrumentation may help us unveil more diverse metabolites, including hormones at the much higher mass resolution, sensitivity, and even higher spatial resolutions.

On the other hand, genome-wide spatial transcriptomics is also emerging in plant research and recently have been reported for germinating barley grains at the spatial resolution of about 55 μm using 10x Genomics Visium (Peirats-Llobet et al., 2023). Also, the recently introduced Stereo-seq, a single-cell spatial enhanced resolution omics sequencing, enables *in situ* visualization of gene expression in Arabidopsis leaf cells at an exceptionally high spatial resolution of up to 500 nm (Xia et al., 2022). Studying spatiotemporal developmental trajectories of specific cell types combined with spatial metabolomics and spatial transcriptomics to reveal metabolomic changes and transcriptome reprogramming will benefit our understanding of the processes confined to specific cell types. Further, a systems biology approach that integrates multiple omics data, computational modeling, and prediction of the cellular functions may further help us understand the biological mechanism underlying complex traits like spike PTD or grain number determination. Given these, with several pertinent questions on spike PTD/spikelet survival remaining to be addressed (Figure 4.44A), I feel that applying recently developed technologies, or those currently in development in addition to the available information, will allow us to fill the knowledge gaps rapidly.

6. Summary

In many cereal crops, not all the initiated floret primordia develop to become fertile florets that form grains. Arrest and cessation of IM or SM apex followed by the basipetal degeneration of apical spikelet/florets and their axes are widespread among cereals (Bonnett, 1966). This phenomenon generally happens during the pre-anthesis phase of reproductive development in the cereal inflorescences possessing indeterminate meristems. Pre-anthesis tip degeneration (PTD) varies among cereal species depending on the position of indeterminate meristems. In barley (*Hordeum vulgare* L.), one of the major temperate cereals in tribe Triticeae, PTD starts with growth arrest of the IM dome, followed basipetally by the degeneration of spikelet primordia and the central axis. Due to its quantitative nature and environmental sensitivity, inflorescence PTD constitutes a complex, multilayered trait affecting final grain number. Reducing spikelet/floret loss during the pre-anthesis phase of reproductive development represents an opportunity to increase grain yield in barley and related cereals. However, the molecular mechanism behind spike PTD in barley remains elusive.

In the present study, spike developmental and histological studies were performed in two-rowed barley cv. Bowman and six-rowed cv. Morex under standardized growth conditions. Based on the findings on the number of spikelet primordia initiated, onset, and extent of apical degeneration, spike PTD in barley appears to be a highly predictable and heritable trait under standardized growth conditions, consistent with a developmentally programmed mechanism. To elucidate the molecular underpinnings of spike PTD, the present study combined metabolomics and transcriptomic approaches by analyzing dividing spikes of two- and six-rowed barley cultivars into degenerating apical and viable central and basal regions at stages before and during the onset of PTD over two weeks. These multi-omics studies revealed that barley spike PTD is accompanied by sugar depletion, amino acid degradation, and abscisic acid responses involving transcriptional regulators of senescence, defense, and light signaling. Photosynthesis, spike greening, and energy metabolism are significant contributors to proper spikelet growth and differentiation and were restricted to basal and central parts. Based on transcriptome analyses, barley *GRASSY TILLERS1* (*HvGT1*), encoding an HD-ZIP class I transcription factor, was identified as a novel modulator of spike PTD. A gene-edited knockout mutant of *HvGT1* delayed PTD with more differentiated apical spikelets and increased final spikelet number, suggesting a

possible means to increase grain number in cereals. Altogether, this study proposes a molecular framework that leads to barley spike PTD, the manipulation of which may increase yield potential in barley and other related cereals. Moreover, the putative gene candidates for spike PTD identified here may serve as an excellent resource for exploiting their natural allelic variants; at the same time, their functional validation and editing may lead to an increase in grain yield potential in barley and other related cereals.

In addition, the present study demonstrated spatial metabolomics in the developing barley inflorescence for the first time using the matrix-assisted laser/desorption ionization (MALDI) mass spectrometry imaging (MSI) technique. MALDI MSI was performed in the longitudinal sections of barley spikes from spikelet initiation and spike growth phases in the mass range between 80 and 1000Da, led to the detection of molecular ions of diverse classes, including amino acids, sugars, polyamines, chlorophyll, and lipids. Preliminary data analysis revealed highly tissue-specific and developmental differences for the metabolites distributed in the developing spike sections. Further, performing MALDI MSI in wild-type Bowman and a mutant *tst2.b* defective in normal spike development revealed the significance of detected metabolites on spikelet development and growth. This led to the identification of novel metabolic pathways governing barley inflorescence development. Polyamines, spermidine/spermine were found distributed specifically in IM and SMs, while lipid signals LPC (16:0) were found localized in vascular cells. Weak or distorted distribution of these signals in the *tst2.b* mutant reveals their possible functions on normal spikelet development, spike growth, and PTD. Altogether, MALDI MSI in barley spike meristems reveals novel metabolic pathways that open new questions and research directions.

7. Zusammenfassung

Bei vielen Getreidearten entwickeln sich nicht alle induzierten Blütenprimordien zu fruchtbaren, kornbildenden Blüentrieben. Die Entwicklungsunterbrechung bzw. der Abbruch der IM- oder SM-Apices, gefolgt von der basipetalen Degeneration der apikalen Ährchen/Blütchen und ihrer Achsen, sind bei Getreidearten weit verbreitet. Dieses Phänomen tritt in der Regel in der Vor-Blüte-Phase der reproduktiven Entwicklung von Getreideblütenständen auf, die nicht determinierte Meristeme besitzen. Die Degeneration des Apikalmeristems vor der Anthese (PTD) variiert je nach Position der nicht determinierten Meristeme bei verschiedenen Getreidearten. Bei Gerste (*Hordeum vulgare* L.), einer der wichtigsten Getreidearten der gemäßigten Zonen im Stamm der Triticeae, beginnt die PTD mit dem Wachstumsstillstand der IM-Kuppel, gefolgt von der Degeneration der Ährchenprimordien und der zentralen Achse. Aufgrund ihres quantitativen Charakters und ihrer Empfindlichkeit gegenüber Umwelteinflüssen ist die PTD in den Blütenständen ein komplexes, vielschichtiges Merkmal, das die endgültige Kornzahl beeinflusst. Die Verringerung des Ährchen-/Blütenverlustes während der Vor-Blüte-Phase der Reproduktionsentwicklung stellt eine Möglichkeit dar, den Kornertrag bei Gerste und verwandten Getreidearten zu steigern. Der molekulare Mechanismus, der dem apikalen Ährchenverlust bei Gerste zugrunde liegt, ist jedoch nach wie vor ungeklärt.

In der vorliegenden Studie wurden Ährenentwicklung und histologische Untersuchungen an zweizeiliger Gerste cv. Bowman und sechszeiliger Gerste cv. Morex unter standardisierten Wachstumsbedingungen durchgeführt. Basierend auf den Erkenntnissen über die Anzahl der gebildeten Ährchenprimordien, den Beginn und das Ausmaß der apikalen Degeneration scheint die Ährchen-PTD bei Gerste unter standardisierten Wachstumsbedingungen ein hochgradig vorhersagbares und vererbbares Merkmal zu sein, das mit einem entwicklungsprogrammierten Mechanismus übereinstimmt. Um die molekularen Grundlagen der Ährchen-PTD aufzuklären, wurden in der vorliegenden Studie Metabolomik- und Transkriptomik-Ansätze kombiniert, indem Ähren von zwei- und sechszeiligen Gerstensorten in degenerierende apikale und lebensfähige zentrale und basale Regionen in Stadien vor und während des Auftretens der PTD über zwei Wochen analysiert wurden. Diese Multi-omics-Studien ergaben, dass die PTD der Gerstenähre mit Zuckerabbau, Aminosäureabbau und Abscisinsäure-Reaktionen einhergeht, an denen

Transkriptionsregulatoren der Seneszenz, der Verteidigung und der Lichtsignalgebung beteiligt sind. Photosynthese, Ergrünen der Ähre und Energiestoffwechsel tragen wesentlich zum Wachstum und zur Differenzierung der Ährchen bei und sind auf die basalen und zentralen Teile beschränkt. Auf der Grundlage von Transkriptomanalysen wurde Gerste *GRASSY TILLERS1 (HvGT1)*, das für einen HD-ZIP-Klasse-I-Transkriptionsfaktor kodiert, als ein neuartiger Modulator der Ährchen-PTD identifiziert. Eine gen-editierte Knockout-Mutante von *HvGT1* verzögerte die PTD mit differenzierteren apikalen Ährchen und einer erhöhten Anzahl der endgültigen Ährchen, was auf einen möglichen Weg zur Erhöhung der Kornzahl bei Getreide hindeutet. Insgesamt wird in dieser Studie ein molekularer Rahmen vorgeschlagen, der zur PTD der Gerstenähre führt und dessen Beeinflussung das Ertragspotenzial von Gerste und anderen verwandten Getreidearten erhöhen könnte. Darüber hinaus können die hier identifizierten mutmaßlichen Genkandidaten für die Ährchen-PTD als hervorragende Ressource für die Nutzung ihrer natürlichen Allelvarianten dienen; gleichzeitig kann ihre funktionelle Validierung und Bearbeitung zu einer Steigerung des Kornertragspotenzials bei Gerste und anderen verwandten Getreidearten führen.

Darüber hinaus wurde in der vorliegenden Studie zum ersten Mal die räumliche Metabolomik in Gersten-Blütenstandsmeristemen mit Hilfe der MALDI-Massenspektrometrie (MSI) nachgewiesen. MALDI MSI wurde in den Längsschnitten von Gerstenähren aus den Phasen der Ährenbildung und des Ährenwachstums im Massenbereich zwischen 80 und 1000Da durchgeführt und führte zum Nachweis von Molekülen verschiedener Klassen, darunter Aminosäuren, Zucker, Polyamine, Chlorophyll und Lipide. Die vorläufige Datenanalyse ergab sehr gewebespezifische und entwicklungsbedingte Unterschiede bei den Metaboliten, die in den sich entwickelnden Ährenabschnitten verteilt sind. Die Durchführung von MALDI MSI in Bowman-Wildtypen und einer *tst2.b*-Mutante, bei der die normale Ährenentwicklung gestört ist, zeigte die Bedeutung der nachgewiesenen Metaboliten für die Entwicklung und das Wachstum der Ährchen. Dies führte zur Identifizierung neuer Stoffwechselwege, die die Entwicklung der Gerstenblütenstände steuern. Polyamine, Spermidin/Spermin wurden spezifisch in IM und SM verteilt gefunden, während Lipidsignale LPC (16:0) in Gefäßzellen lokalisiert wurden. Die schwache oder verzerrte Verteilung dieser Signale in der *tst2.b*-Mutante lässt auf ihre möglichen Funktionen für die normale Ährchenentwicklung, das Ährenwachstum und die PTD

schließen. Insgesamt zeigt die MALDI MSI in Gerstenährenmeristemem neue Stoffwechselwege auf, die neue Fragen und Forschungsrichtungen eröffnen.

8. References

- ABBAI, R., SINGH, V. K., NACHIMUTHU, V. V., SINHA, P., SELVARAJ, R., VIPPARLA, A. K., SINGH, A. K., SINGH, U. M., VARSHNEY, R. K. & KUMAR, A. 2019. Haplotype analysis of key genes governing grain yield and quality traits across 3K RG panel reveals scope for the development of tailor-made rice with enhanced genetic gains. *Plant Biotechnology Journal*, 17, 1612-1622.
- ACHARYA, B. R., JEON, B. W., ZHANG, W. & ASSMANN, S. M. 2013. Open Stomata 1 (OST1) is limiting in abscisic acid responses of Arabidopsis guard cells. *New Phytologist*, 200, 1049-1063.
- ACOSTA, I. F., LAPARRA, H., ROMERO, S. P., SCHMELZ, E., HAMBERG, M., MOTTINGER, J. P., MORENO, M. A. & DELLAPORTA, S. L. 2009. tasselseed1 Is a Lipoyxygenase Affecting Jasmonic Acid Signaling in Sex Determination of Maize. *Science*, 323, 262-265.
- AHARONI, N. & RICHMOND, A. E. 1978. Endogenous Gibberellin and Abscisic Acid Content as Related to Senescence of Detached Lettuce Leaves 1. *Plant Physiology*, 62, 224-228.
- AHKAMI, A. H., LISCHEWSKI, S., HAENSCH, K. T., PORFIROVA, S., HOFMANN, J., ROLLETSCHEK, H., MELZER, M., FRANKEN, P., HAUSE, B., DRUEGE, U. & HAJIREZAEI, M. R. 2009. Molecular physiology of adventitious root formation in *Petunia hybrida* cuttings: involvement of wound response and primary metabolism. *New Phytologist*, 181, 613-625.
- ALABDULLAH, A. K., BORRILL, P., MARTIN, A. C., RAMIREZ-GONZALEZ, R. H., HASSANI-PAK, K., UAUY, C., SHAW, P. & MOORE, G. 2019. A Co-Expression Network in Hexaploid Wheat Reveals Mostly Balanced Expression and Lack of Significant Gene Loss of Homeologous Meiotic Genes Upon Polyploidization. *Frontiers in Plant Science*, 10.
- ALCÁZAR, R., GARCÍA, A. V., KRONHOLM, I., DE MEAUX, J., KOORNNEEF, M., PARKER, J. E. & REYMOND, M. 2010. Natural variation at Strubbelig Receptor Kinase 3 drives immune-triggered incompatibilities between *Arabidopsis thaliana* accessions. *Nature Genetics*, 42, 1135-1139.
- ALEXANDROV, T. 2020. Spatial Metabolomics and Imaging Mass Spectrometry in the Age of Artificial Intelligence. *Annu Rev Biomed Data Sci*, 3, 61-87.
- ALI, A., XU, P., RIAZ, A. & WU, X. 2019. Current Advances in Molecular Mechanisms and Physiological Basis of Panicle Degeneration in Rice. *Int J Mol Sci*, 20.
- ALQUDAH, A. M. & SCHNURBUSCH, T. 2014. Awn primordium to tipping is the most decisive developmental phase for spikelet survival in barley. *Funct Plant Biol*, 41, 424-436.
- ALQUDAH, A. M., SHARMA, R. & BÖRNER, A. 2021. Insight into the genetic contribution of maximum yield potential, spikelet development and abortion in barley. *Plants, People, Planet*, 3, 721-736.
- ALVAREZ, M. E., SAVOURE, A. & SZABADOS, L. 2022. Proline metabolism as regulatory hub. *Trends Plant Sci*, 27, 39-55.
- AMANDA, D., FREY, F. P., NEUMANN, U., PRZYBYL, M., ŠIMURA, J., ZHANG, Y., CHEN, Z., GALLAVOTTI, A., FERNIE, A. R., LJUNG, K. & ACOSTA, I. F. 2022. Auxin boosts energy generation pathways to fuel pollen maturation in barley. *Curr Biol*, 32, 1798-1811.e8.
- ARISNABARRETA, S. & MIRALLES, D. J. 2006. Floret development and grain setting in near isogenic two- and six-rowed barley lines (*Hordeum vulgare* L.). *Field Crops Research*, 96, 466-476.

- AUBUCHON-ELDER, T., CONEVA, V., GOAD, D. M., JENKINS, L. M., YU, Y., ALLEN, D. K. & KELLOGG, E. A. 2020. Sterile Spikelets Contribute to Yield in Sorghum and Related Grasses. *Plant Cell*, 32, 3500-3518.
- AVILA-OSPINA, L., CLÉMENT, G. & MASCLAUX-DAUBRESSE, C. 2017. Metabolite Profiling for Leaf Senescence in Barley Reveals Decreases in Amino Acids and Glycolysis Intermediates. *Agronomy*, 7, 15.
- AVILA-OSPINA, L., MARMAGNE, A., TALBOTEC, J., KRUPINSKA, K. & MASCLAUX-DAUBRESSE, C. 2015. The identification of new cytosolic glutamine synthetase and asparagine synthetase genes in barley (*Hordeum vulgare* L.), and their expression during leaf senescence. *J Exp Bot*, 66, 2013-26.
- BADR, A., M, K., SCH, R., RABEY, H. E., EFFGEN, S., IBRAHIM, H. H., POZZI, C., ROHDE, W. & SALAMINI, F. 2000. On the Origin and Domestication History of Barley (*Hordeum vulgare*). *Molecular Biology and Evolution*, 17, 499-510.
- BAIK, B.-K. & ULLRICH, S. E. 2008. Barley for food: Characteristics, improvement, and renewed interest. *Journal of Cereal Science*, 48, 233-242.
- BAILEY-SERRES, J., PARKER, J. E., AINSWORTH, E. A., OLDROYD, G. E. D. & SCHROEDER, J. I. 2019. Genetic strategies for improving crop yields. *Nature*, 575, 109-118.
- BALAZADEH, S., RIANO-PACHON, D. M. & MUELLER-ROEBER, B. 2008. Transcription factors regulating leaf senescence in *Arabidopsis thaliana*. *Plant Biol (Stuttg)*, 10 Suppl 1, 63-75.
- BALAZADEH, S., SCHILDHAUER, J., ARAÚJO, W. L., MUNNÉ-BOSCH, S., FERNIE, A. R., PROOST, S., HUMBECK, K. & MUELLER-ROEBER, B. 2014. Reversal of senescence by N resupply to N-starved *Arabidopsis thaliana*: transcriptomic and metabolomic consequences. *Journal of Experimental Botany*, 65, 3975-3992.
- BANCAL, P. 2008. Positive contribution of stem growth to grain number per spike in wheat. *Field Crops Research*, 105, 27-39.
- BANCAL, P. 2009. Early development and enlargement of wheat floret primordia suggest a role of partitioning within spike to grain set. *Field Crops Research*, 110, 44-53.
- BARKLEY, A. N. & WANG, L. M. 2008. Application of TILLING and EcoTILLING as Reverse Genetic Approaches to Elucidate the Function of Genes in Plants and Animals. *Current Genomics*, 9, 212-226.
- BAUER, E., SCHMUTZER, T., BARILAR, I., MASCHER, M., GUNDLACH, H., MARTIS, M. M., TWARDZIOK, S. O., HACKAUF, B., GORDILLO, A., WILDE, P., SCHMIDT, M., KORZUN, V., MAYER, K. F. X., SCHMID, K., SCHÖN, C.-C. & SCHOLZ, U. 2017. Towards a whole-genome sequence for rye (*Secale cereale* L.). *The Plant Journal*, 89, 853-869.
- BEGCY, K., NOSENKO, T., ZHOU, L.-Z., FRAGNER, L., WECKWERTH, W. & DRESSELHAUS, T. 2019. Male Sterility in Maize after Transient Heat Stress during the Tetrad Stage of Pollen Development1 [OPEN]. *Plant Physiology*, 181, 683-700.
- BENGOA LUONI, S., ASTIGUETA, F. H., NICOSIA, S., MOSCHEN, S., FERNANDEZ, P. & HEINZ, R. 2019. Transcription Factors Associated with Leaf Senescence in Crops. *Plants*, 8, 411.
- BENJAMINI, Y. & HOCHBERG, Y. 1995. CONTROLLING THE FALSE DISCOVERY RATE - A PRACTICAL AND POWERFUL APPROACH TO MULTIPLE TESTING. *Journal of the Royal Statistical Society Series B-Statistical Methodology*, 57, 289-300.

- BHANDARI, D. R., WANG, Q., FRIEDT, W., SPENGLER, B., GOTTWALD, S. & RÖMPP, A. 2015. High resolution mass spectrometry imaging of plant tissues: towards a plant metabolite atlas. *Analyst*, 140, 7696-7709.
- BI, X., VAN ESSE, W., MULKI, M. A., KIRSCHNER, G., ZHONG, J., SIMON, R. & VON KORFF, M. 2019. CENTRORADIALIS Interacts with FLOWERING LOCUS T-Like Genes to Control Floret Development and Grain Number. *Plant Physiol*, 180, 1013-1030.
- BINENBAUM, J., WEINSTAIN, R. & SHANI, E. 2018. Gibberellin Localization and Transport in Plants. *Trends Plant Sci*, 23, 410-421.
- BJARNHOLT, N., LI, B., D'ALVISE, J. & JANFELT, C. 2014. Mass spectrometry imaging of plant metabolites – principles and possibilities. *Natural Product Reports*, 31, 818-837.
- BLAZQUEZ, M. A., NELSON, D. C. & WEIJERS, D. 2020. Evolution of Plant Hormone Response Pathways. *Annu Rev Plant Biol*, 71, 327-353.
- BLEECKER, A. B. & PATTERSON, S. E. 1997. Last exit: Senescence, abscission, and meristem arrest in Arabidopsis. *Plant Cell*, 9, 1169-1179.
- BODEN, S. A., WEISS, D., ROSS, J. J., DAVIES, N. W., TREVASKIS, B., CHANDLER, P. M. & SWAIN, S. M. 2014. EARLY FLOWERING3 Regulates Flowering in Spring Barley by Mediating Gibberellin Production and FLOWERING LOCUS T Expression. *Plant Cell*, 26, 1557-1569.
- BOMMERT, P., LUNDE, C., NARDMANN, J., VOLLBRECHT, E., RUNNING, M., JACKSON, D., HAKE, S. & WERR, W. 2005. thick tassel dwarf1 encodes a putative maize ortholog of the Arabidopsis CLAVATA1 leucine-rich repeat receptor-like kinase. *Development*, 132, 1235-1245.
- BOMMERT, P., NAGASAWA, N. S. & JACKSON, D. 2013. Quantitative variation in maize kernel row number is controlled by the FASCIATED EAR2 locus. *Nature Genetics*, 45, 334-337.
- BOMMERT, P. & WHIPPLE, C. 2018. Grass inflorescence architecture and meristem determinacy. *Semin Cell Dev Biol*, 79, 37-47.
- BONNETT, O. T. 1966. *Inflorescences of Maize, Wheat, Rye, Barley, and Oats: Their Initiation and Development*, University of Illinois, College of Agriculture, Agricultural Experiment Station.
- BORISJUK, L., HORN, P., CHAPMAN, K., JAKOB, P. M., GÜNDEL, A. & ROLLETSCHEK, H. 2023. Seeing plants as never before. *New Phytologist*, n/a.
- BORRAS-GELONCH, G., REBETZKE, G. J., RICHARDS, R. A. & ROMAGOSA, I. 2012. Genetic control of duration of pre-anthesis phases in wheat (*Triticum aestivum* L.) and relationships to leaf appearance, tillering, and dry matter accumulation. *Journal of Experimental Botany*, 63, 69-89.
- BORRILL, P., HARRINGTON, S. A., SIMMONDS, J. & UAUY, C. 2019. Identification of Transcription Factors Regulating Senescence in Wheat through Gene Regulatory Network Modelling. *Plant Physiol*, 180, 1740-1755.
- BOUSSORA, F., ALLAM, M., GUASMI, F., FERCHICHI, A., RUTTEN, T., HANSSON, M., YOUSSEF, H. M. & BORNER, A. 2019. Spike developmental stages and ABA role in spikelet primordia abortion contribute to the final yield in barley (*Hordeum vulgare* L.). *Bot Stud*, 60, 13.
- BRAY, N. L., PIMENTEL, H., MELSTED, P. & PACTER, L. 2016. Near-optimal probabilistic RNA-seq quantification. *Nature Biotechnology*, 34, 525-527.
- BREEZE, E., HARRISON, E., MCHATTIE, S., HUGHES, L., HICKMAN, R., HILL, C., KIDDLE, S., KIM, Y. S., PENFOLD, C. A., JENKINS, D., ZHANG, C., MORRIS, K., JENNER, C., JACKSON, S., THOMAS, B., TABRETT, A., LEGAIE, R., MOORE, J. D., WILD, D. L., OTT, S., RAND, D., BEYNON, J., DENBY, K.,

- MEAD, A. & BUCHANAN-WOLLASTON, V. 2011. High-resolution temporal profiling of transcripts during Arabidopsis leaf senescence reveals a distinct chronology of processes and regulation. *Plant Cell*, 23, 873-94.
- BROWN, R. H. & BREGITZER, P. 2011. A Ds Insertional Mutant of a Barley miR172 Gene Results in Indeterminate Spikelet Development. *Crop Science*, 51, 1664-1672.
- BROWNING, B. L., ZHOU, Y. & BROWNING, S. R. 2018. A One-Penny Imputed Genome from Next-Generation Reference Panels. *American Journal of Human Genetics*, 103, 338-348.
- BUCHANAN-WOLLASTON, V., PAGE, T., HARRISON, E., BREEZE, E., LIM, P. O., NAM, H. G., LIN, J.-F., WU, S.-H., SWIDZINSKI, J., ISHIZAKI, K. & LEAVER, C. J. 2005. Comparative transcriptome analysis reveals significant differences in gene expression and signalling pathways between developmental and dark/starvation-induced senescence in Arabidopsis. *The Plant Journal*, 42, 567-585.
- BULL, H., CASAO, M. C., ZWIREF, M., FLAVELL, A. J., THOMAS, W. T. B., GUO, W., ZHANG, R., RAPAOTE-FLORES, P., KYRIAKIDIS, S., RUSSELL, J., DRUKA, A., MCKIM, S. M. & WAUGH, R. 2017. Barley SIX-ROWED SPIKE3 encodes a putative Jumonji C-type H3K9me2/me3 demethylase that represses lateral spikelet fertility. *Nature Communications*, 8, 936.
- BURGESS, A. J., MASCLAUX-DAUBRESSE, C., STRITTMATTER, G., WEBER, A. P. M., TAYLOR, S. H., HARBINSON, J., YIN, X., LONG, S., PAUL, M. J., WESTHOFF, P., LORETO, F., CERIOTTI, A., SALTENIS, V. L. R., PRIBIL, M., NACRY, P., SCHARFF, L. B., JENSEN, P. E., MULLER, B., COHAN, J. P., FOULKES, J., ROGOWSKY, P., DEBAEKE, P., MEYER, C., NELISSEN, H., INZÉ, D., KLEIN LANKHORST, R., PARRY, M. A. J., MURCHIE, E. H. & BAEKELANDT, A. 2022. Improving crop yield potential: Underlying biological processes and future prospects. *Food and Energy Security*.
- BURROWS, V. D. 1986. Breeding oats for food and feed: conventional and new techniques and materials.
- CALLENS, C., FERNANDEZ-GOMEZ, J., TUCKER, M. R., ZHANG, D. & WILSON, Z. A. 2022. Heat stress responses vary during floret development in European spring barley cultivars. *Front Plant Sci*, 13, 918730.
- CAUGHLIN, S., PARK, D. H., YEUNG, K. K., CECETTO, D. F. & WHITEHEAD, S. N. 2017. Sublimation of DAN Matrix for the Detection and Visualization of Gangliosides in Rat Brain Tissue for MALDI Imaging Mass Spectrometry. *J Vis Exp*.
- CHA, J.-Y., KIM, M. R., JUNG, I. J., KANG, S. B., PARK, H. J., KIM, M. G., YUN, D.-J. & KIM, W.-Y. 2016. The Thiol Reductase Activity of YUCCA6 Mediates Delayed Leaf Senescence by Regulating Genes Involved in Auxin Redistribution. *Frontiers in Plant Science*, 7.
- CHELLAMUTHU, V. R., ERMILOVA, E., LAPINA, T., LUDDECKE, J., MINAEVA, E., HERRMANN, C., HARTMANN, M. D. & FORCHHAMMER, K. 2014. A widespread glutamine-sensing mechanism in the plant kingdom. *Cell*, 159, 1188-1199.
- CHEN, D., SHAO, Q., YIN, L., YOUNIS, A. & ZHENG, B. 2019. Polyamine Function in Plants: Metabolism, Regulation on Development, and Roles in Abiotic Stress Responses. *Frontiers in Plant Science*, 9.
- CHOW, C.-N., LEE, T.-Y., HUNG, Y.-C., LI, G.-Z., TSENG, K.-C., LIU, Y.-H., KUO, P.-L., ZHENG, H.-Q. & CHANG, W.-C. 2018. PlantPAN3.0: a new and updated

- resource for reconstructing transcriptional regulatory networks from ChIP-seq experiments in plants. *Nucleic Acids Research*, 47, D1155-D1163.
- CHRISTIANSEN, M. W. & GREGERSEN, P. L. 2014. Members of the barley NAC transcription factor gene family show differential co-regulation with senescence-associated genes during senescence of flag leaves. *J Exp Bot*, 65, 4009-22.
- CHRISTIANSEN, M. W., HOLM, P. B. & GREGERSEN, P. L. 2011. Characterization of barley (*Hordeum vulgare* L.) NAC transcription factors suggests conserved functions compared to both monocots and dicots. *BMC Research Notes*, 4, 302.
- CHROBOK, D., LAW, S. R., BROUWER, B., LINDEN, P., ZIOLKOWSKA, A., LIEBSCH, D., NARSAI, R., SZAL, B., MORITZ, T., ROUHIER, N., WHELAN, J., GARDESTROM, P. & KEECH, O. 2016. Dissecting the Metabolic Role of Mitochondria during Developmental Leaf Senescence. *Plant Physiol*, 172, 2132-2153.
- CHUCK, G., MEELEY, R., IRISH, E., SAKAI, H. & HAKE, S. 2007. The maize tasselseed4 microRNA controls sex determination and meristem cell fate by targeting Tasselseed6/indeterminate spikelet1. *Nature Genetics*, 39, 1517-1521.
- CLARK, M. A., DOMINGO, N. G. G., COLGAN, K., THAKRAR, S. K., TILMAN, D., LYNCH, J., AZEVEDO, I. L. & HILL, J. D. 2020. Global food system emissions could preclude achieving the 1.5°C and 2°C climate change targets. *Science*, 370, 705-708.
- COTTRELL, J. E., EASTON, R. H., DALE, J. E., WADSWORTH, A. C., ADAM, J. S., CHILD, R. D. & HOAD, G. V. 1985. A comparison of spike and spikelet survival in mainstem and tillers of barley. *Annals of Applied Biology*, 106, 365-377.
- COULTER, M., ENTIZNE, J. C., GUO, W., BAYER, M., WONNEBERGER, R., MILNE, L., SCHREIBER, M., HAANING, A., MUEHLBAUER, G. J., MCCALLUM, N., FULLER, J., SIMPSON, C., STEIN, N., BROWN, J. W. S., WAUGH, R. & ZHANG, R. 2022. BaRTv2: a highly resolved barley reference transcriptome for accurate transcript-specific RNA-seq quantification. *The Plant Journal*, 111, 1183-1202.
- DAGHMA, D. S., KUMLEHN, J. & MELZER, M. 2011. The use of cyanobacteria as filler in nitrocellulose capillaries improves ultrastructural preservation of immature barley pollen upon high pressure freezing. *Journal of Microscopy*, 244, 79-84.
- DALL'OSTO, L., CAZZANIGA, S., NORTH, H., MARION-POLL, A. & BASSI, R. 2007. The *Arabidopsis* *aba4-1* mutant reveals a specific function for neoxanthin in protection against photooxidative stress. *Plant Cell*, 19, 1048-64.
- DAMPANABOINA, L., JIAO, Y., CHEN, J., GLADMAN, N., CHOPRA, R., BUROW, G., HAYES, C., CHRISTENSEN, S. A., BURKE, J., WARE, D. & XIN, Z. 2019. Sorghum MSD3 Encodes an ω -3 Fatty Acid Desaturase that Increases Grain Number by Reducing Jasmonic Acid Levels. *International Journal of Molecular Sciences*, 20, 5359.
- DANEVA, A., GAO, Z., VAN DURME, M. & NOWACK, M. K. 2016. Functions and Regulation of Programmed Cell Death in Plant Development. *Annu Rev Cell Dev Biol*, 32, 441-468.
- DAVIES, P. J. & GAN, S. 2012. Towards an integrated view of monocarpic plant senescence. *Russian Journal of Plant Physiology*, 59, 467-478.
- DELLAPORTA, S. L. & CALDERON-URREA, A. 1994. The Sex Determination Process in Maize. *Science*, 266, 1501-1505.
- DELONG, A., CALDERON-URREA, A. & DELLAPORTA, S. L. 1993. Sex determination gene TASSELSEED2 of maize encodes a short-chain alcohol

- dehydrogenase required for stage-specific floral organ abortion. *Cell*, 74, 757-768.
- DELORME, V. G., MCCABE, P. F., KIM, D. J. & LEAVER, C. J. 2000. A matrix metalloproteinase gene is expressed at the boundary of senescence and programmed cell death in cucumber. *Plant Physiol*, 123, 917-27.
- DIGEL, B., PANKIN, A. & VON KORFF, M. 2015. Global Transcriptome Profiling of Developing Leaf and Shoot Apices Reveals Distinct Genetic and Environmental Control of Floral Transition and Inflorescence Development in Barley. *Plant Cell*, 27, 2318-34.
- DOBRENEL, T., CALDANA, C., HANSON, J., ROBAGLIA, C., VINCENTZ, M., VEIT, B. & MEYER, C. 2016. TOR Signaling and Nutrient Sensing. *Annu Rev Plant Biol*, 67, 261-85.
- DODSWORTH, S. 2009. A diverse and intricate signalling network regulates stem cell fate in the shoot apical meristem. *Developmental Biology*, 336, 1-9.
- DOENCH, J. G., HARTENIAN, E., GRAHAM, D. B., TOTHOVA, Z., HEGDE, M., SMITH, I., SULLENDER, M., EBERT, B. L., XAVIER, R. J. & ROOT, D. E. 2014. Rational design of highly active sgRNAs for CRISPR-Cas9-mediated gene inactivation. *Nature Biotechnology*, 32, 1262-1267.
- DONG, Y., LI, B. & AHARONI, A. 2016a. More than Pictures: When MS Imaging Meets Histology. *Trends Plant Sci*, 21, 686-698.
- DONG, Y., LI, B., MALITSKY, S., ROGACHEV, I., AHARONI, A., KAFTAN, F., SVATOŠ, A. & FRANCESCHI, P. 2016b. Sample Preparation for Mass Spectrometry Imaging of Plant Tissues: A Review. *Frontiers in Plant Science*, 7.
- DONG, Z., XIAO, Y., GOVINDARAJULU, R., FEIL, R., SIDDOWAY, M. L., NIELSEN, T., LUNN, J. E., HAWKINS, J., WHIPPLE, C. & CHUCK, G. 2019. The regulatory landscape of a core maize domestication module controlling bud dormancy and growth repression. *Nat Commun*, 10, 3810.
- DRECCER, M. F., WOCKNER, K. B., PALTA, J. A., MCINTYRE, C. L., BORGOGNONE, M. G., BOURGAULT, M., REYNOLDS, M. & MIRALLES, D. J. 2014. More fertile florets and grains per spike can be achieved at higher temperature in wheat lines with high spike biomass and sugar content at booting. *Funct Plant Biol*, 41, 482-495.
- DRISSNER, D., KUNZE, G., CALLEWAERT, N., GEHRIG, P., TAMASLOUKHT, M. B., BOLLER, T., FELIX, G., AMRHEIN, N. & BUCHER, M. 2007. Lyso-Phosphatidylcholine Is a Signal in the Arbuscular Mycorrhizal Symbiosis. *Science*, 318, 265-268.
- DRUKA, A., FRANCKOWIAK, J., LUNDQVIST, U., BONAR, N., ALEXANDER, J., HOUSTON, K., RADOVIC, S., SHAHINNIA, F., VENDRAMIN, V., MORGANTE, M., STEIN, N. & WAUGH, R. 2010. Genetic Dissection of Barley Morphology and Development. *Plant Physiology*, 155, 617-627.
- EGGERT, K. & VON WIREN, N. 2017. Response of the plant hormone network to boron deficiency. *New Phytologist*, 216, 868-881.
- ELLIS, C. M., NAGPAL, P., YOUNG, J. C., HAGEN, G., GUILFOYLE, T. J. & REED, J. W. 2005. AUXIN RESPONSE FACTOR1 and AUXIN RESPONSE FACTOR2 regulate senescence and floral organ abscission in *Arabidopsis thaliana*. *Development*, 132, 4563-4574.
- ELLIS, R. P. & KIRBY, E. J. M. 1980. A comparison of spring barley grown in England and in Scotland. 2. Yield and its components. *The Journal of Agricultural Science*, 95, 111 - 115.

- EMWAS, A.-H. M. 2015. The Strengths and Weaknesses of NMR Spectroscopy and Mass Spectrometry with Particular Focus on Metabolomics Research. *In*: BJERRUM, J. T. (ed.) *Metabonomics: Methods and Protocols*. New York, NY: Springer New York.
- ENOMOTO, H., SENSU, T., YUMOTO, E., YOKOTA, T. & YAMANE, H. 2018. Derivatization for detection of abscisic acid and 12-oxo-phytodienoic acid using matrix-assisted laser desorption/ionization imaging mass spectrometry. *Rapid Communications in Mass Spectrometry*, 32, 1565-1572.
- EVELAND, A. L. & JACKSON, D. P. 2012. Sugars, signalling, and plant development. *J Exp Bot*, 63, 3367-77.
- FAN, M., ZHANG, X., NAGARAJAN, R., ZHAI, W., RAUF, Y., JIA, H., MA, Z. & YAN, L. 2023. Natural variants and editing events provide insights into routes for spike architecture modification in common wheat. *The Crop Journal*, 11, 148-156.
- FAO. 2022. *Food and Agriculture Organization Corporate Statistical Database* [Online]. [Accessed].
- FAOSTAT, 2023a. <https://www.fao.org/faostat/en/#data/QCL>
- FAOSTAT, 2023b. <https://www.fao.org/faostat/en/#data/TCL>
- FEENSTRA, A. D., ALEXANDER, L. E., SONG, Z., KORTE, A. R., YANDEAU-NELSON, M. D., NIKOLAU, B. J. & LEE, Y. J. 2017. Spatial Mapping and Profiling of Metabolite Distributions during Germination. *Plant Physiol*, 174, 2532-2548.
- FENG, H.-Y., WANG, Z.-M., KONG, F.-N., ZHANG, M.-J. & ZHOU, S.-L. 2011. Roles of Carbohydrate Supply and Ethylene, Polyamines in Maize Kernel Set. *Journal of Integrative Plant Biology*, 53, 388-398.
- FENG, Q., DE RYCKE, R., DAGDAS, Y. & NOWACK, M. K. 2022. Autophagy promotes programmed cell death and corpse clearance in specific cell types of the Arabidopsis root cap. *Current Biology*, 32, 2110-2119.e3.
- FENG, X., LIU, W. X., CAO, F. B., WANG, Y. Z., ZHANG, G. P., CHEN, Z. H. & WU, F. B. 2020. Overexpression of HvAKT1 improves drought tolerance in barley by regulating root ion homeostasis and ROS and NO signaling. *Journal of Experimental Botany*, 71, 6587-6600.
- FERRANTE, A., SAVIN, R. & SLAFER, G. A. 2013. Floret development and grain setting differences between modern durum wheats under contrasting nitrogen availability. *J Exp Bot*, 64, 169-84.
- FERRANTE, A., SAVIN, R. & SLAFER, G. A. 2020. Floret development and spike fertility in wheat: Differences between cultivars of contrasting yield potential and their sensitivity to photoperiod and soil N. *Field Crops Research*, 256, 107908.
- FIGUEROA, C. M. & LUNN, J. E. 2016. A Tale of Two Sugars: Trehalose 6-Phosphate and Sucrose. *Plant Physiol*, 172, 7-27.
- FISCHER-KILBIENSKI, I., MIAO, Y., ROITSCH, T., ZSCHIESCHE, W., HUMBECK, K. & KRUPINSKA, K. 2010. Nuclear targeted AtS40 modulates senescence associated gene expression in Arabidopsis thaliana during natural development and in darkness. *Plant Mol Biol*, 73, 379-90.
- FORDE, B. G. & LEA, P. J. 2007. Glutamate in plants: metabolism, regulation, and signalling. *J Exp Bot*, 58, 2339-58.
- GALLAGHER, J. P., MAN, J., CHIARAMIDA, A., ROZZA, I., PATTERSON, E. L., POWELL, M., SCHRAGER-LAVELLE, A., MULTANI, D. S., MEELEY, R. & BARTLETT, M. E. 2023. Duplicate transcription factors GT1 and VRS1 regulate branching and fertile flower number in maize and Brachypodium distachyon. *bioRxiv*, 2023.03.15.532786.

- GAN, S. 2003. Mitotic and postmitotic senescence in plants. *Sci Aging Knowledge Environ*, 2003, Re7.
- GAN, S. & AMASINO, R. M. 1995. Inhibition of Leaf Senescence by Autoregulated Production of Cytokinin. *Science*, 270, 1986-1988.
- GAN, S. & AMASINO, R. M. 1997. Making Sense of Senescence (Molecular Genetic Regulation and Manipulation of Leaf Senescence). *Plant Physiol*, 113, 313-319.
- GAO, S., GAO, J., ZHU, X., SONG, Y., LI, Z., REN, G., ZHOU, X. & KUAI, B. 2016. ABF2, ABF3, and ABF4 Promote ABA-Mediated Chlorophyll Degradation and Leaf Senescence by Transcriptional Activation of Chlorophyll Catabolic Genes and Senescence-Associated Genes in Arabidopsis. *Molecular Plant*, 9, 1272-1285.
- GAO, Z., DANEVA, A., SALANENKA, Y., VAN DURME, M., HUYSMANS, M., LIN, Z., DE WINTER, F., VANNESTE, S., KARIMI, M., VAN DE VELDE, J., VANDEPOELE, K., VAN DE WALLE, D., DEWETTINCK, K., LAMBRECHT, B. N. & NOWACK, M. K. 2018. KIRA1 and ORESARA1 terminate flower receptivity by promoting cell death in the stigma of Arabidopsis. *Nature Plants*, 4, 365-375.
- GARIBAY-HERNÁNDEZ, A., KESSLER, N., JÓZEFOWICZ, A. M., TÜRKSOY, G. M., LOHWASSER, U. & MOCK, H.-P. 2021. Untargeted metabolotyping to study phenylpropanoid diversity in crop plants. *Physiologia Plantarum*, 173, 680-697.
- GAUFICHON, L., REISDORF-CREN, M., ROTHSTEIN, S. J., CHARDON, F. & SUZUKI, A. 2010. Biological functions of asparagine synthetase in plants. *Plant Science*, 179, 141-153.
- GHAFFARI, M. R., SHAHINNIA, F., USADEL, B., JUNKER, B., SCHREIBER, F., SREENIVASULU, N. & HAJIREZAEI, M. R. 2016. The Metabolic Signature of Biomass Formation in Barley. *Plant and Cell Physiology*, 57, 1943-1960.
- GHIGLIONE, H. O., GONZALEZ, F. G., SERRAGO, R., MALDONADO, S. B., CHILCOTT, C., CURA, J. A., MIRALLES, D. J., ZHU, T. & CASAL, J. J. 2008. Autophagy regulated by day length determines the number of fertile florets in wheat. *Plant J*, 55, 1010-24.
- GLADMAN, N., JIAO, Y., LEE, Y. K., ZHANG, L., CHOPRA, R., REGULSKI, M., BUROW, G., HAYES, C., CHRISTENSEN, S. A., DAMPANABOINA, L., CHEN, J., BURKE, J., WARE, D. & XIN, Z. 2019. Fertility of Pedicellate Spikelets in Sorghum Is Controlled by a Jasmonic Acid Regulatory Module. *International Journal of Molecular Sciences*, 20, 4951.
- GOL, L., HARALDSSON, E. B. & VON KORFF, M. 2021. Ppd-H1 integrates drought stress signals to control spike development and flowering time in barley. *J Exp Bot*, 72, 122-136.
- GÓMEZ-PORRAS, J. L., RIAÑO-PACHÓN, D. M., DREYER, I., MAYER, J. E. & MUELLER-ROEBER, B. 2007. Genome-wide analysis of ABA-responsive elements ABRE and CE3 reveals divergent patterns in Arabidopsis and rice. *BMC Genomics*, 8, 260.
- GOMEZ, F. M., CARRION, C. A., COSTA, M. L., DESEL, C., KIESELBACH, T., FUNK, C., KRUPINSKA, K. & GUIAMET, J. 2019. Extra-plastidial degradation of chlorophyll and photosystem I in tobacco leaves involving 'senescence-associated vacuoles'. *Plant J*, 99, 465-477.
- GONZÁLEZ-GRANDÍO, E., PAJORO, A., FRANCO-ZORRILLA, J. M., TARANCÓN, C., IMMINK, R. G. H. & CUBAS, P. 2017. Abscisic acid signaling is controlled by a BRANCHED1/HD-ZIP I cascade in Arabidopsis axillary buds. *Proceedings of the National Academy of Sciences*, 114, E245-E254.
- GONZÁLEZ-NAVARRO, O. E., GRIFFITHS, S., MOLERO, G., REYNOLDS, M. P. & SLAFER, G. A. 2015. Dynamics of floret development determining differences

- in spike fertility in an elite population of wheat. *Field Crops Research*, 172, 21-31.
- GONZALEZ, F. G., MIRALLES, D. J. & SLAFER, G. A. 2011. Wheat floret survival as related to pre-anthesis spike growth. *J Exp Bot*, 62, 4889-901.
- GRAHAM, L. E., SCHIPPERS, J. H. M., DIJKWEL, P. P. & WAGSTAFF, C. 2018. Ethylene and Senescence Processes. *Annual Plant Reviews online*.
- GRUBER, A. R., LORENZ, R., BERNHART, S. H., NEUBÖCK, R. & HOFACKER, I. L. 2008. The Vienna RNA Websuite. *Nucleic Acids Research*, 36, W70-W74.
- GUENDEL, A., HILO, A., ROLLETSCHEK, H. & BORISJUK, L. 2021. Probing the Metabolic Landscape of Plant Vascular Bundles by Infrared Fingerprint Analysis, Imaging and Mass Spectrometry. *Biomolecules*, 11, 1717.
- GUENDEL, A., ROLLETSCHEK, H., WAGNER, S., MUSZYNSKA, A. & BORISJUK, L. 2018. Micro Imaging Displays the Sucrose Landscape within and along Its Allocation Pathways. *Plant Physiology*, 178, 1448-1460.
- GUIBOILEAU, A., YOSHIMOTO, K., SOULAY, F., BATAILLÉ, M.-P., AVICE, J.-C. & MASCLAUX-DAUBRESSE, C. 2012. Autophagy machinery controls nitrogen remobilization at the whole-plant level under both limiting and ample nitrate conditions in Arabidopsis. *New Phytologist*, 194, 732-740.
- GUO, Z., CHEN, D. & SCHNURBUSCH, T. 2015. Variance components, heritability and correlation analysis of anther and ovary size during the floral development of bread wheat. *J Exp Bot*, 66, 3099-111.
- GUO, Z., CHEN, D. & SCHNURBUSCH, T. 2018. Plant and Floret Growth at Distinct Developmental Stages During the Stem Elongation Phase in Wheat. *Front Plant Sci*, 9, 330.
- GUO, Z. & SCHNURBUSCH, T. 2015. Variation of floret fertility in hexaploid wheat revealed by tiller removal. *J Exp Bot*, 66, 5945-58.
- GUO, Z., SLAFER, G. A. & SCHNURBUSCH, T. 2016. Genotypic variation in spike fertility traits and ovary size as determinants of floret and grain survival rate in wheat. *J Exp Bot*, 67, 4221-30.
- HANIF, M. & LANGER, R. H. M. 1972. The Vascular System of the Spikelet in Wheat (*Triticum aestivum*). *Annals of Botany*, 36, 721-727.
- HANKIN, J. A., BARKLEY, R. M. & MURPHY, R. C. 2007. Sublimation as a method of matrix application for mass spectrometric imaging. *Journal of the American Society for Mass Spectrometry*, 18, 1646-1652.
- HARA-NISHIMURA, I. & HATSUGAI, N. 2011. The role of vacuole in plant cell death. *Cell Death & Differentiation*, 18, 1298-1304.
- HARTWIG, T., CHUCK, G. S., FUJIOKA, S., KLEMPIEN, A., WEIZBAUER, R., POTLURI, D. P. V., CHOE, S., JOHAL, G. S. & SCHULZ, B. 2011. Brassinosteroid control of sex determination in maize. *Proceedings of the National Academy of Sciences*, 108, 19814-19819.
- HE, Y., FUKUSHIGE, H., HILDEBRAND, D. F. & GAN, S. 2002. Evidence supporting a role of jasmonic acid in Arabidopsis leaf senescence. *Plant Physiol*, 128, 876-84.
- HEIDSTRA, R. & SABATINI, S. 2014. Plant and animal stem cells: similar yet different. *Nature Reviews Molecular Cell Biology*, 15, 301-312.
- HEINEMANN, B. & HILDEBRANDT, T. M. 2021. The role of amino acid metabolism in signaling and metabolic adaptation to stress-induced energy deficiency in plants. *J Exp Bot*, 72, 4634-4645.
- HEINZ, S., BENNER, C., SPANN, N., BERTOLINO, E., LIN, Y. C., LASLO, P., CHENG, J. X., MURRE, C., SINGH, H. & GLASS, C. K. 2010. Simple Combinations of Lineage-Determining Transcription Factors Prime cis-

- Regulatory Elements Required for Macrophage and B Cell Identities. *Molecular Cell*, 38, 576-589.
- HENSEL, G., KASTNER, C., OLESZCZUK, S., RIECHEN, J. & KUMLEHN, J. 2009. Agrobacterium-mediated gene transfer to cereal crop plants: current protocols for barley, wheat, triticale, and maize. *Int J Plant Genomics*, 2009, 835608.
- HENSEL, L. L., NELSON, M. A., RICHMOND, T. A. & BLEECKER, A. B. 1994. The Fate of Inflorescence Meristems Is Controlled by Developing Fruits in Arabidopsis. *Plant Physiology*, 106, 863-876.
- HEYNEKE, E., WATANABE, M., ERBAN, A., DUAN, G., BUCHNER, P., WALTHER, D., KOPKA, J., HAWKESFORD, M. J. & HOEFGEN, R. 2019. Effect of Senescence Phenotypes and Nitrate Availability on Wheat Leaf Metabolome during Grain Filling. *Agronomy*, 9.
- HILDEBRANDT, T. M., NUNES NESI, A., ARAUJO, W. L. & BRAUN, H. P. 2015. Amino Acid Catabolism in Plants. *Mol Plant*, 8, 1563-79.
- HOFFIE, R. E., OTTO, I., PEROVIC, D., BUDHAGATAPALLI, N., HABEKUß, A., ORDON, F. & KUMLEHN, J. 2021. Targeted Knockout of Eukaryotic Translation Initiation Factor 4E Confers Bymovirus Resistance in Winter Barley. *Frontiers in Genome Editing*, 3.
- HOLLMANN, J., GREGERSEN, P. L. & KRUPINSKA, K. 2014. Identification of predominant genes involved in regulation and execution of senescence-associated nitrogen remobilization in flag leaves of field grown barley. *J Exp Bot*, 65, 3963-73.
- HU, P., TAN, Y., WEN, Y., FANG, Y., WANG, Y., WU, H., WANG, J., WU, K., CHAI, B., ZHU, L., ZHANG, G., GAO, Z., REN, D., ZENG, D., SHEN, L., XUE, D., QIAN, Q. & HU, J. 2022. LMPA Regulates Lesion Mimic Leaf and Panicle Development Through ROS-Induced PCD in Rice. *Frontiers in Plant Science*, 13.
- HUANG, H., LIU, B., LIU, L. & SONG, S. 2017. Jasmonate action in plant growth and development. *J Exp Bot*, 68, 1349-1359.
- HUANG, T. & JANDER, G. 2017. Abscisic acid-regulated protein degradation causes osmotic stress-induced accumulation of branched-chain amino acids in Arabidopsis thaliana. *Planta*, 246, 737-747.
- HUANG, Y., KAMAL, R., SHANMUGARAJ, N., RUTTEN, T., THIRULOGACHANDAR, V., ZHAO, S., HOFFIE, I., HENSEL, G., RAJARAMAN, J., MOYA, Y. A. T., HAJIREZAEI, M. R., HIMMELBACH, A., POURSAEBANI, N., LUNDQVIST, U., KUMLEHN, J., STEIN, N., VON WIRÉN, N., MASCHER, M., MELZER, M. & SCHNURBUSCH, T. 2023. A molecular framework for grain number determination in barley. *Sci Adv*, 9, eadd0324.
- JAMSHEER, K. M., JINDAL, S. & LAXMI, A. 2019. Evolution of TOR-SnRK dynamics in green plants and its integration with phytohormone signaling networks. *J Exp Bot*, 70, 2239-2259.
- JAYAKODI, M., PADMARASU, S., HABERER, G., BONTHALA, V. S., GUNDLACH, H., MONAT, C., LUX, T., KAMAL, N., LANG, D. I., HIMMELBACH, A., ENS, J., ZHANG, X. Q., ANGESSA, T. T., ZHOU, G. F., TAN, C., HILL, C., WANG, P. H., SCHREIBER, M., BOSTON, L. B., PLOTT, C., JENKINS, J., GUO, Y., FIEBIG, A., BUDAK, H., XU, D. D., ZHANG, J., WANG, C. C., GRIMWOOD, J., SCHMUTZ, J., GUO, G. G., ZHANG, G. P., MOCHIDA, K., HIRAYAMA, T., SATO, K., CHALMERS, K. J., LANGRIDGE, P., WAUGH, R., POZNIAK, C. J., SCHOLZ, U., MAYER, K. F. X., SPANNAGL, M., LI, C. D., MASCHER, M. & STEIN, N. 2020. The barley pan-genome reveals the hidden legacy of mutation breeding. *Nature*, 588, 22.

- JE, B. I., GRUEL, J., LEE, Y. K., BOMMERT, P., AREVALO, E. D., EVELAND, A. L., WU, Q., GOLDSHMIDT, A., MEELEY, R., BARTLETT, M., KOMATSU, M., SAKAI, H., JÖNSSON, H. & JACKSON, D. 2016. Signaling from maize organ primordia via FASCIATED EAR3 regulates stem cell proliferation and yield traits. *Nature Genetics*, 48, 785-791.
- JE, B. I., XU, F., WU, Q., LIU, L., MEELEY, R., GALLAGHER, J. P., CORCILIOUS, L., PAYNE, R. J., BARTLETT, M. E. & JACKSON, D. 2018. The CLAVATA receptor FASCIATED EAR2 responds to distinct CLE peptides by signaling through two downstream effectors. *eLife*, 7, e35673.
- JEHANZEB, M., ZHENG, X. & MIAO, Y. 2017. The Role of the S40 Gene Family in Leaf Senescence. *Int J Mol Sci*, 18.
- JIA, H., LI, M., LI, W., LIU, L., JIAN, Y., YANG, Z., SHEN, X., NING, Q., DU, Y., ZHAO, R., JACKSON, D., YANG, X. & ZHANG, Z. 2020. A serine/threonine protein kinase encoding gene KERNEL NUMBER PER ROW6 regulates maize grain yield. *Nat Commun*, 11, 988.
- JIAO, Y., LEE, Y. K., GLADMAN, N., CHOPRA, R., CHRISTENSEN, S. A., REGULSKI, M., BUROW, G., HAYES, C., BURKE, J., WARE, D. & XIN, Z. 2018. MSD1 regulates pedicellate spikelet fertility in sorghum through the jasmonic acid pathway. *Nature Communications*, 9, 822.
- JING, H.-C., STURRE, M. J. G., HILLE, J. & DIJKWEL, P. P. 2002. Arabidopsis onset of leaf death mutants identify a regulatory pathway controlling leaf senescence. *The Plant Journal*, 32, 51-63.
- JONES, K., KIM, D. W., PARK, J. S. & KHANG, C. H. 2016. Live-cell fluorescence imaging to investigate the dynamics of plant cell death during infection by the rice blast fungus *Magnaporthe oryzae*. *BMC Plant Biol*, 16, 69.
- KABBAGE, M., KESSENS, R., BARTHOLOMAY, L. C. & WILLIAMS, B. 2017. The Life and Death of a Plant Cell. *Annu Rev Plant Biol*, 68, 375-404.
- KADOTA, K., YE, J., NAKAI, Y., TERADA, T. & SHIMIZU, K. 2006. ROKU: a novel method for identification of tissue-specific genes. *BMC Bioinformatics*, 7, 294.
- KAMAL, R., MUQADDASI, Q. H. & SCHNURBUSCH, T. 2022. Genetic association of spikelet abortion with spike, grain, and shoot traits in highly-diverse six-rowed barley. *Front Plant Sci*, 13, 1015609.
- KAMAL, R., MUQADDASI, Q. H., ZHAO, Y. & SCHNURBUSCH, T. 2021. Spikelet abortion in six-rowed barley is mainly influenced by final spikelet number, with potential spikelet number acting as a suppressor trait. *Journal of Experimental Botany*, 73, 2005-2020.
- KAN, C.-C., CHUNG, T.-Y., JUO, Y.-A. & HSIEH, M.-H. 2015. Glutamine rapidly induces the expression of key transcription factor genes involved in nitrogen and stress responses in rice roots. *BMC Genomics*, 16, 731.
- KASPAR, S., PEUKERT, M., SVATOS, A., MATROS, A. & MOCK, H.-P. 2011. MALDI-imaging mass spectrometry – An emerging technique in plant biology. *PROTEOMICS*, 11, 1840-1850.
- KATO, Y., KAMOSHITA, A. & YAMAGISHI, J. 2008. Preflowering Abortion Reduces Spikelet Number in Upland Rice (*Oryza sativa* L.) under Water Stress. *Crop Science*, 48, 2389-2395.
- KELLOGG, E. A. 2022. Genetic control of branching patterns in grass inflorescences. *Plant Cell*, 34, 2518-2533.
- KELLOGG, E. A., CAMARA, P. E., RUDALL, P. J., LADD, P., MALCOMBER, S. T., WHIPPLE, C. J. & DOUST, A. N. 2013. Early inflorescence development in the grasses (Poaceae). *Front Plant Sci*, 4, 250.

- KENNEDY, S. P., LYNCH, J. P., SPINK, J. & BINGHAM, I. J. 2018. Grain number and grain filling of two-row malting barley in response to variation in post-anthesis radiation: Analysis by grain position on the ear and its implications for yield improvement and quality. *Field Crops Research*, 225, 74-82.
- KIM, H. & HONG, S. 2019. Role of the circadian clock in fine-tuning the process of leaf senescence in plants. *Translational Medicine of Aging*, 3, 26-30.
- KIM, H., KIM, H. J., VU, Q. T., JUNG, S., MCCLUNG, C. R., HONG, S. & NAM, H. G. 2018a. Circadian control of ORE1 by PRR9 positively regulates leaf senescence in Arabidopsis. *Proc Natl Acad Sci U S A*, 115, 8448-8453.
- KIM, H. J., PARK, J. H., KIM, J., KIM, J. J., HONG, S., KIM, J., KIM, J. H., WOO, H. R., HYEON, C., LIM, P. O., NAM, H. G. & HWANG, D. 2018b. Time-evolving genetic networks reveal a NAC troika that negatively regulates leaf senescence in Arabidopsis. *Proc Natl Acad Sci U S A*, 115, E4930-E4939.
- KIM, J. 2019. Sugar metabolism as input signals and fuel for leaf senescence. *Genes & Genomics*, 41, 737-746.
- KIM, J., KANG, H., PARK, J., KIM, W., YOO, J., LEE, N., KIM, J., YOON, T. Y. & CHOI, G. 2016. PIF1-Interacting Transcription Factors and Their Binding Sequence Elements Determine the in Vivo Targeting Sites of PIF1. *Plant Cell*, 28, 1388-405.
- KIM, J. H., WOO, H. R., KIM, J., LIM, P. O., LEE, I. C., CHOI, S. H., HWANG, D. & NAM, H. G. 2009. Trifurcate Feed-Forward Regulation of Age-Dependent Cell Death Involving miR164 in Arabidopsis. *Science*, 323, 1053-1057.
- KIM, J. I., MURPHY, A. S., BAEK, D., LEE, S.-W., YUN, D.-J., BRESSAN, R. A. & NARASIMHAN, M. L. 2011. YUCCA6 over-expression demonstrates auxin function in delaying leaf senescence in Arabidopsis thaliana. *Journal of Experimental Botany*, 62, 3981-3992.
- KINOSHITA, T., YAMADA, K., HIRAIWA, N., KONDO, M., NISHIMURA, M. & HARA-NISHIMURA, I. 1999. Vacuolar processing enzyme is up-regulated in the lytic vacuoles of vegetative tissues during senescence and under various stressed conditions. *Plant J*, 19, 43-53.
- KIRBY, E. J. M. & APPLEYARD, M. 1981. *Cereal Development Guide*, Cereal Unit, National Agricultural Centre.
- KIRBY, E. J. M. & ELLIS, R. P. 1980. A comparison of spring barley grown in England and in Scotland. 1. Shoot apex development. *The Journal of Agricultural Science*, 95, 101 - 110.
- KIRCHOFF, B. K. & CLAßEN-BOCKHOFF, R. 2013. Inflorescences: concepts, function, development and evolution. *Annals of Botany*, 112, 1471-1476.
- KITAGAWA, M. & JACKSON, D. 2019. Control of Meristem Size. *Annu Rev Plant Biol*, 70, 269-291.
- KLEIN, H., GALLAGHER, J., DEMESA-AREVALO, E., ABRAHAM-JUAREZ, M. J., HEENEY, M., FEIL, R., LUNN, J. E., XIAO, Y., CHUCK, G., WHIPPLE, C., JACKSON, D. & BARTLETT, M. 2022. Recruitment of an ancient branching program to suppress carpel development in maize flowers. *Proc Natl Acad Sci U S A*, 119.
- KNUDSEN, S., WENDT, T., DOCKTER, C., THOMSEN, H. C., RASMUSSEN, M., EGEVANG JØRGENSEN, M., LU, Q., VOSS, C., MUROZUKA, E., ØSTERBERG, J. T., HARHOLT, J., BRAUMANN, I., CUESTA-SEIJO, J. A., KALE, S. M., BODEVIN, S., TANG PETERSEN, L., CARCIOFI, M., PEDAS, P. R., OPSTRUP HUSUM, J., NIELSEN, M. T. S., NIELSEN, K., JENSEN, M. K., MØLLER, L. A., GOJKOVIC, Z., STRIEBECK, A., LENGELER, K., FENNESSY, R. T., KATZ, M., GARCIA SANCHEZ, R., SOLODOVNIKOVA, N., FÖRSTER,

- J., OLSEN, O., MØLLER, B. L., FINCHER, G. B. & SKADHAUGE, B. 2022. FIND-IT: Accelerated trait development for a green evolution. *Science Advances*, 8, eabq2266.
- KOEPPEL, I., HERTIG, C., HOFFIE, R. & KUMLEHN, J. 2019. Cas Endonuclease Technology—A Quantum Leap in the Advancement of Barley and Wheat Genetic Engineering. *International Journal of Molecular Sciences*, 20, 2647.
- KOMATSUDA, T., POURKHEIRANDISH, M., HE, C., AZHAGUVEL, P., KANAMORI, H., PEROVIC, D., STEIN, N., GRANER, A., WICKER, T., TAGIRI, A., LUNDQVIST, U., FUJIMURA, T., MATSUOKA, M., MATSUMOTO, T. & YANO, M. 2007. Six-rowed barley originated from a mutation in a homeodomain-leucine zipper I-class homeobox gene. *Proceedings of the National Academy of Sciences*, 104, 1424-1429.
- KOPPOLU, R., ANWAR, N., SAKUMA, S., TAGIRI, A., LUNDQVIST, U., POURKHEIRANDISH, M., RUTTEN, T., SEILER, C., HIMMELBACH, A., ARIYADASA, R., YOUSSEF, H. M., STEIN, N., SREENIVASULU, N., KOMATSUDA, T. & SCHNURBUSCH, T. 2013. Six-rowed spike4 (Vrs4) controls spikelet determinacy and row-type in barley. *Proceedings of the National Academy of Sciences*, 110, 13198-13203.
- KOPPOLU, R., CHEN, S. & SCHNURBUSCH, T. 2022. Evolution of inflorescence branch modifications in cereal crops. *Curr Opin Plant Biol*, 65, 102168.
- KOPPOLU, R. & SCHNURBUSCH, T. 2019. Developmental pathways for shaping spike inflorescence architecture in barley and wheat. *Journal of Integrative Plant Biology*, 61, 278-295.
- KOYAMA, T. 2014. The roles of ethylene and transcription factors in the regulation of onset of leaf senescence. *Frontiers in Plant Science*, 5.
- KRUPINSKA, K., DÄHNHARDT, D., FISCHER-KILBIENSKI, I., KUCHAROWICZ, W., SCHARRENBERG, C., TRÖSCH, M. & BUCK, F. 2013. Identification of WHIRLY1 as a Factor Binding to the Promoter of the Stress- and Senescence-Associated Gene HvS40. *Journal of Plant Growth Regulation*, 33, 91-105.
- KRUPINSKA, K., HAUSSUHL, K., SCHAFFER, A., VAN DER KOOIJ, T. A., LECKBAND, G., LORZ, H. & FALK, J. 2002. A novel nucleus-targeted protein is expressed in barley leaves during senescence and pathogen infection. *Plant Physiol*, 130, 1172-80.
- LACOMBE, B. & ACHARD, P. 2016. Long-distance transport of phytohormones through the plant vascular system. *Curr Opin Plant Biol*, 34, 1-8.
- LANGRIDGE, P. 2018. Economic and Academic Importance of Barley. In: STEIN, N. & MUEHLBAUER, G. J. (eds.) *The Barley Genome*. Cham: Springer International Publishing.
- LASTDRAGER, J., HANSON, J. & SMEEKENS, S. 2014. Sugar signals and the control of plant growth and development. *J Exp Bot*, 65, 799-807.
- LAW, C. W., CHEN, Y., SHI, W. & SMYTH, G. K. 2014. voom: precision weights unlock linear model analysis tools for RNA-seq read counts. *Genome Biology*, 15, R29.
- LAW, S. R., CHROBOK, D., JUVANY, M., DELHOMME, N., LINDEN, P., BROUWER, B., AHAD, A., MORITZ, T., JANSSON, S., GARDESTROM, P. & KEECH, O. 2018. Darkened Leaves Use Different Metabolic Strategies for Senescence and Survival. *Plant Physiol*, 177, 132-150.
- LEE, J., KANG, M. H., KIM, J. Y. & LIM, P. O. 2021. The Role of Light and Circadian Clock in Regulation of Leaf Senescence. *Front Plant Sci*, 12, 669170.
- LEE, O. R., KIM, S. J., KIM, H. J., HONG, J. K., RYU, S. B., LEE, S. H., GANGULY, A. & CHO, H. T. 2010. Phospholipase A(2) is required for PIN-FORMED protein

- trafficking to the plasma membrane in the Arabidopsis root. *Plant Cell*, 22, 1812-25.
- LEE, S. & MASCLAUX-DAUBRESSE, C. 2021. Current Understanding of Leaf Senescence in Rice. *International Journal of Molecular Sciences*, 22, 4515.
- LEIBOFF, S., STRABLE, J., JOHNSTON, R., FEDERICI, S., SYLVESTER, A. W. & SCANLON, M. J. 2021. Network analyses identify a transcriptomic proximodistal prepattern in the maize leaf primordium. *New Phytologist*, 230, 218-227.
- LEYMARIE, J., ROBAYO-ROMERO, M. E., GENDREAU, E., BENECH-ARNOLD, R. L. & CORBINEAU, F. 2008. Involvement of ABA in Induction of Secondary Dormancy in Barley (*Hordeum vulgare* L.) Seeds. *Plant and Cell Physiology*, 49, 1830-1838.
- LI, G., KUIJER, H. N. J., YANG, X., LIU, H., SHEN, C., SHI, J., BETTS, N., TUCKER, M. R., LIANG, W., WAUGH, R., BURTON, R. A. & ZHANG, D. 2021. MADS1 maintains barley spike morphology at high ambient temperatures. *Nat Plants*, 7, 1093-1107.
- LI, G., SIDDIQUI, H., TENG, Y., LIN, R., WAN, X.-Y., LI, J., LAU, O.-S., OUYANG, X., DAI, M., WAN, J., DEVLIN, P. F., DENG, X. W. & WANG, H. 2011. Coordinated transcriptional regulation underlying the circadian clock in Arabidopsis. *Nature Cell Biology*, 13, 616-622.
- LI, J. R., YU, K., WEI, J. R., MA, Q., WANG, B. Q. & YU, D. 2010. Gibberellin retards chlorophyll degradation during senescence of Paris polyphylla. *Biologia Plantarum*, 54, 395-399.
- LI, Z., LIU, P., ZHANG, X., ZHANG, Y., MA, L., LIU, M., GUAN, Z., ZHANG, Y., LI, P., ZOU, C., HE, Y., GAO, S., PAN, G. & SHEN, Y. 2020. Genome-wide association studies and QTL mapping uncover the genetic architecture of ear tip-barrenness in maize. *Physiologia Plantarum*, 170, 27-39.
- LI, Z., PENG, J., WEN, X. & GUO, H. 2013. Ethylene-insensitive3 is a senescence-associated gene that accelerates age-dependent leaf senescence by directly repressing miR164 transcription in Arabidopsis. *Plant Cell*, 25, 3311-28.
- LIANG, C., WANG, Y., ZHU, Y., TANG, J., HU, B., LIU, L., OU, S., WU, H., SUN, X., CHU, J. & CHU, C. 2014. OsNAP connects abscisic acid and leaf senescence by fine-tuning abscisic acid biosynthesis and directly targeting senescence-associated genes in rice. *Proc Natl Acad Sci U S A*, 111, 10013-8.
- LIANG, Z., LUO, J., WEI, B., LIAO, Y. & LIU, Y. 2021. Trehalose can alleviate decreases in grain number per spike caused by low-temperature stress at the booting stage by promoting floret fertility in wheat. *Journal of Agronomy and Crop Science*, 207, 717-732.
- LIM, P. O., KIM, H. J. & NAM, H. G. 2007. Leaf senescence. *Annu Rev Plant Biol*, 58, 115-36.
- LIU, L., GALLAGHER, J., AREVALO, E. D., CHEN, R., SKOPELITIS, T., WU, Q., BARTLETT, M. & JACKSON, D. 2021a. Enhancing grain-yield-related traits by CRISPR-Cas9 promoter editing of maize CLE genes. *Nature Plants*, 7, 287-294.
- LIU, L., LINDSAY, P. L. & JACKSON, D. 2021b. Next Generation Cereal Crop Yield Enhancement: From Knowledge of Inflorescence Development to Practical Engineering by Genome Editing. *Int J Mol Sci*, 22.
- LIU, L., WHITE, M. J. & MACRAE, T. H. 1999. Transcription factors and their genes in higher plants. *European Journal of Biochemistry*, 262, 247-257.

- LIU, X. L., HUANG, M., FAN, B., BUCKLER, E. S. & ZHANG, Z. W. 2016. Iterative Usage of Fixed and Random Effect Models for Powerful and Efficient Genome-Wide Association Studies. *Plos Genetics*, 12, 24.
- LIU, Z., MARELLA, C. B. N., HARTMANN, A., HAJIREZAEI, M. R. & VON WIREN, N. 2019. An Age-Dependent Sequence of Physiological Processes Defines Developmental Root Senescence. *Plant Physiol*, 181, 993-1007.
- LIVAK, K. J. & SCHMITTGEN, T. D. 2001. Analysis of Relative Gene Expression Data Using Real-Time Quantitative PCR and the 2- $\Delta\Delta$ CT Method. *Methods*, 25, 402-408.
- LOVE, M. I., HUBER, W. & ANDERS, S. 2014. Moderated estimation of fold change and dispersion for RNA-seq data with DESeq2. *Genome Biology*, 15, 38.
- LU, Z., MARAND, A. P., RICCI, W. A., ETHRIDGE, C. L., ZHANG, X. & SCHMITZ, R. J. 2019. The prevalence, evolution and chromatin signatures of plant regulatory elements. *Nature Plants*, 5, 1250-1259.
- LUO, Y., ZHANG, M., LIU, Y., LIU, J., LI, W., CHEN, G., PENG, Y., JIN, M., WEI, W., JIAN, L., YAN, J., FERNIE, A. R. & YAN, J. 2022. Genetic variation in YIGE1 contributes to ear length and grain yield in maize. *New Phytologist*, 234, 513-526.
- LV, Y., SHAO, G., JIAO, G., SHENG, Z., XIE, L., HU, S., TANG, S., WEI, X. & HU, P. 2021. Targeted mutagenesis of POLYAMINE OXIDASE 5 that negatively regulates mesocotyl elongation enables the generation of direct-seeding rice with improved grain yield. *Mol Plant*, 14, 344-351.
- LYNCH, J. H. & DUDAREVA, N. 2020. Aromatic Amino Acids: A Complex Network Ripe for Future Exploration. *Trends Plant Sci*, 25, 670-681.
- MA, B., YIN, C. C., HE, S. J., LU, X., ZHANG, W. K., LU, T. G., CHEN, S. Y. & ZHANG, J. S. 2014. Ethylene-induced inhibition of root growth requires abscisic acid function in rice (*Oryza sativa* L.) seedlings. *PLoS Genet*, 10, e1004701.
- MANTEGAZZA, O., GREGIS, V., MENDES, M. A., MORANDINI, P., ALVES-FERREIRA, M., PATREZE, C. M., NARDELI, S. M., KATER, M. M. & COLOMBO, L. 2014. Analysis of the arabidopsis REM gene family predicts functions during flower development. *Annals of Botany*, 114, 1507-1515.
- MAO, C., LU, S., LV, B., ZHANG, B., SHEN, J., HE, J., LUO, L., XI, D., CHEN, X. & MING, F. 2017. A Rice NAC Transcription Factor Promotes Leaf Senescence via ABA Biosynthesis. *Plant Physiol*, 174, 1747-1763.
- MASCHER, M., WICKER, T., JENKINS, J., PLOTT, C., LUX, T., KOH, C. S., ENS, J., GUNDLACH, H., BOSTON, L. B., TULPOVÁ, Z., HOLDEN, S., HERNÁNDEZ-PINZÓN, I., SCHOLZ, U., MAYER, K. F. X., SPANNAGL, M., POZNIAK, C. J., SHARPE, A. G., ŠIMKOVÁ, H., MOSCOU, M. J., GRIMWOOD, J., SCHMUTZ, J. & STEIN, N. 2021. Long-read sequence assembly: a technical evaluation in barley. *The Plant Cell*, 33, 1888-1906.
- MATALLANA-RAMIREZ, L. P., RAUF, M., FARAGE-BARHOM, S., DORTAY, H., XUE, G. P., DROGE-LASER, W., LERS, A., BALAZADEH, S. & MUELLER-ROEBER, B. 2013. NAC transcription factor ORE1 and senescence-induced BIFUNCTIONAL NUCLEASE1 (BFN1) constitute a regulatory cascade in Arabidopsis. *Mol Plant*, 6, 1438-52.
- MATSUMOTO, T., TANAKA, T., SAKAI, H., AMANO, N., KANAMORI, H., KURITA, K., KIKUTA, A., KAMIYA, K., YAMAMOTO, M., IKAWA, H., FUJII, N., HORI, K., ITOH, T. & SATO, K. 2011. Comprehensive Sequence Analysis of 24,783 Barley Full-Length cDNAs Derived from 12 Clone Libraries *Plant Physiology*, 156, 20-28.

- MATTOO, A. K. & SOBIESZCZUK-NOWICKA, E. 2019. Polyamine as Signaling Molecules and Leaf Senescence. *Senescence Signalling and Control in Plants*.
- MAZZONI-PUTMAN, S. M., BRUMOS, J., ZHAO, C., ALONSO, J. M. & STEPANOVA, A. N. 2021. Auxin Interactions with Other Hormones in Plant Development. *Cold Spring Harb Perspect Biol*, 13.
- MCKIM, S. M., KOPPOLU, R. & SCHNURBUSCH, T. 2018. Barley Inflorescence Architecture. *The Barley Genome*.
- MENG, Z.-D., ZHANG, F.-J., DING, Z.-H., SUN, Q., WANG, L., GUO, Q.-F. & WANG, H.-G. 2007. Inheritance of Ear Tip-Barrenness Trait in Maize. *Agricultural Sciences in China*, 6, 628-633.
- MERELO, P., GONZÁLEZ-CUADRA, I. & FERRÁNDIZ, C. 2022. A cellular analysis of meristem activity at the end of flowering points to cytokinin as a major regulator of proliferative arrest in Arabidopsis. *Current Biology*, 32, 749-762.e3.
- METSALU, T. & VILO, J. 2015. ClustVis: a web tool for visualizing clustering of multivariate data using Principal Component Analysis and heatmap. *Nucleic Acids Research*, 43, W566-W570.
- MHAMDI, A. & VAN BREUSEGEM, F. 2018. Reactive oxygen species in plant development. *Development*, 145.
- MILHINHOS, A. & MIGUEL, C. M. 2013. Hormone interactions in xylem development: a matter of signals. *Plant Cell Reports*, 32, 867-883.
- MIRALLES, D. J., KATZ, S. D., COLLOCA, A. & SLAFER, G. A. 1998. Floret development in near isogenic wheat lines differing in plant height. *Field Crops Research*, 59, 21-30.
- MIRALLES, D. J. & RICHARDS, R. A. 2000. Responses of Leaf and Tiller Emergence and Primordium Initiation in Wheat and Barley to Interchanged Photoperiod. *Annals of Botany*, 85, 655-663.
- MIRALLES, D. J., RICHARDS, R. A. & SLAFER, G. A. 2000. Duration of the stem elongation period influences the number of fertile florets in wheat and barley. *Australian Journal of Plant Physiology*, 27, 931-940.
- MONCUR, M. W., SCIENTIFIC, C. & RESEARCH, I. R. O. D. O. L. U. 1981. *Floral Initiation in Field Crops: An Atlas of Scanning Electron Micrographs*, Division of Land Use Research, CSIRO.
- MONTINI, L., CROCOLL, C., GLEADOW, R. M., MOTAWIA, M. S., JANFELT, C. & BJARNHOLT, N. 2020. Matrix-Assisted Laser Desorption/Ionization-Mass Spectrometry Imaging of Metabolites during Sorghum Germination1 [OPEN]. *Plant Physiology*, 183, 925-942.
- MORRIS, K., -MACKERNESS, S. A.-H., PAGE, T., JOHN, C. F., MURPHY, A. M., CARR, J. P. & BUCHANAN-WOLLASTON, V. 2000. Salicylic acid has a role in regulating gene expression during leaf senescence. *The Plant Journal*, 23, 677-685.
- NAGY, G., VELIČKOVIĆ, D., CHU, R. K., CARRELL, A. A., WESTON, D. J., IBRAHIM, Y. M., ANDERTON, C. R. & SMITH, R. D. 2019. Towards resolving the spatial metabolome with unambiguous molecular annotations in complex biological systems by coupling mass spectrometry imaging with structures for lossless ion manipulations. *Chemical Communications*, 55, 306-309.
- NING, Q., JIAN, Y., DU, Y., LI, Y., SHEN, X., JIA, H., ZHAO, R., ZHAN, J., YANG, F., JACKSON, D., LIU, L. & ZHANG, Z. 2021. An ethylene biosynthesis enzyme controls quantitative variation in maize ear length and kernel yield. *Nat Commun*, 12, 5832.

- NISHIMURA, M., BHUSAWANG, P., STRZALKA, K. & AKAZAWA, T. 1982. Developmental formation of glutamine synthetase in greening pumpkin cotyledons and its subcellular localization. *Plant Physiol*, 70, 353-6.
- NOH, Y.-S. & AMASINO, R. M. 1999. Identification of a promoter region responsible for the senescence-specific expression of SAG12. *Plant Molecular Biology*, 41, 181-194.
- NORTH, H. M., DE ALMEIDA, A., BOUTIN, J. P., FREY, A., TO, A., BOTRAN, L., SOTTA, B. & MARION-POLL, A. 2007. The Arabidopsis ABA-deficient mutant *aba4* demonstrates that the major route for stress-induced ABA accumulation is via neoxanthin isomers. *Plant J*, 50, 810-24.
- O'CONNOR, D. L., RUNIONS, A., SLUIS, A., BRAGG, J., VOGEL, J. P., PRUSINKIEWICZ, P. & HAKE, S. 2014. A division in PIN-mediated auxin patterning during organ initiation in grasses. *PLoS Comput Biol*, 10, e1003447.
- O'NEILL, K. C. & LEE, Y. J. 2020. Visualizing Genotypic and Developmental Differences of Free Amino Acids in Maize Roots With Mass Spectrometry Imaging. *Frontiers in Plant Science*, 11.
- OLSEN, K. M. & WENDEL, J. F. 2013. A bountiful harvest: genomic insights into crop domestication phenotypes. *Annu Rev Plant Biol*, 64, 47-70.
- OLVERA-CARRILLO, Y., VAN BEL, M., VAN HAUTEGEM, T., FENDRYCH, M., HUYSMANS, M., SIMASKOVA, M., VAN DURME, M., BUSCAILL, P., RIVAS, S., S. COLL, N., COPPENS, F., MAERE, S. & NOWACK, M. K. 2015. A Conserved Core of Programmed Cell Death Indicator Genes Discriminates Developmentally and Environmentally Induced Programmed Cell Death in Plants *Plant Physiology*, 169, 2684-2699.
- ONO, Y., WADA, S., IZUMI, M., MAKINO, A. & ISHIDA, H. 2013. Evidence for contribution of autophagy to Rubisco degradation during leaf senescence in *Arabidopsis thaliana*. *Plant, Cell & Environment*, 36, 1147-1159.
- OTEGUI, M. S. 2017. Vacuolar degradation of chloroplast components: autophagy and beyond. *Journal of Experimental Botany*, 69, 741-750.
- OUGHAM, H. J., LATIPOVA, G. & VALENTINE, J. 1996. Morphological and biochemical characterization of spikelet development in naked oats (*Avena sativa*). *New Phytologist*, 134, 5-12.
- PALMER, A., PHAPALE, P., CHERNYAVSKY, I., LAVIGNE, R., FAY, D., TARASOV, A., KOVALEV, V., FUCHSER, J., NIKOLENKO, S., PINEAU, C., BECKER, M. & ALEXANDROV, T. 2017. FDR-controlled metabolite annotation for high-resolution imaging mass spectrometry. *Nature Methods*, 14, 57-60.
- PARK, J. H., OH, S. A., KIM, Y. H., WOO, H. R. & NAM, H. G. 1998. Differential expression of senescence-associated mRNAs during leaf senescence induced by different senescence-inducing factors in *Arabidopsis*. *Plant Mol Biol*, 37, 445-54.
- PAZHAMALA, L. T., KUDAPA, H., WECKWERTH, W., MILLAR, A. H. & VARSHNEY, R. K. 2021. Systems biology for crop improvement. *The Plant Genome*, 14, e20098.
- PEI, Y., DENG, Y., ZHANG, H., ZHANG, Z., LIU, J., CHEN, Z., CAI, D., LI, K., DU, Y., ZANG, J., XIN, P., CHU, J., CHEN, Y., ZHAO, L., LIU, J. & CHEN, H. 2022. EAR APICAL DEGENERATION1 regulates maize ear development by maintaining malate supply for apical inflorescence. *The Plant Cell*, 34, 2222-2241.
- PEIRATS-LLOBET, M., YI, C., LIEW, L. C., BERKOWITZ, O., NARSAI, R., LEWSEY, M. G. & WHELAN, J. 2023. Spatially Resolved Transcriptomic Analysis of the Germinating Barley Grain. *bioRxiv*, 2023.01.24.525109.

- PENG, C., UYGUN, S., SHIU, S. H. & LAST, R. L. 2015. The Impact of the Branched-Chain Ketoacid Dehydrogenase Complex on Amino Acid Homeostasis in Arabidopsis. *Plant Physiol*, 169, 1807-20.
- PÉREZ-GIANMARCO, T. I., SLAFER, G. A. & GONZÁLEZ, F. G. 2018. Photoperiod-sensitivity genes shape floret development in wheat. *Journal of Experimental Botany*, 70, 1339-1348.
- PERREAU, F., FREY, A., EFFROY-CUZZI, D., SAVANE, P., BERGER, A., GISSOT, L. & MARION-POLL, A. 2020. ABSCISIC ACID-DEFICIENT4 Has an Essential Function in Both cis-Violaxanthin and cis-Neoxanthin Synthesis. *Plant Physiology*, 184, 1303-1316.
- PEUKERT, M. 2013. *Spatiotemporal distributions of metabolites involved in barley grain development with emphasis on endosperm formation*.
- PEUKERT, M., THIEL, J., PESHEV, D., WESCHKE, W., VAN DEN ENDE, W., MOCK, H. P. & MATROS, A. 2014. Spatio-Temporal Dynamics of Fructan Metabolism in Developing Barley Grains. *Plant Cell*, 26, 3728-3744.
- PIEPER, R., TOMÉ, F., PANKIN, A. & VON KORFF, M. 2020. FLOWERING LOCUS T4 delays flowering and decreases floret fertility in barley. *Journal of Experimental Botany*, 72, 107-121.
- POULSEN, L. R., LOPEZ-MARQUES, R. L., PEDAS, P. R., MCDOWELL, S. C., BROWN, E., KUNZE, R., HARPER, J. F., POMORSKI, T. G. & PALMGREN, M. 2015. A phospholipid uptake system in the model plant Arabidopsis thaliana. *Nat Commun*, 6, 7649.
- POURKHEIRANDISH, M. & KOMATSUDA, T. 2022. Grain Disarticulation in Wild Wheat and Barley. *Plant and Cell Physiology*, 63, 1584-1591.
- POURSAREBANI, N., TRAUTWIG, C., MELZER, M., NUSSBAUMER, T., LUNDQVIST, U., RUTTEN, T., SCHMUTZER, T., BRANDT, R., HIMMELBACH, A., ALTSCHMIED, L., KOPPOLU, R., YOUSSEF, H. M., SIBOUT, R., DALMAIS, M., BENDAHMANE, A., STEIN, N., XIN, Z. & SCHNURBUSCH, T. 2020. COMPOSITUM 1 contributes to the architectural simplification of barley inflorescence via meristem identity signals. *Nat Commun*, 11, 5138.
- PRIETO, P., OCHAGAVÍA, H., SAVIN, R., GRIFFITHS, S. & SLAFER, G. A. 2018. Dynamics of floret initiation/death determining spike fertility in wheat as affected by Ppd genes under field conditions. *Journal of Experimental Botany*, 69, 2633-2645.
- PRUSINKIEWICZ, P., ERASMUS, Y., LANE, B., HARDER, L. D. & COEN, E. 2007. Evolution and Development of Inflorescence Architectures. *Science*, 316, 1452-1456.
- QIN, L., ZHANG, Y., LIU, Y., HE, H., HAN, M., LI, Y., ZENG, M. & WANG, X. 2018. Recent advances in matrix-assisted laser desorption/ionisation mass spectrometry imaging (MALDI-MSI) for in situ analysis of endogenous molecules in plants. *Phytochem Anal*, 29, 351-364.
- RADCHUK, V., TRAN, V., HILO, A., MUSZYNSKA, A., GÜNDEL, A., WAGNER, S., FUCHS, J., HENSEL, G., ORTLEB, S., MUNZ, E., ROLLETSCHEK, H. & BORISJUK, L. 2021. Grain filling in barley relies on developmentally controlled programmed cell death. *Communications Biology*, 4, 428.
- RAE, G. M., DAVID, K. & WOOD, M. 2013. The Dormancy Marker <i>DRM1/ARP</i> Associated with Dormancy but a Broader Role <i>In Planta</i>. *Developmental Biology Journal*, 2013, 632524.
- RAE, G. M., UVERSKY, V. N., DAVID, K. & WOOD, M. 2014. DRM1 and DRM2 expression regulation: potential role of splice variants in response to stress and

- environmental factors in Arabidopsis. *Molecular Genetics and Genomics*, 289, 317-332.
- RAMIREZ-GONZALEZ, R. H., BORRILL, P., LANG, D., HARRINGTON, S. A., BRINTON, J., VENTURINI, L., DAVEY, M., JACOBS, J., VAN EX, F., PASHA, A., KHEDIKAR, Y., ROBINSON, S. J., CORY, A. T., FLORIO, T., CONCIA, L., JUERY, C., SCHOONBEEK, H., STEUERNAGEL, B., XIANG, D., RIDOUT, C. J., CHALHOUB, B., MAYER, K. F. X., BENHAMED, M., LATRASSE, D., BENDAHMANE, A., INTERNATIONAL WHEAT GENOME SEQUENCING, C., WULFF, B. B. H., APPELS, R., TIWARI, V., DATLA, R., CHOLET, F., POZNIAK, C. J., PROVART, N. J., SHARPE, A. G., PAUX, E., SPANNAGL, M., BRAUTIGAM, A. & UAUY, C. 2018. The transcriptional landscape of polyploid wheat. *Science*, 361.
- RAMSAY, L., COMADRAN, J., DRUKA, A., MARSHALL, D. F., THOMAS, W. T. B., MACAULAY, M., MACKENZIE, K., SIMPSON, C., FULLER, J., BONAR, N., HAYES, P. M., LUNDQVIST, U., FRANCKOWIAK, J. D., CLOSE, T. J., MUEHLBAUER, G. J. & WAUGH, R. 2011. INTERMEDIUM-C, a modifier of lateral spikelet fertility in barley, is an ortholog of the maize domestication gene TEOSINTE BRANCHED 1. *Nature Genetics*, 43, 169-172.
- RAY, D. K., RAMANKUTTY, N., MUELLER, N. D., WEST, P. C. & FOLEY, J. A. 2012. Recent patterns of crop yield growth and stagnation. *Nature Communications*, 3, 1293.
- RAY, D. K., SLOAT, L. L., GARCIA, A. S., DAVIS, K. F., ALI, T. & XIE, W. 2022. Crop harvests for direct food use insufficient to meet the UN's food security goal. *Nature Food*, 3, 367-374.
- REINBOTHE, C., SPRINGER, A., SAMOL, I. & REINBOTHE, S. 2009. Plant oxylipins: role of jasmonic acid during programmed cell death, defence and leaf senescence. *FEBS J*, 276, 4666-81.
- RICHMOND, A. E. & LANG, A. 1957. Effect of Kinetin on Protein Content and Survival of Detached Xanthium Leaves. *Science*, 125, 650-651.
- RODRIGUEZ-LEAL, D., XU, C., KWON, C.-T., SOYARS, C., DEMESA-AREVALO, E., MAN, J., LIU, L., LEMMON, Z. H., JONES, D. S., VAN ECK, J., JACKSON, D. P., BARTLETT, M. E., NIMCHUK, Z. L. & LIPPMAN, Z. B. 2019. Evolution of buffering in a genetic circuit controlling plant stem cell proliferation. *Nature Genetics*, 51, 786-792.
- ROSTOKS, N., SCHMIERER, D., KUDRNA, D. & KLEINHOF, A. 2003. Barley putative hypersensitive induced reaction genes: genetic mapping, sequence analyses and differential expression in disease lesion mimic mutants. *Theoretical and Applied Genetics*, 107, 1094-1101.
- ROTTET, S., BESAGNI, C. & KESSLER, F. 2015. The role of plastoglobules in thylakoid lipid remodeling during plant development. *Biochimica et Biophysica Acta (BBA) - Bioenergetics*, 1847, 889-899.
- ROY, S., SAXENA, S., SINHA, A. & NANDI, A. K. 2020. DORMANCY/AUXIN ASSOCIATED FAMILY PROTEIN 2 of Arabidopsis thaliana is a negative regulator of local and systemic acquired resistance. *Journal of Plant Research*, 133, 409-417.
- SAKUMA, S., GOLAN, G., GUO, Z., OGAWA, T., TAGIRI, A., SUGIMOTO, K., BERNHARDT, N., BRASSAC, J., MASCHER, M., HENSEL, G., OHNISHI, S., JINNO, H., YAMASHITA, Y., AYALON, I., PELEG, Z., SCHNURBUSCH, T. & KOMATSUDA, T. 2019. Unleashing floret fertility in wheat through the mutation of a homeobox gene. *Proc Natl Acad Sci U S A*, 116, 5182-5187.

- SAKUMA, S., LUNDQVIST, U., KAKEI, Y., THIRULOGACHANDAR, V., SUZUKI, T., HORI, K., WU, J., TAGIRI, A., RUTTEN, T., KOPPOLU, R., SHIMADA, Y., HOUSTON, K., THOMAS, W. T. B., WAUGH, R., SCHNURBUSCH, T. & KOMATSUDA, T. 2017. Extreme Suppression of Lateral Floret Development by a Single Amino Acid Change in the VRS1 Transcription Factor *Plant Physiology*, 175, 1720-1731.
- SAKUMA, S., POURKHEIRANDISH, M., HENSEL, G., KUMLEHN, J., STEIN, N., TAGIRI, A., YAMAJI, N., MA, J. F., SASSA, H., KOBA, T. & KOMATSUDA, T. 2013. Divergence of expression pattern contributed to neofunctionalization of duplicated HD-Zip I transcription factor in barley. *New Phytologist*, 197, 939-948.
- SAKUMA, S. & SCHNURBUSCH, T. 2020. Of floral fortune: tinkering with the grain yield potential of cereal crops. *New Phytol*, 225, 1873-1882.
- SALAZAR-DIAZ, K., DONG, Y., PAPDI, C., FERRUZCA-RUBIO, E. M., OLEA-BADILLO, G., RYABOVA, L. A. & DINKOVA, T. D. 2021. TOR senses and regulates spermidine metabolism during seedling establishment and growth in maize and Arabidopsis. *iScience*, 24, 103260.
- SCHILDHAUER, J., WIEDEMUTH, K. & HUMBECK, K. 2008. Supply of nitrogen can reverse senescence processes and affect expression of genes coding for plastidic glutamine synthetase and lysine-ketoglutarate reductase/saccharopine dehydrogenase. *Plant Biology*, 10, 76-84.
- SCHIPPERS, J. H., SCHMIDT, R., WAGSTAFF, C. & JING, H. C. 2015. Living to Die and Dying to Live: The Survival Strategy behind Leaf Senescence. *Plant Physiol*, 169, 914-30.
- SCHIPPERS, J. H. M. 2015. Transcriptional networks in leaf senescence. *Current Opinion in Plant Biology*, 27, 77-83.
- SCHIPPERS, J. H. M., FOYER, C. H. & VAN DONGEN, J. T. 2016. Redox regulation in shoot growth, SAM maintenance and flowering. *Current Opinion in Plant Biology*, 29, 121-128.
- SCHOOOF, H., LENHARD, M., HAECKER, A., MAYER, K. F. X., JÜRGENS, G. & LAUX, T. 2000. The Stem Cell Population of Arabidopsis Shoot Meristems Is Maintained by a Regulatory Loop between the CLAVATA and WUSCHEL Genes. *Cell*, 100, 635-644.
- SCHREIBER, M., MASCHER, M., WRIGHT, J., PADMARASU, S., HIMMELBACH, A., HEAVENS, D., MILNE, L., CLAVIJO, B. J., STEIN, N. & WAUGH, R. 2020. A Genome Assembly of the Barley 'Transformation Reference' Cultivar Golden Promise. *G3 Genes/Genomes/Genetics*, 10, 1823-1827.
- SCHWARZ, P. & LI, Y. 2010. Malting and Brewing Uses of Barley. *Barley*.
- SEILER, C., HARSHAVARDHAN, V. T., REDDY, P. S., HENSEL, G., KUMLEHN, J., ESCHEN-LIPPOLD, L., RAJESH, K., KORZUN, V., WOBUS, U., LEE, J., SELVARAJ, G. & SREENIVASULU, N. 2014. Abscisic acid flux alterations result in differential abscisic acid signaling responses and impact assimilation efficiency in barley under terminal drought stress. *Plant Physiol*, 164, 1677-96.
- SENTHIL-KUMAR, M. & MYSORE, K. S. 2011. Caveat of RNAi in Plants: The Off-Target Effect. In: KODAMA, H. & KOMAMINE, A. (eds.) *RNAi and Plant Gene Function Analysis: Methods and Protocols*. Totowa, NJ: Humana Press.
- SEO, J., LEE, H. Y., CHOI, H., CHOI, Y., LEE, Y., KIM, Y. W., RYU, S. B. & LEE, Y. 2008. Phospholipase A2beta mediates light-induced stomatal opening in Arabidopsis. *J Exp Bot*, 59, 3587-94.
- SHANMUGARAJ, N., RUTTEN, T., SVATOŠ, A., SCHNURBUSCH, T. & MOCK, H.-P. 2023a. Fast and Reproducible Matrix Deposition for MALDI Mass

- Spectrometry Imaging with Improved Glass Sublimation Setup. *Journal of the American Society for Mass Spectrometry*, 34, 513-517.
- SHANMUGARAJ, N., RAJARAMAN, J., SANDIP, K., KAMAL, R., HUANG, Y., THIRULOGACHANDAR, V., BUDHAGATAPALLI, N., MOYA, Y. A.T., HAJIREZAEI, M.R., GARIBAY, A., RUTTEN, T., KUMLEHN, J., HENSEL, G., MELZER, M., VON WIRÉN, N., MOCK, H.P., and SCHNURBUSCH, T. 2023b Spatiotemporal multi-omics analyses reveal a multilayered regulation of developmentally programmed pre-anthesis tip degeneration of the barley inflorescence. *The Plant Cell* (Accepted).
- SHANNON, P., MARKIEL, A., OZIER, O., BALIGA, N. S., WANG, J. T., RAMAGE, D., AMIN, N., SCHWIKOWSKI, B. & IDEKER, T. 2003. Cytoscape: A software environment for integrated models of biomolecular interaction networks. *Genome Research*, 13, 2498-2504.
- SHARMA, V. K., CARLES, C. & FLETCHER, J. C. 2003. Maintenance of stem cell populations in plants. *Proceedings of the National Academy of Sciences*, 100, 11823-11829.
- SHAW, D. S. & HONEYCHURCH, K. C. 2022. Nanosensor Applications in Plant Science. *Biosensors*, 12, 675.
- SHAW, L. M., LYU, B., TURNER, R., LI, C., CHEN, F., HAN, X., FU, D. & DUBCOVSKY, J. 2019. FLOWERING LOCUS T2 regulates spike development and fertility in temperate cereals. *J Exp Bot*, 70, 193-204.
- ŠIMÁŠKOVÁ, M., DANEVA, A., DOLL, N., SCHILLING, N., CUBRÍA-RADÍO, M., ZHOU, L., DE WINTER, F., AESAERT, S., DE RYCKE, R., PAUWELS, L., DRESSELHAUS, T., BRUGIÈRE, N., SIMMONS, C. R., HABBEN, J. E. & NOWACK, M. K. 2022. KIL1 terminates fertility in maize by controlling silk senescence. *The Plant Cell*, 34, 2852-2870.
- SIMURA, J., ANTONIADI, I., SIROKA, J., TARKOWSKA, D., STRNAD, M., LJUNG, K. & NOVAK, O. 2018. Plant Hormonomics: Multiple Phytohormone Profiling by Targeted Metabolomics. *Plant Physiology*, 177, 476-489.
- SINGH, R. K., SOOD, P., PRASAD, A. & PRASAD, M. 2021. Advances in omics technology for improving crop yield and stress resilience. *Plant Breeding*, 140, 719-731.
- SKYLAR, A., SUNG, F., HONG, F., CHORY, J. & WU, X. 2011. Metabolic sugar signal promotes Arabidopsis meristematic proliferation via G2. *Dev Biol*, 351, 82-9.
- SLAFER, G. A., FOULKES, M. J., REYNOLDS, M. P., MURCHIE, E. H., CARMO-SILVA, E., FLAVELL, R., GWYN, J., SAWKINS, M. & GRIFFITHS, S. 2022. A 'wiring diagram' for sink strength traits impacting wheat yield potential. *Journal of Experimental Botany*, 74, 40-71.
- SOBIESZCZUK-NOWICKA, E. 2017. Polyamine catabolism adds fuel to leaf senescence. *Amino Acids*, 49, 49-56.
- SOBIESZCZUK-NOWICKA, E., PALUCH-LUBAWA, E., MATTOO, A. K., ARASIMOWICZ-JELONEK, M., GREGERSEN, P. L. & PACAK, A. 2019. Polyamines - A New Metabolic Switch: Crosstalk With Networks Involving Senescence, Crop Improvement, and Mammalian Cancer Therapy. *Front Plant Sci*, 10, 859.
- SREENIVASULU, N. & SCHNURBUSCH, T. 2012. A genetic playground for enhancing grain number in cereals. *Trends Plant Sci*, 17, 91-101.
- SUN, L., ZHANG, H., LI, D., HUANG, L., HONG, Y., DING, X. S., NELSON, R. S., ZHOU, X. & SONG, F. 2013. Functions of rice NAC transcriptional factors,

- ONAC122 and ONAC131, in defense responses against *Magnaporthe grisea*. *Plant Mol Biol*, 81, 41-56.
- SVATOŠ, A. & MOCK, H.-P. 2013. MALDI Mass Spectrometric Imaging of Plants. *The Handbook of Plant Metabolomics*.
- TAMARY, E., NEVO, R., NAVEH, L., LEVIN-ZAIDMAN, S., KISS, V., SAVIDOR, A., LEVIN, Y., EYAL, Y., REICH, Z. & ADAM, Z. 2019. Chlorophyll catabolism precedes changes in chloroplast structure and proteome during leaf senescence. *Plant Direct*, 3, e00127.
- TAN, M., CHENG, D., YANG, Y., ZHANG, G., QIN, M., CHEN, J., CHEN, Y. & JIANG, M. 2017. Co-expression network analysis of the transcriptomes of rice roots exposed to various cadmium stresses reveals universal cadmium-responsive genes. *BMC Plant Biology*, 17, 194.
- TAYLOR, M. J., LUKOWSKI, J. K. & ANDERTON, C. R. 2021. Spatially Resolved Mass Spectrometry at the Single Cell: Recent Innovations in Proteomics and Metabolomics. *Journal of the American Society for Mass Spectrometry*, 32, 872-894.
- THEUNE, M. L., BLOSS, U., BRAND, L. H., LADWIG, F. & WANKE, D. 2019. Phylogenetic Analyses and GAGA-Motif Binding Studies of BBR/BPC Proteins Lend to Clues in GAGA-Motif Recognition and a Regulatory Role in Brassinosteroid Signaling. *Front Plant Sci*, 10, 466.
- THIEL, J., KOPPOLU, R., TRAUTWIG, C., HERTIG, C., KALE, S. M., ERBE, S., MASCHER, M., HIMMELBACH, A., RUTTEN, T., ESTEBAN, E., PASHA, A., KUMLEHN, J., PROVART, N. J., VANDERAUWERA, S., FROHBERG, C. & SCHNURBUSCH, T. 2021. Transcriptional landscapes of floral meristems in barley. *Science Advances*, 7, eabf0832.
- THIRULOGACHANDAR, V., GOVIND, G., HENSEL, G., KALE, S. M., KUHLMANN, M., ESCHEN-LIPPOLD, L., RUTTEN, T., KOPPOLU, R., RAJARAMAN, J., PALAKOLANU, S. R., SEILER, C., SAKUMA, S., JAYAKODI, M., LEE, J., KUMLEHN, J., KOMATSUDA, T., SCHNURBUSCH, T. & SREENIVASULU, N. 2021a. Dosage of duplicated and antifunctionalized homeobox proteins influences spikelet development in barley. *bioRxiv*, 2021.11.08.467769.
- THIRULOGACHANDAR, V., KOPPOLU, R. & SCHNURBUSCH, T. 2021b. Strategies of grain number determination differentiate barley row types. *J Exp Bot*, 72, 7754-7768.
- THIRULOGACHANDAR, V. & SCHNURBUSCH, T. 2021. 'Spikelet stop' determines the maximum yield potential stage in barley. *J Exp Bot*, 72, 7743-7753.
- THOMAS, H. 2013. Senescence, ageing and death of the whole plant. *New Phytol*, 197, 696-711.
- THOMAS, H., OUGHAM, H. J., WAGSTAFF, C. & STEAD, A. D. 2003. Defining senescence and death. *Journal of Experimental Botany*, 54, 1127-1132.
- ULLRICH, S. E. 2014. Chapter 1 - The Barley Crop: Origin and Taxonomy, Production, and End Uses. In: SHEWRY, P. R. & ULLRICH, S. E. (eds.) *Barley (Second Edition)*. AACC International Press.
- VAN DER GRAAFF, E., SCHWACKE, R., SCHNEIDER, A., DESIMONE, M., FLÜGGE, U.-I. & KUNZE, R. 2006. Transcription Analysis of Arabidopsis Membrane Transporters and Hormone Pathways during Developmental and Induced Leaf Senescence. *Plant Physiology*, 141, 776-792.
- VAN DOORN, W. G. & WOLTERING, E. J. 2004. Senescence and programmed cell death: substance or semantics? *J Exp Bot*, 55, 2147-53.

- VAN ESSE, G. W., WALLA, A., FINKE, A., KOORNNEEF, M., PECINKA, A. & VON KORFF, M. 2017. Six-Rowed Spike3 (VRS3) Is a Histone Demethylase That Controls Lateral Spikelet Development in Barley. *Plant Physiol*, 174, 2397-2408.
- VAN HAUTEGEM, T., WATERS, A. J., GOODRICH, J. & NOWACK, M. K. 2015. Only in dying, life: programmed cell death during plant development. *Trends Plant Sci*, 20, 102-113.
- VESCOVI, M., RIEFLER, M., GESSUTI, M., NOVÁK, O., SCHMÜLLING, T. & LO SCHIAVO, F. 2012. Programmed cell death induced by high levels of cytokinin in Arabidopsis cultured cells is mediated by the cytokinin receptor CRE1/AHK4. *J Exp Bot*, 63, 2825-32.
- VIEHWEGER, K., DORDSCHBAL, B. & ROOS, W. 2002. Elicitor-activated phospholipase A(2) generates lysophosphatidylcholines that mobilize the vacuolar H(+) pool for pH signaling via the activation of Na(+)-dependent proton fluxes. *Plant Cell*, 14, 1509-25.
- WADDINGTON, S. R., CARTWRIGHT, P. M. & WALL, P. C. 1983. A QUANTITATIVE SCALE OF SPIKE INITIAL AND PISTIL DEVELOPMENT IN BARLEY AND WHEAT. *Annals of Botany*, 51, 119-130.
- WANG, C., DAI, S., ZHANG, Z.-L., LAO, W., WANG, R., MENG, X. & ZHOU, X. 2021. Ethylene and salicylic acid synergistically accelerate leaf senescence in Arabidopsis. *Journal of Integrative Plant Biology*, 63, 828-833.
- WANG, J. & ZHANG, Z. 2021. GAPIT Version 3: Boosting Power and Accuracy for Genomic Association and Prediction. *Genomics, Proteomics & Bioinformatics*, 19, 629-640.
- WANG, S. & BLUMWALD, E. 2014. Stress-induced chloroplast degradation in Arabidopsis is regulated via a process independent of autophagy and senescence-associated vacuoles. *Plant Cell*, 26, 4875-88.
- WANG, Y. & JIAO, Y. 2018. Auxin and above-ground meristems. *J Exp Bot*, 69, 147-154.
- WANG, Y., KUMAISHI, K., SUZUKI, T., ICHIHASHI, Y., YAMAGUCHI, N., SHIRAKAWA, M. & ITO, T. 2020. Morphological and Physiological Framework Underlying Plant Longevity in Arabidopsis thaliana. *Frontiers in Plant Science*, 11.
- WANG, Y. & LI, J. 2008. Molecular basis of plant architecture. *Annu Rev Plant Biol*, 59, 253-79.
- WANG, Y., SHIRAKAWA, M. & ITO, T. 2022. Dynamic Changes in Reactive Oxygen Species in the Shoot Apex Contribute to Stem Cell Death in Arabidopsis thaliana. *International Journal of Molecular Sciences*, 23, 3864.
- WANG, Y., YU, H., TIAN, C., SAJJAD, M., GAO, C., TONG, Y., WANG, X. & JIAO, Y. 2017. Transcriptome Association Identifies Regulators of Wheat Spike Architecture. *Plant Physiology*, 175, 746-757.
- WANG, Z., CAO, W., DAI, T. & ZHOU, Q. 2001. Effects of exogenous hormones on floret development and grain set in wheat. *Plant Growth Regulation*, 35, 225-231.
- WARE, A., WALKER, C. H., ŠIMURA, J., GONZÁLEZ-SUÁREZ, P., LJUNG, K., BISHOPP, A., WILSON, Z. A. & BENNETT, T. 2020. Auxin export from proximal fruits drives arrest in temporally competent inflorescences. *Nature Plants*, 6, 699-707.
- WATANABE, M., BALAZADEH, S., TOHGE, T., ERBAN, A., GIAVALISCO, P., KOPKA, J., MUELLER-ROEBER, B., FERNIE, A. R. & HOEFGEN, R. 2013. Comprehensive dissection of spatiotemporal metabolic shifts in primary,

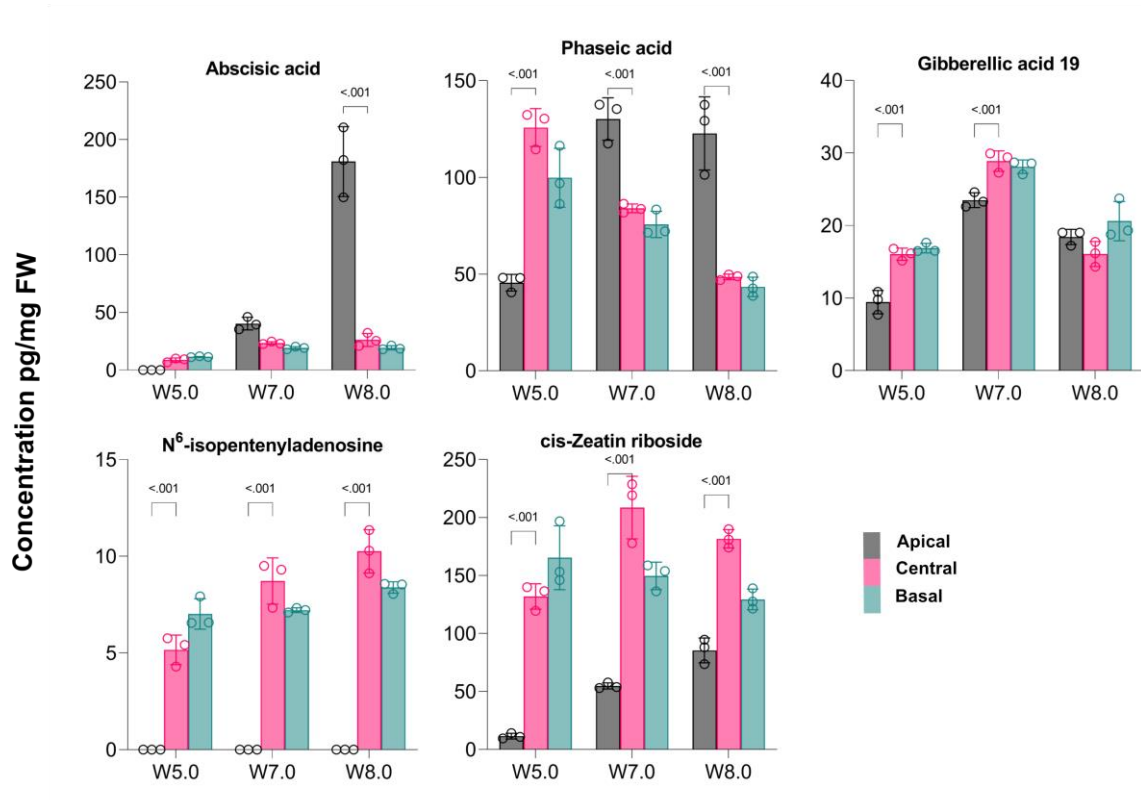
- secondary, and lipid metabolism during developmental senescence in *Arabidopsis*. *Plant Physiol*, 162, 1290-310.
- WELCH, R. W. 2012. *The Oat Crop: Production and Utilization*, Springer Netherlands.
- WENG, J. K., YE, M., LI, B. & NOEL, J. P. 2016. Co-evolution of Hormone Metabolism and Signaling Networks Expands Plant Adaptive Plasticity. *Cell*, 166, 881-893.
- WHIPPLE, C. J., KEBROM, T. H., WEBER, A. L., YANG, F., HALL, D., MEELEY, R., SCHMIDT, R., DOEBLEY, J., BRUTNELL, T. P. & JACKSON, D. P. 2011. grassy tillers1 promotes apical dominance in maize and responds to shade signals in the grasses. *Proc Natl Acad Sci U S A*, 108, E506-12.
- WILLIAMS, L. & FLETCHER, J. C. 2005. Stem cell regulation in the *Arabidopsis* shoot apical meristem. *Current Opinion in Plant Biology*, 8, 582-586.
- WIND, J., SMEEKENS, S. & HANSON, J. 2010. Sucrose: Metabolite and signaling molecule. *Phytochemistry*, 71, 1610-1614.
- WOJCIECHOWSKA, N., SOBIESZCZUK-NOWICKA, E. & BAGNIEWSKA-ZADWORNA, A. 2018. Plant organ senescence – regulation by manifold pathways. *Plant Biology*, 20, 167-181.
- WOLDE, G. M. & SCHNURBUSCH, T. 2019. Inferring vascular architecture of the wheat spikelet based on resource allocation in the branched head(t) (bh(t)-A1) near isogenic lines. *Funct Plant Biol*, 46, 1023-1035.
- WONG, N., LIU, W. & WANG, X. 2015. WU-CRISPR: characteristics of functional guide RNAs for the CRISPR/Cas9 system. *Genome Biology*, 16, 218.
- WOO, H. R., KIM, H. J., LIM, P. O. & NAM, H. G. 2019. Leaf Senescence: Systems and Dynamics Aspects. *Annu Rev Plant Biol*, 70, 347-376.
- WU, H., QU, X., DONG, Z., LUO, L., SHAO, C., FORNER, J., LOHMANN, J. U., SU, M., XU, M., LIU, X., ZHU, L., ZENG, J., LIU, S., TIAN, Z. & ZHAO, Z. 2020a. WUSCHEL triggers innate antiviral immunity in plant stem cells. *Science*, 370, 227-231.
- WU, Q., XU, F., LIU, L., CHAR, S. N., DING, Y., JE, B. I., SCHMELZ, E., YANG, B. & JACKSON, D. 2020b. The maize heterotrimeric G protein $\beta 2$ subunit controls shoot meristem development and immune responses. *Proceedings of the National Academy of Sciences*, 117, 1799-1805.
- WÜRSCHUM, T., LEISER, W. L., LANGER, S. M., TUCKER, M. R. & LONGIN, C. F. H. 2018. Phenotypic and genetic analysis of spike and kernel characteristics in wheat reveals long-term genetic trends of grain yield components. *Theoretical and Applied Genetics*, 131, 2071-2084.
- WYBOUW, B. & DE RYBEL, B. 2019. Cytokinin - A Developing Story. *Trends Plant Sci*, 24, 177-185.
- XIA, K., SUN, H.-X., LI, J., LI, J., ZHAO, Y., CHEN, L., QIN, C., CHEN, R., CHEN, Z., LIU, G., YIN, R., MU, B., WANG, X., XU, M., LI, X., YUAN, P., QIAO, Y., HAO, S., WANG, J., XIE, Q., XU, J., LIU, S., LI, Y., CHEN, A., LIU, L., YIN, Y., YANG, H., WANG, J., GU, Y. & XU, X. 2022. The single-cell stereo-seq reveals region-specific cell subtypes and transcriptome profiling in *Arabidopsis* leaves. *Developmental Cell*, 57, 1299-1310.e4.
- XU, X., CROW, M., RICE, B. R., LI, F., HARRIS, B., LIU, L., DEMESA-AREVALO, E., LU, Z., WANG, L., FOX, N., WANG, X., DRENKOW, J., LUO, A., CHAR, S. N., YANG, B., SYLVESTER, A. W., GINGERAS, T. R., SCHMITZ, R. J., WARE, D., LIPKA, A. E., GILLIS, J. & JACKSON, D. 2021. Single-cell RNA sequencing of developing maize ears facilitates functional analysis and trait candidate gene discovery. *Developmental Cell*, 56, 557-568.e6.
- XUE, G. P., WAY, H. M., RICHARDSON, T., DRENTH, J., JOYCE, P. A. & MCINTYRE, C. L. 2011. Overexpression of TaNAC69 leads to enhanced

- transcript levels of stress up-regulated genes and dehydration tolerance in bread wheat. *Mol Plant*, 4, 697-712.
- YADAV, A. K., CARROLL, A. J., ESTAVILLO, G. M., REBETZKE, G. J. & POGSON, B. J. 2019. Wheat drought tolerance in the field is predicted by amino acid responses to glasshouse-imposed drought. *J Exp Bot*, 70, 4931-4948.
- YAMAGUCHI, N., WU, M. F., WINTER, C. M., BERNS, M. C., NOLE-WILSON, S., YAMAGUCHI, A., COUPLAND, G., KRIZEK, B. A. & WAGNER, D. 2013. A molecular framework for auxin-mediated initiation of flower primordia. *Dev Cell*, 24, 271-82.
- YAMBURENKO, M. V., ZUBO, Y. O. & BORNER, T. 2015. Abscisic acid affects transcription of chloroplast genes via protein phosphatase 2C-dependent activation of nuclear genes: repression by guanosine-3'-5'-bis(diphosphate) and activation by sigma factor 5. *Plant J*, 82, 1030-1041.
- YAN, S., LIU, Q., LI, W., YAN, J. & FERNIE, A. R. 2022. Raffinose Family Oligosaccharides: Crucial Regulators of Plant Development and Stress Responses. *Critical Reviews in Plant Sciences*, 41, 286-303.
- YANG, H., NUKUNYA, K., DING, Q. & THOMPSON, B. E. 2021. Tissue-specific transcriptomics reveal functional differences in floral development. *Plant Physiology*, 188, 1158-1173.
- YANG, J., WORLEY, E. & UDVARDI, M. 2014. A NAP-AAO3 regulatory module promotes chlorophyll degradation via ABA biosynthesis in Arabidopsis leaves. *Plant Cell*, 26, 4862-74.
- YIN, Z., HUANG, W., FERNIE, A. R. & YAN, S. 2023. Mass spectrometry imaging techniques: a versatile toolbox for plant metabolomics. *Trends in Plant Science*, 28, 250-251.
- YOSHIDA, A., SASAO, M., YASUNO, N., TAKAGI, K., DAIMON, Y., CHEN, R., YAMAZAKI, R., TOKUNAGA, H., KITAGUCHI, Y., SATO, Y., NAGAMURA, Y., USHIJIMA, T., KUMAMARU, T., IIDA, S., MAEKAWA, M. & KYOZUKA, J. 2013. TAWAWA1, a regulator of rice inflorescence architecture, functions through the suppression of meristem phase transition. *Proceedings of the National Academy of Sciences*, 110, 767-772.
- YOUNG, T. E. & GALLIE, D. R. 2000. Regulation of programmed cell death in maize endosperm by abscisic acid. *Plant Mol Biol*, 42, 397-414.
- YOUSSEF, H. M., EGGERT, K., KOPPOLU, R., ALQUDAH, A. M., POURSAEBANI, N., FAZELI, A., SAKUMA, S., TAGIRI, A., RUTTEN, T., GOVIND, G., LUNDQVIST, U., GRANER, A., KOMATSUDA, T., SREENIVASULU, N. & SCHNURBUSCH, T. 2017. VRS2 regulates hormone-mediated inflorescence patterning in barley. *Nat Genet*, 49, 157-161.
- YOUSSEF, H. M. & HANSSON, M. 2019. Crosstalk among hormones in barley spike contributes to the yield. *Plant Cell Reports*, 38, 1013-1016.
- YU, G. 2020. Using ggtree to Visualize Data on Tree-Like Structures. *Current Protocols in Bioinformatics*, 69, e96.
- YU, X., LIU, Z. & SUN, X. 2022. Single-cell and spatial multi-omics in the plant sciences: Technical advances, applications, and perspectives. *Plant Communications*, 100508.
- ZEKI, Ö. C., EYLEM, C. C., REÇBER, T., KIR, S. & NEMUTLU, E. 2020. Integration of GC-MS and LC-MS for untargeted metabolomics profiling. *Journal of Pharmaceutical and Biomedical Analysis*, 190, 113509.
- ZENG, J., DONG, Z., WU, H., TIAN, Z. & ZHAO, Z. 2017. Redox regulation of plant stem cell fate. *The EMBO Journal*, 36, 2844-2855.

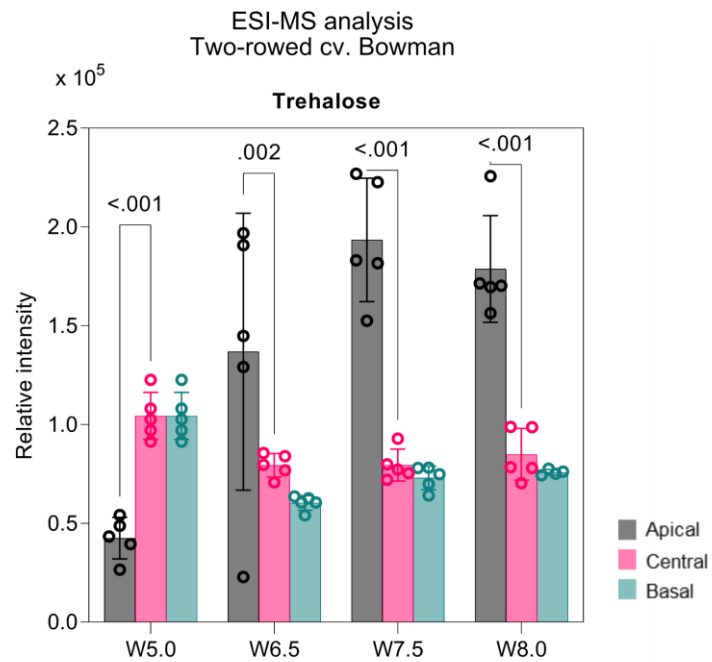
- ZHANG, D. & YUAN, Z. 2014. Molecular control of grass inflorescence development. *Annu Rev Plant Biol*, 65, 553-78.
- ZHANG, L., ZHU, X., ZHAO, Y., GUO, J., ZHANG, T., HUANG, W., HUANG, J., HU, Y., HUANG, C.-H. & MA, H. 2022. Phylotranscriptomics Resolves the Phylogeny of Pooideae and Uncovers Factors for Their Adaptive Evolution. *Molecular Biology and Evolution*, 39.
- ZHANG, W., PENG, K., CUI, F., WANG, D., ZHAO, J., ZHANG, Y., YU, N., WANG, Y., ZENG, D., WANG, Y., CHENG, Z. & ZHANG, K. 2021. Cytokinin oxidase/dehydrogenase OsCKX11 coordinates source and sink relationship in rice by simultaneous regulation of leaf senescence and grain number. *Plant Biotechnology Journal*, 19, 335-350.
- ZHANG, Y., WU, R., QIN, G., CHEN, Z., GU, H. & QU, L. J. 2011. Over-expression of WOX1 leads to defects in meristem development and polyamine homeostasis in Arabidopsis. *J Integr Plant Biol*, 53, 493-506.
- ZHAO, Z., ZHANG, J. W., LU, S. H., ZHANG, H., LIU, F., FU, B., ZHAO, M. Q. & LIU, H. 2020. Transcriptome divergence between developmental senescence and premature senescence in *Nicotiana tabacum* L. *Sci Rep*, 10, 20556.
- ZHENG, C., ZHU, Y., WANG, C. & GUO, T. 2016. Wheat Grain Yield Increase in Response to Pre-Anthesis Foliar Application of 6-Benzylaminopurine Is Dependent on Floret Development. *PLoS One*, 11, e0156627.
- ZHOU, Y. Y., ZHOU, B., PACHE, L., CHANG, M., KHODABAKHSHI, A. H., TANASEICHUK, O., BENNER, C. & CHANDA, S. K. 2019. Metascape provides a biologist-oriented resource for the analysis of systems-level datasets. *Nature Communications*, 10, 10.
- ZHU, C., BORTESI, L., BAYSAL, C., TWYMAN, R. M., FISCHER, R., CAPELL, T., SCHILLBERG, S. & CHRISTOU, P. 2017. Characteristics of Genome Editing Mutations in Cereal Crops. *Trends in Plant Science*, 22, 38-52.
- ZHU, F., ALSEEKH, S., KOPER, K., TONG, H., NIKOLOSKI, Z., NAAKE, T., LIU, H., YAN, J., BROTMAN, Y., WEN, W., MAEDA, H., CHENG, Y. & FERNIE, A. R. 2022. Genome-wide association of the metabolic shifts underpinning dark-induced senescence in Arabidopsis. *Plant Cell*, 34, 557-578.
- ZIMMER, C. M., UBERT, I. P., PACHECO, M. T. & FEDERIZZI, L. C. 2019. Variable expressivity and heritability of multiflorous spikelets in oat panicles. *Experimental Agriculture*, 55, 829-842.
- ZOHARY, D., HOPF, M. & WEISS, E. 2012. *Domestication of Plants in the Old World: The origin and spread of domesticated plants in Southwest Asia, Europe, and the Mediterranean Basin*, Oxford University Press.
- ZWIREK, M., WAUGH, R. & MCKIM, S. M. 2019. Interaction between row-type genes in barley controls meristem determinacy and reveals novel routes to improved grain. *New Phytologist*, 221, 1950-1965.

9. Appendix

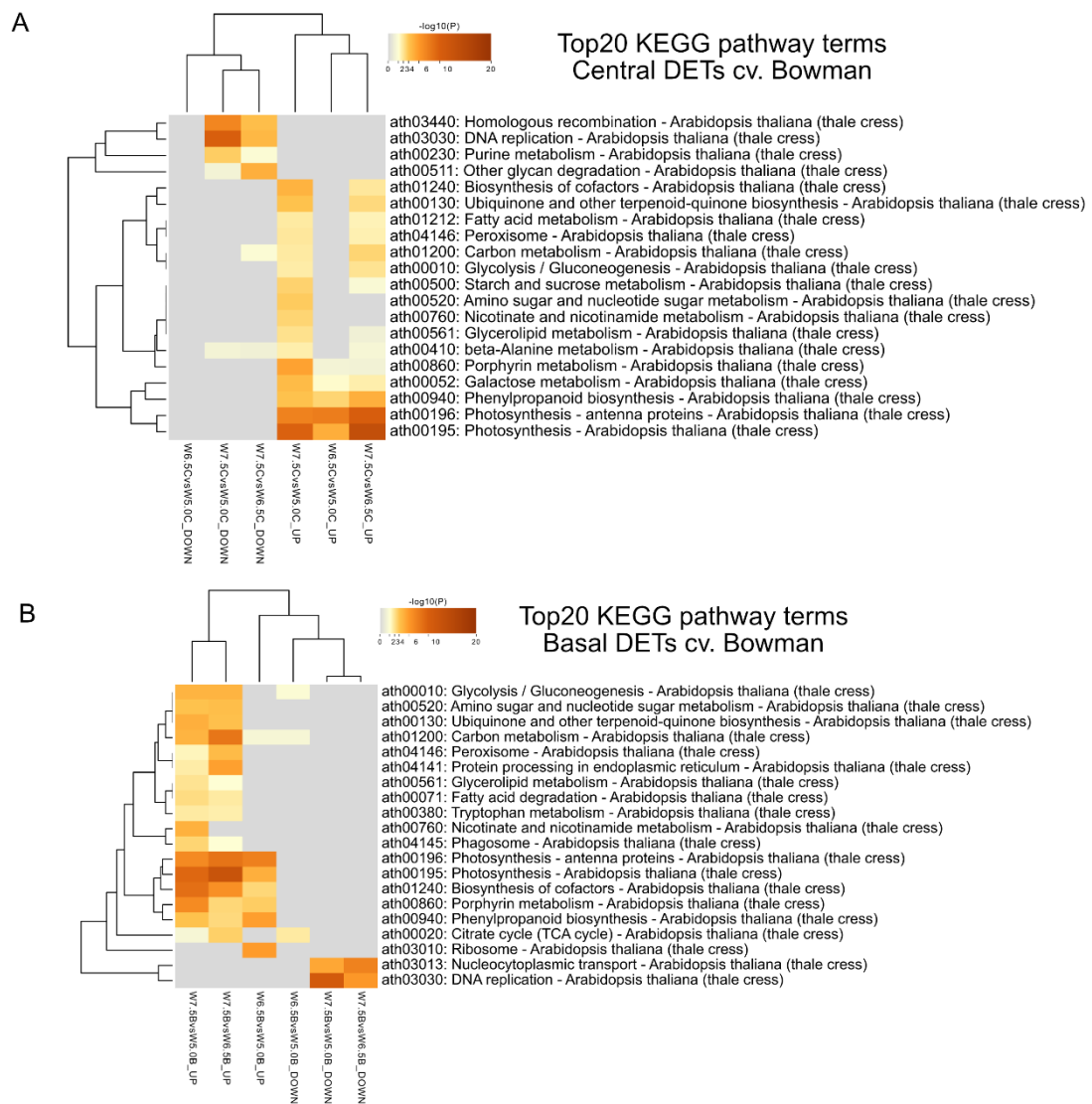
Bowman (Greenhouse)



Appendix Figure 1. Absolute levels of phytohormones in spike sections of barley cv. Bowman in greenhouse. Hormonal levels in three spikes of Bowman under long-day conditions in the greenhouse. Under greenhouse conditions, visible death initiation happens at around stage W7.0 in Bowman. Plots show means \pm SD with significant p values calculated from three to four biological replicates. Significance was tested by Two-way ANOVA with Tukey's multiple comparison test to evaluate the difference between apical, central, and basal positions at each stage. W, Waddington scale.

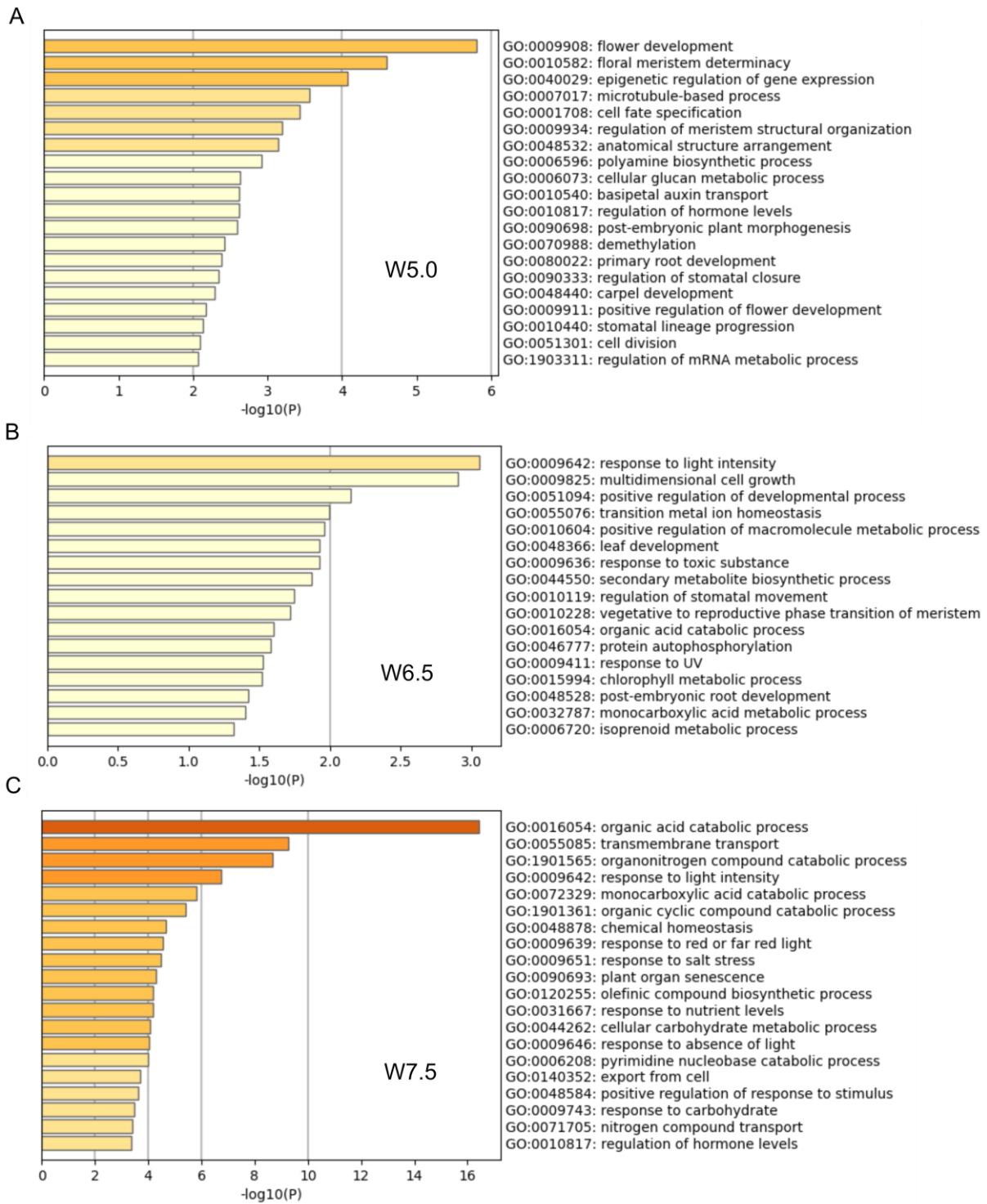


Appendix Figure 2. Relative contents of Trehalose along the spike. Relative distribution of trehalose in the three spike positions of Bowman measured by ESI-MS analysis. The relative quantitation of trehalose was based on the most intense ion, $[M+H-H_2O]^+$ m/z 325.1138. A- apical, C-central, B- Basal. Bar shows mean with standard deviation from five biological replication. A- apical, C-central, B- Basal. W, Waddington scale.



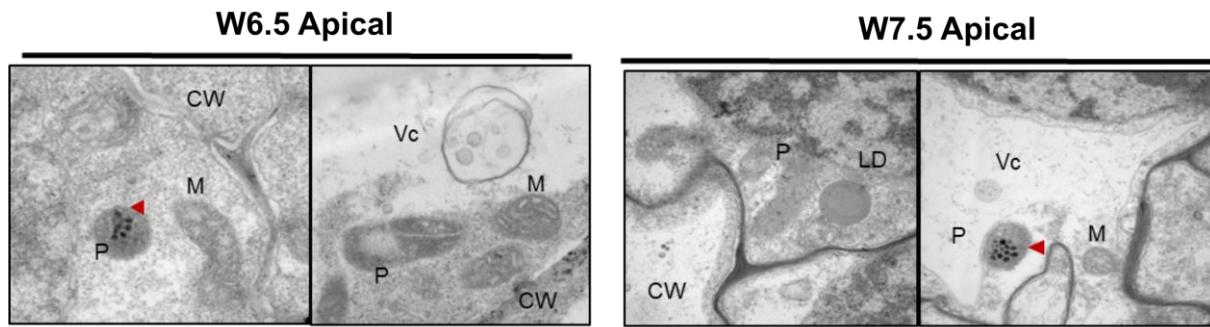
Appendix Figure 3. KEGG pathway enrichment analysis for differentially expressed genes (DEGs) in spike central (A) and basal (B) parts. Color saturation corresponds to the degree of enrichment. A- apical, C-central, B- Basal. W, Waddington scale.

Top20 GO terms for apically enriched genes in cv. Bowman



Appendix Figure 4. Gene Ontology (GO) enrichment analysis for apically enriched genes in cv. Bowman. (A-C) Stage-wise enrichment of top 20 biological processes terms. Color saturation corresponds to the degree of enrichment. A- apical, C-central, B- Basal. W, Waddington scale.

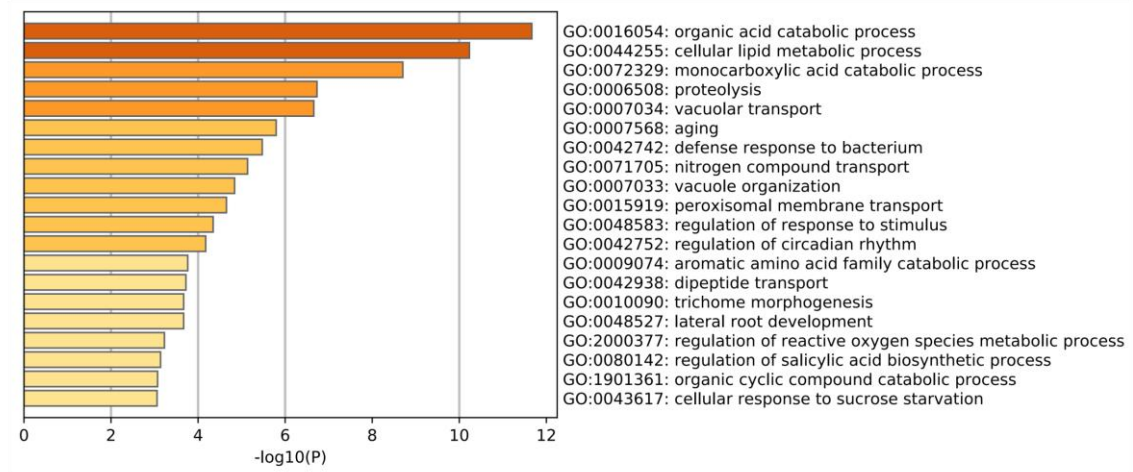
Bowman (Two-rowed)



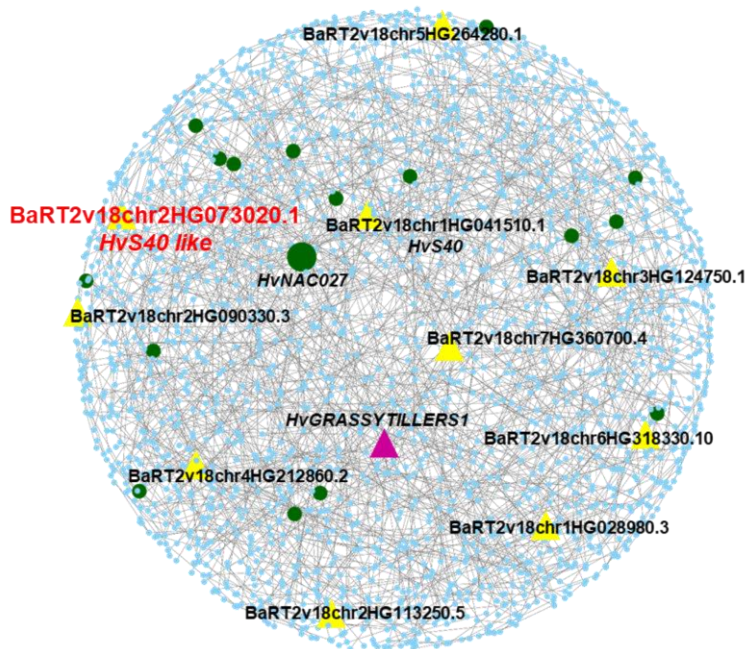
Appendix Figure 5. Transmission electron microscope (TEM) images of longitudinal sections of Bowman spikes in the apical part at W6.5 and W7.5 stages. P, plastid; M, mitochondria; CW, cell-wall; Vc, vesicles; LD, lipid droplets. W, Waddington scale.

A

Top 20 GO terms for co-expressed genes in PTD-associated gene network module in cv. Bowman - Yellow module

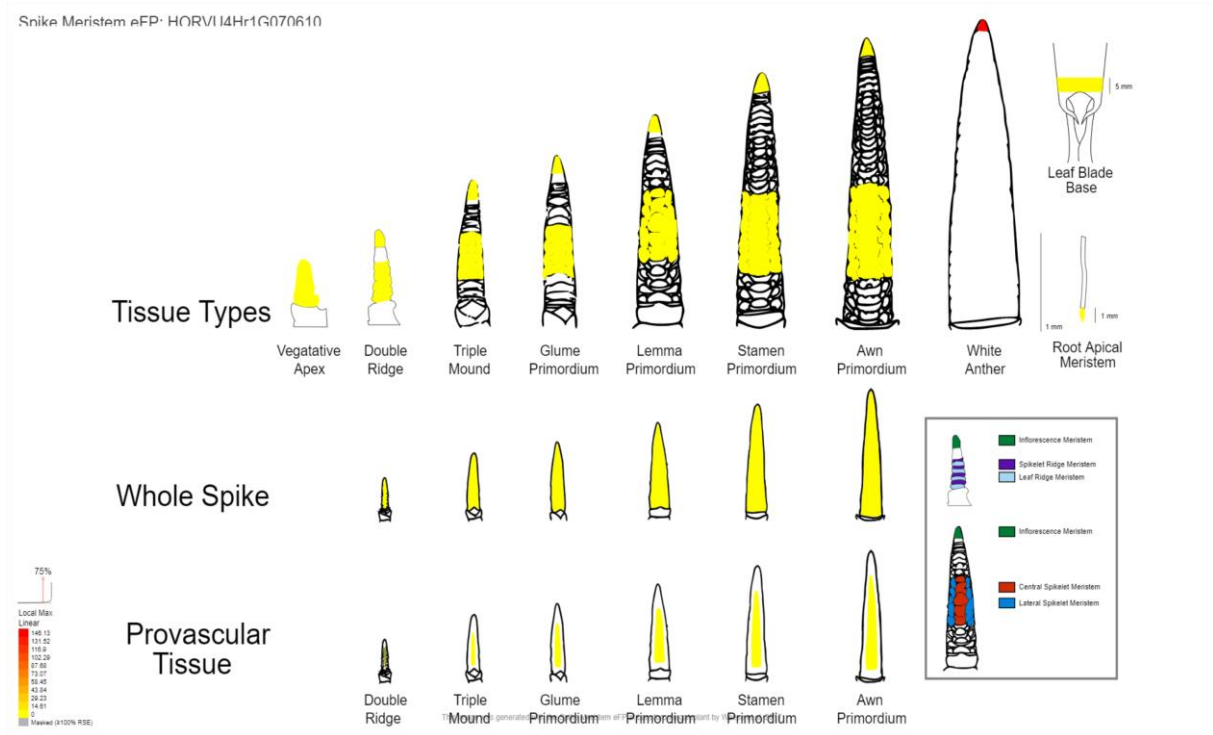


B

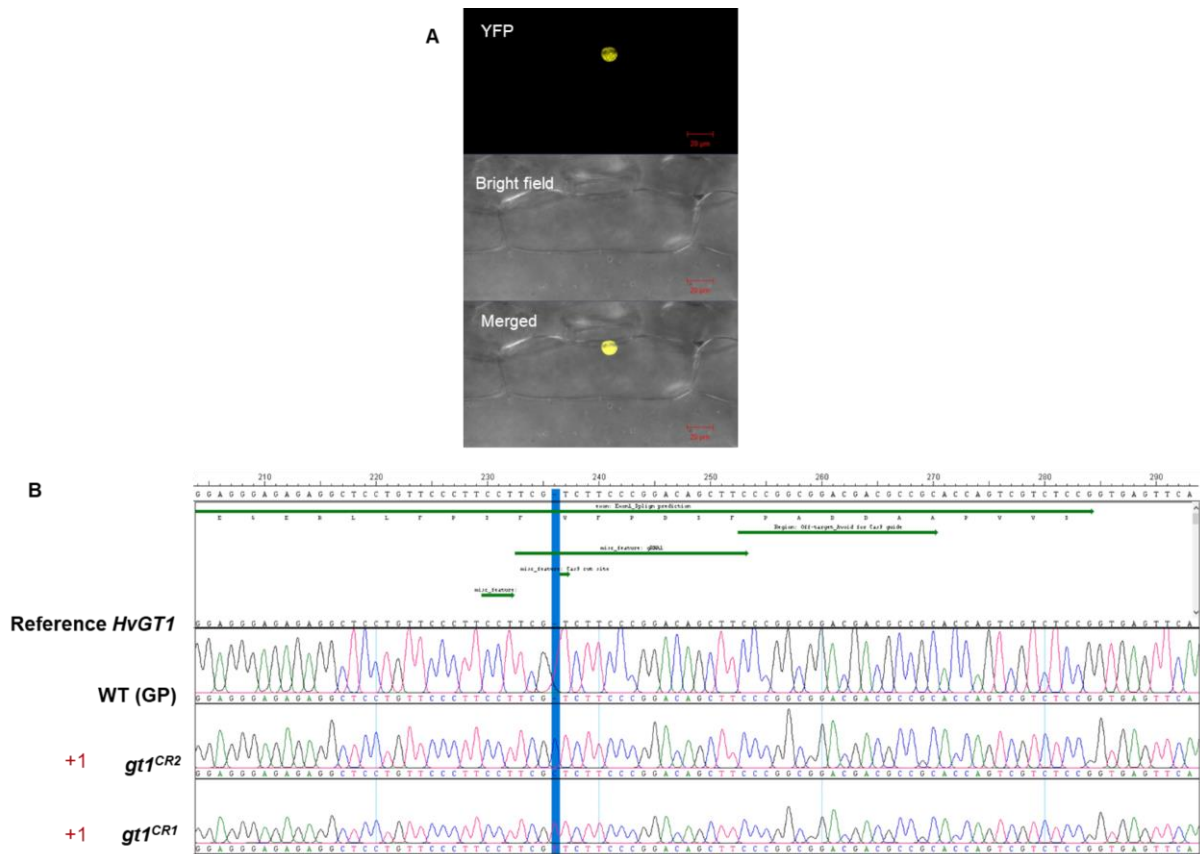


Appendix Figure 6. WGCNA co-expression module in cv. Bowman. (A) Top 20 terms enriched in the PTD-associated module (yellow). **(B)** Gene regulatory networks of PTD-associated module in Bowman. The top 10 hub genes are presented as yellow triangles, and the senescence-associated *Hvs40-like* gene is highlighted in red. Magenta colored triangle highlight *HvGT1* and NAC transcription factors in green circles.

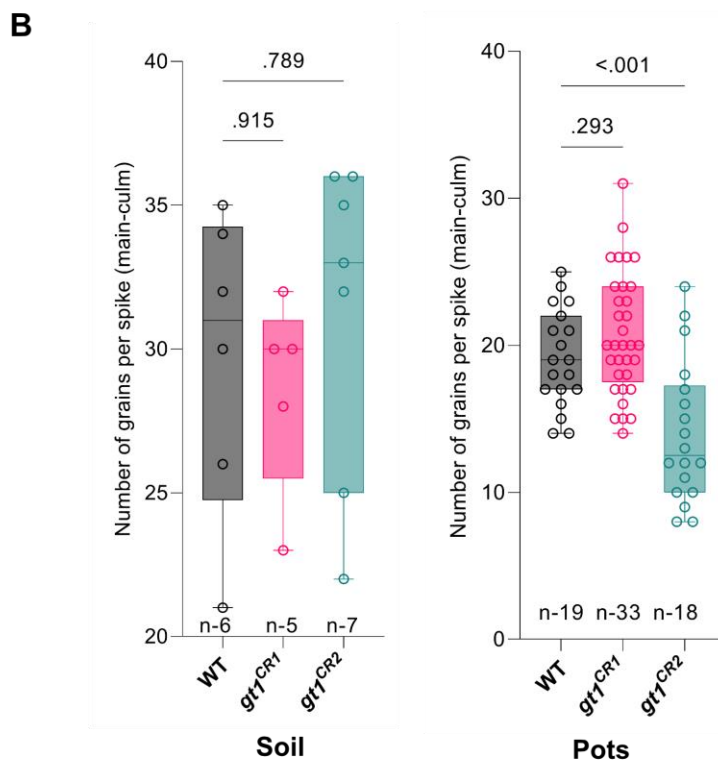
Hv GRASSY TILLERS1(*HvGT1*)



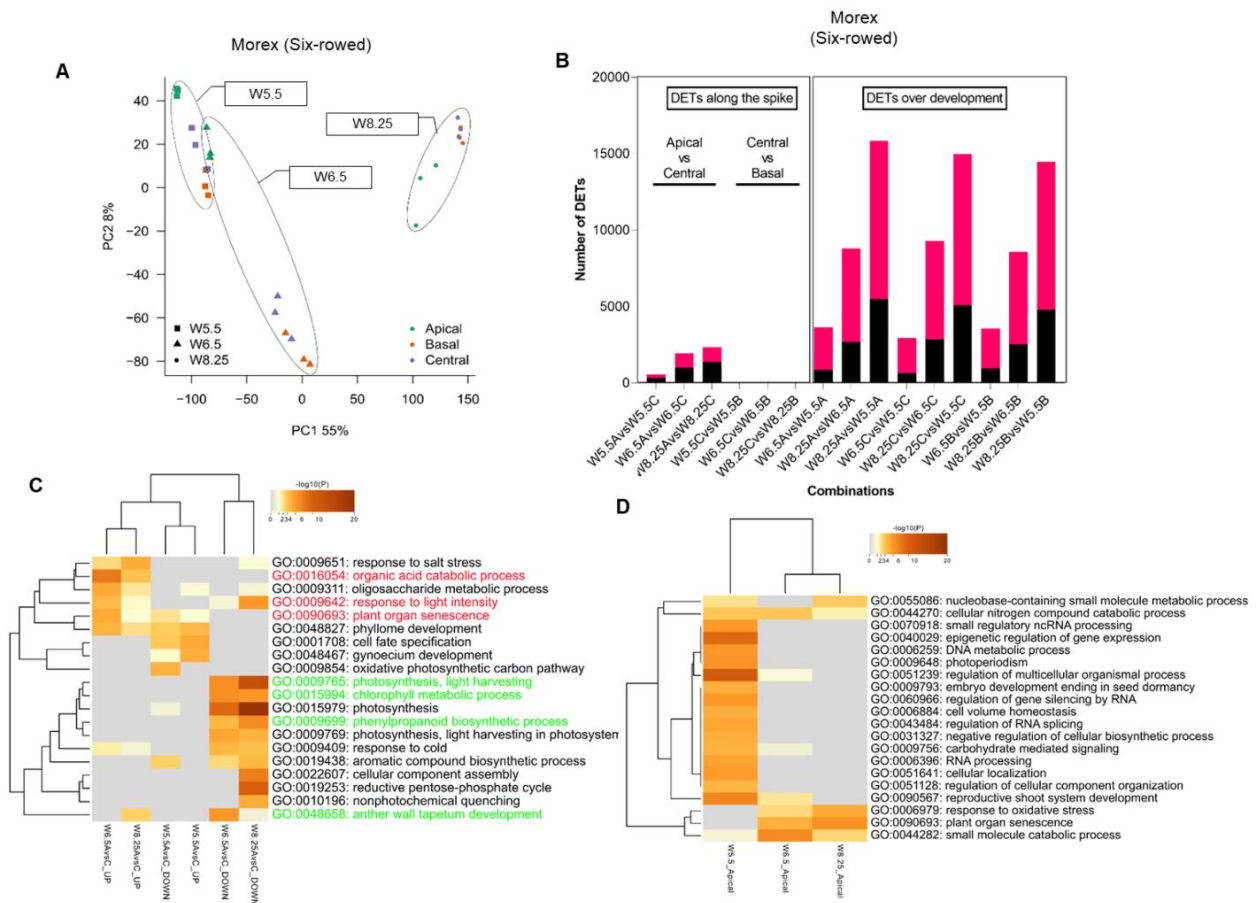
Appendix Figure 7. *GT1* expression in IM found in independent barley spike transcriptome atlas database. IM dome-specific expression of *HvGT1* in barley spike meristem at white anther stage (W5.0) in cv. Bowman. (http://bar.utoronto.ca/eplant_barley/)



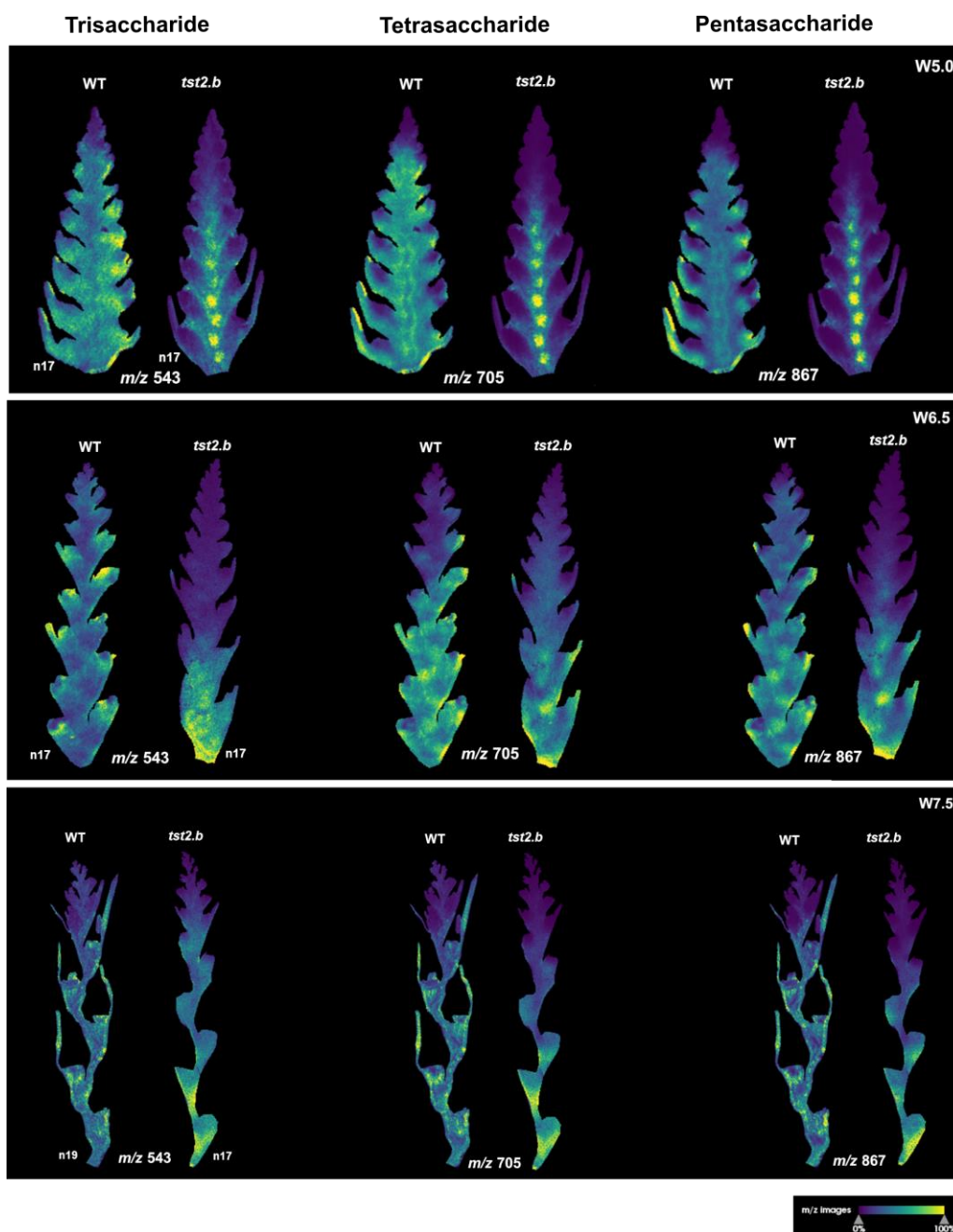
Appendix Figure 8. HvGT1 localization and mutation screening in gene-edited *Hvgt1* knockout lines. (A) HvGT-YFP fusion protein targets to the nucleus in barley leaf epidermis. **(B)** DNA sequences of independent T1 lines (WT, *gt1^{CR1}* & *gt1^{CR2}*) in the background of two-rowed cv. Golden Promise.



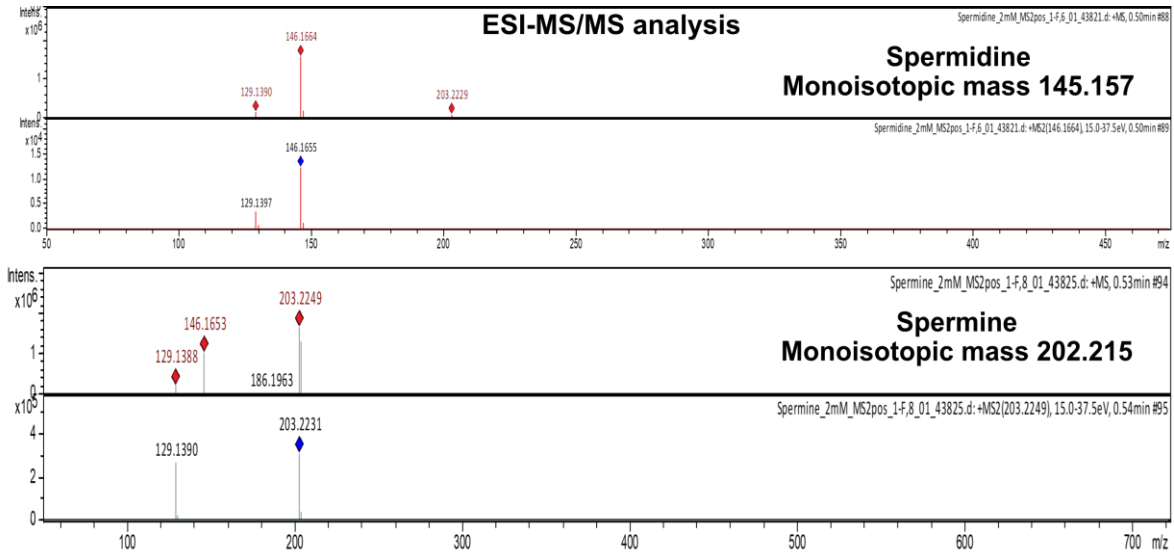
Appendix Figure 9. Mutation in barley *GT1* does not contribute to grain yield. (A-B) Mature spikes of azygous WT and *gt1* mutant at harvest. White arrow points the unfilled chaff of extra-survived spikelets in *gt1* mutant. Scale bar – 1 cm. **(C-D)** Box plot shows the final grain number after harvest in the main-culm spikes of WT and *gt1* mutant lines grown under greenhouse directly in soil (C) and in pots (D) (Methods section 2.1). Plots show means \pm SD with all replicate values. Significant levels are determined from the Unpaired Student's *t*-test with Welch's correction. W, Waddington scale.



Appendix Figure 10. Position-specific transcriptome analysis in six-rowed cv. Morex. (A) Principal component analysis (PCA) of normalized expression levels (counts per million, cpm) of all expressed transcripts. **(B)** The number of differentially expressed transcripts (\log_2 FC > 1) between 15 pairwise combinations. **(C)** Top 20 GO terms enriched for the differential expressed transcripts (DETs) between degenerating apical and viable central parts. **(D)** Top 20 GO terms enriched for the apically enriched transcripts. Color saturation corresponds to the degree of enrichment. A- apical, C-central, B- Basal, W, Waddington scale.



Appendix Figure 11. Spatial distribution of oligosaccharides identified by MALDI MSI in barley inflorescence meristem sections. Distribution of disaccharide signal in Bowman and BW.*tst2.b* mutant sections. Distributions are presented in the divided apical sections at W5.0, W6.5 and W7.5. All three signals were detected as potassium adducts $[M+K]^+$. Images are shown as normalized single ion intensity maps with 15- μm pixel size generated from Scils lab software. The color map corresponds to the intensity of ions. n, rachis node; W, Waddington scale.



Appendix Figure 12. Identification of candidate ion m/z 146.1 as polyamine. ESI-MS/MS fragmentation pattern using spermidine and spermine standards.

Appendix Table 1. Primers used in this study

qRT-PCR			
Gene	MorexV3 ID	Forward (5'-3')	Reverse(5'-3')
<i>HvNCED1</i> (Leymarie et al., 2008)	HORVU.MOREX.r3.5HG0426410.1	CCAGCACTAATCGATTCC	GAGAGTGGTGATGAGTAA
<i>HvACTIN</i>	HORVU.MOREX.r3.5HG0457850.1	AAGTACAGTGTCTGGATTGGAGGG	AAGTACAGTGTCTGGATTGGAGGG
Subcellular localisation			
<i>HvGT1-Topo</i>	HORVU.MOREX.r3.4HG0399240.1	CACCATGAGCCCCGAGGAGGGAGAG	GCTGAACTGATCGTACGCCCTC
Site-directed mutagenesis/ mutational screening			
	Remarks		
<i>HvGT1_exon1gR1</i>	<i>Cas9</i> gRNA for <i>HvGT1</i>	TGGCGAAGCTGTCCGGGAAGACGA	AAACTCGTCTCCCGACAGCTTC
<i>HvGT1-1207F/1893R</i>	PCR amplification and mutation detection	CAGGCTCACAGACTCGGAC	CTCCTCCTCGATGAGCTTGC
<i>zCas9</i>	PCR amplification and mutation detection	CGGCCTCGATATTGGGACTAACTCT	CTTATCTGTGGAGTCCACGAGCTTC
<i>HptII</i>	PCR amplification and mutation detection	AGCTGCGCCGATGGTTTCTACAA	CATCGCCTCGCTCCAGTCAATG

10. Abbreviations

mg	Milligram
mm	Millimeter
µm	Micrometer
µg	Microgram
µl	Microliter
µM	Micromolar
mM	Millimolar
mL	Milliliter
pmole	Picomolar
pg	Picogram
g	Gram
%	Percent
°C	degree Celsius
ABA	Abscisic acid
AA	Amino Acid
AP	Awn primordium
CAN	Acetonitrile
BLAST	Basic Local Alignment Search Tool
BM	Branch Meristem
bp	base pair
cDNA	Complementary DNA
CDS	Coding sequence
CK	Cytokinins
CRISPR	Clustered Regularly Interspaced Short Palindromic Repeats
CS	Central Spikelet
cZR	cis-Zeatin Riboside
DHB	2,5-dihydroxybenzoic acid
DNA	Deoxyribonucleic acid
DR	Double Ridge
EDTA	Ethylenediaminetetraacetic acid
ESI	Electrospray ionization
FAO	The Food and Agriculture Organization
FW	Fresh weight
FDR	False discovery rate
FM	Floret Meristem
GA	Gibberellic acid
GFP	Green Fluorescence Protein
Gb	Gigabase
GO	Gene ontology
GP	Glume Primordium
gRNA	Guide RNA
GWAS	Genome-Wide Association Study
H ₂ O ₂	Hydrogen peroxide
<i>Hv</i>	<i>Hordeum vulgare</i>
IAA	Indole-3-acetic acid
IM	Inflorescence Meristem
ITO	Indium tin oxide
Kb	Kilobase pairs

LC-MS	Liquid Chromatography-Mass Spectrometry
LPC	Lysophosphatidylcholine
LP	Lemma Primordium
LS	Lateral Spikelet
LSM	Lateral Spikelet Meristem
mRNA	messenger RNA
miRNA	micro RNA
Mb	Megabase pairs
ML	maximum likelihood
m/z	Mass-to-charge
MSI	Mass spectrometry imaging
MALDI	Matrix-assisted laser desorption/ionization
MeOH	Methanol
N	Nitrogen
NCED	9- <i>cis</i> -epoxycarotenoid dioxygenase
NGS	Next Generation Sequencing
NIL	Nearly isogenic lines
<i>Os</i>	<i>Oryza sativa</i>
PCD	Programmed cell death
PTD	Pre-anthesis tip degeneration
p-value	Probability value
PCA	Principle component analyses
PCR	Polymerase Chain Reaction
PEG	Polyethylene glycol
RT-qPCR	Reverse transcriptase-quantitative Polymerase Chain Reaction
RNA	Ribonucleic acid
ROS	Reactive oxygen species
RNA-seq	RNA sequencing
SAM	Shoot Apical Meristem
SEM	Scanning Electron Microscopy
SM	Spikelet Meristem
SNP	Single Nucleotide Polymorphism
SP	Stamen Primordium
SPM	Spikelet Pair Meristem
Spd	Spermidine
Spm	Spermine
SD	Standard deviation
TF	Transcription Factor
TOF	Time-of-flight
TM	Triple Mound
TSM	Triple-Spikelet Meristem
TEM	Transmission electron microscope
WGS	Whole-genome sequencing
W	Waddington
WT	Wild-type
<i>Zm</i>	<i>Zea mays</i>

11. Curriculum Vitae

Name: Nandhakumar Shanmugaraj

Gender: Male

Date of birth: 28.04.1994

Place of birth: Salem, Tamil Nadu, India

Education

PhD.

November 2017 – present

Martin Luther University Halle-Wittenberg, Germany

Thesis title: Spatiotemporal multi-omics analyses of the barley (*Hordeum vulgare* L.) inflorescence reveal a multilayered regulation of developmentally programmed pre-anthesis tip degeneration

Supervisor: Prof. Dr. Thorsten Schnurbusch, Co-supervisor: Dr. Hans-Peter Mock

M.Sc.

June 2017

Tamil Nadu Agricultural University (TNAU), India

Major: Agriculture (Biotechnology)

Thesis: Development and characterization of insect-resistant transgenic rice plants

Supervisor: Associate Prof. Dr. Balakrishnan Natarajan

CGPA – 8.92/10

B.Tech.

April 2015

Tamil Nadu Agricultural University (TNAU), India

Major: Biotechnology

Project: Agrobacterium-mediated transformation in *indica* rice with *cry2AX1* gene

Supervisor: Prof. Dr. Sudhakar Duraialagaraja

CGPA – 8.59/10

Research experience

Doctoral student, IPK Gatersleben

November 2017- present

Supervisor: *Prof. Dr. Thorsten Schnurbusch*, Co-supervisor: *Dr. Hans-Peter Mock*

- The research elucidates the molecular basis of pre-anthesis tip degeneration (PTD) in barley inflorescence.
- Spatiotemporal transcriptome, metabolome, and hormonal changes were captured using RNA sequencing and targeted metabolite profiling.

- Novel genes regulating PTD have been identified and functionally validated barley *GRASSY TILLERS1(GT1)* as one of the candidate genes, using CRISPR/Cas9-mediated mutagenesis.
- In addition, to capture the local metabolic changes during early spike meristems in barley, a spatial metabolomics technique MALDI Mass spectrometry imaging (MSI) platform was established and performed. With this, novel metabolic pathways shaping early spike development in barley have been identified.
- Moreover, the laser-captured microdissection (LCM) technique was utilized to capture transcriptional signatures between dying and viable tissues at high-spatial resolution. For this, a low-input total RNA extraction protocol was established with LCM spike tissues.

Master's student,

June 2016- June 2017

Bt Laboratory, Department of Plant biotechnology
Tamil Nadu Agricultural University (TNAU), India
Advisor: Associate Prof. Dr. Balakrishnan Natarajan

- Development and characterization of insect-resistant transgenic rice plants.
- *Agrobacterium*-mediated transformation of *indica* rice with a novel *cry2A* gene isolated from indigenous *Bt* strain.
- Testing the efficacy of transgenic rice lines expressing *cry2A* gene against target insect pests (Rice leaf folder, yellow stem borer, rice armyworm).

Publications

Shanmugaraj, N.*, Svatos, A., Twan, R., Mock, H.P., and Schnurbusch, T., (2023) "*Fast and reproducible matrix deposition for MALDI mass spectrometry imaging with improved glass sublimation setup*" Journal of the American Society for Mass Spectrometry. 34(3): 513-517. *Corresponding author

Huang, Y., Kamal, R., **Shanmugaraj, N.**, Rutten, T., Thirulogachandar, V., Zhao, S., Hoffie, I., Hensel, G., Rajaraman, J., Moya¹, Y. A. T., Hajirezaei, M-R., Himmelbach, A., Poursarebani, N., Lundqvist, U., Kumlehn, J., Stein, N., von Wirén, N., Mascher, M., Melzer, M., Schnurbusch, T., (2023) "*A molecular framework for grain number determination in barley*". Science Advances. 9(9): eadd0324.

Shanmugaraj, N., Rajaraman, J., Sandip, K., Kamal, R., Huang, Y., Thirulogachandar, V., Budhagatapalli, N., Moya, Y. A.T., Hajirezaei, M.R., Garibay, A., Rutten, T., Kumlehn, J., Hensel, G., Melzer, M., von Wirén, N., Mock, H.P., and Schnurbusch, T., (2023) "*Multilayered regulation of developmentally programmed pre-anthesis tip degeneration of the barley inflorescence*". The Plant Cell.

Shanmugaraj, N., Huang, Y., Garibay, A., D'Auria, J., Mock, H.P., and Schnurbusch, T., "Metabolic signals shaping early inflorescence meristem development in barley" (In preparation).

Oral presentations

Shanmugaraj, N., Thirulogachandar, V., Kale, S., Hajirezaei, M-R., von Wirén, N., Mock, H-P., and Schnurbusch, T. *Comprehensive understanding of apical spikelet abortion in barley inflorescence by tissue-specific multi-omics analyses*. Cold Spring Harbor meeting: Plant Genomes, Systems Biology and Engineering (Virtual), December 2021.

Shanmugaraj, N., Natarajan, B., Duraialagaraja, S., and Varadharajalu, U. *Development of multiple lepidopteran insect-resistant transgenic rice plants expressing a novel cry2A gene*. National level technical symposium Bioconcorrenza, Coimbatore, India, March 2017.

Selected Poster presentations

Shanmugaraj, N., Huang, Y., Mock, H-P., Schnurbusch, T. *Shaping of the barley inflorescence meristem—the discovery of metabolic signals*. FASEB SRC: The Mechanism of Plant development, Vermont, USA, July 2022.

Shanmugaraj, N., Thirulogachandar, V., Kale, S., Hajirezaei, M-R., von Wirén, N., Mock, H-P., and Schnurbusch, T. *Understanding the molecular basis of apical spikelet abortion on barley inflorescence*. Plant science students conference (IPK Gatersleben), June 2021.

Shanmugaraj, N., Thirulogachandar, V., Kale, S., Hajirezaei, M-R., von Wirén, N., Mock, H-P., and Schnurbusch, T. *Influence of tissue-specific transcriptomic and metabolomic changes on apical spikelet abortion in barley inflorescence*. EMBO workshop: International Plant systems biology (virtual), April 2021.

Shanmugaraj, N., Thirulogachandar, V., Kale, S., Hajirezaei, M-R., von Wirén, N., Mock, H-P., and Schnurbusch, T. *Studying apical spikelet abortion in barley inflorescences by spatiotemporal profiling of hormones and primary metabolome*. Plant biology 2020 virtual worldwide summit organized by the American society of plant biologist (ASPB), July 2020.

12. Eidesstattliche Erklärung/Declaration under Oath

Ich erkläre an Eides statt, dass ich die Arbeit selbstständig und ohne fremde Hilfe verfasst, keine anderen als die von mir angegebenen Quellen und Hilfsmittel benutzt und die den benutzten Werken wörtlich oder inhaltlich entnommenen Stellen als solche kenntlich gemacht habe.

I declare under penalty of perjury that this thesis is my own work entirely and has been written without any help from other people. I used only the sources mentioned and included all the citations correctly both in word or content.

Datum / Date

Unterschrift des Antragstellers /

Signature of the applicant